

Design of a Suitable Controller for Automatic Generation Control of Multi-Area Power System

**A Thesis Submitted
In Partial Fulfillment of the Requirements
for the Degree of**

DOCTOR OF PHILOSOPHY

by

RAVI CHOUDHARY
(2K18/Ph.D/EE/17)

**Under the Supervision of
Prof. J.N. Rai, Delhi Technological University, Delhi
and
Dr. Yogendra Arya, J.C. Bose University of Science and
Technology, YMCA, Faridabad, Haryana**



To the

Department of Electrical Engineering

**DELHI TECHNOLOGICAL UNIVERSITY
(Formerly Delhi College of Engineering)
Shahbad Daultapur, Main Bawana Road, Delhi-110042. India**

October, 2024



DELHI TECHNOLOGICAL UNIVERSITY
(Formerly Delhi College of Engineering)
Shahbad Daultapur, Main Bawana Road, Delhi-110042

CANDIDATE'S DECLARATION

I declare that I have carried out the research work presented in this thesis entitled **“Design of a Suitable Controller for Automatic Generation Control of Multi-Area Power System”** for the award of Doctor of Philosophy, submitted in the Department of Electrical Engineering, Delhi Technological University, New Delhi. I also declare that the thesis embodies the results of original work and studies carried out by me, and the contents of the thesis do not form the basis for the award of any other degree to me or anybody else from this or any other university or institution.

Ravi Choudhary
(2K18/Ph.D/EE/17)

Date:



DELHI TECHNOLOGICAL UNIVERSITY

(Formerly Delhi College of Engineering)
Shahbad Daultapur, Main Bawana Road, Delhi-110042

CERTIFICATE BY THE SUPERVISORS(s)

It is certified that **Ravi Choudhary (2K18/Ph.D/EE/17)** has carried out the research work presented in this thesis entitled “**Design of a Suitable Controller for Automatic Generation Control of Multi-Area Power System**” for the award of Doctor of Philosophy from Department of Electrical Engineering, Delhi Technological University, Delhi, under our supervision. The thesis embodies results of original work, and studies are carried out by the student himself and the contents of the thesis do not form the basis for the award of any other degree to the candidate or to anybody else from this or any other University/Institution.

Prof. J.N. Rai, Supervisor
Professor
Department of Electrical Engineering
Delhi Technological University,
Bawana road, Delhi-110042, India

Dr. Yogendra Arya,
Joint-Supervisor,
Associate Professor
Department of Electrical Engineering
J.C. Bose University of Science and
Technology, YMCA,
Faridabad-121006, India

The Ph.D. viva-voce of Mr. Ravi Choudhary, research scholar has been held on 25-09-2024.

ACKNOWLEDGEMENTS

Completion of this Ph.D. thesis was achievable with the support of several people. I would like to express my sincere gratitude to all of them. First of all, I am extremely grateful to my Supervisor Prof. J.N. Rai and Joint-Supervisor Dr. Yogendra Arya, for their priceless guidance, scholarly inputs, constant and unconditional support I received throughout the research work. This feat was possible only because of the unconditional support provided by my supervisors. I consider it as a big opportunity to do my Ph.D. under their guidance and to learn from their research erudition and knowledge. I thank my supervisors again for their assistance and support.

I owe my most sincere gratitude to Prof. Rachna Garg, Head, Department of Electrical Engineering, Delhi Technological University (DTU), Delhi, for her constant support throughout the duration of this work. Besides the moral support, she has provided all infrastructural facilities required for successful completion of this work.

I would also like to thank Prof. Mukhtiar Singh, Prof. Bharat Bhushan and other faculties in the Department of Electrical Engineering, DTU, Delhi, who have inspired and motivated me to carry out this ambitious work to its logical end.

I am at a loss of words to describe adequately the motivation, constructive criticism, invaluable suggestions and support I have received from Dr. Narender Kumar, Professor, Electrical Engineering Department, DTU, throughout my research work. He and his unconditional support were always with me during this research work. I would also like to thank Dr. Ajendra Singh (foreman) for his guidance and unconditional support during the research work.

I thank the college management, Director and HOD of Electronics Engineering Department, Dr. Archana Balyan of my institute for deputing me to pursue Ph.D. degree.

The completion of this work came at the expense of my long hours of absence from home. No words are adequate to express my indebtedness to my family for all the pains and suffering they have undergone to bring me up to this stage. I am extremely thankful to all my relatives too for their sincere good wishes.

(Ravi Choudhary)

ABSTRACT

The prime objective of automatic generation control (AGC) is to adjust the active power generation in response to variable power demands and hence AGC is required to maintain scheduled system frequency and scheduled tie-line power flows with neighboring control areas at desired tolerance values. A sizeable fall in frequency might badly affect the timing of electric clocks, magnetizing currents in transformers/induction motors, constant speed of AC motors, continuous operation of processes and synchronous operation of various units in power system. Additionally, power system may face a serious instability problem at substantial drop in the frequency. In steady state, automatically these variations must be zero. Enhanced power system stability is achieved with the proper design of supplementary controller adopted in an AGC system. However, continuous growth in size and complexity, stochastically changing power demands, system modeling errors, alterations in electric power system structures and variations in the system parameters over the time has turned AGC task into a challenging one. Consequently, conventional control strategies may be incompetent to handle such unpredictable variations in an AGC system. Hence, the researchers over the world are trying to propose several novel control strategies that fuse knowledge, techniques and methodologies from varied sources to tackle AGC problem of power system effectively. The literature survey indicates that several researchers tried to tackle AGC issue in traditional system. It presents various types of controllers optimized using various conventional and intelligent soft computing techniques. The literature survey also unveils that the performance of AGC system depends chiefly on the sort of intelligent technique exploited and structure of the controller. Hence, the goal of the present study is to propose different types of new supplementary controller structures for various types of traditional power systems.

The presented work is divided into ten chapters. Chapter 1 presents the introduction of AGC topic. Chapter 2 deals with a critical review of AGC schemes in power system. Chapter 3 stresses on the modeling of power systems under the study. The simulation work is presented in Chapter 4.

In Chapter 4, the AGC study is initially implemented on a single-area single-source thermal system. From the results attained in the study, it is authenticated that the single-area single-source non-reheat thermal system shows superior performances in comparison to the single-area single-source reheat thermal system. ALO and GNA tuned PI/PID controllers are employed in the thermal system and compared for the dynamic response. The values of overshoots, undershoots, settling times, and performance index, validated the dominance of GNA tuned controllers for single-area thermal system.

In Chapter 5, the study is conducted on two-area reheat/non-reheat thermal systems. GNA tuned PI/PID/2DOF-PID controllers are employed. The performance of GNA tuned controller is revealed significantly superior in terms of lesser numerical values compared to conventional controllers based on DE/TLBO/hSFS-PS optimization algorithms.

In Chapter 6, the study is conducted on single-area multi-source thermal-hydro-gas interconnected system and two-area multi-source thermal-hydro-gas interconnected system. In first attempt, a new fractional order proportional tilt integral derivative (FOPTID)+1 controller optimized using GNA is proposed for different electric power system. The results of FOPTID+1 controller are found to be superior compared to FOPID/PID controller optimized with GNA algorithm. Yet, FOPTID+1 controller has resulted superior performance compared to the published results with conventional controllers PI/PID. The performance of FOPTID+1 controller is revealed significantly superior in terms of lesser numerical values of settling times (STs), undershoots/overshoots and ITAE compared to conventional controllers based on DE/TLBO/hSFS-PS optimization algorithms.

Next, in Chapter 7, the study is conducted on single-area single-source nuclear system, single-area multi-source hydro-nuclear system, single-area multi-source hydro-nuclear-gas system. A new GNA optimized, FOPI-FOPTID controller is proposed for power system. It is observed that proposed controller shows superior results in terms of lesser values of STs/USs/OSs compared to GNA optimized FOPI-FOPID/FOPID/PID controllers. To show the effectiveness of the method, the

approach is further extended to two-area multi-source hydro-nuclear system and two-area multi-source hydro-nuclear-gas system. The proposed controller has revealed the superior performance in terms of lesser values of STs/ USs/OSs compared to GNA optimized FOPI-FOPID/FOPID/PID controllers.

Next, in Chapter 8, the study is conducted on single-area multi-source and two-area multi-source interconnected traditional thermal-hydro-gas power system without nonlinearities. A new WHO optimized, FOID-FOPTID controller is proposed for power system. It is observed that proposed controller shows superior results in terms of lesser values of STs/USs/OSs compared to WHO optimized FOTID/TID/PID controllers. Further, results are superior with the proposed controller compared to the recently published DE/TLBO/hSFS-PS optimized conventional controllers. To show the effectiveness of the method, the approach is further extended to two-area multi-source thermal-hydro-gas systems with nonlinearities. The analysis of the simulation results discloses the efficacy of WHO optimized FOID-FOPTID controller for power systems.

In the next step of the study in Chapter 9, an attempt is made to propose efficacy of energy storage systems (ESS), for traditional single-area multi-source thermal-hydro-gas system and two-area multi-source thermal-hydro-gas system. The critical analysis of the obtained results revealed the worth of ESS for the enhanced performance of dynamic responses in terms of less numerical value of STs/USs/OSs. It is also experienced that WHO optimized FOID-FOPTID controller is robust since it satisfies the AGC requirements when the system parameters are varied in regulated environment.

Finally, Chapter 10 presents an overview of the major contributions made out of, the research work presented in the thesis. The scope for future work in the area of AGC of power systems is also presented.

CONTENTS

Candidate's Declaration		ii
Certificate		iii
Acknowledgement		iv-v
Abstract		vi-viii
Contents		ix-xiii
List of Figures		xiv-xvi
List of Tables		xvii-xix
Nomenclature		xx-xxii
CHAPTER 1:	INTRODUCTION	1-10
1.1	General	1
1.2	Automatic generation control (AGC)	2
1.3	Control loops in AGC system	3
1.4	AGC implementation	5
1.5	Objectives of the thesis	7
1.6	Outline of the thesis	8
CHAPTER 2:	LITERATURE SURVEY	11-25
2.1	Introduction	11
2.2	AGC study based on traditional system with RES	13
2.3	AGC study based on deregulated environment	15
2.4	AGC study based on secondary controllers	16
2.4.1	AGC study based on classical secondary controllers	17
2.4.2	AGC study based on modern and intelligent secondary controllers	17
2.4.2.1	Intelligent secondary controllers	18
2.4.2.2	Degrees of freedom (DOF) secondary controllers	19
2.4.2.3	Advance secondary controllers	19
2.4.2.4	Other control techniques	20
2.5	AGC study based on HVDC transmission	20
2.6	AGC study based on FACTS devices	21
2.7	AGC study based on various optimization techniques	22
2.8	AGC study based on energy storage system	23
2.9	AGC study based on hybrid power system	24
2.10	Conclusion	25

CHAPTER 3:	DEVELOPMENT OF MATHEMATICAL MODELS FOR AGC OF POWER SYSTEMS	26-43
3.1	Introduction	26
3.2	Mathematical modeling of power system	28
3.2.1	Modeling of thermal power system	30
3.2.2	Modeling of hydro power system	32
3.2.3	Modeling of gas power system	34
3.2.4	Modeling of tie-line	35
3.3	Power system models under investigation	36
3.4	Conclusion	42
CHAPTER 4:	AGC OF SINGLE-AREA THERMAL POWER SYSTEM USING ALO AND GNA OPTIMIZED PID CONTROLLERS	44-62
4.1	Introduction	44
4.2	Antlion optimization algorithm (ALO)	44
4.2.1	Inspiration	45
4.2.2	Mathematical model of the behavior of antlions	45
4.2.3	Random walk of ants	47
4.2.4	Trapping in antlion's pits	47
4.2.5	Building trap	48
4.2.6	Sliding ants towards antlion	48
4.2.7	Hunting the prey and re-building the pit	50
4.2.8	Elitism	50
4.3	Global neighbourhood algorithm (GNA)	51
4.4	Systems investigated	53
4.5	PID controller	53
4.6	Optimization problem	54
4.7	Simulation results and discussion	55
4.7.1	Single-area thermal system with ALO tuned PI/PID controller	55
4.7.2	Single-area thermal system with GNA tuned PI/PID controller	58
4.8	Comparison of ALO and GNA	60
4.9	Conclusion	62
CHAPTER 5:	AGC OF MULTI-AREA THERMAL POWER SYSTEM USING GNA OPTIMIZED 2DOF-PID CONTROLLER	63-68

5.1	Introduction	63
5.2	Investigated system	63
5.3	Two degree-of-freedom PID (2DOF-PID) controller	64
5.4	Optimization problem	65
5.5	Simulation results and discussions	66
5.6	Conclusion	68
CHAPTER 6:	MULTI SOURCE MULTI-AREA POWER SYSTEM WITH OPTIMIZED FOPTID+1 CONTROLLER	69-83
6.1	Introduction	69
6.2	Systems investigated	70
6.3	FO proportional tilt integral derivative (FOPTID+1) controller	71
6.4	Optimization problem	73
6.5	Simulation results and discussions	75
6.5.1	Multi-area thermal-hydro-gas system with GNA tuned 2DOF-PID and FOPTID+1 controllers	75
6.5.2	Comparison with other controllers	78
6.5.3	Two-area thermal-hydro-gas system with GDB/GRC nonlinearities	80
6.6	Conclusion	83
CHAPTER 7:	GNA OPTIMIZED FOPI-FOPTID CONTROLLER	84-103
7.1	Introduction	84
7.2	System investigated	85
7.3	Cascade FOPI-FOPTID controller	85
7.4	Optimization problem	86
7.5	Simulation results and discussion	87
7.5.1	Single-area thermal-hydro-gas system	87
7.5.2	Single-area nuclear power system	89
7.5.3	Single-area hydro-nuclear system	91
7.5.4	Single-area hydro-nuclear-gas system	93
7.5.5	Two-area hydro-nuclear system	95
7.5.6	Two-area hydro-nuclear-gas system	97
7.5.7	Two-area hydro-nuclear-gas system with GDB/GRC/TD	101
7.6	Conclusion	102
CHAPTER 8:	WHO OPTIMIZED FOID-FOPTID CONTROLLER	104-125
8.1	Introduction	104

8.2	Wild horse optimization (WHO) algorithm	104
8.2.1	Generate initial population	105
8.2.2	Grazing behavior	106
8.2.3	Horse mating behavior	107
8.2.4	Group leadership	109
8.2.5	Selection and exchange of leaders	109
8.3	Systems investigated	109
8.4	Cascade fractional order integral derivative (FOID)- Fractional order proportional tilt integral derivative (FOPTID) controller	110
8.5	Optimization problem	111
8.6	Simulation results and discussion	112
8.6.1	Single-area non-reheat thermal system	112
8.6.2	Single-area reheat-thermal system	114
8.6.3	Single-area thermal-hydro-gas system	115
8.6.4	Two-area thermal-hydro-gas system	119
8.6.5	Two-area thermal-hydro-gas system with GDB/GRC	122
8.7	Conclusion	125
CHAPTER 9:	USE OF ENERGY STORAGE SYSTEMS	126-139
9.1	Introduction	126
9.2	Energy storage system (ESSs)	126
9.2.1	Capacitive energy storage (CES)	127
9.2.2	Superconducting magnetic energy storage (SMES)	128
9.2.3	Redox flow battery (RFB)	129
9.3	Systems investigated	130
9.4	Simulation results and discussions	130
9.4.1	Single-area thermal-hydro-gas system with ESS	130
9.4.2	Two-area thermal-hydro-gas system with ESS	132
9.4.3	Two-area thermal-hydro-gas system with GDB/GRC and ESS	138
9.4.4	Sensitivity analysis	138
9.5	Conclusion	139
CHAPTER 10:	CONCLUSIONS, FUTURE SCOPE, AND SOCIAL IMPACT	140-144
10.1	Overview of the work	140
10.2	Scope for the future research	143

REFERENCES	145-168
APPENDIX : SYSTEM DATA	169-172
BIODATA	173
LIST OF PUBLICATIONS	174

LIST OF FIGURES

Fig. No.	Caption	Page No.
Fig. 1.1	Control loops in AGC system	4
Fig. 3.1	Generalized model of multi area interconnected PS	29
Fig. 3.2	Transfer function model (TFM) of reheated steam turbine	32
Fig. 3.3	TFM of hydro turbine	34
Fig. 3.4	TFM of gas turbine	35
Fig. 3.5	TFM of tie-line	36
Fig. 3.6	TFM of single-area non-reheat thermal PS	36
Fig. 3.7	TFM of single-area reheat thermal PS	37
Fig. 3.8	TFM of single-area non-reheat with GRC thermal PS	37
Fig. 3.9	TFM single-area reheat with GRC thermal PS	37
Fig. 3.10	TFM of single-area THG PS	38
Fig. 3.11	TFM of single-area nuclear PS	38
Fig. 3.12	TFM of single-area hydro-nuclear PS	38
Fig. 3.13	TFM of two-area thermal PS	39
Fig. 3.14	TFM of two-area THG PS	39
Fig. 3.15	TFM of two-area THG PS with GRC/GDB	40
Fig. 3.16	TFM of two-area hydro-nuclear PS	41
Fig. 3.17	TFM of two-area HNG PS with GRC/GDB/TD	42
Fig. 4.1	(a) Geometrical shape of trap, (b) Cone shaped pit, (c) Random motion of ant, and (d) Antlion catching its prey	45
Fig. 4.2	Flowchart of ALO	49
Fig. 4.3	Flowchart of GNA	52
Fig. 4.4	Single area reheat thermal PS with GRC and PID controller	53
Fig. 4.5	Structure of PID controller	53
Fig. 4.6	Single-area thermal system response (ΔF) with ALO tuned controller: (a) Non-reheat, (b) Reheat, (c) Non-reheat with GRC, and (d) Reheat with GRC.	56
Fig. 4.7	Single-area thermal system response (ΔF) with GNA tuned controller: (a) Non-reheat, (b) Reheat, (c) Non-reheat with GRC, and (d) Reheat with GRC	59
Fig. 4.8	Single-area thermal system response (ΔF) with ALO and GNA tuned controller: (a) Non-reheat, (b) Reheat, (c) Non-reheat with GRC, and (d) Reheat with GRC	61
Fig. 5.1	Two-area non-reheat thermal system with 2DOF-PID controller	64
Fig. 5.2	Structure of 2DOF-PID controller	65
Fig. 5.3	Two-area thermal system response: (a) Convergence curves, (b) ΔF_1 , (c) ΔF_2 , and (d) ΔP_{tie12}	67
Fig. 6.1	Structure of FOPTID+1 controller	74

Fig. 6.2	Two-area THG system with FOPTID+1 controller	76
Fig. 6.3	Two-area THG responses: (a) ΔF_1 , (b) ΔF_2 , and (c) $\Delta P_{tie_{12}}$	77
Fig. 6.4	Two-area THG responses: (a) ΔF_1 , (b) ΔF_2 , and (c) $\Delta P_{tie_{12}}$	79
Fig. 6.5	Two-area THG PS with FOPTID+1 controller	81
Fig. 6.6	Multi-area THG responses with GDB/GRC: (a) ΔF_1 , (b) ΔF_2 , and (c) $\Delta P_{tie_{12}}$	82
Fig. 7.1	Cascade FOPI-FOPTID controller structure	86
Fig. 7.2	Single-area THG system	88
Fig. 7.3	Single-area THG system response (ΔF)	88
Fig. 7.4	Single-area nuclear system with GNA optimized FOPI-FOPTID controller	89
Fig. 7.5	Single-area nuclear system response: (a) Convergence curve and (b) ΔF	90
Fig. 7.6	Single-area hydro-nuclear system	91
Fig. 7.7	Single-area hydro-nuclear (HN) system frequency deviation response (ΔF)	92
Fig. 7.8	Single-area HNG system	93
Fig. 7.9	Single-area HNG system frequency deviation response (ΔF)	94
Fig. 7.10	Two-area HN PS with optimized FOPI-FOPTID controller	95
Fig. 7.11	Two-area HN system response: (a) ΔF_1 , (b) ΔF_2 , and (c) $\Delta P_{tie_{12}}$	97
Fig. 7.12	Two-area HNG system	98
Fig. 7.13	Two-area HNG system response: (a) ΔF_1 , (b) ΔF_2 , and (c) $\Delta P_{tie_{12}}$	99
Fig. 7.14	Two-area HNG system with GDB/GRC/Time-delay (TD)	100
Fig. 7.15	Two-area HNG system response with GDB/GRC/TD: (a) ΔF_1 , (b) ΔF_2 , and (c) $\Delta P_{tie_{12}}$	102
Fig. 8.1	Formation of groups from original population	105
Fig. 8.2	Departure of foals from a group, crossover and reproduction	107
Fig. 8.3	Flowchart WHO	108
Fig. 8.4	Structure of FOID-FOPTID controller	111
Fig. 8.5	Single-area non-reheat thermal system	112
Fig. 8.6	Single-area non-reheat thermal system response: (a) ΔF and (b) convergence curve	113
Fig. 8.7	Single-area reheat thermal system	114
Fig. 8.8	Single-area reheat thermal system response ΔF	114
Fig. 8.9	Single-area THG system	115
Fig. 8.10	Single-area THG system response ΔF	116
Fig. 8.11	Single-area THG system response with optimized FOID-FOPTID controller	117
Fig. 8.12	Two-area THG system	119
Fig. 8.13	Two-area THG system response without GDB/GRC (a) ΔF_1 , (b) ΔF_2 , and (c) $\Delta P_{tie_{12}}$	121
Fig. 8.14	Two-area THG system with GDB/GRC	122

Fig. 8.15	Two-area THG system response with GDB/GRC response (a) ΔF_1 , (b) ΔF_2 , and (c) $\Delta P_{tie_{12}}$	124
Fig. 9.1	Block CES linearized model	127
Fig. 9.2	SMES schematic diagram	127
Fig. 9.3	RFB schematic diagram	128
Fig. 9.4	Single-area THG system with ESSs	130
Fig. 9.5	Single-area THG system response (ΔF) with ESS	131
Fig. 9.6	Two-area THG system without ESS	133
Fig. 9.7	Two-area THG system response with ESS response (a) ΔF_1 , (b) ΔF_2 , and (c) $\Delta P_{tie_{12}}$	134
Fig. 9.8	Two-area THG system with GDB/GRC and ESS	135
Fig. 9.9	Two-area THG system response with GDB/GRC and ESS (a) ΔF_1 , (b) ΔF_2 , and (c) $\Delta P_{tie_{12}}$	136
Fig. 9.10	Sensitivity analysis for two-area THG system with GDB/GRC and ESS (a) ΔF_1 , (b) ΔF_2 , and (c) $\Delta P_{tie_{12}}$	137

LIST OF TABLES

Table No.	Caption	Page
Table 4.1	ALO optimized gain parameters of single-area thermal system for PI and PID controllers	55
Table 4.2	System results (ΔF) in terms of ST/OS/US/ITAE for single-area thermal system with ALO tuned PI and PID controller at $\Delta P_d = 0.01$ puMW	56
Table 4.3	GNA optimized gain parameters of single-area thermal system for PI and PID controller	58
Table 4.4	System results (ΔF) in terms of ST/OS/US/ITAE for single-area thermal system with GNA tuned PI and PID controller at $\Delta P_d = 0.01$ puMW	58
Table 4.5	System results (ΔF) in terms of ST/OS/US/ITAE for single-area thermal system (ΔF) with ALO and GNA tuned PI and PID controller at $\Delta P_d = 0.01$ puMW	60
Table 5.1	Tuned parameters of two-area non-reheat thermal system	66
Table 5.2	ST/OS/US/ITAE in two-area non-reheat thermal system at $\Delta P_{d1} = 0.01$ puMW with GNA optimized controllers	67
Table 6.1	Tuned parameters of two-area thermal system without GDB/GRC with GNA optimized controllers	76
Table 6.2	ST/OS/US/ITAE in two-area THG system at $\Delta P_{d1} = 0.01$ puMW with GNA optimized controllers	77
Table 6.3	Tuned parameters of two-area THG system with GNA optimized controllers	78
Table 6.4	ST/OS/US/ITAE in two-area THG system without GDB/GRC at $\Delta P_{d1} = 0.01$ puMW with GNA optimized FOPTID+1 controller.	79
Table 6.5	Tuned parameters of two-area THG system with GDB/GRC with GNA optimized FOPTID+1 controller	82
Table 6.6	ST/OS/US/ITAE in two-area THG system with GDB/GRC at $\Delta P_{d1} = 0.01$ puMW with GNA optimized FOPTID+1 controller.	83
Table 7.1	Tuned parameters of single-area THG system with GNA optimized controllers	88
Table 7.2	ST/OS/US/ITAE in single-area THG system at $\Delta P_{d1} = 0.01$ puMW	89
Table 7.3	Tuned parameters of single-area nuclear system with GNA optimized controllers	90

Table 7.4	ST/OS/US/ITAE in single-area nuclear system at $\Delta P_{d1} = 0.01$ puMW	90
Table 7.5	Tuned parameters of single-area hydro-nuclear system with GNA optimized controller	91
Table 7.6	ST/OS/US/ITAE in single-area hydro-nuclear system at $\Delta P_{d1} = 0.01$ puMW	92
Table 7.7	Tuned parameters of single-area HNG PS with GNA optimized FOPI-FOPTID controller	93
Table 7.8	ST/OS/US/ITAE in single-area HNG system at $\Delta P_{d1} = 0.01$ puMW	94
Table 7.9	Tuned parameters of two-area HNG system with GNA optimized controllers	96
Table 7.10	ST/OS/US/ITAE in two-area HN system at $\Delta P_{d1} = 0.01$ puMW with GNA optimized FOPI-FOPTID controller	97
Table 7.11	Tuned parameters of two-area HNG system with GNA optimized controllers	99
Table 7.12	ST/OS/US/ITAE in two-area HNG system at $\Delta P_{d1} = 0.01$ puMW	99
Table 8.1	Tuned parameters of single-area non-reheat thermal system with GNA and WHO optimized PID controller	113
Table 8.2	ST/OS/US/ITAE in single-area non-reheat thermal system at $\Delta P_{d1} = 0.01$ puMW	113
Table 8.3	Tuned parameters of single-area reheat thermal system without GRC with GNA and WHO optimized PID controller	114
Table 8.4	ST/OS/US/ITAE in single-area reheat thermal system at $\Delta P_{d1} = 0.01$ puMW	115
Table 8.5	Tuned parameters of single-area THG system with GNA and WHO optimized controllers	116
Table 8.6	ST/OS/US/ITAE in single-area THG system at $\Delta P_{d1} = 0.01$ puMW	116
Table 8.7	Tuned parameters of single-area THG system with WHO optimized controllers	117
Table 8.8	ST/OS/US/ITAE in single-area THG system at $\Delta P_{d1} = 0.01$ puMW	118
Table 8.9	Tuned parameters of two-area THG system with WHO optimized controllers	120
Table 8.10	ST/OS/US/ITAE in two-area THG system at $\Delta P_{d1} = 0.01$ puMW	121
Table 8.11	Tuned parameters of two-area THG system with GDB/GRC with WHO optimized controllers	123
Table 8.12	ST/OS/US/ITAE in two-area THG system with GDB/GRC at $\Delta P_{d1} = 0.01$ puMW	124
Table 9.1	Tuned parameters of single-area THG system with WHO optimized FOID-FOPTID controller and ESSs	131
Table 9.2	ST/OS/US/ITAE in single-area THG system at $\Delta P_{d1} = 0.01$ puMW	132
Table 9.3	Tuned parameters of two-area THG system with ESSs	133

Table 9.4	ST/OS/US/ITAE in two-area THG system with ESS at $\Delta P_{d1} = 0.01$ puMW	135
Table 9.5	Optimized parameters of two-area THG system with GDB/GRC and ESS	136
Table 9.6	ST/OS/US/ITAE in two-area THG system with GDB/GRC and ESS at $\Delta P_{d1} = 0.01$ puMW	137

NOMENCLATURE

Symbols	Name of the parameter/constant
F	: Frequency
U_{PS}	: Incremental change in power generation function
U_P	: Input signal to primary control loop
U_S	: Input signal to secondary control loop
U_{LS}	: Incremental change in load shading function
U_{TU}	: Incremental change in tripping unit function
β	: Area frequency response characteristic
R_t	: Thermal power generation regulation constant
R_h	: Hydro power generation regulation constant
R_g	: Gas power generation regulation constant
T_{SG}	: Steam turbine governor time constant
T_t	: Steam turbine time constant
K_r	: Coefficient of reheater steam turbine
T_r	: Steam turbine reheater time constant
T_{RH}	: Hydro turbine speed governor transient droop time constant
T_{GH}	: Hydro turbine speed governor main servo time constant
T_{RS}	: Hydro turbine speed governor reset time
T_W	: Nominal starting time of water in penstock
X	: Gas turbine speed governor lead time constant
Y	: Gas turbine speed governor lag time constant
a, b & c	: Gas turbine constant of valve positioner
T_{CR}	: Gas turbine combustion reaction time delay
T_F	: Gas turbine fuel time constant
T_{CD}	: Gas turbine compressor discharge volume time constant
P_{Gh}	: Output power of hydro turbine
P_{Gt}	: Output power of thermal turbine
P_{Gg}	: Output power of gas turbine
P_G	: Power output
P_g	: Total power output
$P_{12 \max}$: Maximum power flow from area-1 to area-2
P_C	: Control signal or speed changer setting
α_{12}	: Area size ratio
ACE	: Area control error
K_{PS}	: Gain constant of power system

T_{PS}	:	Time constant of power system
D	:	Load frequency constant
T_{12}	:	Tie-line synchronization power coefficient
H	:	Inertia constant
F_r	:	Rated frequency
P_r	:	Power rating of each control area
ΔF	:	Frequency deviation
$\Delta P_{tie_{12}}$:	Tie-line power deviation between area-1 and area-2
ΔP_{Gt}	:	Deviation in thermal turbine output
ΔP_{Rt}	:	Deviation in intermediate state of reheat turbine
ΔX_t	:	Deviation in steam turbine governor output
ΔP_{Gh}	:	Deviation in hydro turbine output
ΔX_h	:	Deviation in output of mechanical hydraulic governor of hydro turbine
ΔP_{RH}	:	Deviation in intermediate state of hydro turbine governor in
ΔP_{Gg}	:	Deviation in gas turbine output
ΔP_{FC}	:	Deviation in intermediate state of fuel system and combustor of gas turbine
ΔP_{VP}	:	Deviation in valve positioner of gas turbine
ΔP_G	:	Deviation in total power output
ΔP_d	:	Deviation in load disturbance
ΔP_L	:	Deviation in power demand
J	:	Performance Index
ACO	:	Ant colony optimization algorithm
ALO	:	Ant lion optimizer
AGC	:	Automatic generation control
CES	:	Capacitive energy storage
DE	:	Differential evolution
DOF	:	Degree of freedom
ESS	:	Energy storage system
GNA	:	Global neighborhood algorithm
GWO	:	Grey wolf optimization
GRC	:	Generation rate constraint
GDB	:	Governor dead-band
HNG	:	Hydro nuclear gas
h-SFS:PS	:	Hybrid stochastic fractal search pattern search
ITAE	:	Integral time absolute error

IPSO	:	Improved particle swarm optimization algorithm
PFA	:	Path finder algorithm
PS	:	Power system
K_G	:	Gas power generation contribution
K_H	:	Hydro power generation contribution
K_T	:	Thermal power generation contribution
K_N	:	Nuclear power generation contribution
PID	:	Proportional integral derivative
TID	:	Tilt integral derivative
FOID	:	Fractional order integral derivative
FOPID	:	Fractional order PID
FOTID	:	Fractional order TID
ST/OS/US	:	Settling time/overshoot/undershoot
R	:	Speed governor (SG) regulation parameter
RFB	:	Redox flow battery
SCA	:	Sine cosine algorithm
SMES	:	Superconducting magnetic energy storage
X	:	Gas turbine (GT) SG lead TC
TLBO	:	Teaching learning based optimization algorithm
T_{PS}	:	PS time constant
TFM	:	Transfer function model
THG	:	Thermal hydro gas
WHO	:	Wild horse optimization algorithm

CHAPTER 1

INTRODUCTION

1.1 General

Electricity is a basic commodity necessary for the people's overall development and welfare. One of the major objectives is to deliver good power quality and reliable electrical energy at a realistic price to the clients. It is a big challenge to control output power in large-scale power systems (PSs). For abnormal conditions, the tie-lines [1] provide inter-area assistance to interlinked areas and are availed for contractual energy exchange among multiple areas. A coherent group of generators represents control areas or regions of a complex PS. During the busiest times of the day, there is a greater demand for a constant power supply, the real and reactive power demands consistently diverge with the rising or falling drift. There is a steady variation in generating the real and reactive power for matching the load fluctuations. The inconsistency occurs after the system frequency deviation from its nominal value, concerning the generated power and the load demand. Consequently, It would be useless to use manual control to keep an accurate power balance. A practical method for efficiently controlling the power generated by electric generators is Automatic Generation Control, or AGC.

The demand for power is increasing as the number of customers grows. To fulfill this demand with uninterrupted power, commercial, and superior quality of power, modern PSs are developing from controlled settings to intricate PSs. In the contemporary electric PSs, the goal of engineering is to control operations using intelligent techniques. As a

result, advanced AGC controllers are needed to manage frequency deviations, tie-line power flows, and power outputs. This study introduces both conventional controllers and new controller structures optimized using antlion optimization algorithm, global neighborhood algorithm, and wild horse optimization techniques.

1.2 Automatic Generation Control (AGC)

To ensure efficient as well as stable electric power, maintaining the nominal voltage and frequency is essential, to minimize wear-tear on consumer equipment. Mismatches in active power between the generator and load can lead to frequency variations, while voltage deviations are mainly caused by reactive power imbalances. Reactive power is not transmitted on lines to reduce transmission losses, involves only capital costs, and is generated close to the demand. By monitoring the generation active power balance can be realized.

An imbalance in real power primarily affects system frequency for small load changes but keeps bus voltage levels constant, while an imbalance in reactive power primarily fluctuates bus voltage levels with persistent system frequency. Real power-frequency (p-f) is an independent control issue as well as reactive power-voltage (q-v) is an identical control problem [1-6]. The goal of AGC is to keep various bus voltages and currents functioning at frequencies that are relatively close to designated nominal values. Tie-line power flows connecting linked locations sustain the designated nominal values. The total power commitment of the entire system is optimally shared by isolated generators. The planning of a true AGC controller ensures the two leading functionalities mentioned above. The third function is the active power dispatch, alternate set of control.

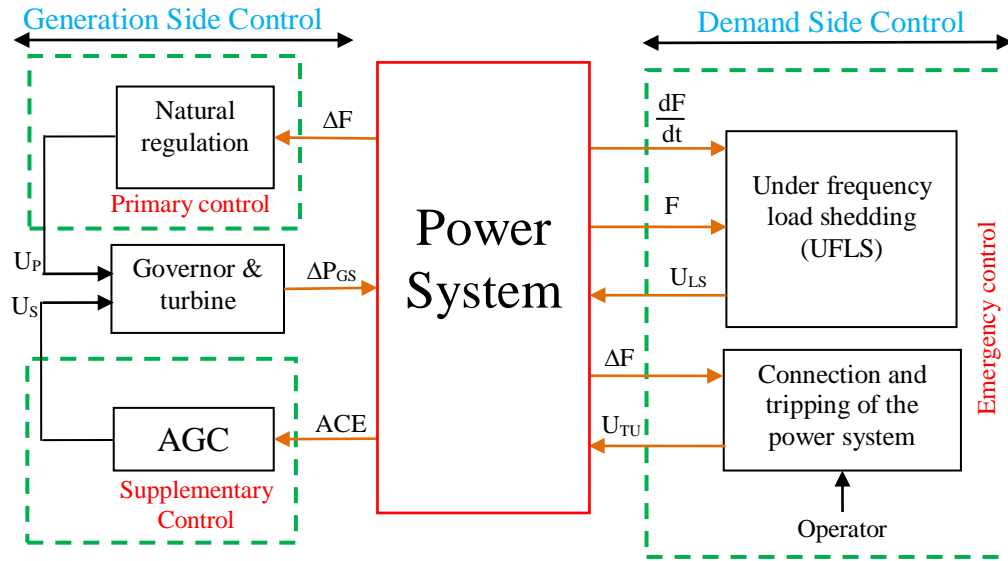


Fig. 1.1 Control loops in AGC system.

1.3 Control Loops in AGC System

In order to implement AGC in a PS, the primary and supplementary AGC loops perform several regulatory operations. Fig 1.1 illustrates the structure of the control loops. The primary AGC loop is responsible for generator speed control to regulate the real power generation. The supplementary AGC loop is essential for managing the frequency, units' real power generation, and net interchange. The speed governor in this loop receives a signal from a feedback system called the area control error (ACE). Frequency deviation (ΔF) is combined with tie-line power deviation (ΔP_{tie}) to form ACE. By use of ACE, this additional loop provides feedback, and the incremental change (U_S) incorporates it into the primary control loop through an appropriate controller. Generator determines the incremental change in power generation (ΔP_{GS}), by input data fed through the primary (U_P) or supplementary (U_S) control loops.

In the event of a major fault, the rapid frequency oscillations are associated with a significant demand-generation discrepancy. The controller's capacity in AGC is limited to

rectify frequency changes through the supplementary control loop. To mitigate the risk of cascading incidents that could disrupt power supply, strategies for protection such as underfrequency load shedding (UFLS) and emergency control situations are introduced. Should the supplementary controller fail to control undesirable changes in operating conditions, the UFLS and protection systems act as tertiary controls. The Under Frequency Load Shedding (UFLS) control system is designed to monitor signals such as frequency and its rate of change. Based on this data, a proper increment function (U_{LS}) for load shedding is created. In the meantime, the protection unit is in charge of generating an increment change (U_{TU}) that will cause the PS network to trip, helping to restore the PS to its standard operating state.

The operation and control of PSs involve a wide range of response times, which necessitates a hierarchical approach to implementing control functions. To address this issue, the problem is divided into smaller sub-problems using time decomposition methods [7]. The control of a PSs involves the following main groups classified by time perspective: Governor actions, which typically occur within a few seconds, are responsible for controlling the speed of generators and maintaining the stability of the PSs. AGC operates over several seconds and is responsible for adjusting the power output of generators to match the changing load and maintain system frequency. Economic dispatching, which occurs over a matter of minutes, involves optimizing the generation of power to meet demand at the lowest possible cost. Unit commitment, spanning hours, involves decisions about which generating units to start up, shut down, or run at varying output levels to meet anticipated demand while taking operating limits and fuel costs into

account. Additionally, it's worth noting that there are other functions with different response times.

For instance, maintenance scheduling follows a day-by-day schedule, involving planning for maintenance activities to ensure the reliability and availability of the PS. On the other hand, relay action is faster than governor action and is crucial for rapidly isolating faults and protecting the PS from harm.

The temporal dynamics of control functions within PSs exhibit hierarchical characteristics. Control operations at higher levels, notably unified control (UC), are orchestrated across interconnected PS tiers, while those at lower levels, At the level of individual power plants, policies including governor action, AGC, and economic dispatch control are implemented. Nevertheless, this does not universally hold true. For instance, it is conceivable for boiler control at the power plant level to manifest a slower response time compared to system-level AGC.

1.4 AGC Implementation

For implementing AGC schemes, the control actions are usually determined for each control area of a PS at dispatch center. PSs frequency, data concerned with tie-line flows, and unit MW loadings is telemetered to dispatch center, where the control actions are evaluated by a digital computer. The control signals are transmitted via the same telemetered channels to the generating units for necessary actions. The normal practice is to transmit raise or lower pulses of varying lengths of the units. However, the control equipment at the power plants changes the reference set-points of the units up or down in proportion to the pulse length.

The interconnected PS involves some control areas, which are controlled independently but in a similar manner. In this system, generation control is decentralized within each control area. Power transfer between control areas is facilitated by tie-lines. Not all generators within a control area participate in AGC; only a select few contribute to this function.

Earlier traditional schemes for controlling PSs like, proportional integral (PI)/PI derivative (PID) [9] were frequently employed in the AGC. However, recent studies have shown that fractional order (FO) controllers, such as FOPID [10], offer superior performance compared to traditional controllers. Additionally, controllers with two degrees of freedom, such as 2DOF-PID [11], have demonstrated improved dynamic responses over conventional controllers.

The energy storage system (ESS) may permit flexible generation and delivery of stable electricity for meeting demands of customers. ESS has fast response time, high storage efficiency, flexible and reliable, complete charge and discharge, strengths; high power capacity, stability, and quality, no moving parts, and no environmental hazard [12-14]. ESS has been used in the lately published research such as flywheel energy storage (FES), superconducting magnetic energy storage (SMES), ultra capacitor (UC), redox flow battery (RFB), capacitive energy storage (CES), etc. The ESS has opportunities and potentials like large storage capacity, unique application and transmission characteristics, innovating room temperature super conductors, further R & D improvement, reduced costs, and enhancing power capacities of present grids.

Multi-area thermal-hydro-gas (THG) and multi-area hydro-nuclear-gas (HNG) systems are examined, considering within several PS nonlinearities, including time delay

(TD), governor dead-band (GDB), and generation rate constraint (GRC). Despite being optimized for linear systems, the controller demonstrates robust performance including nonlinearities. But with these restrictions in place, the system's performance suffers greatly, particularly for PSs with GRC alone in contrast to linear PSs.

1.5 Objectives of the Thesis

Several articles have examined AGC and proposed various control strategies to enhance PSs' dynamic performance. The planning of AGC controllers has evolved over time, integrated classical, modern control, and intelligent techniques. However, there is still a need for further investigation into PSs to comprehensively address key issues.

Most studies on optimal AGC for interconnected PSs rely on single-source models. It's important to assess the efficacy of optimal control approaches in multi-source PSs. Additionally, existing studies in AGC heavily favor conventional PI/PID controllers. This calls for the application of new controller structures with optimization algorithms, to both single-area and multi-area PSs, including testing of suitable evolutionary algorithms. such as global antlion optimization (ALO), neighborhood algorithm (GNA), and wild horse optimization (WHO).

Given the above discussion, the reason behind this thesis and the primary objectives are described as follows:

1. To design PI, PID, 2DOF-PID, FOPID, 2DOF-FOPID etc. controllers for AGC of various PSs.

2. To find the optimal controller parameters by employing antlion optimization (ALO), global neighbourhood algorithm (GNA), and wild horse optimization (WHO) algorithms.
3. To compare the designed controllers and establish the superiority of suggested method over the existing controllers.
4. To assess the robustness of the recommended controller.
5. To assess the robustness of the suggested controller, it is necessary to investigate how system nonlinearities such as GRC, GDB, and TD affect the system's efficiency of single-area single-source, and multi-area multi-source PSs.
6. To investigate how energy storage systems (ESS) impact AGC.

1.6 Outline of the thesis

The thesis structure is divided into ten chapters. The breakup of summary is chapter-wise as follows:

Chapter 1: It provides a concise overview of operational and control aspects, with a focus on identifying primary, secondary, and emergency controls in PSs operating in interconnected environments. It also discusses Automatic Generation Control (AGC) and associated information.

Chapter 2: It begins with a brief description of AGC schemes in PSs and then offers a comprehensive review of recent literature on AGC for interconnected PSs. The chapter covers advanced control concepts such as 2DOF-PID, FOPID, FOTID, cascaded control, and AGC schemes incorporating intellectual optimization algorithms.

Chapter 3: It focuses on developing transfer function models of THG PSs comprising of speed governor systems, turbines, and linked components. It includes the design of linear and non-linear models, considering practical aspects. The chapter also discusses the development of dynamic models for single/multi-area interconnected PSs incorporating single and multiple sources.

Chapter 4: It stretches on the investigation of optimized PI/PID controllers for AGC in single-area thermal PSs, both with/without GRC. Utilizing Ant Lion Optimization (ALO) and Global Neighbourhood Algorithm (GNA) techniques, the optimized gains of AGC controllers are determined. The chapter discusses dynamic plots, overshoots, undershoots, and performance index values. A comparison between the two techniques is made to determine the best algorithm, and simulation results are obtained.

Chapter 5: It delves on the investigation of Global Neighbourhood Algorithm (GNA) optimized PI/PID/FOPTID controllers for multi-area thermal PSs AGC. Superiority of GNA tuned FOPTID controller is established over PI/PID controllers in this chapter.

Chapter 6: The GNA technique is employed to design a FOPTID+1 controller for multi-area interconnected THG PSs with or without governor dead-band (GDB) and GRC nonlinearities. Simulation results are then compared for the FOPTID+1 controller with other recently published controllers.

Chapter 7: It demonstrate the AGC studies on single-area single-source nuclear PS, single-area multi-source THG/HN/HNG, and multi-area multi-source hydro-nuclear/HNG PSs employing GNA optimized cascade FOPI-FOPTID supplementary controller. Non-linearities GDB/GRC/TD, are also deliberated. The dominance of FOPI-

FOPTID controller is demonstrated over GNA optimized PID/FOPID/FOPI-FOPID, and FOPTID+1 structured controllers.

Chapter 8: A WHO tuned cascade fractional order ID-fractional order PTID (FOID-FOPTID) supplementary controller is projected for investigations on single-area single/multi-source, and multi-area multi-source THG PS. Dynamic responses reflects that the proposed FOID-FOPTID controller outperforms WHO optimized PID/TID/FOTID/FOPID, GNA optimized FOPI-FOPTID/FOPTID+1 and many existing controllers.

Chapter 9: A desirable performance is achieved using energy storage systems (ESSs) with WHO optimized FOID-FOPTID controller. To confirm its robustness, the controller is additionally tested with a extensive range of system parameters. Variation of $\pm 25\%$ of the system parameters reveals the controller is efficient.

Chapter 10: The thesis demonstrates a review on synthesis of the significant findings derived from the research presented here. Additionally, it delineates the possibilities for future exploration and advancement in the field of AGC across diverse interconnected PSs.

CHAPTER 2

LITERATURE SURVEY

2.1 Introduction

Over the years' researchers have considered electrical energy as one of the main inputs. They have presented continuous growth and development in electric PSs all over the world. As the demand for electric power increases, parallel growths have been evident in the power industry structure to cope the situation with large size PSs. Researchers focus on the operation and control features of PSs as it needs to devise and develop more effective operation and control schemes. The utmost features of PSs discussed in Chapter 1 are the AGC of PS.

Initially mechanisms developed in the area of AGC are stated in [1–3]. The controlling system of bulk power transfer in conventional system was the first to proposed by Cohn et al. in [4–5] for interconnected PSs considering the frequency bias setting and utilizing the techniques for time error, tie-line bias control strategy and unplanned interchange rectification for large and multi-area PSs. Later in Quazza et al. [6], has proposed study on area control error; wide growth and extension of interconnected electric PSs, the related need to control generation in the essential areas, and the equitable, reliable power flow amongst them, economic system and area operation relating to the evolution of AGC. Elgerd and Fosha [7] have demonstrated and scrutinized the problem of optimal control scheme for AGC in the interconnected PSs.

From the past five decades there has been a constant work in literature to propose optimal AGC schemes in the beginning of modern control theory including benefits in PS

control, to overcome several limitations of classical approaches [8–9]. Various problems are faced for strategy and execution of control schemes for large and complex PSs. Fractional order [10] controllers have emerged to overcome the disadvantages of classical control schemes. To increase versatility, the controller design uses two degrees of freedom [11]. Addition of ESSs with advance controllers has demonstrated enrichment in the dynamic response of PSs. In various AGC studies, ESSs such as SMES, CES, UC, Battery Energy Storage, RFB, and others have been widely discussed in the literature [12–15]. In addition to advancements in control concepts, significant operational and structural changes have occurred over the past two decades. This review comprehensively examines these advancements in the following sections.

Modern intelligent techniques such as fuzzy logic control [16–17] approach have proven remarkable response. Over a period of more than five decades there has been an endless advancement in the power industry to design and implement some new AGC strategies [18]. The arrival of digital computers to manage huge interconnected structures of PS has further motivated power engineers to design and incorporate new control devices in AGC. Devices incorporating Gate Controlled Series Capacitor (GCSC)-High-Voltage Direct Current (HVDC) link [19], Flexible Alternating Current Transmission System (FACTS) [20] devices/structures such as Thyristor Control Phase Shifter (TCPS) [21], has been considered in many studies. Recently, the design and implementation of AGC structures employing intelligent techniques have been witnessed in the attainment undisturbed output power. These ideas helped the power engineers to handle the PS models effectively which are connected with non-linearities, crude models with insufficient information.

Over the past twenty years, intelligent techniques have been increasingly employed to address the complexities associated with AGC (Automatic Generation Control) in PSs. Meta-heuristic algorithms have gained popularity in optimizing controller parameters in recent years. A thorough literature review on this topic can be found in various national and international publications such as journals, conferences, seminars, books, and magazines etcetera in [22–25].

The following features of PS involved in AGC have been discussed in order to review the relevant literature.

- AGC study based on traditional system with RES
- AGC study based on deregulated environment
- AGC study based on secondary controllers
- AGC study based on HVDC transmission
- AGC study based on FACTS devices
- AGC study based on various optimization techniques
- AGC study based on energy storage system
- AGC study based on hybrid PS

2.2 AGC Study Based on Traditional System With RES

It is extremely important to have a fairly accurate mathematical model of PSs for better insight into the dynamics and optimization aspects of AGC problem. The mathematical model of control area includes the Generator, energy source (i.e. boiler and combustion system) dynamics, load, speed governor, turbine, and tie-line interconnected to other areas. The AGC scheme is predominantly based on linearized models developed over decades [2,4]. Early research focused on deviation in frequency and tie-line power,

pioneered by Cohn [4–5], however optimal control approaches were introduced by Elgerd and Fosha [7].

The study of AGC began with traditional PSs models [8–9] and the consideration of traditional PS configurations with conventional sources [1–18] such as hydro, thermal, hydro-thermal, thermal-hydro-gas (THG), and others. Some studies have expanded to incorporate wind power alongside conventional sources [19–21], with discussions on a THG-wind traditional PS created on full state feedback theory [21], employed an optimal AGC controller. Some studies on conventional sources are implemented with optimization algorithms [22–23]. Various strategies with different generating sources are prevalent in the literature [24–28]. Other sources like dish-stirling solar and geothermal [29–31]; diesel generator [32–38] are included in PSs with other sources. Integration of distributed generation (DG) in modern PSs is incorporated with thermal-gas (TG) system using electric vehicles (EVs), and energy storage system (ESS) [39]. Further, THG [40,41]; electric vehicle [42–44] are included to revolutionize the modern AGC system.

PSs are typically categorized into four sets according to their levels of increasing areas: single/dual/three-area, and four-area PSs, the majority of research work studies are provided on dual area in the AGC of interconnected PSs. Numerous AGC techniques [45] for single-area single/multi-source, two-area single/multi-source, three-area single/multi-source and with four-area single/multi-source PSs, are found in the literature [45–61].

The new investigations are carried out with hybrid energy systems, i.e., integrating the renewable energy sources (RES) [62–69]. Some other RES are PV-wind [70–75]; dish-stirling thermal solar (DSTS) [73,76,77]; solar-thermal PS [78, 79] are utilized to generate pollution free electric power. RES have reduced the electric power load demand

and impact on environment [80]. AGC performance has improved with RES system as suggested by Bevrani et al. in [81]. Development of realistic PS models using RES are further explored in [82–90].

2.3 AGC Study Based on Deregulated Environment

Previously, traditional control strategy was employed in dealing with AGC problem in PSs. The tie-line bias control scheme was implemented assuming that each area is operating in isolation so that the area control could be decided on the basis of the response characteristics of the area-decoupled to the other area. In [7], Fosha and Elgerd have presented a proportional plus integral controller expecting the load disturbances are known and deterministic while ignoring the compensation of load disturbances and steady state errors. The classic AGC PS, which consists of proper planning and operation, is modified to create the deregulated PS. In deregulated PS [88–89], the independent contract administrator receives approves the contracts between generation companies (GENCOs) and distribution companies (DISCOs) to supply area regulation. It is required due to unscheduled generation and load changes and inconsistent frequency bias existing in the system.

Every governor reacts instantly to a change in frequency brought about by variations in the load, irrespective of how they are selected for AGC. The governor response is defined as area regulation contracts, and the cost of area regulation is allocated among the players by the ratio of their participation. Besides addressing the operational structures likely to result in from deregulation, the possible approaches to AGC, and associated technical issues, i.e., standards and algorithms related to optimal and robust controller

were described by [90–95] and later, they reported an AGC scheme for hybrid electric power markets.

The AGC schemes in deregulated systems are investigated on solar-thermal, conventional thermal, wind, and EV is proposed in [96]. The approaches resulted in favorable effects in handling the increased strain of the system operator caused by the deregulated environment. In most of the literature reported so far, attempts have been made to adapt well-tested classical AGC schemes of deregulated PSs. A deregulated PS is comprised of three distinct entities, such as GENCOs, transmission companies (TRANSCOs), and DISCOs, however the bidding rules and protocols between GENCOs and DISCOs are provided by an independent system operator (ISO). The DISCOs and GENCOs belonging to the same/outside control area can interact each other [97–98]. For contract violation DISCOs may demand more than the fixed price this can be managed by GENCOs in that control area. Such an additional claim is termed as local load instead of contracted load. Various techniques are implemented for deregulated PSs as prevalent in literature [99–113]. The relation between DISCOs and GENCOs is represented by DISCO participation matrix (DPM), with elements pronounced as the contract participation factor (cpf).

2.4 AGC Study Based on Secondary Controllers

Initially the classical control theory [2] studies were applied on AGC of single-input and single-output (SISO) type PS models. Due to the limitations of regulator designs based on classical control theory, new ideas were invited to deal this limitation.

The classic control theory struggles to effectively manage the intricate PS structures inherent in multi-input and multi-output (MIMO) systems. Addressing these

complexities, modern control theory offers advanced strategies for optimal system control design. This includes the proposal of optimal AGC regulators depending on specific system performance criteria, made possible through the application of modern control theory.

2.4.1 AGC Study Based on Classical Secondary Controllers

The stability of a system is increased by minimizing the steady state error with classical controllers such as integer order (IO) includes integral (I) [114], I/proportional-integral (PI)/proportional integral derivative (PID) [115], however incorporating double-derivative with integral constitutes IDD/PID/PIDD [116] controllers. Later on filter coefficient was added in PID to enhance the system stability with employing controllers like 2DOF-PIDN-PDN [117], FOPI-IDDN [118] etc. These controllers have proved better performance over PID controllers. The stability criterion improved more with fractional order (FO) controllers by adding extra parameters λ and μ as integral and differential operators, respectively. FO controllers have shown remarkable performance over IO controllers such as FOPID [119]. Later on MPC-FOPIDN [120] was designed with a filter coefficient N adding to FOPID for enhancement of the system stability. New FO tilt ID (FOTID) controller was proposed in [121]. Also, enhanced responses are demonstrated with FOTID controller over PID/TID controllers in [122].

2.4.2 AGC Study Based on Modern and Intelligent Secondary Controllers

Advanced and dedicated operation for AGC control schemes has motivated the power engineers to simplify the increasing complexity of modern PS, coupled with the economic and good quality of electricity requirement. Some of elements of a PS are

extremely complex and of non-linear category. The utmost significant factor required to develop such scheme is the most accurate modeling of the system elements. The precise modeling of such elements is possible under numerous operating conditions; therefore, from investigation point of view, their approximated models are developed.

2.4.2.1 Intelligent Secondary Controllers

In recent years, advanced control methods like fuzzy logic control, neural networks, degree of freedom (DOF), and the limitations of traditional control methods have led to an increased use of cascade control approaches. These sophisticated approaches are aimed at effectively managing the implementation, synthesis, and analysis of AGC schemes in PSs. Fuzzy logic control (FLC) leverages system experience and information, along with a comprehensive knowledge base, to tackle uncertainty issues. FLC is particularly effective in addressing uncertainty problems and has been successfully applied in AGC systems, are discussed in [123]. Later, FLC is applied along with RES [124] and with ESS unit [125]. Novel fuzzy theory-based control approaches [126-128], including type-2 FLC, have been proposed to enhance frequency capability and reduce oscillation damping in PSs AGC, as detailed in [129–131]. Additionally, researchers have explored the use of artificial neural networks (ANN) [132] to optimize AGC systems, with considerations for biological nervous system concepts and data classification techniques in a standalone PS AGC network. An optimal ANN for AGC system is proposed in [133]. Furthermore, a non-linear recurrent ANN structure has been demonstrated to enhance performance when applied to interconnected PS studies, as documented in [134].

2.4.2.2 Degrees-of-Freedom (DOF) Secondary Controllers

The DOF controllers have two extra parameters for controlling the regulators with a reference and measured signals. Utilizing Degree of Freedom (DOF) analysis allows for better insight into system dynamics compared to traditional controllers. The 2DOF controller design is founded on the variance between reference and measured signals. By utilizing specified set points, the 2DOF controller calculates a weighted output variance, for each controller. Modified controller structures such as 2DOF-PID [135–139], 2DOF-TID [140] are prevalent in the literature for AGC studies. The 3DOF-PID [141, 142] controller was proposed for AGC study relating the perturbation abolition factor in a 2DOF controller. The superior dynamic response is revealed by 3DOF controller over 2DOF and other conventional controllers.

2.4.2.3 Advance Secondary Controllers

Cascade controller has two loops: outer loop and inner loop. It offers extra advantages over single control loop system for disturbance cancelation rapidly. The outer controller loop PI cascaded with inner controller loop PIDN to form cascaded (CPI-PIDN) controller for a conventional LFC system [143]. Cascade controllers such as TID-PI^λD^μN [144] and IDN-FOPD [145] are proposed for AGC studies. An optimal cascaded 2DOF(PI) and PDF i.e., CC-2DOF (PI)-PDF is projected as a new controller in [146]. Further, a cascaded 1+TD-FOTIDF is projected as an advance controller in [147] comprising of 1+TD and FO TID with a filter (FOTIDF). Various optimization techniques are employed in AGC to obtain systems responses with cascade control for superior dynamic responses compared to conventional/intelligent, and DOF controllers.

2.4.2.4 Other Control Techniques

The text discusses various advanced control techniques used in PSs, specifically focusing on model predictive control (MPC). MPC involves predicting the plant's subsequent response depending on its recent output, and it is effectively applied to AGC problems in PSs and microgrids for enhanced performances [148-152]. The damping of oscillations are enhanced, with a bat-inspired algorithm (BIA)[153] proposed for PSs using optimal control MPC technique. Furthermore, the integration of MPC with new AI techniques is proposed for AGC study with ESS [154].

On the other hand, sliding mode control (SMC) is employed for addressing uncertainties in power generation, characterized by discrete control signals. Full order SMC proves to be effective in solving AGC problems in PSs [155]. Double SMC is proposed for micro-grid system with RES in [156]. A time-delay dependent H-infinity based non-linear SMC is suggested in [157]. Further, improvement in the system dynamics are revealed in AGC schemes with advanced exponential SMC [158], adaptive control techniques [159], and centralized control scheme with vehicle to grid (V2G) smart technique [160]. A centralized control scheme with communication time delay is presented in [161]. Researchers carried out the modern intelligent controllers employing soft computing techniques [162–166] to increase AGC system stability as a whole.

2.5 AGC Study Based on HVDC Transmission

High Voltage Direct Current (HVDC) transmission appeared as a practical solution for transmitting large amounts of power over long distances due to its economic and technical advantages. Furthermore, integrating HVDC connections with existing AC lines resulting into additional profits relating PS stability. Analysis of a DC system's

dampening effects on linked AC systems has been the focus of determination. Virtual synchronous power strategies are developed for AGC study considering the HVDC links [167]. AGC works on HVDC links under conventional systems are proposed in [168–169]. Inertia emulation control (IEC) strategy in Voltage Source Converter based HVDC (VSC-HVDC) system is explored for PS [170]. A VSC-HVDC system is presented with improved vector control method [171]. Transportation of power to the offshore wind farm using VSC-HVDC was explored in [172]. IEC based HVDC link for deregulated system incorporating DG and a FO cascaded controller is proposed in [173]. A static synchronous series compensator (SSSC) incorporating CES based HVDC link for conventional AGC system with PID controller is suggested in [174]. Other various HVDC studies are explored in AGC systems [31,36,48,55,57,102,118,131,143,146, 175–176].

2.6 AGC Study Based on FACTS Devices

Power engineers are driven to simplify the modern PSs growing complexity due to advanced and focused operation for AGC control systems, as well as the need for affordable, high-quality electricity. The implementation of power electronic devices like Rectifiers, Inverters, Static Var Compensators (SVC), SSSC, and Thyristor-Controlled Phase Shifters (TCPS) etc etc, for PS control has gained widespread acceptance constituting Flexible AC Transmission Systems (FACTS). Enhanced versatility is offered by FACTS no matter how the PSs are operated and controlled.

Studies in [177–179] have indicated that with a variety of optimization strategies, the best location for FACTS devices to optimize power in interconnected PSs. Sahu et al. [180] conducted a study on AGC incorporating a TCSC with TIDF controller,

demonstrating improved AGC response. FACTS devices have been discussed in detail with new evolutionary algorithms for PSs in [181]. The FO controllers are employed to design an effective SSSC damping controller with optimization techniques in a deregulated PS [182]. Reactive power planning with SVC and TCSC techniques with optimized with whale optimizer algorithm (WOA) is presented to locate TCSC by determining the power flow analysis method and location of SVC via voltage collapse proximity indication (VCPI) method [183]. UPFC with SMES is proposed with optimized controller for AGC of hybrid deregulated environment [184]. Other studies on AGC with FACTS controllers is given in [20,22,32,50,53,145].

2.7 AGC Study Based on Various Optimization Techniques

Various traditional algorithms such as gradient/random search are known for their slow convergence. Evolutionary algorithms (EAs) are widely used for solving nonlinear and complicated optimization problems. First EA used for optimizing parameters was genetic algorithm (GA) portrayed in AGC studies [185–186]. On the other hand, heuristic/meta-heuristic algorithms, exhibit quicker convergence and require less iterations, leading to global optima solutions instead of local optima. Then various EAs like differential evolution (DE) [187], differential search algorithm (DSA) [188], hybrid bacterial foraging optimization algorithm (BFOA)-particle swarm optimization (PSO) [189], grey wolf optimization (GWO) [190], etc algorithms are carried out in the PSs' AGC. Later on, numerous EAs are employed for optimization of controller parameters determined with meta-heuristic algorithms due to complexity, faster convergence. Some heuristic approaches were carried out like gases brownian motion optimization (GBMO) [191], opposition-based harmonic search (OHS) [192], multi-verse optimization (MVO) [193],

BFOA [194–195], grasshopper optimization algorithm (GOA) [196], sine-cosine algorithm (SCA) [197], whale optimization algorithm (WOA) [198], ant colony optimization (ACO) [199] etc.

Next, an interconnected PS is investigated [200–201] by biogeography-based optimization (BBO) algorithm to enhance the PS performance impressively. Cuckoo search (CS) algorithm in three-area interconnected PS is investigated [202]. Imperialist competitive algorithm (ICA) [203–204] is employed in single/multi-area PS. Spotted hyena optimizer (SHO) with a two stage controller in cascade is employed in [205]. A novel hybrid local unimodal sampling (hLUS) and TLBO algorithm is employed for tuning fuzzy/conventional PID controllers [206]. BAT algorithm optimized PI controller is suggested for reducing fluctuations in a multi-area PS [207]. Various optimization algorithms are proposed in the AGC studies in [208–214]. Wild horse optimizer (WHO) is proposed as new meta-heuristic algorithm for solving complex problems [215]. WHO assisted cascaded controller is employed in multi-area IPS with nonlinearities has demonstrated enhanced performance [216].

2.8 AGC Study Based on Energy Storage System

The addition of an ESS enhances PS stability as well as performance by providing additional storage capacity and helping manage sudden load changes. Initial studies on ESS-AGC with lead-acid batteries have shown promising results. The high energy density and fast response time of battery energy systems (BES) demonstrate their effectiveness in AGC systems [217–219] by swiftly supplying bulk power. Fly wheel energy storage (FES) because of its long life, minimal maintenance requirements, high power density, high round-trip efficiency, and lack of depth of discharge effects is found

beneficial for the frequency regulation of PS [220]. The flexibility of conventional thermal PS is enhanced with FES [221]. Unification of hydrogen aqua electrolyzer (HAE) to RFB is proposed for restructured hybrid PS [222]. HAE-fuel cell combination is proposed for IPS [223]. The fast response time and high efficiency caused the use of SMES for frequency regulation in [224–226]. Next, UC with RFB is employed in PS with RES [227,228]. The use of UC offers high efficiency, extended lifespan, and substantial power capacity. In the context of AGC studies, CES is recommended since it exhibit rapid response to power variations, minimal energy losses, and low maintenance requirements [229–231]. RFB has demonstrated better performance with disturbance rejection and quick storing action in the dual area IPS with RES [232]. A new intelligent fuzzy based controller is employed with RFB in [233]. Next, RFB is proposed in five-area IPS with RES integration stabilizes the frequency [234]. Other applications of ESS in AGC of PS are given in [13,14,16,20,30,32,34,36,37,39,58,64,71–73,90,97,110,131, 143,145,154,174,186,192, 205].

2.9 AGC Study Based on Hybrid Power System

Recently, various research works are implemented on AGC with hybrid PS (HPS) having sources of energy in one control area. A Gaussian-interval type-2 fuzzy PID (GIT2-FPID) is suggested as advance controller for HPSs in [235]. A coordinated frequency control between doubly fed induction generators (DFIGs)-Variable Speed Wind Turbines (VSWT) and BESS hybrid systems is presented in [236]. The split shaft gas turbine plants interconnected with thermal PS, solar photovoltaic-EV is presented in [237]. A four-area thermal-wind PS is studied in [238]. A cascaded PI-PD controller based two-area system connected with thermal-hydro-wind-PV incorporating EVs is suggested in

[239]. A proportional-derivative (PD) proportional-integral (PDn-PI) with filter cascaded controller tuned with innovative coyote optimization algorithm (COA) interconnected with RESs was employed in multi-area PSs [240]. An optimized TID controller employed for a multi-area PS with the application of a PV-thermal environment HPS is proposed [241]. A tuned TDF-TIDF controller is employed in an isolated hybrid micro-grid system [242]. An optimized PID controller is used in a modern PS with RESs and ESS [243]. A robust control approach with optimal fuel cells is utilized for the frequency stability of a diverse-sources PS including renewable source [245]. A novel cascade FOID and tilt controller is employed in interconnected hybrid PS with RESs and EV [246]. A modified TID-MPC controller works well in a hybrid PS with virtual inertia [247]. Various research papers have been published on HPSs for AGC based on new algorithms and optimization techniques in [248–258].

2.10 Conclusion

In this chapter, we have provided a thorough and evaluative overview of the existing literature on Automatic Generation Control (AGC). We have delved into recent advancements, particularly AGC methodologies utilizing artificial intelligence principles such as neural networks. Our analysis identifies multiple AGC approaches documented in the literature and examines their notable characteristics.

CHAPTER 3

DEVELOPMENT OF MATHEMATICAL MODELS FOR AGC OF POWER SYSTEMS

3.1 Introduction

Massive numbers of generators connected by transmission line networks make up the electric PSs, which provides users with power at rated voltage and frequency. The upkeep of these parameters at the rated values is necessary for having high efficiency and minimum loss of the consumer machines. The power supply reliability and standard are determined by the voltage and frequency of a PS. Thus, PSs voltage and frequency are primary characteristics that need to be managed. Frequency deviations in a PS are caused by a real power difference across the generation and the load, whereas voltage fluctuations are the result of a difference in reactive power inside the system. In order to generate the required reactive power, only capital costs are required; fuel is not dispersed over the lines to prevent significant transmission losses. In a PS, generation control can be used to accomplish automatic AGC. As a result, it is believed that the voltage and frequency control loops are disconnected [1,2].

One of the major objective of an interconnected PS is to generate large-scale power to accomplish economic benefits at distant locations from the main load centers. In addition, interconnectivity reduces the reserve capacity of the individual generating stations and also increases consistency of the overall system through backup during emergencies. If a frequency deviation occurs in case of any disturbance in the system a coherent group of the generators in the system start swinging in unison with equal.

Control area is formed by a group of generators regardless of the energy source or utility. Therefore, it is expected on the presence of well-defined control area that typically relates to the geographical and electrical limitations of one or more standards.

An interconnected power system's primary goal is to produce significant amounts of power in order to achieve financial gains at areas that are far from the main load centers. In addition, interconnectivity reduces the reserve capacity of the individual generating stations and also increases consistency of the overall system through backup during emergencies. If a frequency deviation occurs in case of any disturbance in the system a coherent group of the generators in the system start swinging in unison with equal. Control area is formed by a group of generators regardless of the energy source or utility. Therefore, it is expected on the presence of well-defined control area that typically relates to the geographical and electrical limitations of one or more standards.

In addition to their own generations and to eliminate mismatch between generation and demand, there are tie-lines connecting these control zones, for providing contractual exchange of power under normal operating conditions. Therefore, maintaining frequency and power exchanges within the zones at their prescribed levels is a PS's primary control need. Variation in frequency/tie-line power cause sudden fluctuations in the side of load in control area. Frequency and tie-line power deviation combines to result in area control error (ACE), and processed in order to limit the fluctuations to zero level. Based on ACE signal the load frequency regulators are designed which are responsible to increase or decrease the generation by manipulation of speed changer of various generating units following to the action by speed governors.

The most often used natural energy sources in power plants include coal, oil, and natural gas. Other generating natural sources are nuclear energy, and falling water. Since fossil fuels are depleting day by day, therefore, a wide and growing variety of unconventional generation technologies and fuels have also been developed, including cogeneration, solar energy, wind generators, and waste materials. Therefore, the control zones in the current situation are expected to feature a variety of energy sources.

This chapter develops mathematical models of interconnected PSs that are single-area and multi-area, comprising power plants of different characteristics for power generation like, hydro, thermal, gas and nuclear turbines. The dynamic model of the system is established relating every part of the power plant.

3.2 Mathematical Modeling of Power System

Fig. 3.1. displays the generalized structure of two-area interconnected PS diverse/hybrid energy sources. In this model, interconnection of several control areas are demonstrated through a tie-line. P_{ri} and P_{rj} MW represents the power rating of i^{th} and j^{th} control area respectively.

Suppose for i^{th} control area K_{hi} , K_{ti} , and K_{gi} are sharing factors of hydro, thermal and gas power plant respectively for total power generation of i^{th} control area. Suppose P_{Ghi} , P_{Gti} , P_{Ggi} are power generation in MW by hydro, thermal and gas power plants in the i^{th} control area, respectively.

There is no difference between generation and load under typical operating conditions. THG power generations from power plants are given by Eqns. (3.1)-(3.3) [2]:

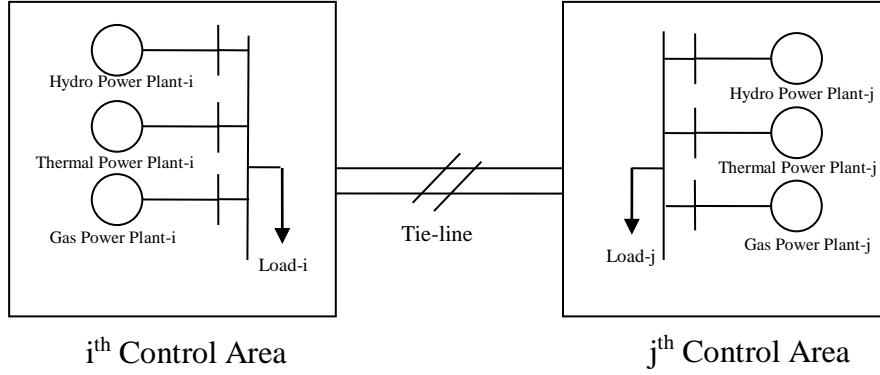


Fig. 3.1 Generalized model of multi-area interconnected PS.

$$P_{Ghi} = K_{hi} P_{Gi} \quad (3.1)$$

$$P_{Gti} = K_{ti} P_{Gi} \quad (3.2)$$

$$P_{Ggi} = K_{gi} P_{Gi} \quad (3.3)$$

Under nominal generation loading, the total power generated, P_{Gi} of i^{th} area is given by Eqns. (3.4-3.5).

$$P_{Gi} = P_{Ghi} + P_{Gti} + P_{Ggi} \quad (3.4)$$

$$P_{Gi} = K_{hi} P_{Gi} + K_{ti} P_{Gi} + K_{gi} P_{Gi} \quad (3.5)$$

$$K_{ti} + K_{hi} + K_{gi} = 1 \quad (3.6)$$

For i^{th} control area, the deviation in power generation (ΔP_{Gi}) with small load perturbation can be framed using Eqn. (3.7);

$$\Delta P_{Gi} = \Delta P_{Ghi} + \Delta P_{Gti} + \Delta P_{Ggi} \quad (3.7)$$

Similarly, for j^{th} area, ΔP_{Gj} is given by Eqn. (3.8);

$$\Delta P_{Gj} = \Delta P_{Ghj} + \Delta P_{Gtj} + \Delta P_{Ggj} \quad (3.8)$$

The load frequency characteristic (D_i), PS gain constant (K_{Pi}), PS time constant (T_{Pi}), and bias constant (β_i) are specified by Eqns. (3.9-3.12) [2].

$$D_i = \frac{\partial P_{Li}}{\partial f_i} \frac{1}{P_{ri}} \quad (3.9)$$

$$K_{PSi} = \frac{1}{D_i} \quad (3.10)$$

$$T_{PSi} = \frac{2H_i}{F_r D_i} \quad (3.11)$$

$$\beta_i = D_i + \frac{1}{R_i} \quad (3.12)$$

Similarly, these parameters for j^{th} area can be defined by Eqns. (3.13-3.16).

$$D_j = \frac{\partial P_{Lj}}{\partial f_j} \frac{1}{P_{rj}} \quad (3.13)$$

$$K_{PSj} = \frac{1}{D_j} \quad (3.14)$$

$$T_{PSj} = \frac{2H_j}{F_r D_j} \quad (3.15)$$

$$\beta_j = D_j + \frac{1}{R_j} \quad (3.16)$$

Synchronous generators in a PS are often powered by prime movers including hydro, thermal, and gas, among others. Every turbine has a speed controlling system installed in order to enable the turn on turbine, functioning at the proper speed, and operate on load in order to provide the necessary amount of power output.

3.2.1 Modeling of Thermal Power System

High-pressure and temperature steam is generated and stored in the boiler by fuel energy, used in coal-burning, oil-burning, and nuclear power plants. In axial flow steam turbines, the energy contained in the steam is subsequently converted into mechanical energy. Each turbine is made up of a collection of stationary, rotating blades arranged in groups/stages. The steam at high-pressure expands to a lower pressure as it passes through the set

of fixed, stationary blades, it gains kinetic energy and accelerates. Following this, when the fluid stream passes through the spinning blades, its momentum and direction change, applying a torque to the turbine shaft and a tangential force to the turbine blade. The pressure of the steam decreases as it moves axially up the turbine shaft, increasing its volume. To account for this shift, the blades' dimension grows from beginning of steam inlet to exhaust. Whole steam turbine is usually separated into three or more stages, each of which is coupled to the others through a shared shaft. splitting the turbine into several stages to preheat the steam in between to boost its enthalpy and, in turn, the steam cycle's total efficiency.

There are three types of steam turbines: non-reheat, single-reheat, and double-reheat systems. Typically designed for usage in units less than 100 MW, non-reheat turbines contain one turbine stage. The single tandem-reheat layout is the most widely utilized turbine configuration for big steam turbines. The controlling system regulates the steam flow in the turbine. The emergency stop valves remain completely open when the generator is matched and the turbine speed and power are adjusted by modifying the position of the valve. The speed measurement gadget provides the governor with a speed signal. An oil servomotor that is managed by the pilot valve serves as both the valve mover and the primary amplifier of the regulating system. The emergency stop valves, which are frequently employed to regulate the turbine's initial start-up, are only utilized to stop the generator in an emergency when the generator is synchronized. For small load perturbation, representation of governing system of steam turbine is given by Eqns. (3.17) [2].

$$\Delta X_{ti}(s) = \left(\frac{1}{1+sT_{gi}} \right) \left(\Delta P_{Ci}(s) - \frac{\Delta F_i(s)}{R_{ti}} \right) \quad (3.17)$$

The steam turbine's output power variation in reaction to a change in the governor setting is shown by:

$$\Delta P_{Gti}(s) = \left(\frac{1}{1+sT_{ti}} \right) \left(\frac{1+sK_{ri}T_{ri}}{1+sT_{ri}} \right) \Delta X_{ti}(s) \quad (3.18)$$

The combination of Eqns. (3.17) & (3.18) results in the block diagram of reheated steam turbine shown in Fig. 3.2.

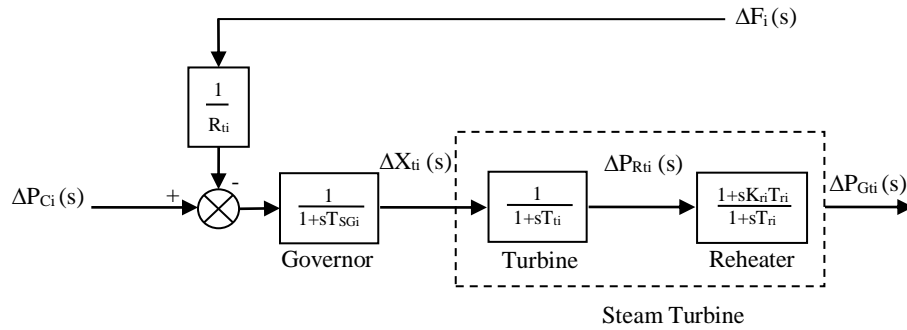


Fig. 3.2 Transfer function model (TFM) of reheated steam turbine.

3.2.2 Modeling of Hydro Power System

Water energy is one of the earliest methods employed for producing electricity. Hydraulic turbines are driven by the force of falling water. Level of the turbine is separated from the upper reservoir by the vertical distance denoted as head. Although there is no clear isolation line, hydroelectric power amenities are classified as high/medium/low-head (run-of-river) plants depending on the size of their heads.

Francis turbines and other reaction turbines are used in the construction of low- and medium-head hydroelectric plants. Turbines usually utilize a lot of water, need wide water passageways, and run slowly due to the relatively low pressure head reaction.

Large diameter generators are the result of low rotating speed. When the turbine is operating, water enters through the spiral case from the intake tunnel or penstock, travels through the movable wicket gates and stay ring, and then exits onto the runner. The water enters the tail-water reservoir through the draft tube after exiting the runner. The movable wicket gates regulate the turbine's power output with their axes parallel to the main shaft. Francis turbine runners feature blades with lower ends fastened to a band and top ends fastened to a crown. The runner has no band or crown for low-head operation, exposing the blades. There are two types of blades: fixed and adjustable. The governor can alter the wicket gate opening and blade angle for runners with changeable blades (Kaplan-type turbine). A piston inside the main shaft that runs on oil is used to modify the blades.

In hydroelectric power plants with high head, Pelton wheel impulse turbines are utilized. A series of fixed nozzles in these turbines transforms the HP water into high-velocity jets of water. The high-velocity water jets strike a series of bowl-shaped buckets that are affixed around the runner's perimeter. These buckets reverse the water's flow, so affecting the entire impact of the water jet on the runner. A needle at the nozzle's center regulates the jet's size, which in turn affects the turbine's power output. The governor is in charge of the needle's movement. In the case of a sudden fall in load, a jet deflector situated just outside the nozzle tip will deflect the jet away from the buckets. For small load perturbation, the change in valve position (ΔX_{hi}) is given by Eqn. (3.19) [2].

$$\Delta X_{hi}(s) = \left(\frac{1}{1+sT_{RHi}} \right) \left(\frac{1+sT_{Ri}}{1+sT_{GHi}} \right) \left(\Delta P_{Ci}(s) - \frac{\Delta F_i(s)}{R_{hi}} \right) \quad (3.19)$$

Due to change in setting of governor, the corresponding change in output power from hydro turbine is represented by Eqn. (3.20).

$$\Delta P_{Ghi}(s) = \left(\frac{1-sT_{Wi}}{1+0.5sT_{Wi}} \right) \Delta X_{hi}(s) \quad (3.20)$$

The Eqns. (3.19) and (3.20) can be represented by Fig. 3.3.

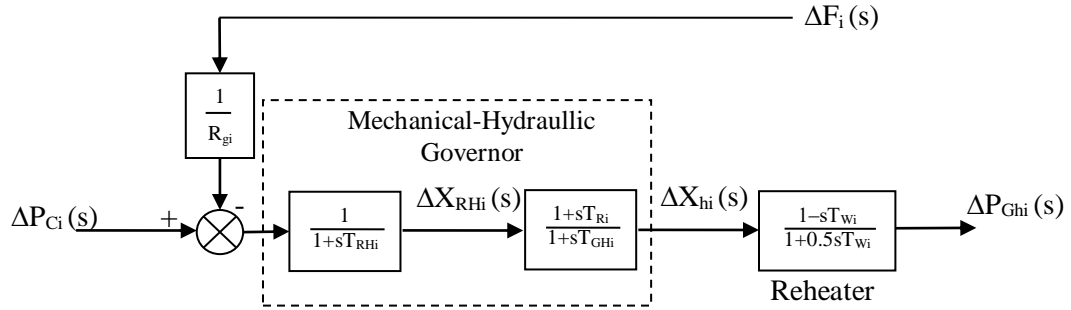


Fig. 3.3 TFM of hydro turbine.

3.2.3 Modeling of Gas Power System

Gas turbines convert fuel's thermal energy into mechanical energy by means of the turbine's hot exhaust gases, negating the need for an intermediary working fluid. The fuel is either natural gas or fuel oil (heavy/medium) whereas working fluid is usually air. The most frequently used type of gas turbine system parts are turbine, compressor and combustion chamber. Air provided by the compressor helps in fuel ignition inside the combustion chamber, whereas fuel has to be transferred by the governor valve. Following the feeding of the hot, compressed air and combustion products into the turbine, the air expands and powers the rotating blades similarly to a steam turbine. After that, the compressor's air is heated using the exhaust gasses. In addition, there exist more intricate cycles that employ compressor cooling in addition with reheating. For small load perturbation, the change in setting of gas turbine governor (ΔX_{gi}), valve positioner (ΔP_{VPi}), fuel & combustor system (ΔP_{FCi}) and gas turbine (ΔP_{Ggi}) are given by following mathematical relations [2];

$$\Delta X_{gi}(s) = \left(\frac{1+sX_i}{1+sY_i} \right) \left(\Delta P_{Ci}(s) - \frac{\Delta F_i(s)}{R_{gi}} \right) \quad (3.21)$$

$$\Delta P_{VPi}(s) = \left(\frac{a_i}{c_i + sb_i} \right) \Delta X_{gi}(s) \quad (3.22)$$

$$\Delta P_{FCi}(s) = \left(\frac{1-sT_{CRi}}{1+sT_{Fi}} \right) \Delta P_{VPi}(s) \quad (3.23)$$

Combining Eqns. (3.21)-(3.23), the overall gas turbine model equation is expressed, with block diagram displayed in Fig. 3.4.

3.2.4 Modeling of Tie-line

The synchronization coefficient (T_{ij}) for a tie-line connecting two PSs control areas is described by Eqn (3.24) [2]:

$$T_{ij} = P_{ij\max} \cos(\delta_i - \delta_j) \quad (3.24)$$

Eqn. (3.25) describes the deviation in tie-line flow ($\Delta P_{tie_{ij}}$) for a modest load fluctuation:

$$\Delta P_{tie_{ij}}(s) = \frac{2\pi T_{ij}}{s} [\Delta F_i(s) - \Delta F_j(s)] \quad (3.25)$$

The block diagram can be designed by the Eqn. (3.25) is displayed in Fig. 3.5.

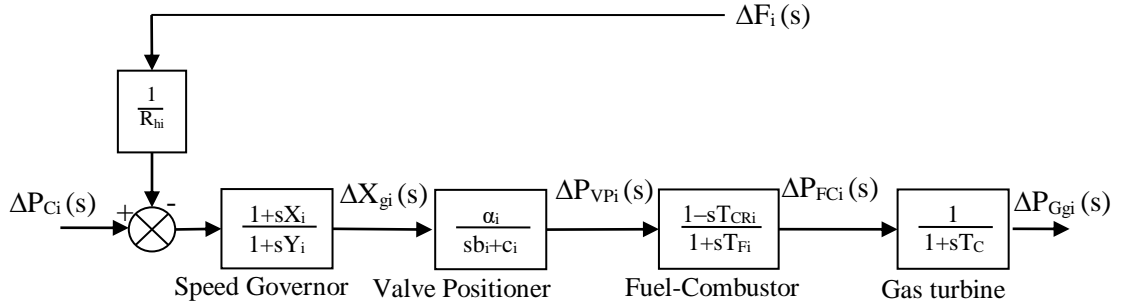


Fig. 3.4 TFM of gas turbine.

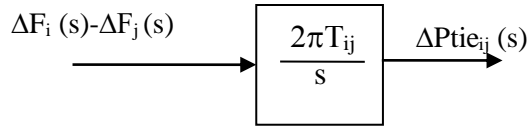


Fig. 3.5 TFM of tie-line.

3.3 Power System Models Under Investigation

The PSs under investigation are modeled in a generalized manner using the Eqns. (3.1-3.25). In this study, various conventional PS models are thoroughly examined. Figs. (3.6-3.9) depict a single-area PS with one non-reheat/reheat PS without/with GRC in each area. Nevertheless, Fig. 3.10 depicts a single-area THG PS. Figs. 3.11 and 3.12 show single-area nuclear and hydro-nuclear (HN) PS respectively. A two-area (multi-area) thermal PS is displayed by Fig. 3.13. THG PS (Two-area multi-source) is displayed by Figs. 3.14 and 3.15 respectively. Two-area HN and HNG system are shown in Figs. 3.16 and 3.17. The ACE is expressed by Eqns. (3.26-3.37) as:

$$ACE_1(s) = \beta_1 \Delta F_1(s) + \Delta P_{tie_{12}}(s), \quad (3.26)$$

$$ACE_2(s) = \beta_2 \Delta F_2(s) + \alpha_{12} \Delta P_{tie_{12}}(s). \quad (3.27)$$

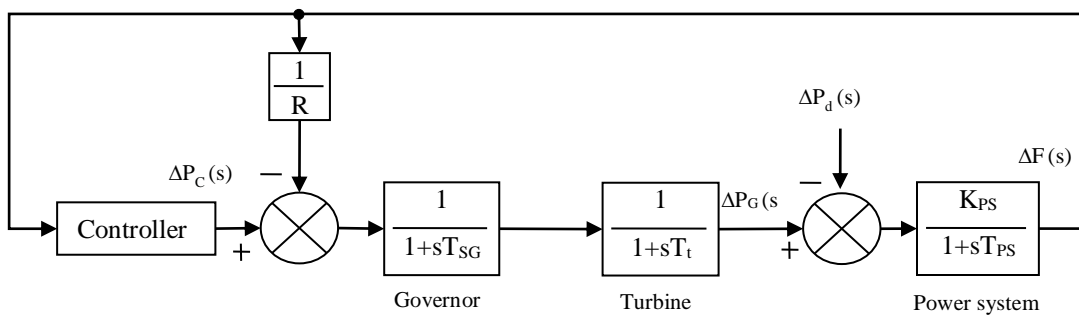


Fig. 3.6 TFM of single-area non-reheat thermal PS.

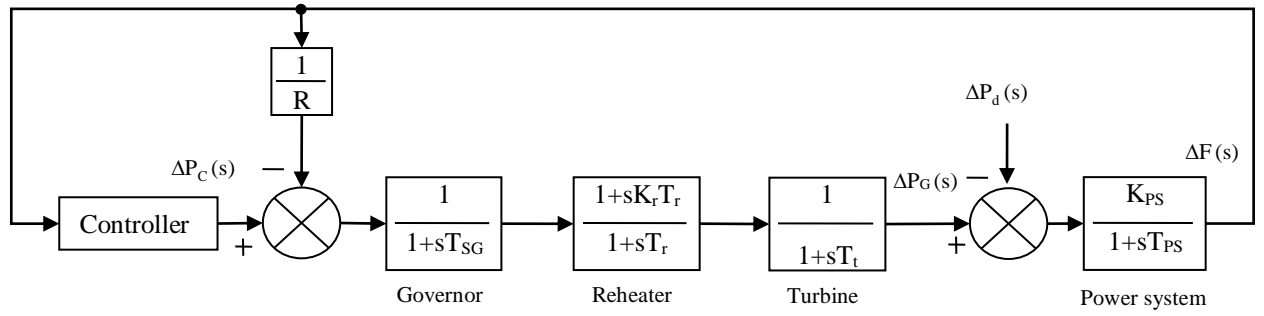


Fig. 3.7 TFM of single-area reheat thermal PS.

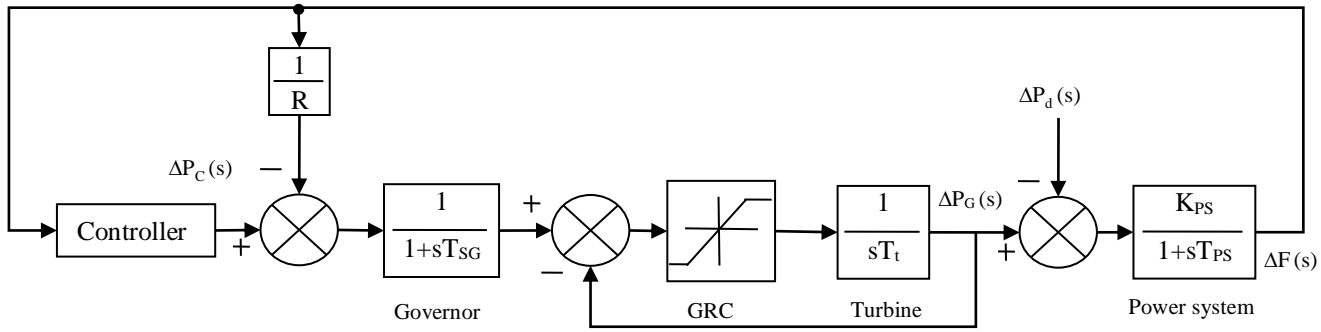


Fig. 3.8 TFM of single-area non-reheat with GRC thermal PS.

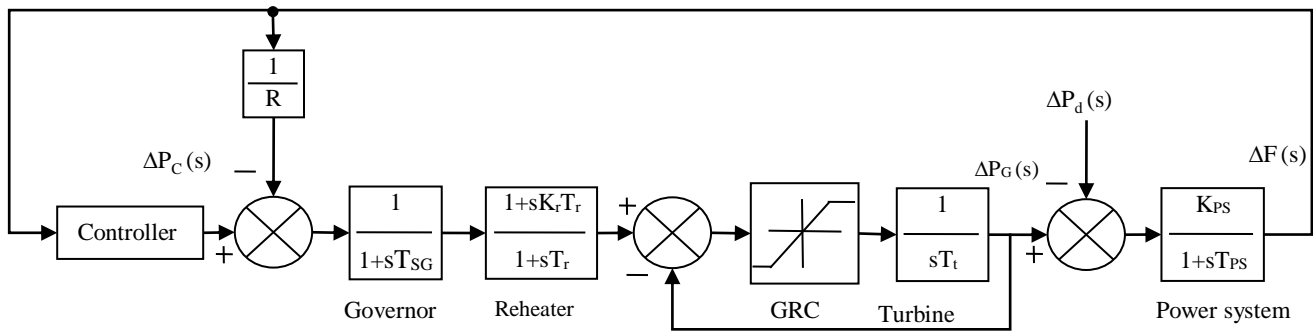


Fig. 3.9 TFM of single-area reheat with GRC thermal PS.

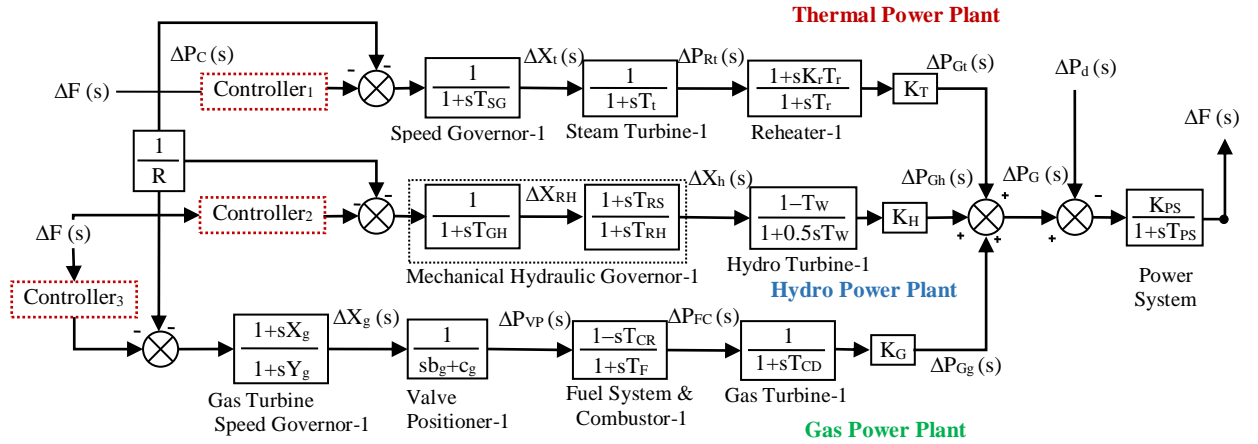


Fig. 3.10 TFM of single-area THG PS.

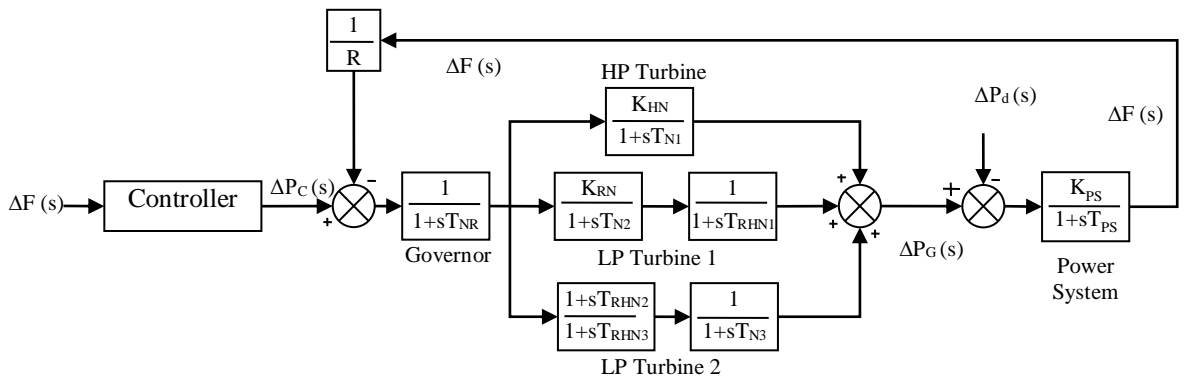


Fig. 3.11 TFM of single-area nuclear PS.

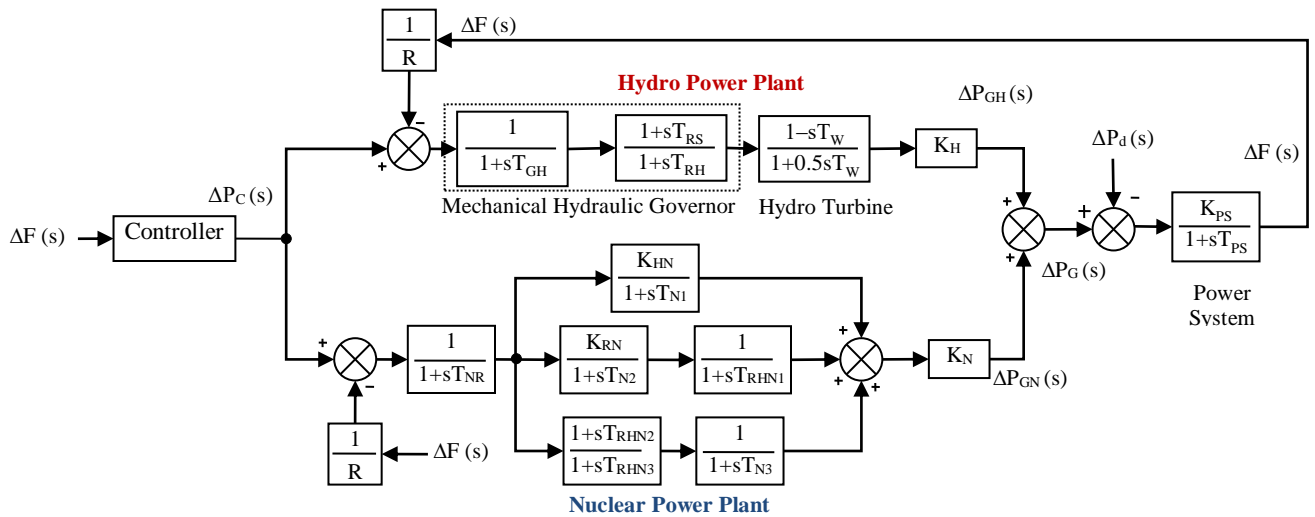


Fig. 3.12 TFM of single-area hydro-nuclear PS.

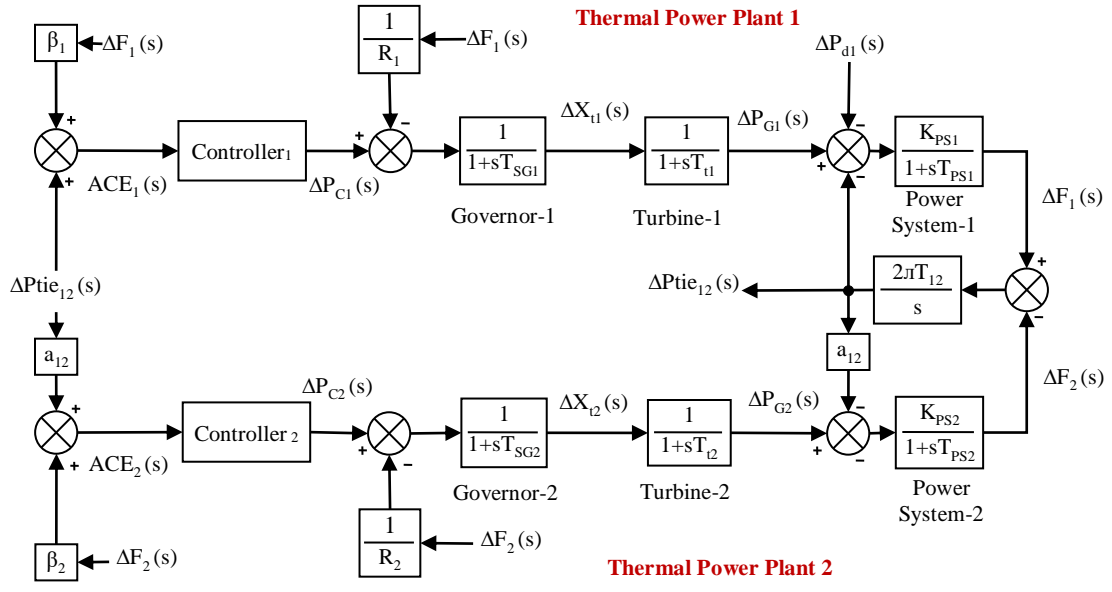


Fig. 3.13 TFM of multi-area thermal PS.

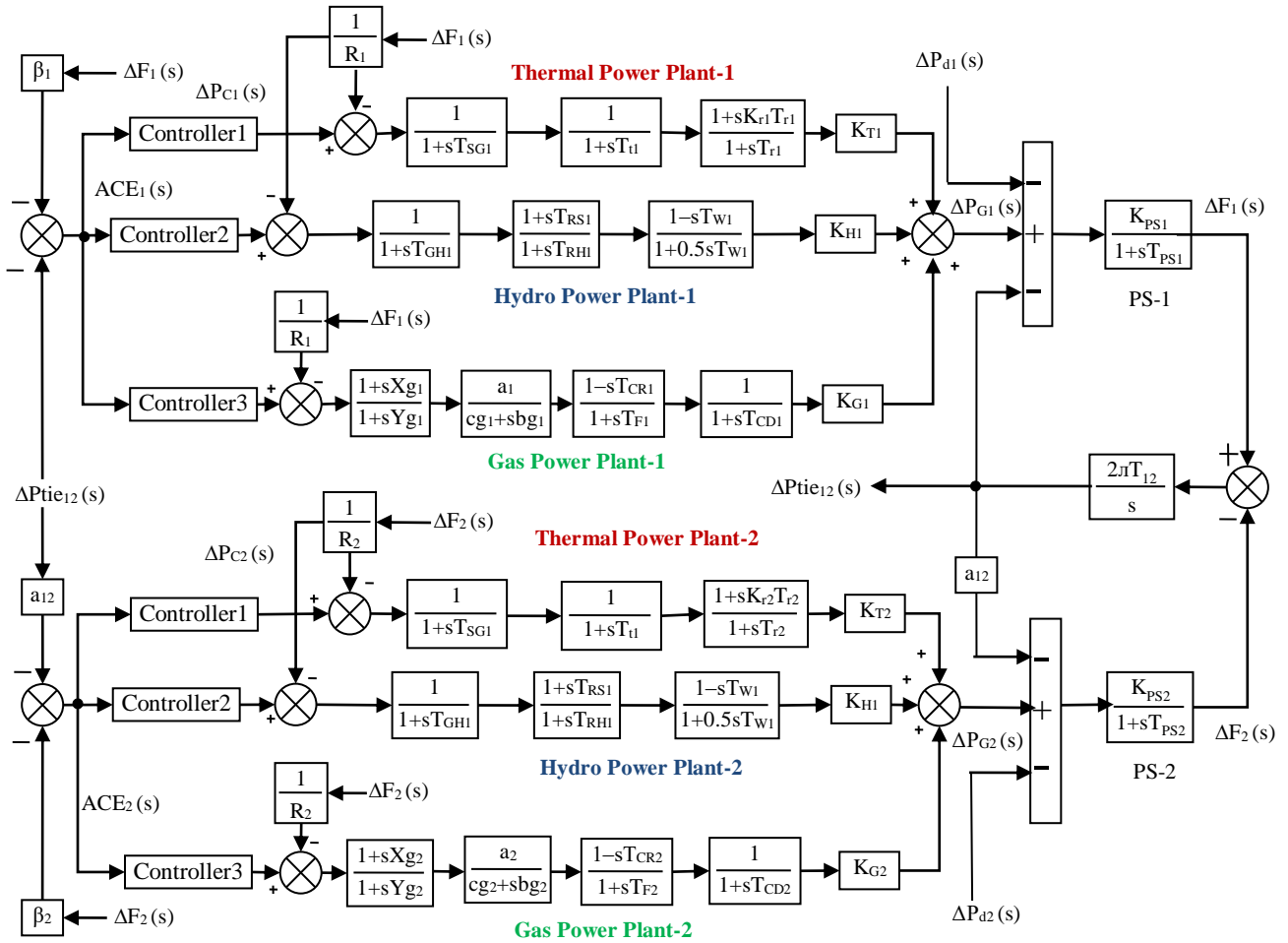


Fig. 3.14 TFM of two-area THG PS.

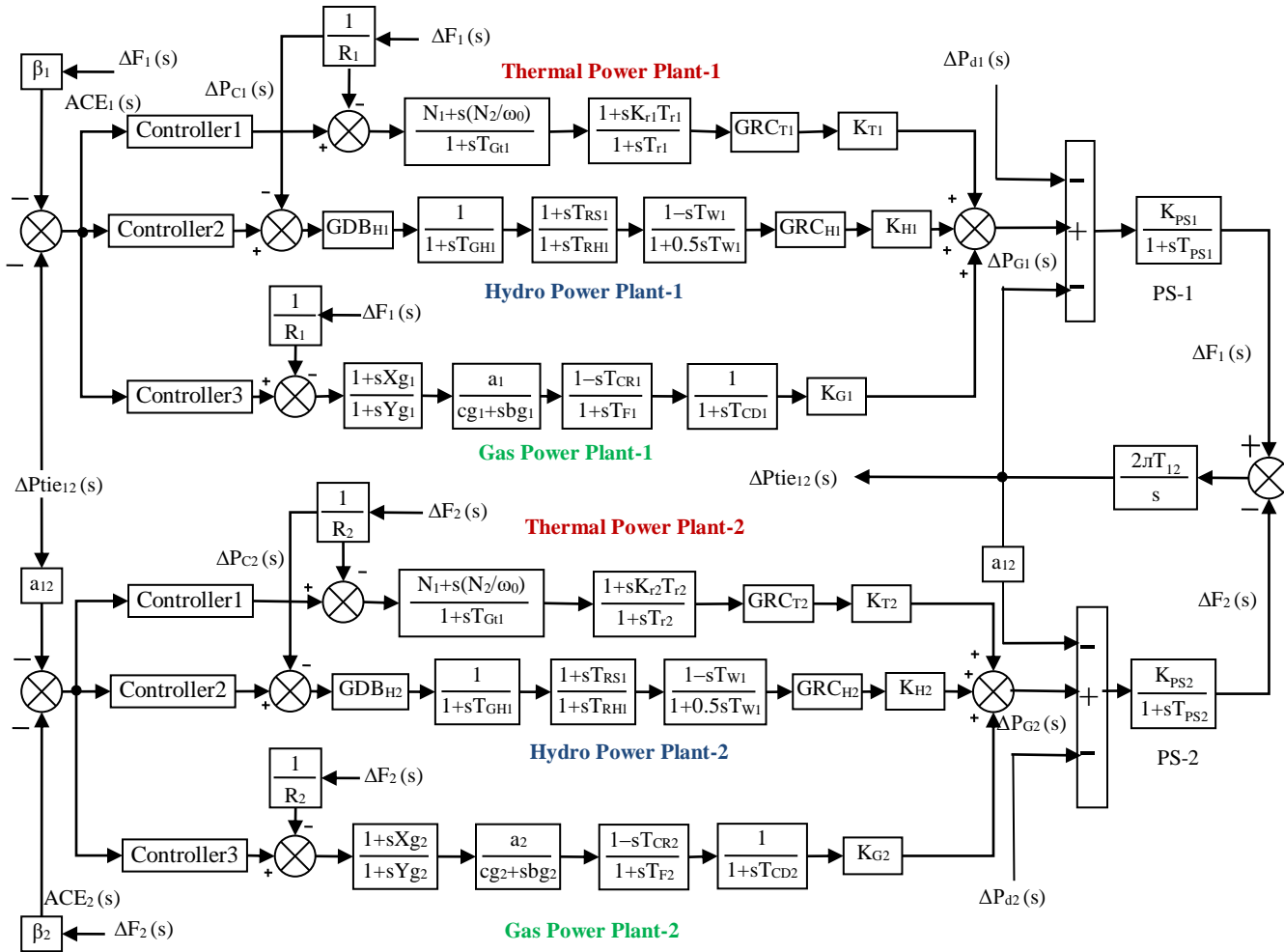


Fig. 3.15 TFM of two-area THG PS with GRC/GDB.

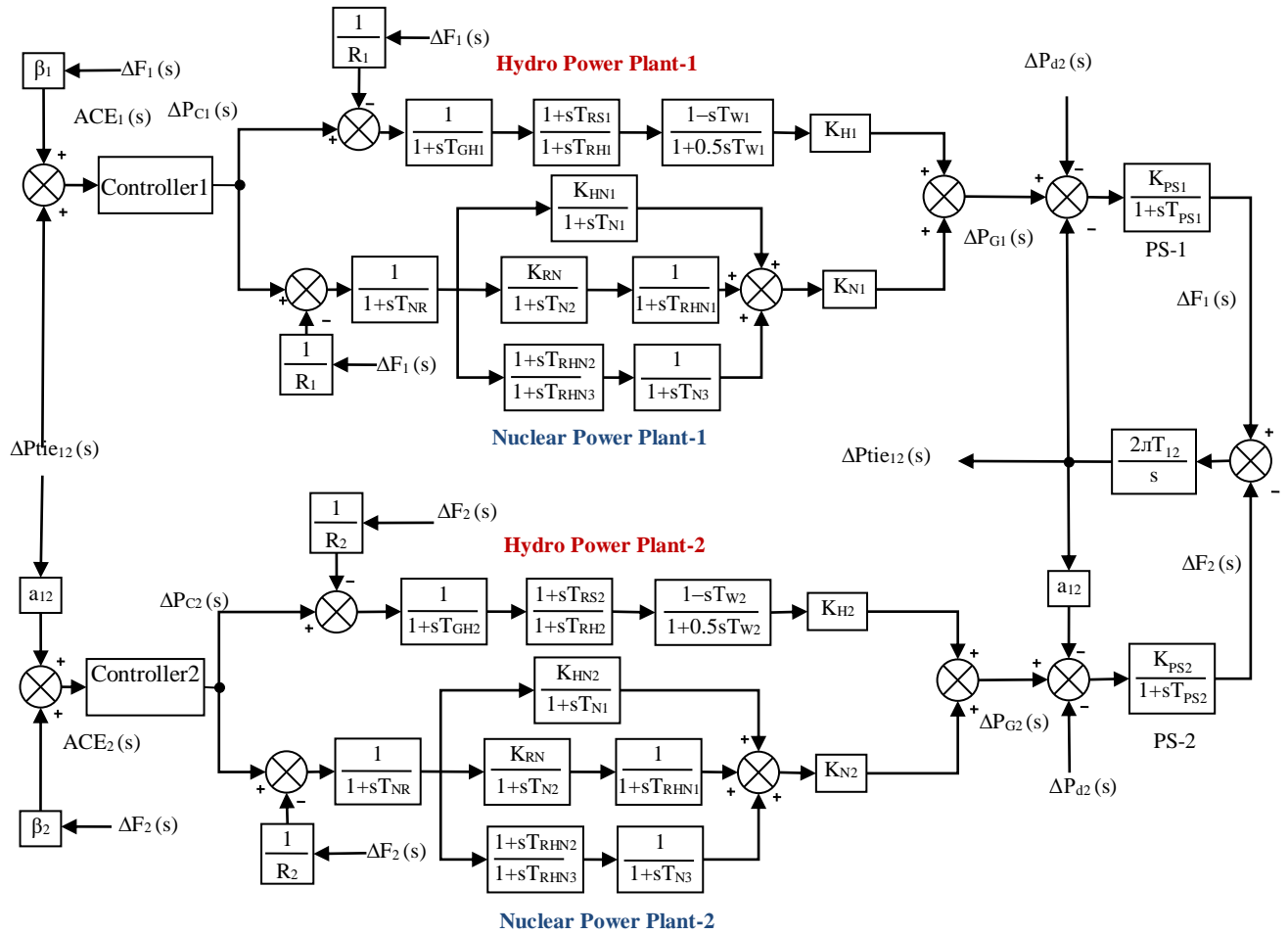


Fig. 3.16 TFM of two-area hydro-nuclear PS.

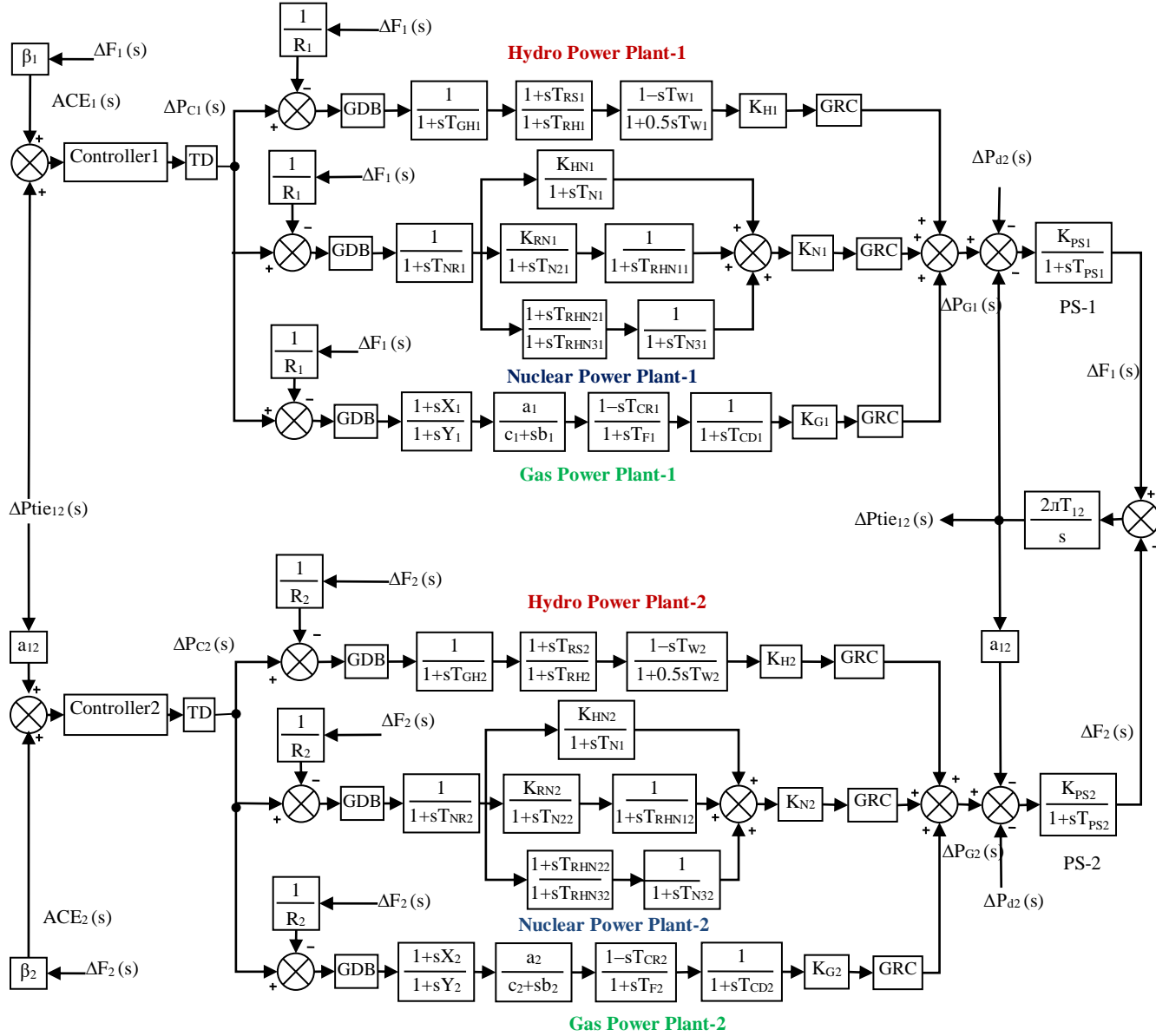


Fig. 3.17 TFM of two-area HNG PS with GDB/GRC/TD.

3.4 Conclusion

This chapter develops the TFM for THG turbines connected with controlling systems, tie-lines, and other parts. A variety of single/multi-area interconnected PSs, including multi-source, multi-unit THG PSs, single-area reheat thermal PSs, and non-reheat thermal PSs, have their TF models constructed. This chapter also designs a number of models for

nuclear single-source multi-unit single PSs, THG PSs (multi-source multi-unit), and HNG PSs (multi-source multi-unit).

CHAPTER 4

AGC OF SINGLE-AREA THERMAL POWER SYSTEM USING ALO AND GNA OPTIMIZED PID CONTROLLERS

4.1 Introduction

The AGC of thermal PSs in a single-area is designed in this chapter. It can be seen from the literature review that the type of optimization technique and secondary controller architecture that are employed have a notable effect on the performance of the AGC systems. The literature contains a variety of clever structures and approaches that are used in relation to classical control schemes. Most research portrays the use of traditional PID controller in industrial processes because of its straightforward design, reliability, affordability, and efficacy for linear systems. An optimization algorithm based on modeling-behavior of antlion is presented here, known as antlion optimization (ALO) algorithm, which is applied for tuning of PI/PID controllers to determine the performance index. Several investigations are identified to demonstrate the dynamic performance of PS model under investigation with ALO tuned AGC regulators. Comparison of ALO optimized PID controllers with GNA optimized PID controllers is tested to prove the dynamic performance of PSs.

4.2 Antlion Optimization (ALO) Algorithm

Recently several intelligent algorithms are available in literature but the probability of best solution is more in evolutionary algorithms. ALO [259] is based on the intelligent

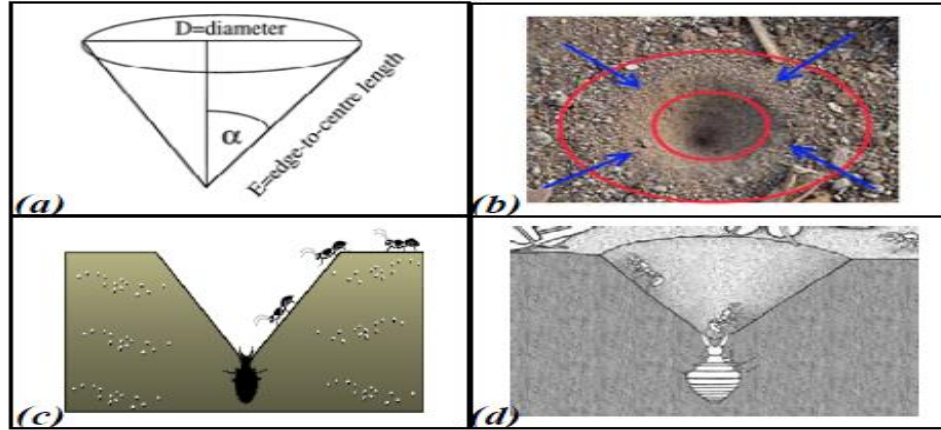


Fig. 4.1 (a) Geometrical shape of trap, (b) Cone shaped pit, (c) Random motion of ant, and (d) Antlion catching its prey [259].

behaviour of antlions naturally to hunt the ants. Five primary processes in hunting prey such as ants roam randomly, traps are built, ants are trapped in traps, prey is caught, and traps are rebuilt. These steps are explained in section 4.2.1-4.2.7.

4.2.1 Inspiration

Antlions are the net-winged insects having two phases in lifecycle: larvae and adult. Total lifespan is up to 3 years. During the larvae phase it mostly hunts the prey while it does mating in the adulthood. The larvae use its big massive jaw to dig a cone- shaped pit in the sand as shown in Fig. 4.1. The larvae try to catch its prey by hiding near the bottom of a pit. Usually insects (mostly ants) moving around the cone shaped pit fall in the trap easily as the edge of the pit is sharp. Antlion catches its prey and consumes it easily, then waits for the next hunt.

4.2.2 Mathematical Model of the Behaviour of Antlions

A random walk of the ants is chosen to move in a search space so that antlions can dig a fittest trap. For modeling of the movement of ants is described by Eqn. (4.1) as:

$$W(t) = [0, csum(2x(t_1) - 1), csum(2x(t_2) - 1), \dots, csum(2x(t_n) - 1)] \quad (4.1)$$

Where, t denotes the step of random walk (here iterations), cumulative sum is denoted as $csum$, highest number of iteration is denoted with n , and $r(t)$ is defined as random number represented by Eqn. (4.2).

$$r(t) = \begin{cases} 1 & \text{if } rand \geq 0.5 \\ 0 & \text{if } rand \leq 0.5 \end{cases} \quad (4.2)$$

A random number is denoted with $rand$ in the range of $[0,1]$. The location of ants is saved and utilized during optimization of matrix denoted as T_{ant} represented by Eqn. (4.3).

$$T_{ant} = \begin{bmatrix} H_{1,1} & H_{1,2} & \dots & H_{1,d} \\ H_{2,1} & H_{2,2} & \dots & H_{2,d} \\ \dots & \dots & \dots & \dots \\ H_{n,1} & H_{n,2} & \dots & H_{n,d} \end{bmatrix} \quad (4.3)$$

Here, $H_{p,q}$ denotes the position value of the q -th variable of the p -th ant. n , d , respectively denotes the number of ants and the number of variables. Let us assign the fitness function in the matrix form represented by Eqn. (4.4).

$$T_{OA} = \begin{bmatrix} f\left(\left[H_{1,1}, H_{1,2}, \dots, H_{1,d}\right]\right) \\ f\left(\left[H_{2,1}, H_{2,2}, \dots, H_{2,d}\right]\right) \\ \dots \\ f\left(\left[H_{n,1}, H_{n,2}, \dots, H_{n,d}\right]\right) \end{bmatrix} \quad (4.4)$$

Where, T_{OA} is the matrix which stores the best value of each ant position as $H_{p,q}$. Objective function is denoted by f . The positions of antlions which are hiding can be stored with best value in the matrix form as $T_{antlion}$ is given by Eqn. (4.5).

$$T_{antlion} = \begin{bmatrix} HL_{1,1} & HL_{1,2} & \dots & HL_{1,d} \\ HL_{2,1} & HL_{2,2} & \dots & HL_{2,d} \\ \dots & \dots & \dots & \dots \\ HL_{n,1} & HL_{n,2} & \dots & HL_{n,d} \end{bmatrix} \quad (4.5)$$

Here, $HL_{i,j}$ is the q -th dimension value of p -th antlion. n , d , respectively denotes the number of antlions and the number of variables. The fitness of each antlion is saved in the matrix form as T_{OAL} is given by Eqn. (4.6).

$$T_{OAL} = \begin{bmatrix} f\left([HL_{1,1}, HL_{1,2}, \dots, HL_{1,d}]\right) \\ f\left([HL_{2,1}, HL_{2,2}, \dots, HL_{2,d}]\right) \\ \dots \\ f\left([HL_{n,1}, HL_{n,2}, \dots, HL_{n,d}]\right) \end{bmatrix} \quad (4.6)$$

4.2.3 Random Walk of Ants

All the random walks are related to the Eqn. (4.1). Ants update their positions with random walk in each optimization step. This walk is limited in the search space using the min-max normalization represented by Eqn. (4.7).

$$W_i^t = \frac{(W_i^t - a_i) \times (b_i - c_i^t)}{(d_i^t - a_i)} + c_i \quad (4.7)$$

Here the lowest and highest of random walks for p -th variable are denoted with a_i and b_i respectively, and the lowest and highest of the p -th variable at the t -th iteration are denoted with c_i^t and d_i^t , respectively.

4.2.4 Trapping in Antlion's Pits

The mathematical equations can be given for the random walks of ants which are affected by antlion's traps represented by Eqns. (4.8-4.9).

$$c_i^t = Antlion_j^t + c^t \quad (4.8)$$

$$d_i^t = Antlion_j^t + d^t \quad (4.9)$$

Where, $Antlion_j^t$ denotes the location of chosen q -th antlion at t -th iteration. The spherical behaviour of the movement of ants are defined by the vectors c and d around a selected antlion.

4.2.5 Building Trap

A roulette wheel is designed to model the antlion's hunting capability. ALO algorithm uses a roulette wheel for fittest antlions by optimization. This is shown in Fig. 4.1(a-d).

4.2.6 Sliding Ants Towards Antlion

Due to the random movement of ants it is more probability that ants will be trapped in a pit. Antlions try to build sharp corners of the traps so that ant cannot escape according to their fitness. This mathematical modeling can be described by the radius of a hyper-sphere using Eqns. (4.10-4.11)

$$c^t = \frac{c^t}{I} \quad (4.10)$$

$$d^t = \frac{d^t}{I} \quad (4.11)$$

Where, c^t and d^t denotes the lowest and highest of all variables at t -th iteration. I is a constant calculated by Eqn. (4.12). the current iteration is denoted with t while total iterations is denoted with N respectively, and p is a constant defined by Eqn. (4.13).

$$I = 10^{p \frac{t}{N}} \quad (4.12)$$

$$p = \begin{cases} 2 & \text{if } p \geq 0.1N \\ 3 & \text{if } p \geq 0.5N \\ 4 & \text{if } p \geq 0.75N \\ 5 & \text{if } p \geq 0.9N \end{cases} \quad (4.13)$$

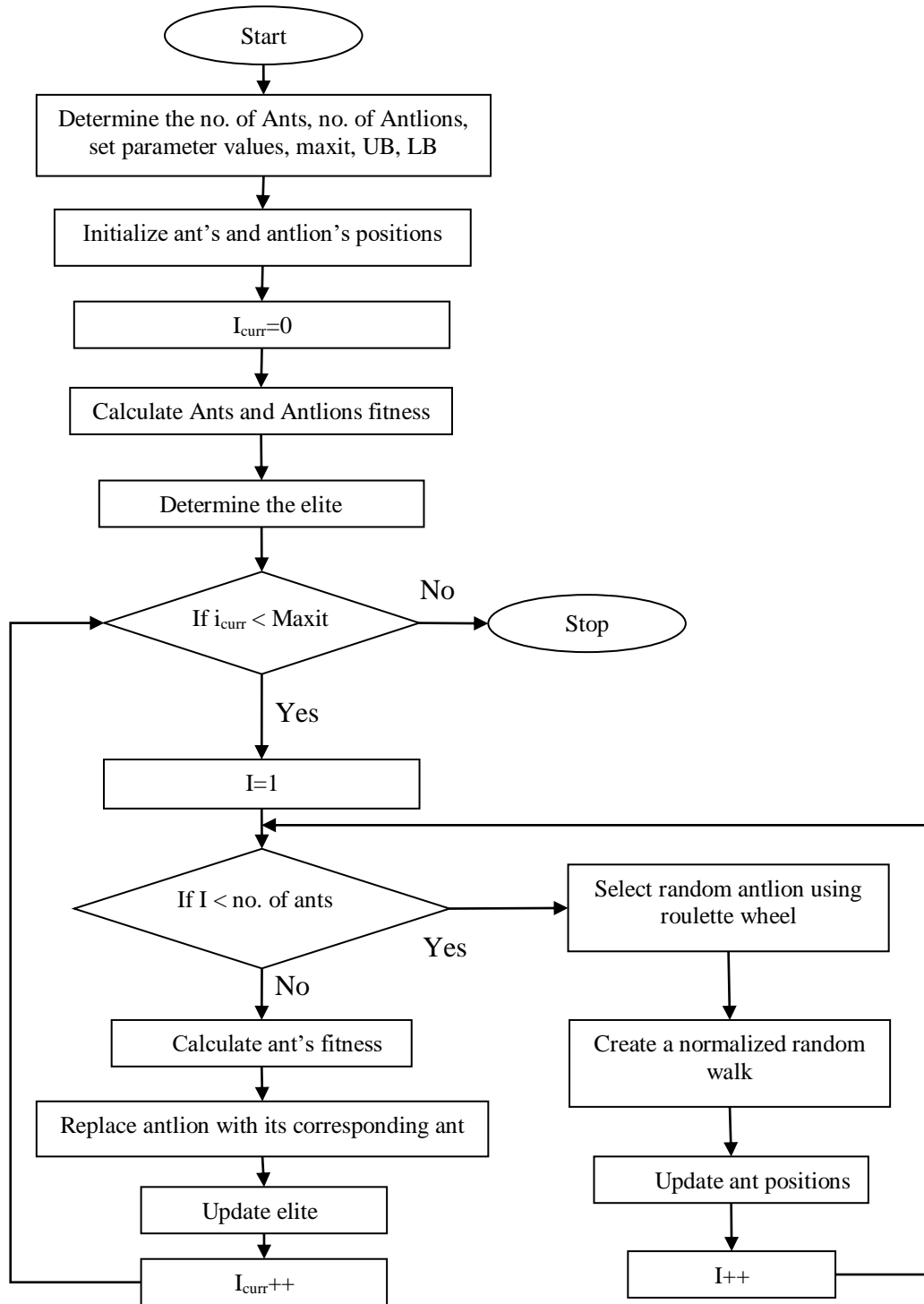


Fig. 4.2 Flowchart of ALO [259].

4.2.7 Hunting the Prey and Re-building the Pit

After hunting and consuming the ants body an antlion has to update the current position with a new fittest position to catch new ants in the pit. Assuming at t -th iteration, the spot of selected q -th antlion as $Antlion_q^t$. Ant_p^t denotes at t -th iteration, the spot of p -th ant.

This condition is given by Eqn. (4.14) as follows:

$$Antlion_q^t = Ant_p^t \text{ if } f(Ant_p^t) > f(Antlion_q^t) \quad (4.14)$$

4.2.8 Elitism

The main advantage of evolutionary algorithms is to maintain the best solution after optimization. Here the best antlion obtained in each iteration is saved and denoted as elite. As a result, each ant moves at random close to the elite group and the fittest antlion according to the roulette wheel is defined by the Eqn. (4.15) as:

$$Ant_i^t = \frac{R_A^t + R_E^t}{2} \quad (4.15)$$

Where, R_A^t is the random walk near the fittest antlion by roulette wheel selection at t -th iteration.

The random walk near the elite is R_E^t at t -th iteration. The advantages of ALO are, it ensures the exploration of search space by the random walk of ants around the antlions. ALO is a population-based algorithm so it rejects local optima and selects the global optima. Convergence of ALO algorithm is observed by the decreasing intensity of ant's movement after specified iterations. The number of parameters to optimize in a PID controller (K_P, K_I, K_D) = 3. Search space selected is 20 and number of iterations is 100. The lower and upper limits is in the range [0-5]. Flowchart of ALO is shown in Fig. 4.2.

4.3 Global Neighbourhood Algorithm (GNA)

The GNA was induced by Allazam and Lewis [260]. To improve the controller parameters, a heuristic method known as the global neighbourhood algorithm (GNA) has been tested. There's a chance that this method will find the optimum values quickly. This kind of algorithm uses iteration to solve complicated issues. As another advantage, local optima avoidance is high due the stochastic nature of evolutionary algorithms. If an evolutionary algorithm is trapped in a local optimum, stochastic operator lead to random changes in the solution and eventually escaping from the local optimum. GNA is a population-based algorithm, so local optima avoidance is intrinsically high. Selecting the global and local search spaces at random ensures that the search space is thoroughly explored. The algorithm is explained as:

1. GNA algorithm generates two sets of space from the random selection denoted as local search space and global search space.
2. Creates T possible values of K_P , K_I , K_D gains from random search space.
3. Calculates objective function after first iteration i.e. minimum value of ITAE.
4. Then optimal value is selected from the comparison with best value and stored as ITAE.
5. After total iterations are over, minimum value of ITAE is best solution.

Here, the controller gains (K_P , K_I , K_D) and other parameters (ITAE, ST, OS, US) are simultaneously optimized using the Objective Function (OF). The number of parameters to optimize in a PID controller (K_P , K_I , K_D) = 3. The initial step is to assign the random values = $T/2 = 50$ and number of iterations is 100. Range of the lower limit and upper limit is 0 and 5, respectively. GNA flowchart is shown in Fig. 4.3.

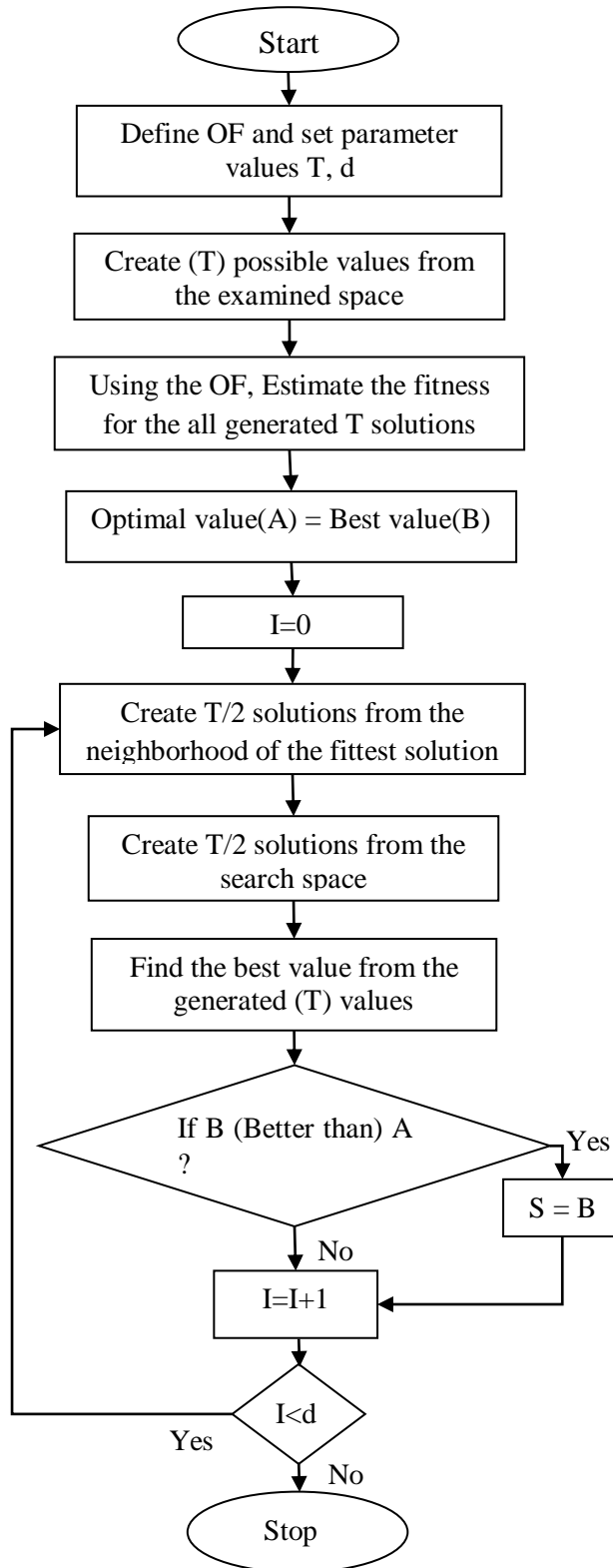


Fig. 4.3 Flowchart of GNA [260].

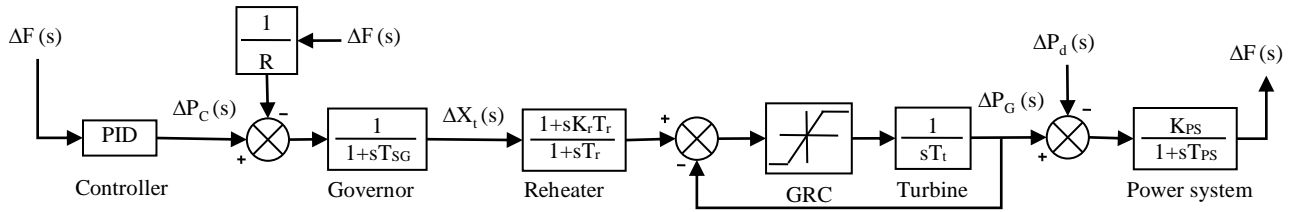


Fig. 4.4 Single-area reheat thermal PS with GRC and PID controller.

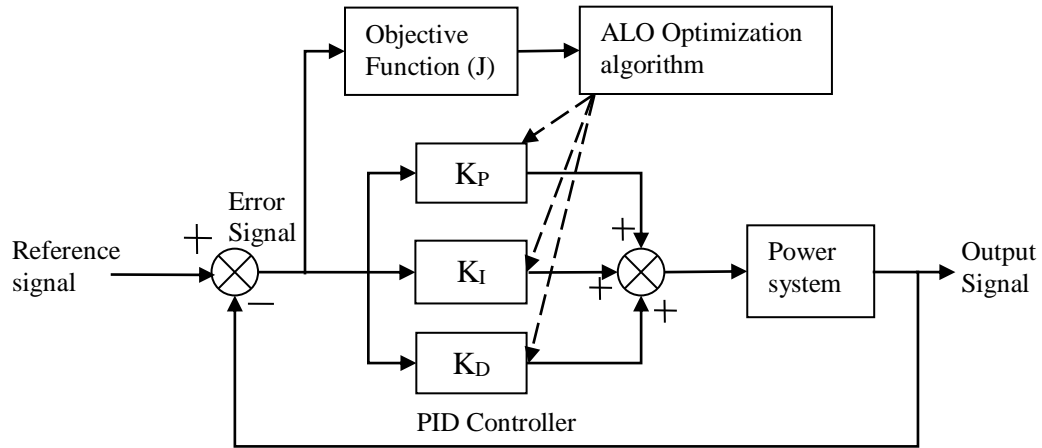


Fig. 4.5 Structure of PID controller.

4.4 Systems Investigated

A single-area, single-source, non-reheat/reheat thermal PS with/without GRC is the subject of investigations. Each section has a 2000 MW rated capacity, with a 1000 MW initial loading. Fig. 4.4 displays the design of the PS that is being studied. The Appendix contains the systems' nominal parameters. Chapter 3 discusses the models that are the subject of the study in detail.

4.5 PID Controller

The derivative, integral, and proportional controllers' outputs are combined to create the PID controller's output. The controller gains are K_P , K_I , and K_D . The PID controller minimizes the steady state error and boosts stability. Fig. 4.5 displays the parallel arrangement of the controller.

$G_{PI}(s)$ and $G_{PID}(s)$ denote the TFs of PI and PID controllers defined by Eqns. (4.16-4.17) as:

$$G_{PI}(s) = K_P + \frac{K_I}{s} \quad (4.16)$$

$$G_{PID}(s) = K_P + \frac{K_I}{s} + K_D s \quad (4.17)$$

The PSs under investigation have PI/PID controllers to overcome the AGC problem. PID controller receives the error input. To obtain the output U or ΔP_C of the PID controller, the error is multiplied by gains and then summed. PC is the system's control input. By minimizing an objective function, the ALO/GNA method can be used to adjust the gains.

4.6 Optimization Problem

An optimization problem's primary aim is to reduce an objective function that has been chosen for the system while taking the proper performance index into account. The choice of an appropriate performance index has a major impact on how well an optimization approach performs. The integral time absolute error (ITAE) used to develop the ALO/GNA-PID controller serves as the study's performance index (PI) which is expressed as J , for single-area PS, is defined by Eqn. (4.18) as:

$$J = \int_0^t t |\Delta F| dt \quad (4.18)$$

The PI/PID controller gains within a few pre-established bounds are the optimization problem's constraints. Therefore, using Eqn. (4.19), the subsequent optimization problem can be used to create the controller design challenge.

$$K_P^{\min} \leq K_P \leq K_P^{\max}, K_I^{\min} \leq K_I \leq K_I^{\max}, K_D^{\min} \leq K_D \leq K_D^{\max} \quad (4.19)$$

Table 4.1 ALO optimized gain parameters of single-area thermal system for PI and PID controllers.					
Type of Single-area Thermal system	Controller used	K_P	K_I	K_D	ITAE
Non-Reheat	ALO:PI	0.34001	0.4802	0	0.031184
	ALO:PID	0.8268	0.999	0.13072	0.0088
Reheat	ALO:PI	1	0.67959	0	0.04849
	ALO:PID	1	1	0.14675	0.03547
Non-Reheat with GRC	ALO:PI	0.1778	0.071348	0	0.2872
	ALO:PID	0.51671	0.080816	0.56511	0.2346
Reheat with GRC	ALO:PI	0.3148	0.08126	0	0.4653
	ALO:PID	0.67785	0.073781	0.552	0.2291

The parameters have been set with a minimum of 0.0 and a maximum of 5.0, respectively. Table 4.1 shows the best final ideal outcomes for the several PS models that were studied. The program created in MATLAB software is used to calculate the numerical values of settling times (STs), undershoots (USs), and overshoots (OSs) of frequency deviation results under SLP in order to explore the comparative assessment between the suggested ALO adjusted PI and PID controllers. The dynamic response speed is shown by the STs, USs, and OSs numerical values.

4.7. Simulation Results and Discussion

4.7.1 Single-Area Thermal System with ALO Tuned PI/PID Controller

At $t = 0$ sec considering a 1% step load perturbation (SLP) in area-1, single-area non-reheat thermal PS is simulated for investigation. Current study shows PI controllers are also constructed for comparison with the suggested PID controllers. A MATLAB algorithm designed for PI/PID controller optimization is accomplished using the system data provided in Appendix to produce the gain parameters displayed in Table 4.1. The

supremacy of the ALO:PID controllers is revealed from its performance obtained in the findings when compared to ALO:PI.

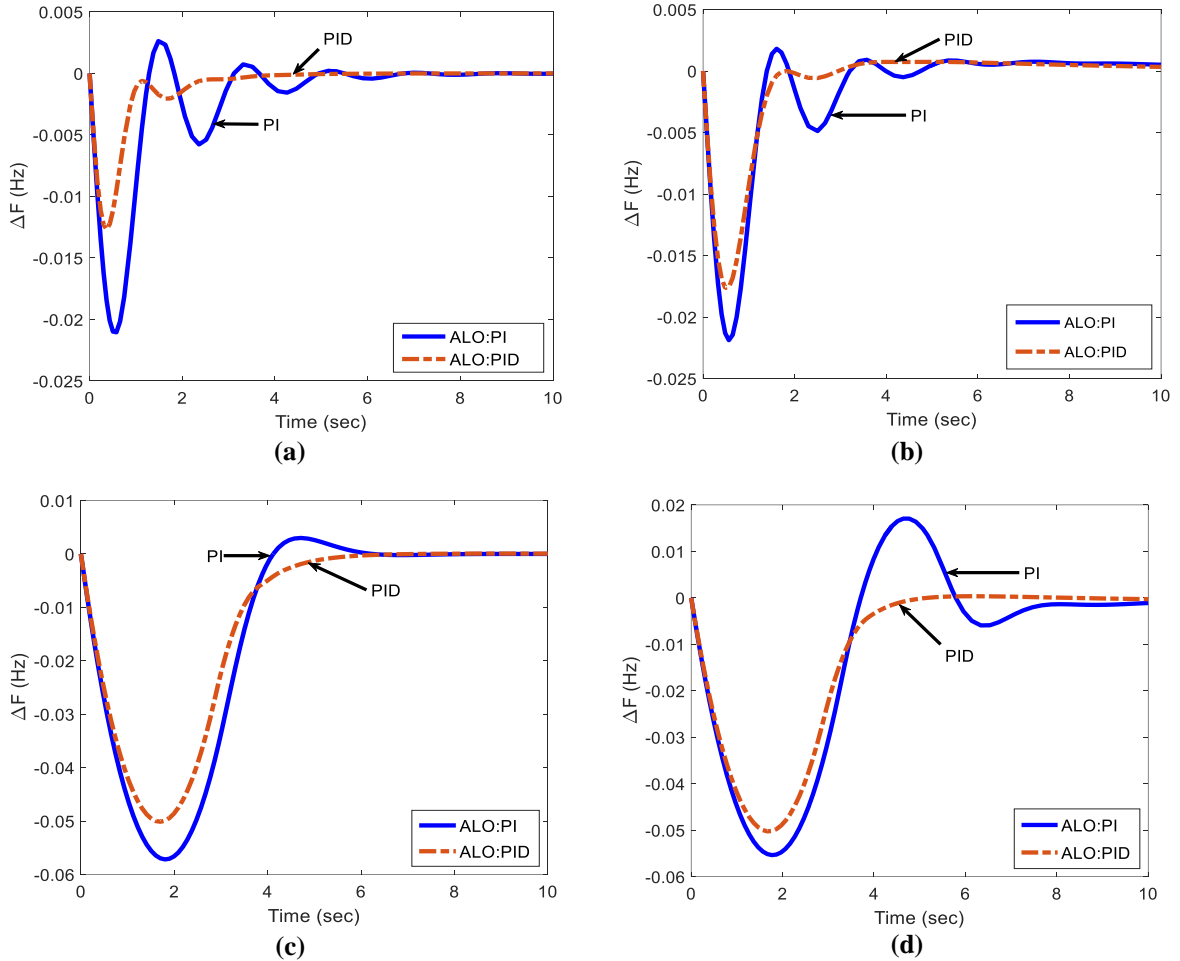


Fig. 4.6 Single-area thermal system responses (ΔF) with ALO tuned PI/PID controllers: (a) Non-reheat, (b) Reheat, (c) Non-reheat with GRC, and (d) Reheat with GRC.

Table 4.2					
System results (ΔF) in terms of ST/OS/US/ITAE for single-area thermal system with ALO tuned PI and PID controllers at $\Delta P_d = 0.01$ puMW.					
Type of Single-area Thermal system	Type of controller	ST (sec)	US (Hz) (-ve)	OS (Hz)	ITAE
Non-Reheat	ALO:PI	4.74	0.021	0.00252	0.031184
	ALO:PID	2.53	0.013	0.00015	0.0088
Reheat	ALO:PI	11.1329	0.022	0.00175	0.04849
	ALO:PID	9.7492	0.018	0.00074	0.03547
Non-Reheat with GRC	ALO:PI	5.5556	0.056	0.00297	0.2872
	ALO:PID	5.1834	0.050	0.00315	0.2346
Reheat with GRC	ALO:PI	10.0110	0.057	0.0171	0.4653
	ALO:PID	4.5697	0.051	0.00042	0.2291

ALO:PID controller is better than those offered by ALO:PI as shown in Figs. 4.6(a-d). The settling times (STs) with mathematical values, undershoots (USs) and overshoots (OSs) for response of frequency deviation is shown in Table 4.2. ST is observed for a tolerance band of ± 0.0005 . The simulation time of 10 sec is considered for ITAE given by Eqn. (4.18). Analysis shows that, as compared to ALO:PI controller, the values of STs/USs/OSs and ITAE values are lowest with ALO:PID controller. Therefore, it can be said that PID controllers outperform PI controllers in terms of performance even at lower ST, US, and OS values. The values of STs, USs, OSs, and ITAE for the ALO:PID controller's ΔF response with reheat system are 2.53 sec, -0.013 Hz, 0.0015 Hz, and 0.0088 , in that order, and with reheat PS are 9.7492 sec, -0.018 Hz, 0.00074 Hz, and 0.03547 , respectively. For non-reheat PS using ALO:PI controller the values of ΔF response are $ST=4.74$ sec, $US= -0.021$ Hz, $OS=0.00252$ Hz and $ITAE=0.031184$, respectively, and with reheat PS values are 11.1329 sec, -0.022 Hz, 0.00175 Hz, and 0.04849 , respectively. It permits the reheat system's slower or less effective operation in comparison to the non-reheat system. The ΔF response values for the ALO:PID controller are 5.1834 sec, -0.050 Hz, 0.00315 Hz, and 0.2346 when using a non-reheat system with GRC, and 4.5697 sec, -0.051 Hz, 0.00042 Hz, and 0.2291 when using a reheat PS with GRC. The ΔF response values for the ALO:PI controller are 5.5556 sec, -0.056 Hz, 0.00297 Hz, and 0.2872 when using a non-reheat system with GRC, and 10.011 sec, -0.057 Hz, 0.0171 Hz, and 0.4653 when using a reheat PS with GRC. Hence, the performance of thermal PS with GRC degrades compared to thermal PS without GRC.

4.7.2 Single-Area Thermal System with GNA Tuned PI/PID Controller

The gain parameters tuned via GNA for PI/PID are shown in Table 4.3. To demonstrate the GNA:PID controller's influence, over the GNA:PI controller, It is evident from the performance attained in results by the GNA:PID controller is better than those offered by GNA:PI controller displayed by Figs. 4.7(a-d). The numeric values of STs, USs and OSs for frequency deviation response is shown in Table 4.4. It is clearly evident from the findings that lowest values of STs/USs/OSs and ITAE are attained with GNA:PID controller in contrast to GNA:PI controller.

Table 4.3 GNA optimized gain parameters of single-area thermal system for PI and PID controllers.					
Type of Single-area Thermal system	Controller used	K_P	K_I	K_D	ITAE
Non-Reheat	GNA:PI	0.3075	0.4681	0	0.0314
	GNA:PID	2.2814	4.6887	0.4279	0.000647
Reheat	GNA:PI	1.5387	1.2359	0	0.0467
	GNA:PID	3.2531	4.5221	0.5535	0.0077
Non-Reheat with GRC	GNA:PI	0.2253	0.0705	0	1.0082
	GNA:PID	4.6970	0.0909	3.4192	0.2154
Reheat with GRC	GNA:PI	0.2609	0.0753	0	0.3769
	GNA:PID	1.6215	0.1153	1.5082	0.3656

Table 4.4 System results (ΔF) in terms of ST/OS/US/ITAE for single-area thermal system with GNA tuned PI and PID controllers at $\Delta P_d = 0.01$ puMW.					
Type of Single- area Thermal system	Type of controller	ST (sec)	US (Hz) (-ve)	OS (Hz)	ITAE
Non-Reheat	GNA:PI	4.85	0.0215	0.00241	0.0314
	GNA:PID	0.52	0.00682	0.000265	0.000647
Reheat	GNA:PI	8.1	0.00508	0.0185	0.0467
	GNA:PID	0.73	0.0087	0.000241	0.0077
Non-Reheat with GRC	GNA:PI	24.37	0.054	0.027	0.7655
	GNA:PID	4.67	0.050	0.000064	0.2154
Reheat with GRC	GNA:PI	17.5	0.056	0.011	0.3769
	GNA:PID	16.7	0.051	0.00498	0.3656

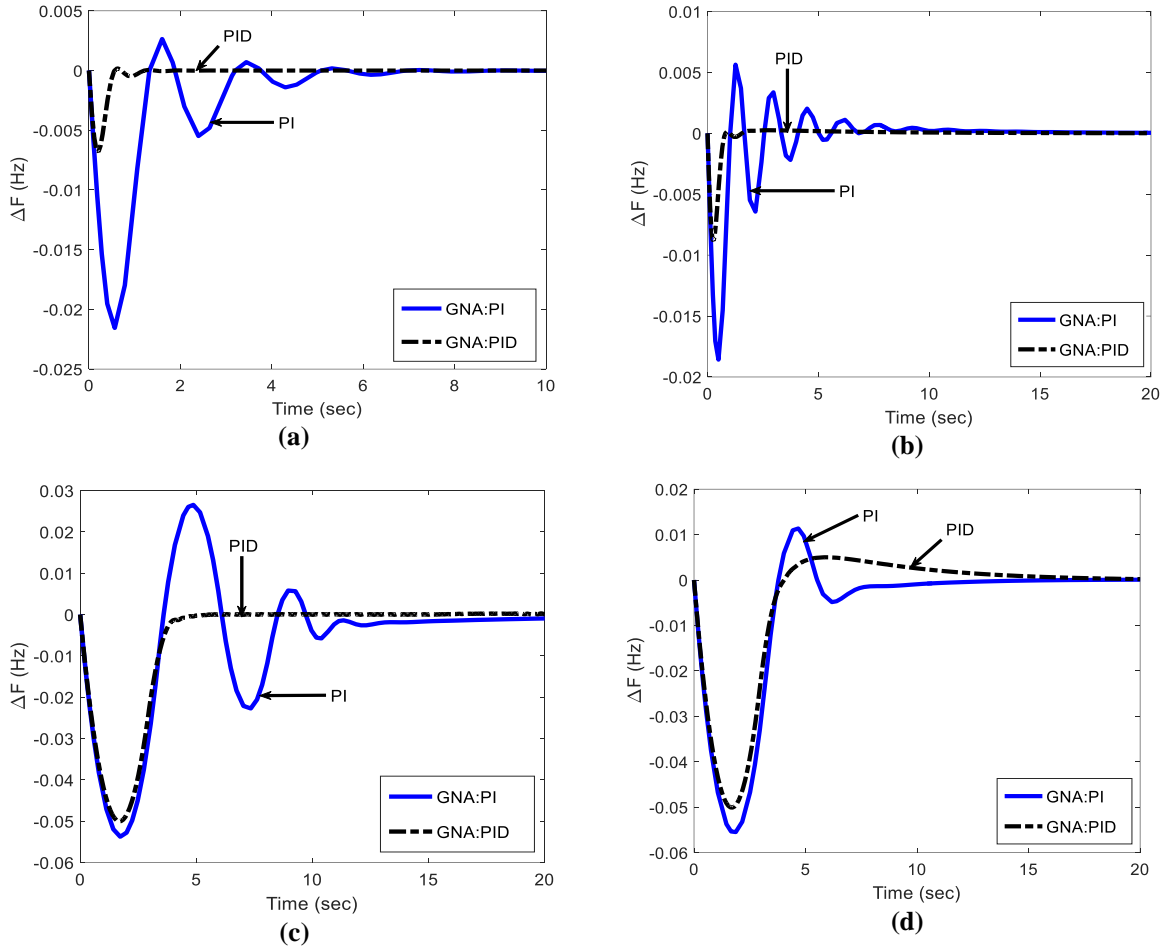


Fig. 4.7 Single-area thermal system response (ΔF) with GNA tuned PI/PID controllers: (a) Non-reheat, (b) Reheat, (c) Non-reheat with GRC, and (d) Reheat with GRC.

Consequently, PID controllers can provide higher performance with lower ST, US, and OS values than PI controllers can. Table 4.4 provides the non-reheat thermal system values. The ΔF response values for the GNA:PID controller are as follows: 0.52 sec, -0.00682 Hz, 0.000265 Hz, and 0.000647, respectively, for the non-reheat system; 0.73 sec, -0.0087 Hz, 0.000241 Hz, and 0.0077, for the reheat PS. With no reheat PS, the GNA:PI controller's ΔF response STs, USs, OSs, and ITAE values are 4.85 sec, -0.0215 Hz, 0.00241 Hz, and 0.0314, respectively; with reheat PS, these values are 8.1 sec, -0.00508 Hz, 0.0185 Hz, and 0.0467, respectively. It illustrates how the performance of the reheat PS is slower or worse than that of the non-reheat system. The ΔF response

values for the GNA:PID controller are 4.67 sec, -0.050 Hz, 0.000064 Hz, and 0.2154 when using a non-reheat system with GRC, and 16.7 sec, -0.051 Hz, 0.000498 Hz, and 0.3656 when using a reheat PS with GRC. The ΔF response values for the GNA:PI controller are as follows: 24.37 sec, -0.054 Hz, 0.027 Hz, and 0.7655 for the non-reheat system with GRC, and 17.5 sec, -0.056 Hz, 0.011 Hz, and 0.3769 for the reheat PS with GRC. Therefore, PID outperforms PI, but system performance sharply declines when GRC is used.

4.8 Comparison of ALO and GNA

ΔF responses for single-area thermal system are displayed in Fig. 4.8(a-d) considering all cases. The STs, USs and OSs for ΔF responses are shown in Table 4.5. The results indicate that in the non-reheat PS, the GNA:PID controller's responses are significantly better than ALO:PID controller's. Following study, it is abundantly clear that, for non-reheat and reheat thermal systems without GRC, the values of STs/USs and ITAE values are least with GNA:PID controller compared to ALO:PID controller. The ΔF response values for the GNA:PID controller are as follows: 0.52 sec, -0.00682 Hz, 0.000265 Hz,

Type of Single- area Thermal system	Type of controller	ST (sec)	US (Hz) (-ve)	OS (Hz)	ITAE
Non-Reheat	ALO:PID	2.53	0.013	0.00015	0.0088
	GNA:PID	0.52	0.00682	0.000265	0.000647
Reheat	ALO:PID	9.7492	0.018	0.00074	0.03547
	GNA:PID	0.73	0.0087	0.000241	0.0077
Non-Reheat with GRC	ALO:PID	5.1834	0.050	0.000063	0.2346
	GNA:PID	4.67	0.050	0.000064	0.2154
Reheat with GRC	ALO:PID	4.5697	0.051	0.00042	0.2291
	GNA:PID	16.7	0.051	0.00498	0.3656

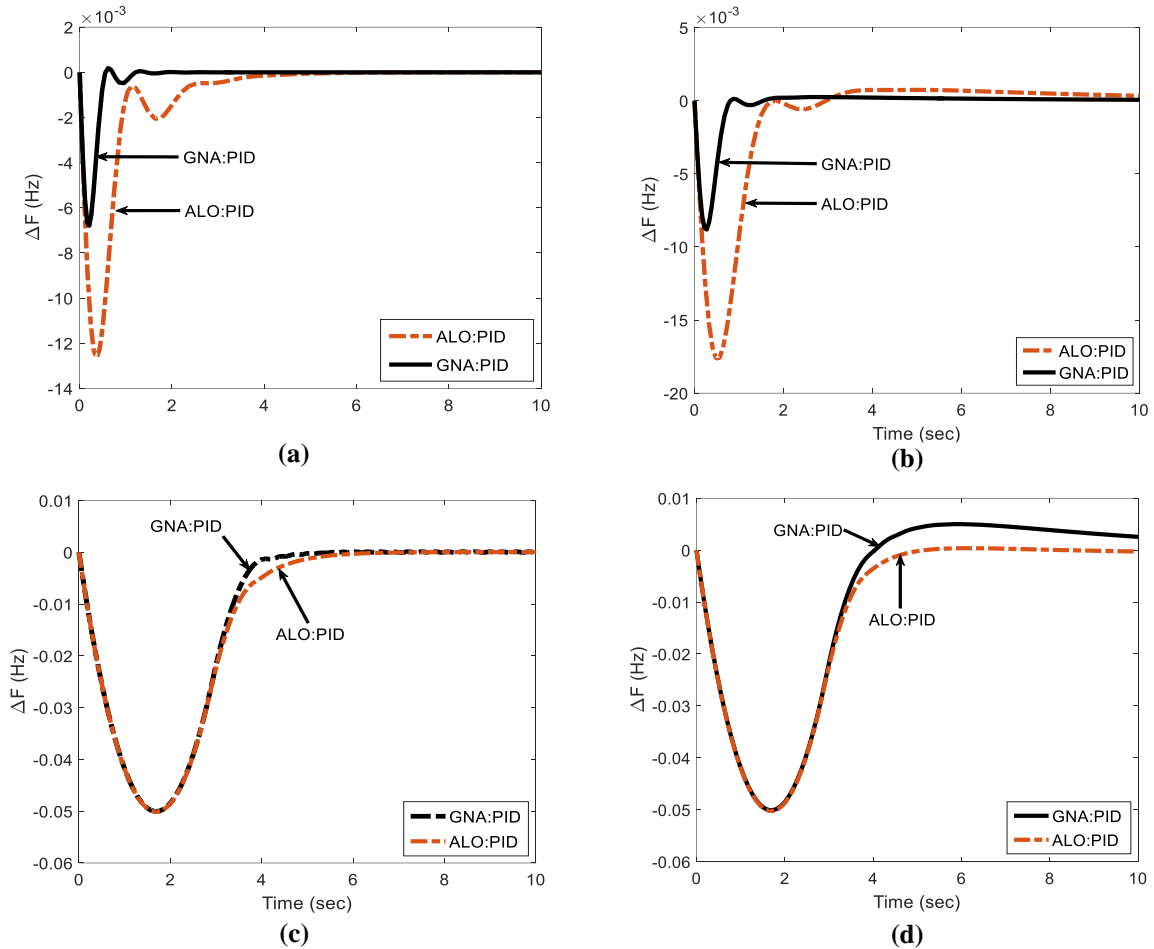


Fig. 4.8 Single-area thermal system response (ΔF) with ALO and GNA tuned PID controller: (a) Non-reheat, (b) Reheat, (c) Non-reheat with GRC, and (d) Reheat with GRC.

and 0.000647, respectively, for the non-reheat system; 0.73 sec, -0.0087 Hz, 0.000241 Hz, and 0.0077, for the reheat PS. These values are lesser than ALO:PID controller. For non-reheat system with GRC values of the ΔF response using GNA:PID controller are $ST=4.67$ sec, $US= -0.050$ Hz, $OS=0.000064$ Hz, and $ITAE=0.2154$ respectively, while reheat PS with GRC values are 16.7 sec, -0.051 Hz, 0.000498 Hz, and 0.3656 respectively. Here, some values GNA:PID are greater than ALO:PID. Hence with GRC, ALO:PID performs somewhat better than GNA:PID. However, in overall cases it is concluded that GNA:PID controller is more capable of providing better performance.

4.9 Conclusion

The outcomes of the ALO-tuned PID and PI controllers are compared for a single-area non-reheat thermal PS, and ST, US, Oss, and ITAE values are used in the comparison analysis. Performance analysis reveals the supremacy of ALO:PID controller over ALO:PI controller. Reheat thermal PSs, non-reheat thermal PSs without GRC, and reheat thermal PSs with GRC are all the subject of additional research. Comparatively speaking, the GNA optimized PID controller outperforms the GNA:PI controller. The performance of thermal PS with GRC degrades compared to thermal PS without GRC.

It is analyzed that GNA optimized PID controllers work better in non-reheat and reheat thermal PSs without GRC than ALO optimized PID controllers. GNA optimized PID controller results minimum values of ST/US/OS/ITAE than ALO optimized PID controller. For non-reheat thermal PS with GRC GNA/ALO optimized PID controller show same value for OS, while ALO:PID controller show less values of OS, more value of ITAE compared to GNA:PID controller. ALO optimized PID controller has given minimum values of ST/OS/ITAE for reheat thermal PS with GRC. Overall the GNA optimized PID controller has proven better results in contrast to ALO optimized PID.

CHAPTER 5

AGC OF MULTI-AREA THERMAL POWER SYSTEM USING GNA OPTIMIZED 2DOF-PID CONTROLLER

5.1 Introduction

A review of the literature makes it evident that the controller's design and objective function choice, in addition to the artificial intelligence methods used, affect the system's performance. Occurrence of disturbance inputs, in two degree-of-freedom-PID (2DOF-PID) controller achievements are better for set-point tracking and regulation than conventional PI/PID controllers. Nevertheless, 2DOF controller designs are less frequently used for AGC situations despite these benefits. In light of the aforementioned, a preliminary effort is carried out to employ a 2DOF-PID controller for the power system's AGC and examine results in this study.

Given the foregoing, an attempt has been made to create the best possible GNA-tuned 2DOF-PID controller design in the AGC of PSs by ITAE performance index minimization. The efficiency of the controller in giving adequate damping characteristics to system oscillations is demonstrated by the simulation results presented.

5.2 Investigated System

An analysis is conducted on a non-reheat thermal system with two areas. One governor, one controller, and one non-reheat turbine are owned by each area of PS. Studied PS has an initial loading capacity of 1000 MW, however each region has a rated capacity of 2000 MW. Two-area PS block diagram that is being studied is displayed in

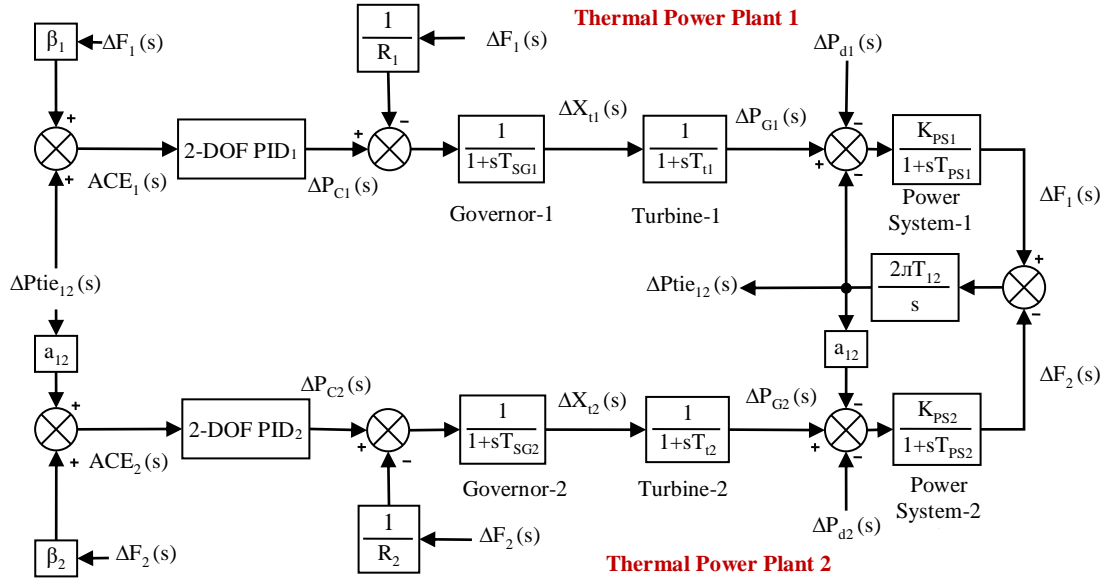


Fig. 5.1 Two-area non-reheat thermal system with 2DOF-PID controller.

Fig. 5.1. The Appendix contains the system's nominal parameters, whereas the Nomenclature part contains the list of symbols.

5.3 Two Degree-of-Freedom-PID (2DOF-PID) Controller

A control system's DOF can be summed up as several independently adjustable closed-loop TFs. Since several performance requirements need to be met while designing a control system, a 2DOF controller has intrinsic advantages over a standard 1DOF control system. According to the variation among an actual data and reference data, the 2DOF controller produces output data (signal). Using the given set point weights, it calculates a weighted modified signal for individual three actions: derivative (D), integral (I), and proportional (P). The optimized gains of the suggested controller are attained. Fig. 5.2 illustrates the construction of the 2DOF-PID controller [24], where reference signal is denoted by $r(s)$, feedback from the measured system output is denoted by $y(s)$, and output signal is denoted by $U(s)$ whereas PW and DW are used to specify the proportional-derivative set point weights. The P, I, and D gains are denoted by K_P , K_I , and K_D ,

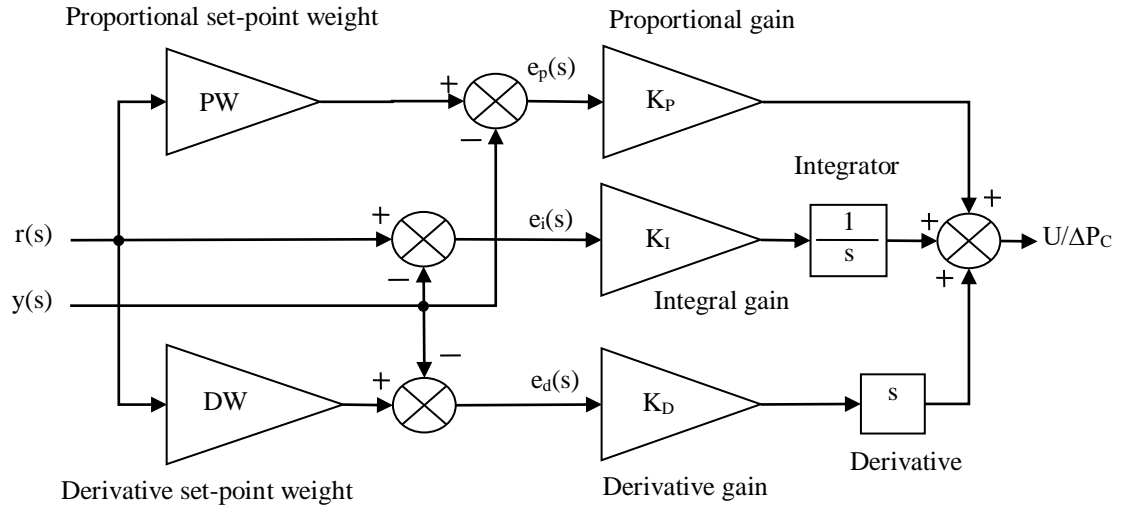


Fig. 5.2 Structure of 2DOF-PID controller.

respectively. For a 2DOF-PID, Errors e_p , e_i , and e_d are given by Eqns. (5.1-5.3), where r and y are the two inputs and u is the output given by Eqns. (5.4-5.5) as follows:

$$e_p = (PW)r - y \quad (5.1)$$

$$e_i = r - y \quad (5.2)$$

$$e_d = (DW)r - y \quad (5.3)$$

Output signal u is calculated by Eqns. (5.4-5.5) as follows:

$$u = (K_P) e_p + \left(\frac{K_I}{s} \right) e_i + (sK_D) e_d \quad (5.4)$$

$$u = K_P ((PW)r - y) + \frac{K_I}{s} (r - y) + sK_D ((DW)r - y) \quad (5.5)$$

5.4 Optimization Problem

AGC problem under consideration is solved by minimization of the objective function (J) denoted with ITAE, defined by Eqn. (5.6). The bounds on the controller parameters are the problem constraints. Consequently, the following optimization problem can be used

Table 5.1 Tuned parameters of two-area non-reheat thermal system.					
Controller type	K_{Pi}	K_{Ii}	K_{Di}	PW_i	DW_i
GNA:PI	K_{P1}	K_{I1}	K_{D1}	PW₁	DW₁
	0.0073	0.6281	0	-	-
	K_{P2}	K_{I2}	K_{D2}	PW₂	DW₂
	0.8298	0.0176	0	-	-
GNA:PID	K_{P1}	K_{I1}	K_{D1}	PW₁	DW₁
	3.8152	4.9981	1.0257	-	-
	K_{P2}	K_{I2}	K_{D2}	PW₂	DW₂
	3.4277	1.1506	2.1627	-	-
GNA:2DOF-PID	K_{P1}	K_{I1}	K_{D1}	PW₁	DW₁
	1.9848	4.3370	1.1758	3.4277	0.0962
	K_{P2}	K_{I2}	K_{D2}	PW₂	DW₂
	4.2074	0.1594	1.8262	3.9090	2.0366

$$J = \int_0^t (|\Delta F_1| + |\Delta F_2| + |\Delta P_{tie}|) dt \quad (5.6)$$

to formulate the design problem. Eqn. (5.7) provides the parameters' lowest and maximum values (K_P , K_I and K_D , PW , DW). 0.0 and 5.0 are the chosen ranges, respectively. Table 5.1 shows the best final ideal outcomes for the different PS models that were studied.

$$\begin{aligned}
K_P^{\min} &\leq K_P \leq K_P^{\max} \\
K_I^{\min} &\leq K_I \leq K_I^{\max} \\
K_D^{\min} &\leq K_D \leq K_D^{\max} \\
PW^{\min} &\leq PW \leq PW^{\max} \\
DW^{\min} &\leq DW \leq DW^{\max}
\end{aligned} \quad (5.7)$$

5.5 Simulation Results and Discussion

Two-area non-reheat thermal PS is simulated for investigation considering a 1% SLP in area-1 at $t = 0$ sec. A MATLAB application was created for the purpose of optimizing PI/PID and 2DOF-PID controllers using GNA, using the system data provided in the Appendix. The finally obtained optimal gain parameters are shown in Table 5.1. Results shown in Figs. 5.3(a-d), validates that GNA:2DOF-PID controller is better than GNA:PI/PID controllers. The mathematical values of STs, USs and OSs for response of

frequency deviation ($\Delta F_1/\Delta F_2$) and tie-line power deviation (ΔP_{tie12}) are portrayed by Table 5.2. The ITAE performance index (J) given by Eqn. (5.6), is another basis for evaluating the controllers' performance. The ST for ΔF_1 is measured in a tolerance

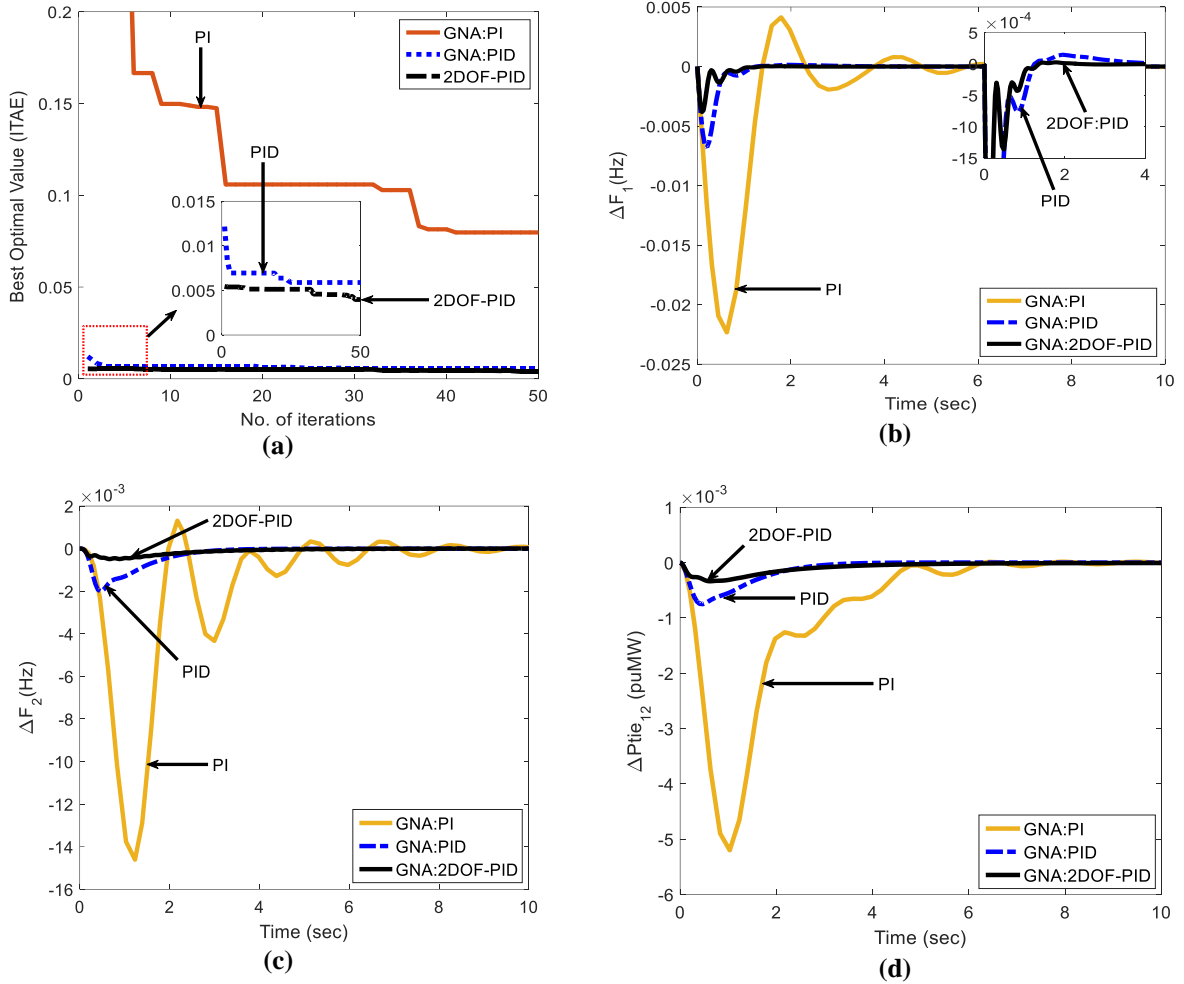


Fig. 5.3 Two-area thermal system responses: (a) Convergence curves, (b) ΔF_1 , (c) ΔF_2 , and (d) ΔP_{tie12} .

Table 5.2 ST/OS/US/ITAE in two-area non-reheat thermal system at $\Delta P_{d1} = 0.01$ puMW with GNA optimized controllers										
Controller structure	ST (sec)			US (-ve) (Hz)		US (-ve) (puMW)	OS (Hz)		OS (puMW)	J
	ΔF_1	ΔF_2	ΔP_{tie12}	ΔF_1	ΔF_2	ΔP_{tie12}	ΔF_1	ΔF_2	ΔP_{tie12}	ITAE
GNA:PI	5.3	6.2	4.17	0.022	0.015	0.0052	0.0042	0.0013	0.0000127	0.0798
GNA:PID	1.02	1.86	1.13	0.00675	0.00202	0.00074	0.000127	0.0000053	0.0000036	0.0054
GNA:2DOF-PID	0.62	2.2	1.65	0.00382	0.00049	0.000335	0.0000286	0.0000043	0.00000213	0.0040

band of ± 0.0005 while $\Delta F_2/\Delta P_{tie12}$ both are measured with tolerance band of ± 0.0002 (2% band). Analysis shows that the values of ITAE, STs, USs, and OSs are the least, with GNA:2DOF-PID controller in contrast to GNA:PI/PID controllers. Therefore, in contrast to PI/PID controllers, 2DOF-PID controllers are further proficient to offer enhancement with lower STs, USs, and OSs values.

For GNA:2DOF-PID controller the values of STs, USs, OSs and ITAE for ΔF_1 response with non-reheat thermal system are 0.62 sec, -0.00382 Hz, 0.0000286 Hz and 0.0040 , respectively, while these values for ΔF_2 response are 2.2 sec, -0.00049 Hz, 0.0000043 Hz and 0.0040 , respectively. For ΔP_{tie12} the STs, USs, OSs are 1.65 sec, -0.000335 Hz, 0.00000213 Hz. For GNA:PID controller the values of STs, USs, OSs and ITAE for ΔF_1 response are 1.02 sec, -0.00675 Hz, 0.000127 Hz and 0.0054 , respectively, while these values for ΔF_2 response in PS are 1.86 sec, -0.00202 Hz, 0.0000053 Hz and 0.0054 respectively. For ΔP_{tie12} the STs, USs, OSs are 1.13 sec, -0.00074 Hz, 0.0000036 Hz. For GNA:PI biggest/worst values are obtained. We see that all values are better with 2DOF-PID compared to others except ST of ΔF_2 and ΔP_{tie12} . Hence, in overall, 2DOF-PID can be recommended to offer a better outcome in AGC of multi-area thermal PSs.

5.6 Conclusion

For two-area PSs' AGC a GNA tuned 2DOF-PID controller is employed. Dynamic response of ΔF_1 with GNA:2DOF-PID has least ST/US/OS and ITAE compared to GNA optimized PI/PID controllers. Similarly dynamic response of $\Delta F_2/\Delta P_{tie12}$ has minimum US/OS compared to GNA optimized PI/PID controllers. It can be concluded from the AGC of multi-area thermal PSs that 2DOF-PID controller out performs the PI/PID.

CHAPTER 6

MULTI-SOURCE MULTI-AREA POWER SYSTEM WITH OPTIMIZED FOPTID+1 CONTROLLER

6.1 Introduction

Persistent evolution in size and complication of PSs, variation in load power demands, deviations in electric system structures and system modeling errors has made necessity of a stable AGC in PSs. As a result, researchers all around the world are working to actively address the AGC problem by recommending novel control mechanisms from a variety of sources. Numerous optimization and control methods, including the classical control, approach bacterial foraging optimization (BFOA) reliant I/PI/PID/IDD [9], differential evolution (DE) reliant PID [26], hybrid stochastic fractal search and pattern search (hSFS-PS) technique reliant PI/PID [27], The TLBO algorithm-tuned PID controller is utilized to efficiently regulate PS fluctuations [28], etc.

Due to its exceptional design performance and added flexibility, fractional calculus (FC) based control techniques have garnered increasing attention in recent years for research. A mathematical idea is called fractional order calculus (FOC). Due to a lack of computational tools and limited physical restrictions over the past 20 years, FOC has not been widely used in control engineering. Researchers have observed in recent years that FO differential equations, as opposed to integer order ones, could more accurately simulate a variety of materials. Using FC, an extension of the integer order PID (IOPID) controller is the FOPID controller. Design of a FOPID controller involves obtaining differential, integrating/differential, integral, and proportional orders. The evolutionary algorithms like, ICA [17], hybrid ALO [19] were used to optimize FO controller. Some

fractional order controllers are implemented in cascaded form such as sine-cosine (SCA) [29] algorithm optimized FO cascade controller (FOPI-FOPID) and FOPI-FOPID in [30], whale optimization [39], improved particle swarm optimization (IPSO) [40] are used in tuning the FO controllers. In context to FO, a diversity of optimization algorithms are present in literature [41,47,51,54,55]. The FO controllers have been observed expedient in AGC incorporating RESs in [58,61]. When the FOC technique is used to regulate an industrial process, multiple advantages are seen, including: robustness to variations in the plant's gain, lack of steady-state error, good rejection of output fluctuations, robustness to high-frequency noise etc.

Given the aforementioned, an effort has been implemented in this chapter to carry out a FOPTID+1 controller for multi-area, multi-source THG PSs' AGC. The controller gains, such as the order of integrator (λ , n), and the order of differentiator (μ), are optimized through GNA.

6.2 Systems Investigated

Studies are accomplished on a multi-source multi-area THG PS without GDB/GRC using GNA tuned 2DOF-PID controller and GNA tuned FOPTID+1 controllers. Both areas of THG PS own one reheat thermal unit, one hydro unit, and one gas generating unit in its each area connected with tie-lines. Each section has a 2000 MW rated capacity, with a 1000 MW initial loading. Further research is stretched on multi-source multi-area THG PS with GDB/GRC. The model of the PSs examined is shown in Fig. 6.2, Fig. 6.4, Fig. 6.6. The Appendix contains the nominal parameters of the PSs, while the Nomenclature section includes the set of symbols.

6.3 FO Proportional Tilt Integral Derivative+1 (FOPTID+1) Controller

FOPTID+1 controller is used in the AGC of PSs first time. The literature has documented numerous instances of the FOPID controller being used in the AGC of different systems. Through FC, the FO controller theory addresses differential equations. The literature has documented numerous instances of the FOPID controller being used in the AGC of different systems. Differential equations are applied through FC, in the FO controller theory. The Fractional Calculus (FC) is the name given to the elaboration of the ordinary calculus. The concept of $d^n y(t)/dt^n$, which is an integer number, is expanded to $d^\alpha y(t)/dt^\alpha$, where α is a non-integer number, with the intention of becoming complex. Numerous definitions, including the Cauchy integral formula, the Riemann-Liouville definition, are available in the literature to illustrate the FO function. In FO calculus, however, the Riemann-Liouville formulation described in Eqn. (6.1) is typically applied [261].

$${}_a D_t^\alpha f(t) = \frac{1}{\Gamma(n-\alpha)} \frac{d^n}{dt^n} \int_a^t (t-\tau)^{n-\alpha-1} f(\tau) d\tau \quad (6.1)$$

Where, $n-1 > \alpha < n$, n is an integer and symbol $\Gamma(\cdot)$ represents Euler's gamma function and is described by Eqn. (6.2).

$$\Gamma(x) = \int_0^\infty e^{-t} t^{(x-1)} dt, \quad x > 0, \quad (6.2)$$

with unique case when $x = n$,

$$\Gamma(n) = (n-1)(n-2) \cdots (2)(1) = (n-1)!. \quad (6.3)$$

For ease of understanding, the fractional differentiation-integration process is demonstrated using the Laplace domain idea. Eqn. (6.4) provides the Laplace transformation of Eqn. (6.1) for the fractional derivative under zero initial condition.

$$L\{{}_a D_t^\alpha f(t)\} = \int_0^\infty e^{-st} {}_a D_t^\alpha f(t) dt$$

$$= s^\alpha F(s) - \sum_{k=0}^{n-1} s^k a D_t^{\alpha-k-1} f(t) \Big|_{t=0} \quad (6.4)$$

The normal Laplace transform is denoted by $L\{f(t)\}$, while the Laplace transform of $f(t)$ is represented by $F(s)$. The $PI\lambda D\mu$ is the generic form of FOPID, and Eqn. (6.5) provides its TF.

$$G_c(s) = K_p + \frac{K_I}{s^\lambda} + K_D s^\mu \quad (6.5)$$

The FOPTID+1 controller TF is defined by Eqn. (6.6).

$$G_{\text{FOPTID+1}}(s) = \left[1 + \left(K_p + \frac{K_T}{s^{1/n}} + \frac{K_I}{s^\lambda} + K_D s^\mu \right) \right] \quad (6.6)$$

Where, proportional, integral, derivative, and tilt-integral gains are represented respectively by K_P , K_I , K_D , and K_T . The order of integration and differentiation is indicated by λ , μ , and n is a non zero real number. Therefore, instead of just five design parameters needed for a FOPID structured controller, seven design parameters are needed for a FOPTID+1 controller structure. The FOPTID+1 orders $\lambda/\mu/n$ and require the proper $K_P/K_I/K_D/K_T$ design. In essence, the orders are any real number rather than an integer.

An ordinary TF would designate poles and zeroes in order of infinite number to appropriately resemble a fractional transfer function. Nonetheless, to obtain an approximate solution using a finite number of poles-zeroes, Oustaloup's CRONE approximation [262] can be applied. Using a higher order filter with an order of $2N + 1$, Oustaloup's recursive distribution gives an excellent estimation of the FO element s^α specified by Eqn. (6.6) in a range of definite frequency band $[\omega_L, \omega_H]$.

$$G_f(s) = s^\alpha = K \prod_{k=-N}^N \frac{s + \omega'_k}{s + \omega_k} \quad (6.6)$$

Where, α is the order of differentiation-integration and $0 < \alpha < 1$, The filter's order is $(2N + 1)$. The gain, denoted as K , ω_k' and ω_k are the zeros/poles of the analog filter, are derived iteratively in the following manner:

$$K = \omega_H^\alpha \quad (6.7)$$

$$\omega_k' = \omega_L \left(\frac{\omega_H}{\omega_L} \right)^{\frac{k + N + \frac{1}{2}(1-\alpha)}{2N + 1}} \quad (6.8)$$

$$\omega_k = \omega_L \left(\frac{\omega_H}{\omega_L} \right)^{\frac{k + N + \frac{1}{2}(1+\alpha)}{2N + 1}} . \quad (6.9)$$

K is changed to give the approximation of a unit gain at a frequency of one rad/s. An important factor that determines the success of the approximation is the selection of N . Low values of N can lead to easier hardware execution and simpler approximations, but the approximations deteriorate as a result of ripple generation in phase and magnitude responses. These waves are eliminated by incrementing N , but doing so will convert the approximation more complex, thereby the hardware implementation is more difficult. The frequency range $[\omega_L, \omega_H]$ is selected as $[10^{-2}, 10^2]$ and $N = 3$ to investigate this study.

6.4 Optimization Problem

According to Eqns. 5.10/(6.11) [26–27], AGC problem under consideration is solved by minimization of the objective function (J) denoted with ITAE.

$$J = \int_0^t t \left(|\Delta F_1| + |\Delta F_2| + |\Delta P_{tie}| \right) dt \quad (6.11)$$

The controller parameter limitations are the problem restraints. Consequently, a challenge to design the FOPTID controller gains with optimization for problem solutions. Every multi-area system's FOPTID+1 controller has seven parameters that need to be

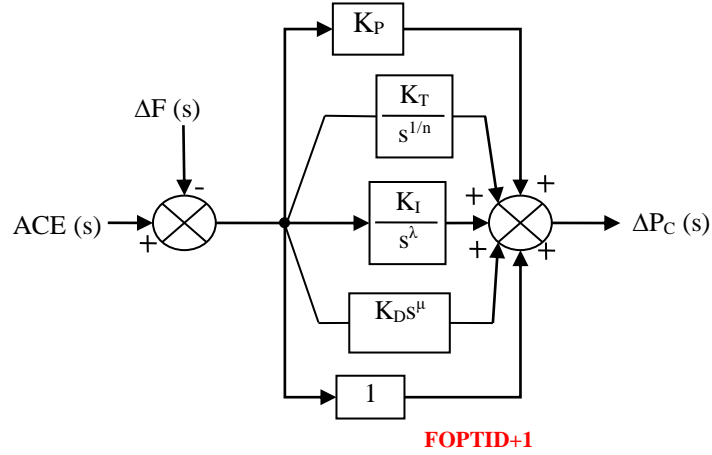


Fig. 6.1 Structure of FOPTID+1 controller.

optimized. The following constraints can be used to define the optimization issue as minimizing J:

$$\begin{aligned}
 K_P^{\min} &\leq K_P \leq K_P^{\max} \\
 K_I^{\min} &\leq K_I \leq K_I^{\max} \\
 K_D^{\min} &\leq K_D \leq K_D^{\max} \\
 \lambda^{\min} &\leq \lambda \leq \lambda^{\max} \\
 \mu^{\min} &\leq \mu \leq \mu^{\max} \\
 K_T^{\min} &\leq K_T \leq K_T^{\max} \\
 n^{\min} &\leq n \leq n^{\max}
 \end{aligned} \tag{6.12}$$

The minimum and maximum values of the parameters are K_P [0 to 5], K_I [0 to 5], K_D [0 to 5], λ [0 to 1], μ [0 to 1], K_T [0 to 5], n [1 to 3], respectively. Errors in control areas-1 and 2, denoted with ACE_1 and ACE_2 respectively specified by Eqns. (6.13) and (6.14) [28].

$$ACE_1(s) = \beta_1 \Delta F_1(s) + \Delta P_{tie_{12}}(s) \tag{6.13}$$

$$ACE_2(s) = \beta_2 \Delta F_2(s) + a_{12} \Delta P_{tie_{12}}(s) \tag{6.14}$$

6.5 Simulation Results and Discussions

6.5.1. Multi-Area Thermal-Hydro-Gas System with GNA Tuned 2DOF-PID and FOPTID+1 Controllers

Using the data in the Appendix, a multi-area i.e., two-area THG PS is simulated, taking into account a 1% SLP at $t = 0$ sec in each regions. Fig. 6.2 portrays the THG units in the PS and situation of SLP inputs. Fig. 6.3 portrays the comparison of proposed GNA tuned FOPTID+1 controller and GNA tuned 2DOF-PID controller investigated THG PS. Figs. 6.3(a-c) portray the dynamic results of investigated PS for ΔF_1 , ΔF_2 and $\Delta P_{tie_{12}}$ responses. Table 6.1 provides the tuned parameters of the recommended controller. It is abundantly evident through dynamic response that, in contrast to the GNA:2DOF-PID controller, the suggested GNA tuned FOPTID+1 controller exhibits significant improvements in PSs. The dynamic response mathematical values of ITAE performance index and STs/USs/OSs are shown in Table 6.2. Numerical values with the GNA optimized FOPTID+1 controller are evident from Table 6.2, smaller ITAE (0.0234), STs ($\Delta F_1 = 1.095$, $\Delta P_{tie_{12}} = 2.20$) and OSs ($\Delta F_1 = 0.000077$, $\Delta F_2 = 0.0000207$, $\Delta P_{tie_{12}} = 0.000008$) are obtained compared to GNA optimized 2DOF-PID controller. However, ST ($\Delta F_2 = 3.82$) and USs ($\Delta F_1 = -0.011$, $\Delta F_2 = -0.00427$, $\Delta P_{tie_{12}} = -0.00125$) are inferior compared to GNA optimized 2DOF-PID controller. But, in overall, we can say that

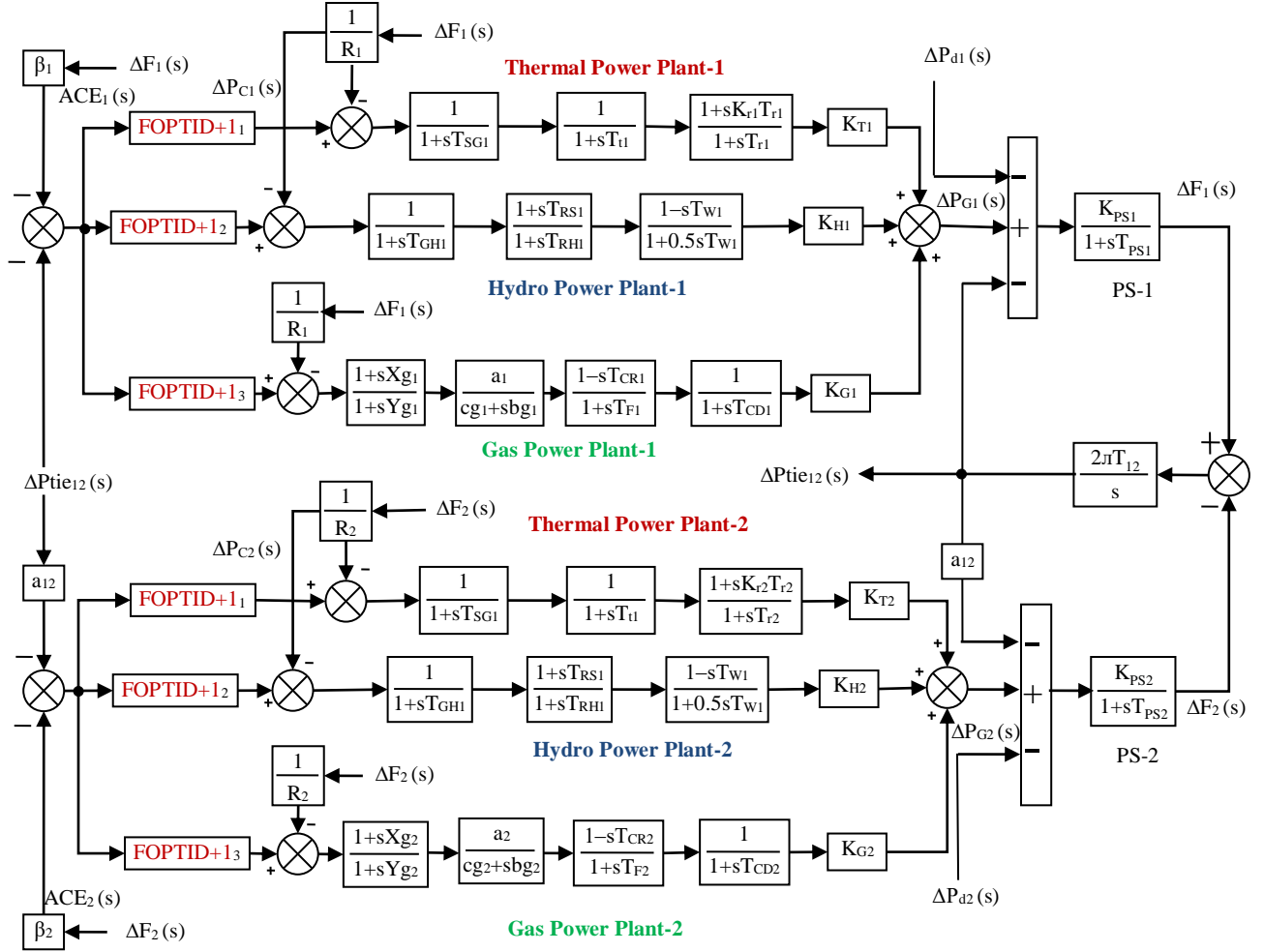


Fig. 6.2 Two-area THG system with FOPTID+1 controller.

Table 6.1 Tuned parameters of two-area THG system without GDB/GRC with GNA optimized controllers.									
Controller type	K_{P_i}	K_{I_i}	K_{D_i}	PW_i	DW_i	λ_i	μ_i	K_{T_i}	n_i
GNA:2DOF-PID	K_{P_1}	K_{I_1}	K_{D_1}	PW_1	DW_1	λ_1	μ_1	K_{T_1}	n_1
	1.4673	2.9375	2.1645	3.6640	1.3032	-	-	-	-
	K_{P_2}	K_{I_2}	K_{D_2}	PW_2	DW_2	λ_2	μ_2	K_{T_2}	n_2
	3.2259	2.7475	0.7883	3.4241	2.400	-	-	-	-
GNA:FOPTID+1	K_{P_3}	K_{I_3}	K_{D_3}	PW_3	DW_3	λ_3	μ_3	K_{T_3}	n_3
	1.4096	3.8593	1.5284	4.9204	4.3314	-	-	-	-
	K_{P_1}	K_{I_1}	K_{D_1}	PW_1	DW_1	λ_1	μ_1	K_{T_1}	n_1
	4.7755	3.8004	4.4043	-	-	0.2375	0.9397	2.5992	1.0272
GNA:FOPTID+1	K_{P_2}	K_{I_2}	K_{D_2}	PW_2	DW_2	λ_2	μ_2	K_{T_2}	n_2
	0.9156	4.4523	0.8350	-	-	0.4252	0.3269	2.8076	1.5676
	K_{P_3}	K_{I_3}	K_{D_3}	PW_3	DW_3	λ_3	μ_3	K_{T_3}	n_3
3.3521	1.9584	3.1068	-	-	0.9652	0.8285	4.1346	1.8134	

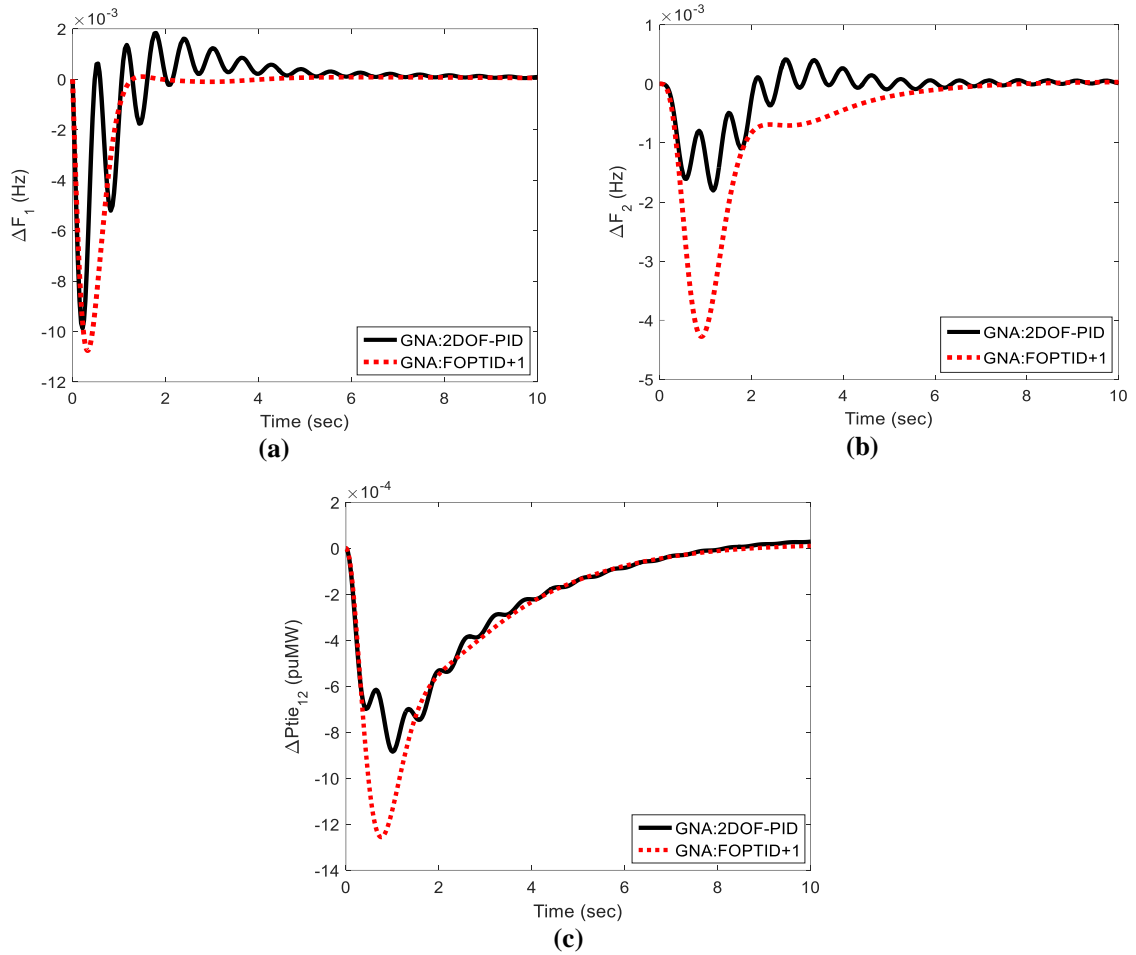


Fig. 6.3 Two-area THG system responses: (a) ΔF_1 , (b) ΔF_2 , and (c) $\Delta P_{tie_{12}}$.

Controller structure	ST (sec)			US (-ve) (Hz)		US (-ve) (puMW)	OS (Hz)		OS (puMW)	J
	ΔF_1	ΔF_2	$\Delta P_{tie_{12}}$	ΔF_1	ΔF_2	$\Delta P_{tie_{12}}$	ΔF_1	ΔF_2	$\Delta P_{tie_{12}}$	ITAE
GNA:2DOF-PID	4.36	1.95	2.31	0.0099	0.0018	0.00088	0.00181	0.000411	0.000029	0.0244
GNA:FOPTID+1	1.095	3.82	2.20	0.011	0.00427	0.00125	0.000077	0.0000207	0.000008	0.0234

response with FOPTID+1 controller is enhanced over 2DOF-PID controller in terms of fast and oscillation less results and less ITAE. Hence, further study is conducted with GNA optimized FOPTID+1 controller.

6.5.2. Comparison with Other Controllers

Research is stretched on a multi-source THG PS without nonlinearities with GNA optimized FOPTID+1 controller as shown in Fig. 6.2. Table 6.3 illustrates the optimized parameters of the suggested controller. Figs. 6.3(a-c) Portrays the dynamic results of PS studied for ΔF_1 , ΔF_2 , and $\Delta P_{tie_{12}}$ responses. Critical scrutiny of responses clearly exposes that considerable improvement is observed with the projected GNA tuned FOPTID+1 controller compared to DE:PID [26], hSFS-PS:PID [27], TLBO:PID [28], and GNA optimized PID/FOPID controllers.

The controllers' performance for a tolerance band of ± 0.0005 is also investigated using performance index (PI) denoted with ITAE given in Table 6.4. It clearly depicts the mathematical values of STs/USs/OSs and performance index, ITAE. Table 6.4 depicts values of GNA optimized PID controller as ITAE (0.047), STs ($\Delta F_1 = 4.9$, $\Delta F_2 = 2.40$, $\Delta P_{tie_{12}} = 2.32$), USs ($\Delta F_1 = -0.012$, $\Delta F_2 = -0.0047$, $\Delta P_{tie_{12}} = -0.00136$) and OSs ($\Delta F_1 = 0.00122$, $\Delta F_2 = 0.000340$, $\Delta P_{tie_{12}} = 0.000118$) while these values with GNA optimized

Controller type	K_{T1}	n_1	K_{P1}	K_{I1}	K_{D1}	λ_1	μ_1
GNA:PID	K_{T1}	n_1	K_{P1}	K_{I1}	K_{D1}	λ_1	μ_1
	-	-	4.7273	4.5144	4.6174	-	-
	K_{T2}	n_2	K_{P2}	K_{I2}	K_{D2}	λ_2	μ_2
	-	-	4.7522	0.3409	1.6493	-	-
	K_{T3}	n_3	K_{P3}	K_{I3}	K_{D3}	λ_3	μ_3
-	-	4.6742	5.2648	1.3591	-	-	
GNA:FOPID	K_{T1}	n_1	K_{P1}	K_{I1}	K_{D1}	λ_1	μ_1
	-	-	4.3785	4.6327	4.1441	0.4962	0.9697
	K_{T2}	n_2	K_{P2}	K_{I2}	K_{D2}	λ_2	μ_2
	-	-	1.0035	4.6215	0.5661	0.9643	0.5380
	K_{T3}	n_3	K_{P3}	K_{I3}	K_{D3}	λ_3	μ_3
-	-	4.5340	3.2785	0.0047	0.4701	0.5190	
GNA:FOPTID+1	K_{T1}	n_1	K_{P1}	K_{I1}	K_{D1}	λ_1	μ_1
	2.5992	1.0272	4.7755	3.8004	4.4043	0.2375	0.9397
	K_{T2}	n_2	K_{P2}	K_{I2}	K_{D2}	λ_2	μ_2
	2.8076	1.5676	0.9156	4.4523	0.8350	0.4252	0.3269
	K_{T3}	n_3	K_{P3}	K_{I3}	K_{D3}	λ_3	μ_3
4.1349	1.8134	3.3521	1.9584	3.1068	0.9652	0.8285	

FOPID controller, ITAE (0.044), STs ($\Delta F_1 = 2.85$, $\Delta F_2 = 4.95$, $\Delta P_{tie_{12}} = 3.67$), USs ($\Delta F_1 = -0.011$, $\Delta F_2 = -0.00536$, $\Delta P_{tie_{12}} = -0.00158$) and OSs ($\Delta F_1 = 0.000059$, $\Delta F_2 = 0.0000518$, $\Delta P_{tie_{12}} = 0.000021$). The lowest values are with GNA optimized FOPTID+1 controller, ITAE (0.0234), STs ($\Delta F_1 = 1.095$, $\Delta F_2 = 3.82$, $\Delta P_{tie_{12}} = 2.20$), USs

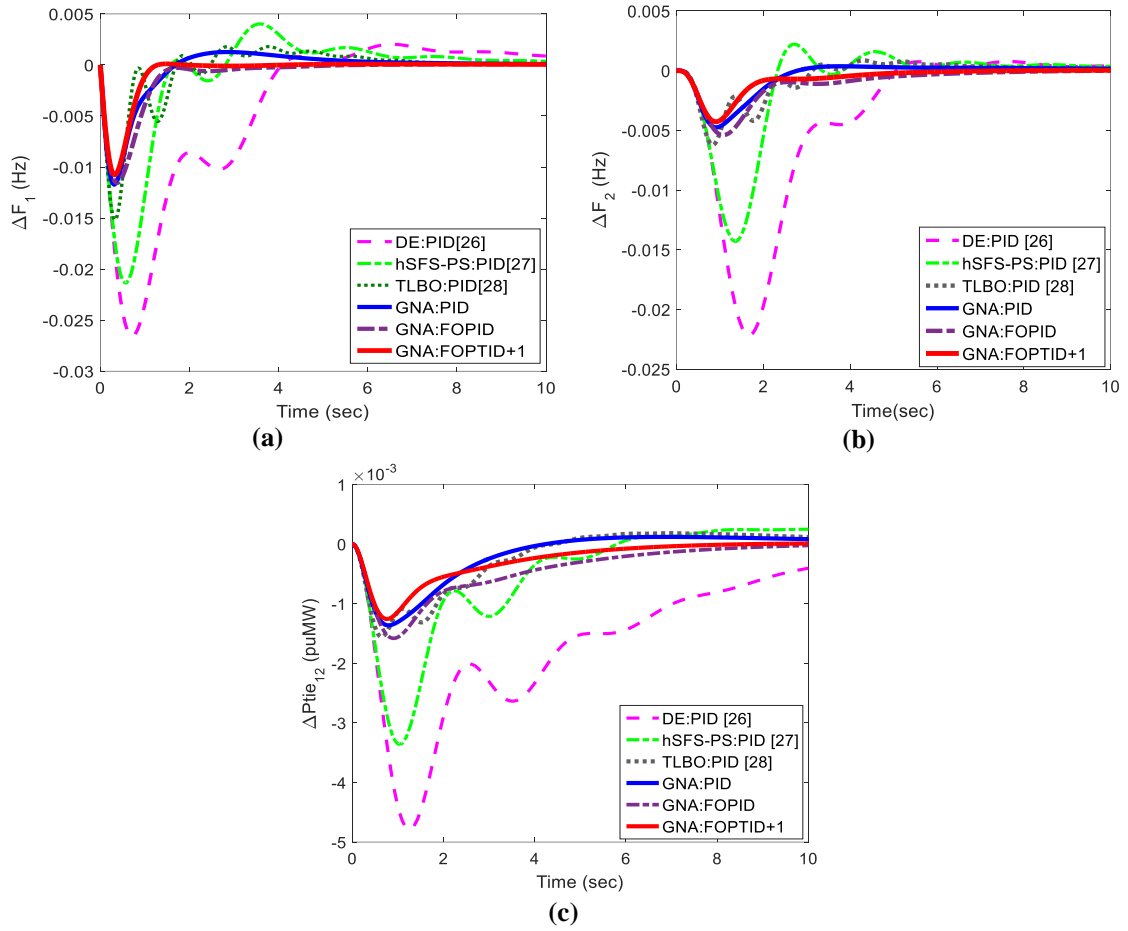


Fig. 6.4 Two-area THG system responses: (a) ΔF_1 , (b) ΔF_2 , and (c) $\Delta P_{tie_{12}}$.

Controller structure	ST (sec)			US (-ve) (Hz)		US (-ve) (puMW)	OS (Hz)		OS (puMW)	J
	ΔF_1	ΔF_2	$\Delta P_{tie_{12}}$	ΔF_1	ΔF_2	$\Delta P_{tie_{12}}$	ΔF_1	ΔF_2	$\Delta P_{tie_{12}}$	ITAE
DE:PID [26]	13.097	8.523	9.222	0.0258	0.0215	0.00471	0.00197	0.000764	0.000187	0.290
hSFS:PID [27]	8.58	7.34	3.885	0.0202	0.0134	0.00325	0.00392	0.00218	0.000246	0.129
TLBO:PID [28]	6.27	5.805	2.796	0.0139	0.0055	0.00155	0.00172	0.000825	0.000179	0.067
GNA:PID	4.9	2.40	2.32	0.012	0.0047	0.00136	0.00122	0.000340	0.000118	0.047
GNA:FOPID	2.85	4.95	3.67	0.011	0.00536	0.00158	0.000059	0.0000518	0.000021	0.044
GNA:FOPTID+1	1.095	3.82	2.20	0.011	0.00427	0.00125	0.000077	0.0000207	0.000008	0.0234

($\Delta F_1 = -0.011$, $\Delta F_2 = -0.00427$, $\Delta P_{tie_{12}} = -0.00125$) and OSs ($\Delta F_1 = 0.000077$, $\Delta F_2 = 0.0000207$, $\Delta P_{tie_{12}} = 0.000008$). The GNA optimized FOPTID+1 controller outperforms the other techniques, according to the results. Table 6.4 shows that the following is the sequence in which the performance is improving: GNA:FOPTID+1 \rightarrow GNA:FOPID \rightarrow GNA:PID \rightarrow TLBO:PID \rightarrow h-SFS:PID \rightarrow DE:PID.

6.5.3. Two-Area Thermal-Hydro-Gas System with GDB/GRC nonlinearities

Further research is stretched on a two-area THG system with nonlinearities like GDB/GRC as shown in Fig. 6.5. One hydro power plant, one gas plant, and one reheat thermal unit are owned by each control area. The closed loop GRC limitations for thermal units are owned by each control area. The closed loop GRC limitations for thermal units are set at $\pm 10\%$ /minute. For hydro units, the GRC (open loop) for raising and lowering the generation is 270%/minute and 360%/minute, respectively. For the hydro unit, 0.02% is selected as the GDB limit. The generalized TFM of the governor incorporates the GDB effect in the thermal unit while accounting for non-linearities. GDB and GRC modeling are described in detail in Chapter 3. The PS parameters are portrayed in the Appendix. Tuned parameters of the suggested controller are given in Table 6.5. Figs. 6.6(a-c) portrays PS dynamic response for ΔF_1 , ΔF_2 , and $\Delta P_{tie_{12}}$. A critical analysis of the answers makes it abundantly evident that, as compared to IPSO:PID/TID/FOPID [40] and PFA:PID/TID/FOTID [41] controllers, significant improvements are shown with the suggested GNA adjusted FOPTID+1 controller. The ITAE, as presented in Table 6.6, is used to evaluate the controller performance for a tolerance band of ± 0.0005 . It depicts the mathematical values of STs/USs/OSs and ITAE respectively. The values of ITAE, STs/USs/OSs with GNA optimized FOPTID+1

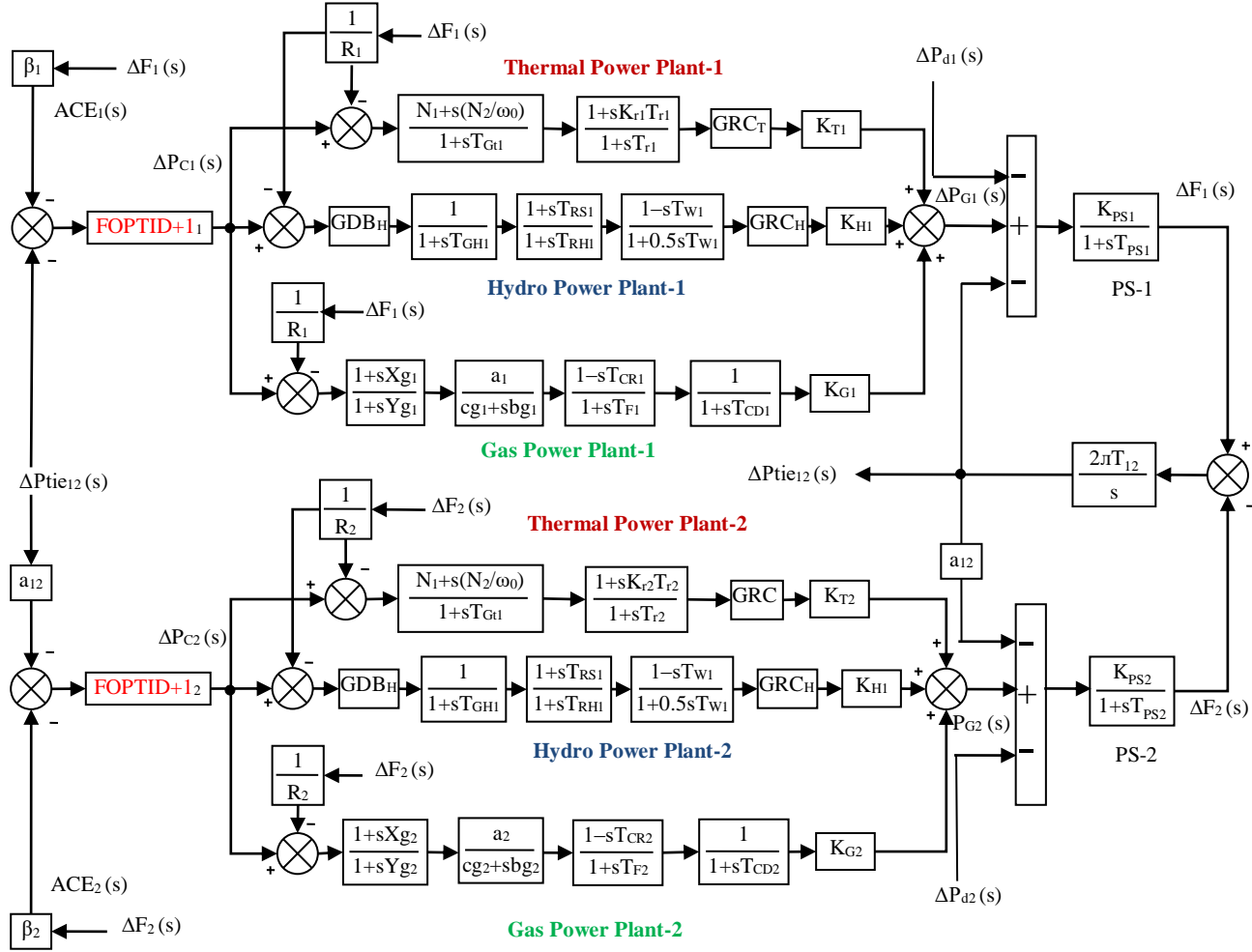


Fig. 6.5 Multi-area THG PS with GDB/GRC and FOPTID+1 controller.

controller are ITAE (0.1107), STs ($\Delta F_1 = 5.05$, $\Delta F_2 = 6.14$, $\Delta P_{tie12} = 4.85$), USs ($\Delta F_1 = -0.0200$, $\Delta F_2 = -0.0170$, $\Delta P_{tie12} = -0.00292$) and OSs ($\Delta F_1 = 0.0042$, $\Delta F_2 = 0.0049$, $\Delta P_{tie12} = 0.000021$). While the values of ITAE, STs/USs/OSs with IPSO optimized FOPID controller are, ITAE (0.4677), STs ($\Delta F_1 = 10.53$, $\Delta F_2 = 10.35$, $\Delta P_{tie12} = 5.38$), USs ($\Delta F_1 = -0.034$, $\Delta F_2 = -0.031$, $\Delta P_{tie12} = -0.0056$) and OSs ($\Delta F_1 = 0.0076$, $\Delta F_2 = 0.0070$, $\Delta P_{tie12} = 0.00065$). The values of ITAE, STs/USs/OSs with PFA optimized FOTID controller are, ITAE (0.4796), STs ($\Delta F_1 = 11.32$, $\Delta F_2 = 10.8$, $\Delta P_{tie12} = 8.14$), USs ($\Delta F_1 = -0.025$, $\Delta F_2 = -0.022$, $\Delta P_{tie12} = -0.00435$) and OSs ($\Delta F_1 = 0.011$, $\Delta F_2 = 0.014$,

$\Delta P_{tie_{12}} = 0.00323$). This proves the superiority of GNA optimized FOPTID+1 controller over the others. Table 6.6 depicts the improvement in the controller performance as: GNA:FOPTID+1 \rightarrow PFA:FOTID \rightarrow IPSO:FOPID.

Table 6.5
Tuned parameters of two-area THG system with GDB /GRC with GNA optimized FOPTID+1 controller.

Controller type	K_{Ti}	n_i	K_{Pi}	K_{Ii}	K_{Di}	λ_i	μ_i
IPSO:FOPID [40]	K_{T1}	n_1	K_{P1}	K_{I1}	K_{D1}	λ_1	μ_1
	-	-	0.8615	1.8463	1.9990	0.6494	0.9990
	K_{T2}	n_2	K_{P2}	K_{I2}	K_{D2}	λ_2	μ_2
	-	-	0.0510	0.3561	1.6478	0.4003	0.9826
PFA:FOTID [41]	K_{T1}	n_1	K_{P1}	K_{I1}	K_{D1}	λ_1	μ_1
	2.0000	3.0000	-	1.9943	1.3884	1.0001	1.3646
	K_{T2}	n_2	K_{P2}	K_{I2}	K_{D2}	λ_2	μ_2
	0.0012	2.9537	-	0.3572	1.9997	0.0008	1.2693
GNA:FOPTID+1	K_{T1}	n_1	K_{P1}	K_{I1}	K_{D1}	λ_1	μ_1
	1.5210	2.7448	1.7940	3.2377	2.9453	0.4890	1.3043
	K_{T2}	n_2	K_{P2}	K_{I2}	K_{D2}	λ_2	μ_2
	1.3494	1.8519	1.9710	1.0164	2.8209	0.7161	1.1277

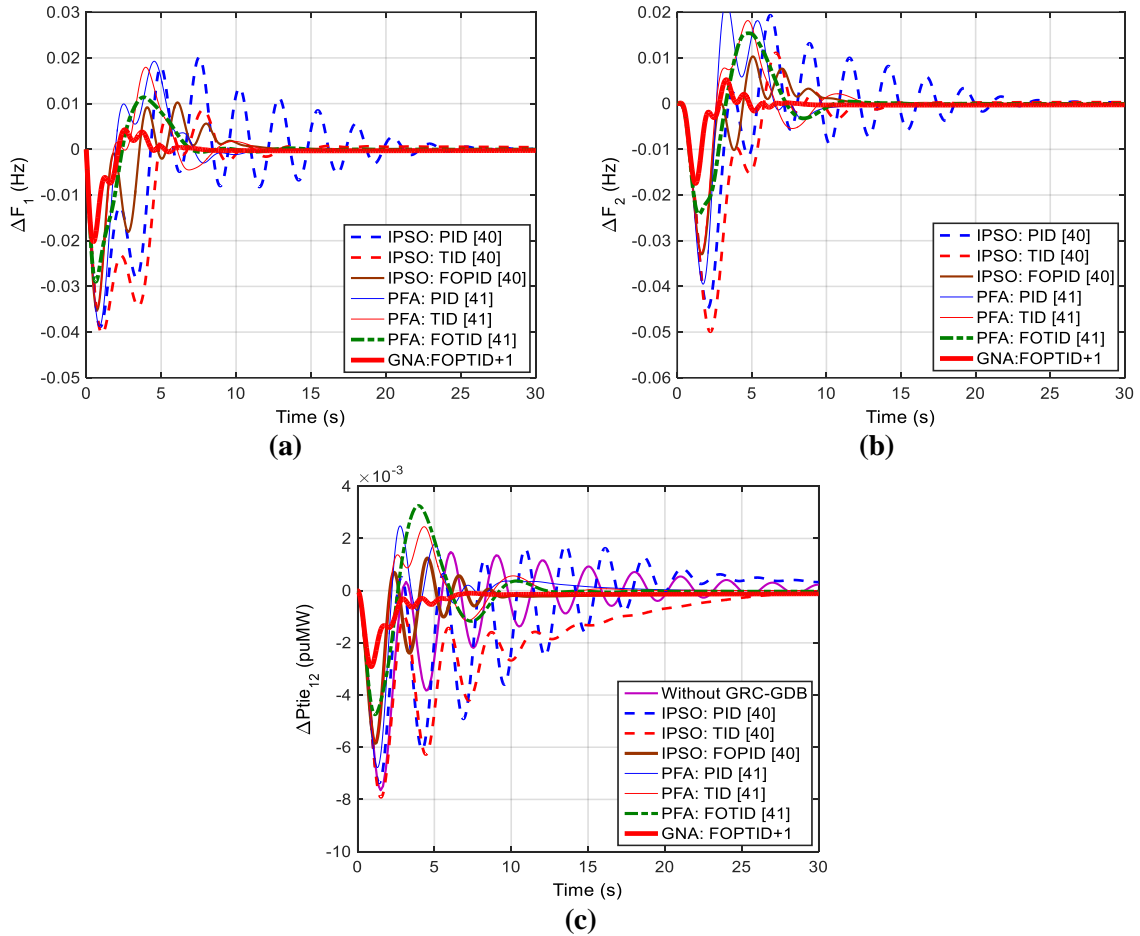


Fig. 6.6 Two-area THG system responses with GDB/GRC: (a) ΔF_1 , (b) ΔF_2 , and (c) $\Delta P_{tie_{12}}$.

Table 6.6 ST/OS/US/ITAE in two-area THG system with GDB/GRC at $\Delta P_{d1} = 0.01$ puMW with GNA optimized FOPTID+1 controller.										
Controller structure	ST (sec)			US (-ve) (Hz)		US (-ve) (puMW)	OS (Hz)		OS (puMW)	J
	ΔF_1	ΔF_2	$\Delta P_{tie_{12}}$	ΔF_1	ΔF_2	$\Delta P_{tie_{12}}$	ΔF_1	ΔF_2	$\Delta P_{tie_{12}}$	ITAE
IPSO: PID [40]	24.46	24.7	24.2	0.039	0.045	0.0074	0.021	0.020	0.00183	1.176
IPSO: TID [40]	14.28	13.75	21.8	0.040	0.049	0.0089	0.0078	0.0089	0.00017	0.9829
IPSO: FOPID [40]	10.53	10.35	5.38	0.034	0.031	0.0056	0.0076	0.0070	0.00065	0.4677
PFA: PID [41]	10.85	11.1	6.51	0.039	0.040	0.0067	0.019	0.023	0.00248	0.6469
PFA: TID [41]	8.96	10.9	9.01	0.034	0.031	0.00563	0.011	0.012	0.00212	0.4382
PFA: FOTID [41]	11.32	10.8	8.14	0.025	0.022	0.00435	0.011	0.014	0.00323	0.4796
GNA:FOPTID+1	5.05	6.14	4.85	0.0200	0.0170	0.00292	0.0042	0.0049	0.000021	0.1107

6.6 Conclusion

The proposed GNA optimized FOPTID+1 controller is recommended for a two-area THG PS without/with GDB/GRC. The performance obtained by the GNA optimized FOPTID+1 controller is clearly superior to that of the GNA optimized 2DOF-PID controller, as evidenced from outcomes. The suggested controller ensures improved dynamic performance over existing IPSO tuned PID/TID/FOPID, PFA tuned PID/TID/FOTID controllers, and GNA tuned PID/FOPID controllers. Consequently, the results establish that the proposed control strategy is effective, robust, and suitable for multiple PSs.

CHAPTER 7

GNA OPTIMIZED FOPI-FOPTID CONTROLLER

7.1 Introduction

To deal with the AGC problem of multi-source PS, new and intelligent control strategies are obligatory. Due to its exceptional design performance and added flexibility, fractional calculus (FC) based control techniques have garnered increasing attention in recent years for research purposes. However, cascaded control approach has shown remarkable performance in the control of AGC to stabilize the disturbances. Hence, a innovative cascade FO controller is designed in this chapter specified as fractional order PI (FOPI)-FO proportional tilt integral derivative (FOPI-FOPTID) controller to investigate the dynamic response of PSs. Single-area THG PS is employed initially with GNA optimized FOPTID+1 and FOPI-FOPTID controllers for comparison of frequency deviation response as well as tuning of controller gains. The analysis is focused on single-area and two-area HN/HNG PSs to demonstrate the quality and scalability of the strategy after a critical examination of single-area nuclear PS. The methodology's sovereignty is established for GNA optimized PID/FOPID/FOPI-FOPID controller by comparing the outcomes with PID controller optimized using ant colony optimization (ACO) [166]. Analyzing the data demonstrates that FOPI-FOPTID performs better in contrast to above controllers in terms of the smallest error criteria, OSs/USs/STs, and tie-line power variations during disturbances.

7.2 Systems Investigated

Further research is probed on a multi-source single-area THG PS without GDB/GRC using GNA optimized FOPTID+1 controller and GNA optimized cascaded FOPI-FOPTID controller. A THG PS own one THG unit in its single-area. Results for the dynamic response with GNA optimized cascaded FOPI-FOPTID controller are much better, so that it can be employed in multi-source single-area HN PS, single-area HNG, and two-area HN/HNG PS with / without GDB/GRC. Both areas of HNG PS own, one mechanical governor based hydro unit, one nuclear unit and one gas unit connected with tie-lines in its each area. PS has an initial loading of 1000 MW. However, the rated capacity of each area is 2000 MW. Figs. 7.2, 7.4, 7.6, 7.8, Fig. 10, and 7.12 display block diagrams of the systems under study. The Appendix contains the systems' nominal parameters, and the Nomenclature section contains the list of symbols.

7.3 Cascade FOPI-FOPTID Controller

The cascaded controllers (CC) like PI-PD [27] and FOPI-FOPD [29] validated superior performance compared to I/PI/PID conventional controllers. PID with filter (PIDN)-FOPD controller [47] validated superior performance compared to I/PI/PIDN controllers. An optimal cascaded fuzzy FOPI-FOPID (CFFOPI-FOPID) controller presented new stable and robust technique superior to other PID/FO controllers [203]. An optimized cascade form of tilt ID (TID) controller i.e., fractional-order ID-T (FID-T) controller for LFC of an interconnected PS incorporating RES in the form of distributed generation (DG) and EV is presented [246]. The FID-T works well over ID-T/I-TD/I-PD and TID controllers. The implementation of cascaded FOPI-FOPTID controller implemented in this study is used in the AGC of PSs first time.

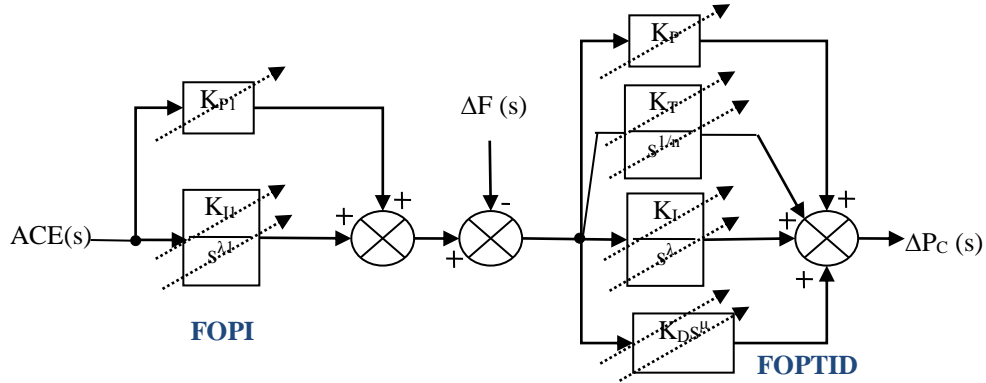


Fig. 7.1 Cascade FOPI-FOPTID controller structure.

The cascaded structure form of FOPI-FOPTID controller is shown in Fig. 7.1 and its TF of FOPI-FOPTID controller is defined by Eqn. (7.1).

$$G_{\text{FOPI-FOPTID}}(s) = \left[\left\{ \left(K_{P1} + \frac{K_{I1}}{s^{\lambda_1}} \right) - \Delta F(s) \right\} \times \left(K_P + \frac{K_T}{s^{1/n}} + \frac{K_I}{s^\lambda} + K_D s^\mu \right) \right] \quad (7.1)$$

Where, gains proportional, integral, derivative and tilt-integral, are denoted as K_P/K_{P1} , K_I/K_{I1} , K_D , K_T , respectively. λ/λ_1 , μ , and n indicate order of integration, order of differentiation, and an unknown positive integer, respectively. It is desirable to optimize ten design parameters in FOPI-FOPTID controller structure. It requires the appropriate design of $K_P/K_{P1}/K_I/K_{I1}/K_D/K_T$ and orders $\lambda/\lambda_1/\mu/n$. Any real numbers are assigned to the orders are however not integers.

7.4 Optimization Problem

The objective function (J) employed single/two-area PS is ITAE as stated in Eqns. (6.11)/(7.2). The controller parameter limitations are the problem restraints. AGC problem under consideration is solved by minimization of the objective function (J) denoted with ITAE.

$$J = \int_0^t t |\Delta F| dt \quad (1\text{-area}) \quad (7.2)$$

$$J = \int_0^t (|\Delta F_1| + |\Delta F_2| + |\Delta P_{tie_{12}}|) dt \quad (2\text{-area})$$

The following limits can be used to define the optimization issue as minimizing J:

$$\begin{aligned}
K_{P1}^{\min} &\leq K_{P1} \leq K_{P1}^{\max} \\
K_{I1}^{\min} &\leq K_{I1} \leq K_{I1}^{\max} \\
\lambda 1^{\min} &\leq \lambda 1 \leq \lambda 1^{\max} \\
K_P^{\min} &\leq K_P \leq K_P^{\max} \\
K_T^{\min} &\leq K_T \leq K_T^{\max} \\
n^{\min} &\leq n \leq n^{\max} \\
K_I^{\min} &\leq K_I \leq K_I^{\max} \\
\lambda^{\min} &\leq \lambda \leq \lambda^{\max} \\
K_D^{\min} &\leq K_D \leq K_D^{\max} \\
\mu^{\min} &\leq \mu \leq \mu^{\max}
\end{aligned} \tag{7.3}$$

The minimum and maximum values of the parameters are K_{P1} [0 to 5], K_{I1} [0 to 5], $\lambda 1$ [0 to 1], K_P [0 to 5], K_T [0 to 5], n [1 to 3], K_I [0 to 5], K_D [0 to 5], λ [0 to 1], μ [0 to 1], K_T [0 to 5], n [1 to 3], respectively. ACE_1 and ACE_2 of area-1 and area-2 are represented, respectively by Eqns. (6.13) and (6.14) in Chapter 6.

7.5 Simulation Results and Discussion

7.5.1. Single-Area Thermal-Hydro-Gas System

Using the data in the Appendix and accounting for a 1% SLP at $t = 0$ sec in both areas, a single-area THG system is simulated. The PS block diagram displayed in Fig. 7.2 clearly depicts the connections of thermal unit, hydro unit, gas unit and position of SLP inputs. Three FOPI-FOPTID cascaded controllers are applied with each plant in this model. Fig. 7.2 depicts the comparison of GNA optimized FOPTID+1 controller and GNA optimized FOPI-FOPTID controllers are presented in this section. Controller gains are depicted in Table 7.1. PS dynamic results of ΔF response are exposed in Fig. 7.3. It is inferred that

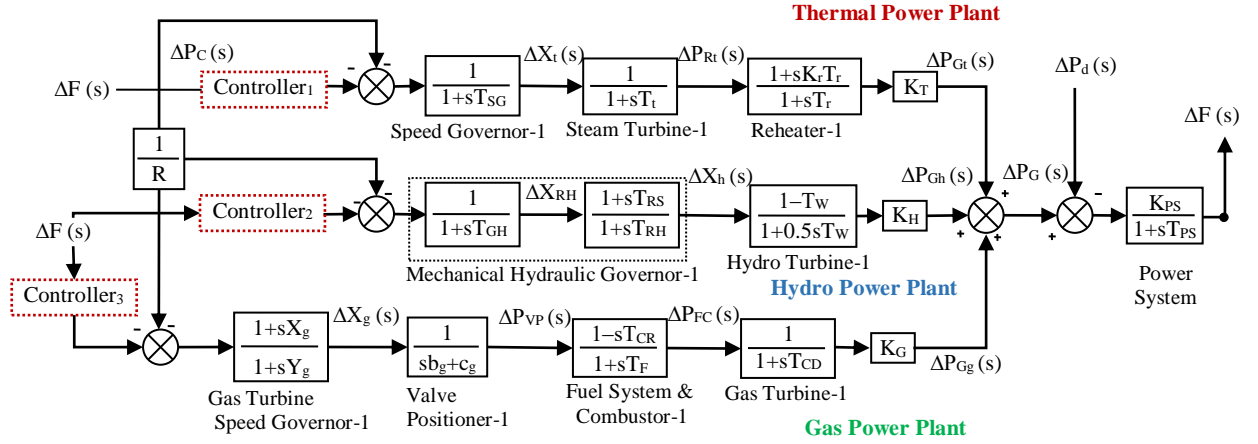


Fig. 7.2 Single-area THG system.

Table 7.1
Tuned parameters of single-area THG system with GNA optimized controllers.

Controller type	K_{Ii}	K_{Di}	λ_i	K_{Ti}	n_i	K_{Pi}	K_{Ii}	K_{Di}	λ_i	μ_i
GNA:FOPTID+1	K_{P4}	K_{I4}	λ_4	K_{T1}	n_1	K_{P1}	K_{I1}	K_{D1}	λ_1	μ_1
	-	-	-	4.3331	1.8018	0.0042	0.4014	4.5687	0.5655	0.8197
	K_{P5}	K_{I5}	λ_5	K_{T2}	n_2	K_{P2}	K_{I2}	K_{D2}	λ_2	μ_2
	-	-	-	3.9237	1.2135	0.0105	4.8913	3.9787	0.5139	0.1900
	K_{P6}	K_{I6}	λ_6	K_{T3}	n_3	K_{P3}	K_{I3}	K_{D3}	λ_3	μ_3
-	-	-	1.1250	1.0184	2.3630	4.9787	4.4989	0.8484	0.5190	
GNA:FOPI-FOPTID	K_{P4}	K_{I4}	λ_4	K_{T1}	n_1	K_{P1}	K_{I1}	K_{D1}	λ_1	μ_1
	0.5067	3.2856	0.0895	3.7045	1.7551	4.3714	2.5027	3.4571	0.8272	0.9999
	K_{P5}	K_{I5}	λ_5	K_{T2}	n_2	K_{P2}	K_{I2}	K_{D2}	λ_2	μ_2
	1.3277	3.9158	0.6931	0.8016	1.8535	1.5357	2.5558	0.7070	0.5988	0.9674
	K_{P6}	K_{I6}	λ_6	K_{T3}	n_3	K_{P3}	K_{I3}	K_{D3}	λ_3	μ_3
2.6324	3.9439	0.2917	3.7142	1.9355	1.7651	4.4996	2.9474	0.768	0.5431	

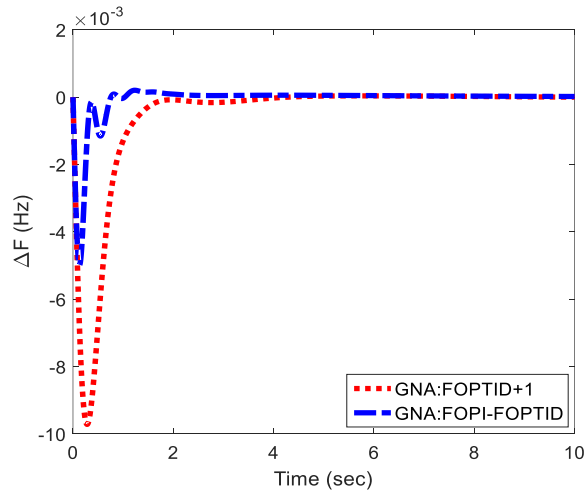


Fig. 7.3 Single-area THG system response (ΔF).

Type of controller	ST (sec)	US (Hz) (-ve)	OS (Hz)	ITAE
GNA:FOPTID+1	1.35	0.0096	0.0000386	0.0042
GNA:FOPI-FOPTID	0.67	0.0049	0.000207	0.0022

substantial enhancement is detected in the AGC of single-area THG PS with the FOPI-FOPTID controller compared to FOPTID+1 controller.

Table 7.2 depicts the dynamic responses of STs/USs/OSs and ITAE with the mathematical values. Table 7.2 infers that ITAE (0.0022), ST (0.67), US (0.0049) with FOPI-FOPTID controller are lesser than FOPTID+1 controller. This shows the superiority of the FOPI-FOPTID controller compared to FOPTID+1 controller. However, OS (0.000207) due to FOPI-FOPTID controller is more than FOPTID+1 controller. GNA optimized FOPI-FOPTID controller is proposed for single-area and multi-area PSs. This study is extended to single-area nuclear PSs and multi-area nuclear PSs.

7.5.2 Single-Area Nuclear Power System

The single-area nuclear PS model with one cascaded FOPI-FOPTID controller is displayed in Fig. 7.4. Table 7.4 infers the enhancement of responses with the suggested controller over existing ACO:PID structured controller [166].

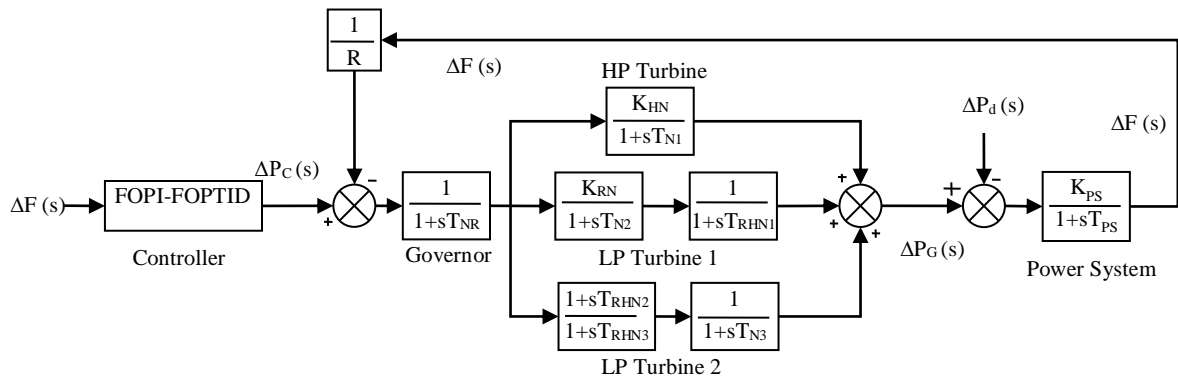


Fig. 7.4 Single-area nuclear system with GNA optimized FOPI-FOPTID controller.

Table 7.3										
Tuned parameters of single-area nuclear system with GNA optimized controllers.										
Controller type	K_{P1}	K_{I1}	λ_1	K_P	K_I	K_D	λ	μ	K_T	n
ACO:PID [58]	–	–	–	0.5100	0.9800	0.2000	–	–	–	–
GNA:PID	–	–	–	3.4959	5.9049	1.4596	–	–	–	–
GNA:FOPID	–	–	–	1.6012	4.9801	1.6020	0.8125	0.8952	–	–
GNA:FOPI - FOPID	-3.0261	-0.1771	-0.1771	1.7308	3.5652	2.330	0.6026	0.6601	–	–
GNA:FOPI - FOPTID	-3.8303	-1.7536	-1.7536	0.6516	3.2888	0.8818	0.5195	0.9090	4.6179	1.8499

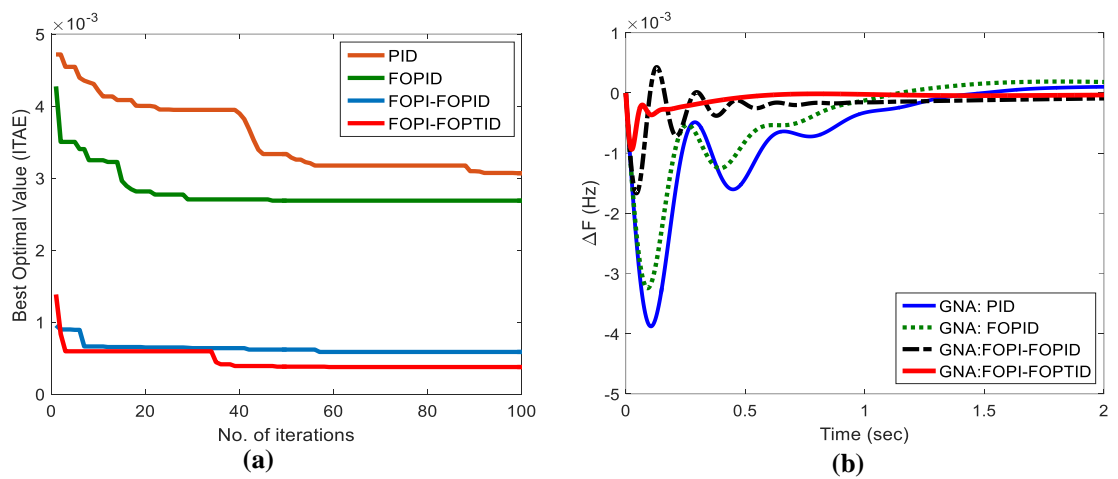


Fig. 7.5 Single-area nuclear system response: (a) Convergence curve and (b) ΔF .

Table 7.4				
ST/OS/US/ITAE in single-area nuclear system at $\Delta P_d = 0.001$ puMW.				
Controller structure	ST(sec)	OS (Hz)	US (-ve) (Hz)	ITAE
ACO: PID [166]	0.858	0.0004573	0.009838	0.020000
GNA: PID	0.775	0.00014700	0.0031680	0.003400
GNA: FOPID	0.860	0.00011630	0.0038770	0.003800
GNA: FOPI-FOPID	0.080	0.00038880	0.001668	0.00120
GNA: FOPI-FOPTID	0.046	0.00001240	0.000885	0.000412

It clearly depicts the connections of a nuclear unit and position of SLP input. The tuned parameters of the suggested, GNA:PID/FOPID/FOPI-FOPID, and ACO:PID [166] are given in Table 7.3. The convergence characteristic of ITAE with different controllers and system dynamic results of ΔF responses are shown in Figs. 7.5(a-b). It inferred with

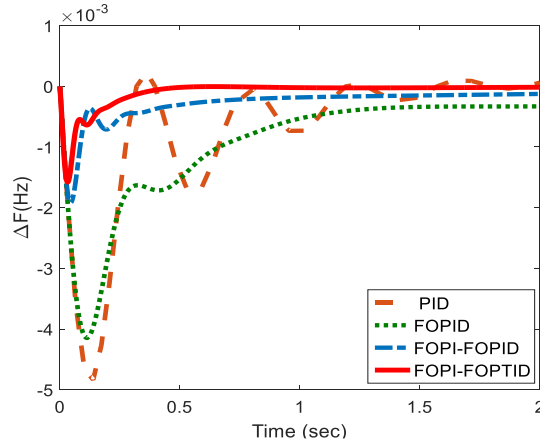


Fig. 7.7 Single-area hydro-nuclear (HN) system frequency deviation response (ΔF).

Table 7.6 ST/OS/US/ITAE in single-area hydro-nuclear system at $\Delta P_d = 0.01$ puMW.				
Controller structure	ST(sec)	OS (Hz)	US (-ve) (Hz)	ITAE
GNA:PID	1.08	0.0002250	0.00483	0.00620
GNA:FOPID	1.039	0.0000855	0.00414	0.00510
GNA:FOPI-FOPID	0.250	0.0000351	0.00192	0.00191
GNA:FOPI-FOPTID	0.145	0.0000156	0.00158	0.00064

It is inferred by responses that substantial enhancement is detected with GNA optimized FOPI-FOPTID controller over GNA optimized FOPI-FOPID, FOPID, and PID controllers. Table 7.6 depicts the mathematical values of the STs/USs/OSs, and ITAE. Table 7.6 reveals that with GNA optimized PID controller values are ST = 1.08 sec, OS = 0.0002250, US = 0.00483, ITAE = 0.00620, while these values with GNA optimized FOPID controller values are ST = 1.039 sec, OS = 0.0000855, US = 0.00414, ITAE = 0.00510.

GNA optimized FOPI-FOPID controller values are ST = 0.25 sec, OS = 0.0000351, US = 0.00192, ITAE = 0.00191. The values for GNA optimized FOPI-FOPTID controller are ST = 0.15 sec, OS = 0.0000156, US = 0.00158, ITAE = 0.00164. The dominance of the GNA optimized FOPI-FOPTID controller is revealed over the others. It is observed that the

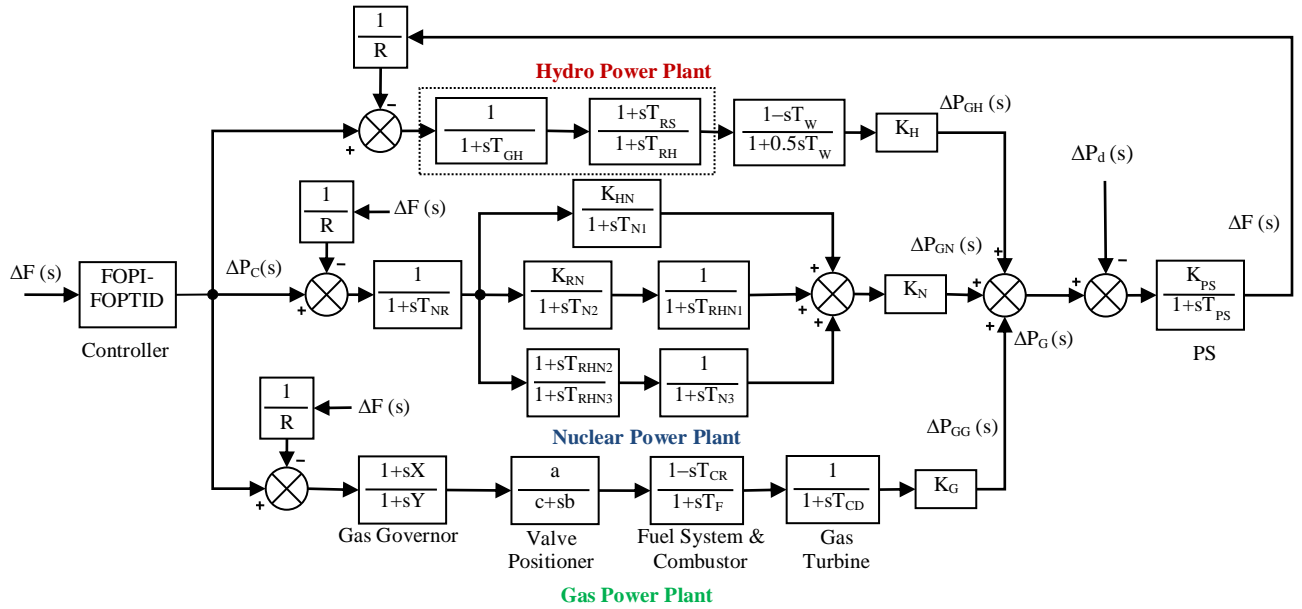


Fig. 7.8 Single-area HNG system.

Table 7.7 Tuned parameters of single-area HNG PS with GNA optimized FOPI-FOPTID controller.										
Controller used	K_{P1}	K_{I1}	$\lambda 1$	K_P	K_I	K_D	λ	μ	K_T	n
GNA:PID	–	–	–	4.8587	5.0392	1.8089	–	–	–	–
GNA:FOPID	–	–	–	3.2096	5.1775	1.6822	0.6008	1.1891	–	–
GNA:FOPI-FOPID	-0.2282	-2.0300	-0.0122	1.9026	3.5176	0.9770	0.6664	1.1150	–	–
GNA:FOPI-FOPTID	-4.7510	-2.6781	-0.8388	0.6771	3.2034	0.4667	0.5602	0.7242	0.8092	1.1653

performance is decreasing in the order: GNA:FOPI-FOPTID → GNA:FOPI-FOPID → GNA:FOPID → GNA:PID.

7.5.4. Single-Area Hydro-Nuclear-Gas System

Further research is carried on a single-area multi-source HNG PS displayed by Fig. 7.8. Each control area owns one mechanical governor dependent hydro power plant, one nuclear plant and one gas plant. One cascaded FOPI-FOPTID controller is applied in this model. The significant parameters are presented in Appendix. Table 7.7 portrays tuned gains of the designed controllers.

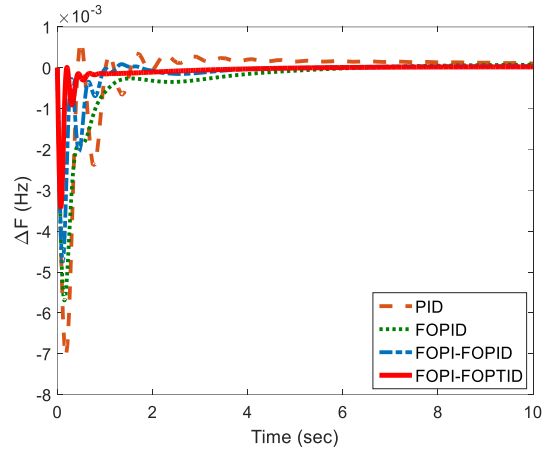


Fig. 7.9 Single-area HNG system frequency deviation response (ΔF).

Table 7.8 ST/OS/US/ITAE in single-area HNG system at $\Delta P_d = 0.01$ puMW.				
Controller structure	ST(sec)	OS (Hz)	US (-ve) (Hz)	ITAE
GNA:PID	1.440	0.000633	0.00752	0.00834
GNA:FOPID	1.123	0.000045	0.00579	0.0051
GNA:FOPI-FOPID	0.875	0.0000762	0.00472	0.0023
GNA:FOPI-FOPTID	0.373	0.0000243	0.00338	0.0013

The system dynamic results of ΔF responses are portrayed by Fig. 7.9. It is inferred that substantial enhancement is detected with the suggested GNA optimized FOPI-FOPTID controller over GNA optimized FOPI-FOPID, FOPID, and PID controllers. The mathematical values of the dynamic responses are depicted in Table 7.8 in terms of STs/USs/OSs and ITAE. Table 7.8 reveals that with GNA optimized PID controller values are ST = 1.440 sec, OS = 0.000633, US = 0.00752, ITAE = 0.00834, while these values with GNA optimized FOPID controller are ST = 1.123 sec, OS = 0.000045, US = 0.00579, ITAE = 0.0051. The values for GNA optimized FOPI-FOPID controller are ST = 0.875 sec, OS = 0.0000762, US = 0.00472, and ITAE = 0.0023. The values for GNA optimized FOPI-FOPTID controller are ST = 0.373 sec, OS = 0.0000243, US = 0.00338, and ITAE = 0.0013. Supremacy of the GNA optimized FOPI-FOPTID controller is revealed over the others in terms of least values of STs, USs, OSs, and ITAE. Table 7.8

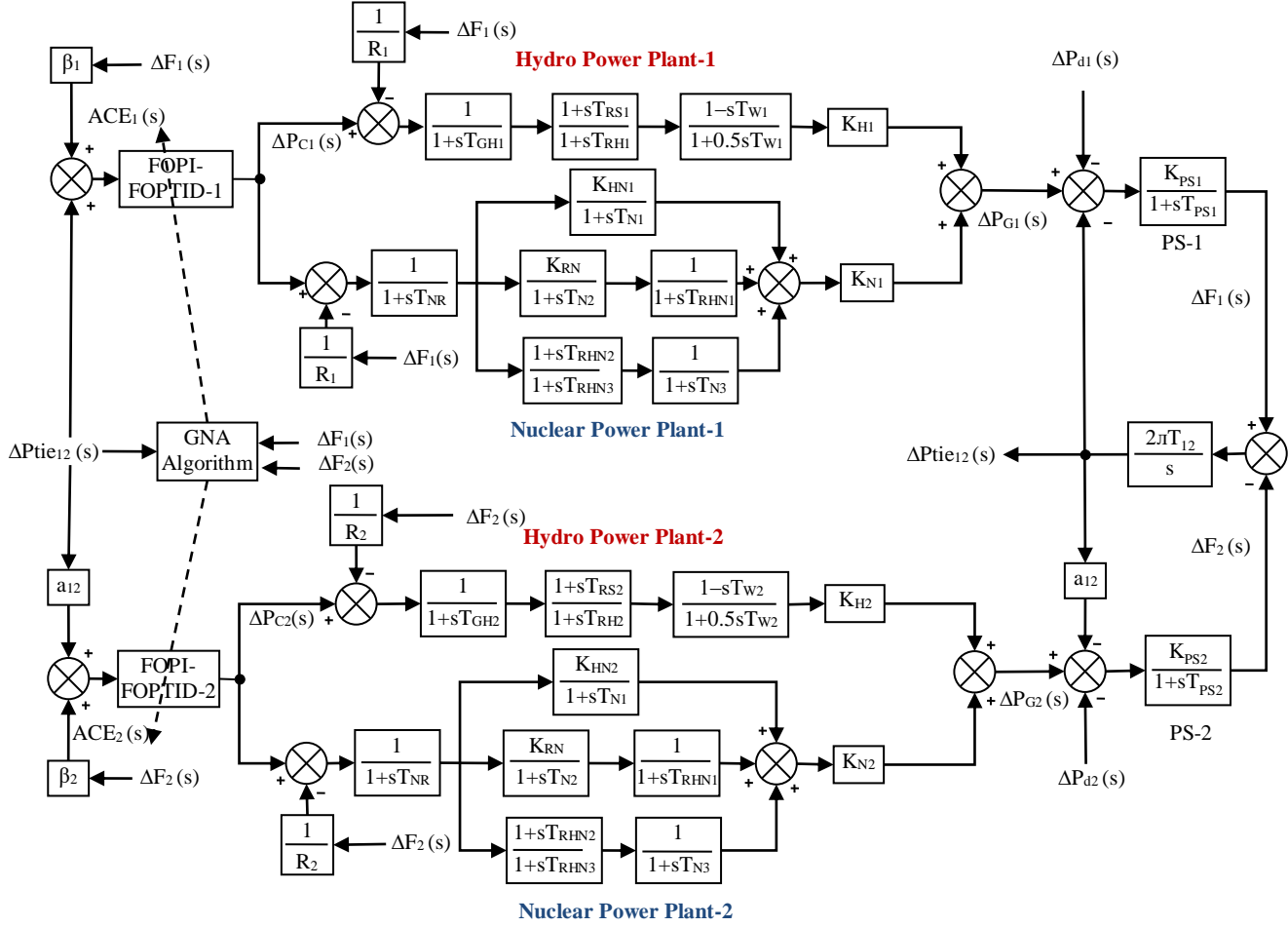


Fig. 7.10 Two-area HN PS with optimized FOPI-FOPTID controller.

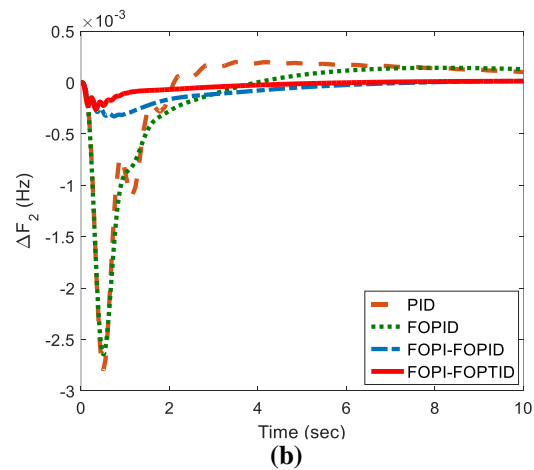
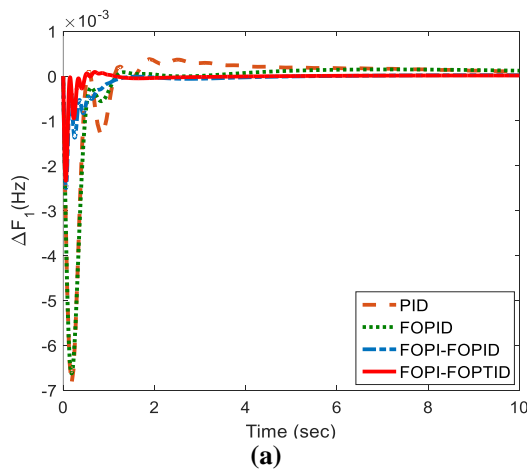
and Fig. 7.9 reveals that the performance is diminishing in the order: GNA:FOPI-FOPTID → GNA:FOPI-FOPID → GNA:FOPID → GNA:PID.

7.5.5. Two-Area Hydro-Nuclear System

Further research is stretched on a two-area multi-source HN PS, displayed by Fig. 7.10. Each control area owns one hydro power plant and one nuclear plant in both areas. One cascaded FOPI-FOPTID controller is applied in each area in this model. Table 7.9 portrays tuned gains for projected controller. PS dynamic results for $\Delta F_1/\Delta F_2/\Delta P_{tie12}$ responses are displayed by Figs. 7.11(a-c). It is inferred that substantial enhancement is detected with the proposed GNA tuned FOPI-FOPTID controller against the GNA

optimized FOPI-FOPID/FOPID/PID controllers. Table 7.10 portrays the mathematical values of STs/USs/OSs, and ITAE. Table 7.10 interprets that with GNA optimized PID controller, the values of ITAE, STs/USs/OSs are ITAE (0.0214), STs ($\Delta F_1 = 1.647$, $\Delta F_2 = 1.580$, $\Delta P_{tie_{12}} = 0.720$) and USs ($\Delta F_1 = -0.0078$, $\Delta F_2 = -0.00357$, $\Delta P_{tie_{12}} = -0.001073$), OSs ($\Delta F_1 = 0.001429$, $\Delta F_2 = 0.000194$, $\Delta P_{tie_{12}} = 0.0000857$). For GNA optimized FOPID controller the values are ITAE (0.0170), STs ($\Delta F_1 = 0.921$, $\Delta F_2 = 0.912$, $\Delta P_{tie_{12}} = 0.833$) and USs ($\Delta F_1 = -0.0066$, $\Delta F_2 = -0.00662$, $\Delta P_{tie_{12}} = -0.000841$), OSs ($\Delta F_1 = 0.000155$, $\Delta F_2 = 0.000088$, $\Delta P_{tie_{12}} = 0.0000576$). For GNA optimized FOPI-FOPID controller the values of are ITAE (0.0046), STs ($\Delta F_1 = 0.541$, $\Delta F_2 = 1.651$, $\Delta P_{tie_{12}} = 1.337$) USs ($\Delta F_1 = -0.0025$, $\Delta F_2 = -0.00033$, $\Delta P_{tie_{12}} = -0.000245$) and OSs ($\Delta F_1 = 0.000012$, $\Delta F_2 = 0.000015$, $\Delta P_{tie_{12}} = 0.0000129$).

Table 7.9 Tuned parameters of two-area HNG system with GNA optimized controllers.										
Controller type	K_{P1}	K_{I1}	$\lambda 1$	K_P	K_I	K_D	λ	μ	K_T	n
GNA:PID	–	–	–	4.5783	5.5438	1.9989	–	–	–	–
GNA:FOPID	–	–	–	4.8174	5.1423	1.9598	0.8178	1.0459	–	–
GNA:FOPI-FOPID	2.0795	0.5382	0.1408	3.3448	4.3270	1.8119	0.4897	1.1820	–	–
GNA:FOPI-FOPTID	3.0645	2.7554	0.1728	4.8744	3.8542	1.0382	0.3984	1.2683	1.2402	1.2362



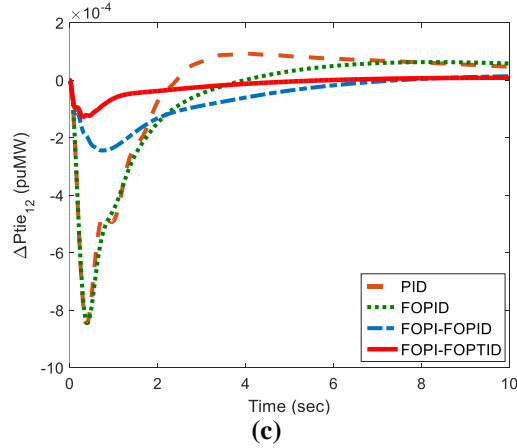


Fig. 7.11 Two-area HN system response: (a) ΔF_1 , (b) ΔF_2 , and (c) $\Delta P_{tie_{12}}$.

Table 7.10 ST/OS/US/ITAE in two-area HN system at $\Delta P_{d1} = 0.01$ puMW with GNA optimized FOPI-FOPTID controller.										
Controller structure	ΔF_1			ΔF_2			$\Delta P_{tie_{12}}$			-
	ST(s)	OS (Hz)	US(-ve) (Hz)	ST (s)	OS (Hz)	US (-ve) (Hz)	ST (s)	OS (Hz)	US (-ve) (Hz)	ITAE
GNA: PID	1.647	0.001429	0.0078	1.580	0.000194	0.00357	0.720	0.0000857	0.001073	0.0214
GNA: FOPID	0.921	0.000155	0.0066	0.912	0.000088	0.00662	0.833	0.0000576	0.000841	0.0170
GNA: FOPI-FOPID	0.541	0.000012	0.0025	1.651	0.000015	0.00033	1.337	0.0000129	0.000245	0.0046
GNA: FOPI-FOPTID	0.278	0.000088	0.0023	0.553	0.000013	0.00025	0.652	0.0000064	0.000126	0.0020

For GNA optimized FOPI-FOPTID controller the values of ITAE, STs/USs/OSs are ITAE (0.0020), STs ($\Delta F_1 = 0.278$, $\Delta F_2 = 0.553$, $\Delta P_{tie_{12}} = 0.652$), USs ($\Delta F_1 = -0.0023$, $\Delta F_2 = -0.00025$, $\Delta P_{tie_{12}} = -0.000126$) and OSs ($\Delta F_1 = 0.000088$, $\Delta F_2 = 0.000013$, $\Delta P_{tie_{12}} = 0.0000064$). It is observed from Table 7.10 that GNA:FOPI-FOPTID provides least STs/USs/USs/ITAE compared to others and performance is decreasing in the order:

GNA:FOPI-FOPTID \rightarrow GNA:FOPI-FOPID \rightarrow GNA:FOPID \rightarrow GNA:PID.

7.5.6. Two-Area Hydro-Nuclear-Gas System

Further research is stretched on a two-area multi-source HNG PS displayed by Fig. 7.12. Each control area owns one hydro power plant, one nuclear plant and one gas plant in both areas. One cascaded FOPI-FOPTID controller is applied in each area in this model. Table 7.11 shows projected controllers' tuned gains. Figs. 7.13(a-c) portrays

$\Delta F_1/\Delta F_2/\Delta P_{tie12}$ responses and it is inferred that significant enhancement is detected with the projected GNA optimized FOPI-FOPTID controller against GNA optimized FOPI-FOPID/ FOPID/ PID controllers. The controller's efficiency is also evaluated using the performance index, ITAE for a tolerance range of ± 0.0005 portrayed in Table 7.12. The ST is considered in the error band of ± 0.0005 (ΔF_1 and ΔF_2) and ± 0.0002 (ΔP_{tie12}) for final value of the result. Table 7.12 interprets the mathematical values of $\Delta F_1/\Delta F_2/\Delta P_{tie12}$

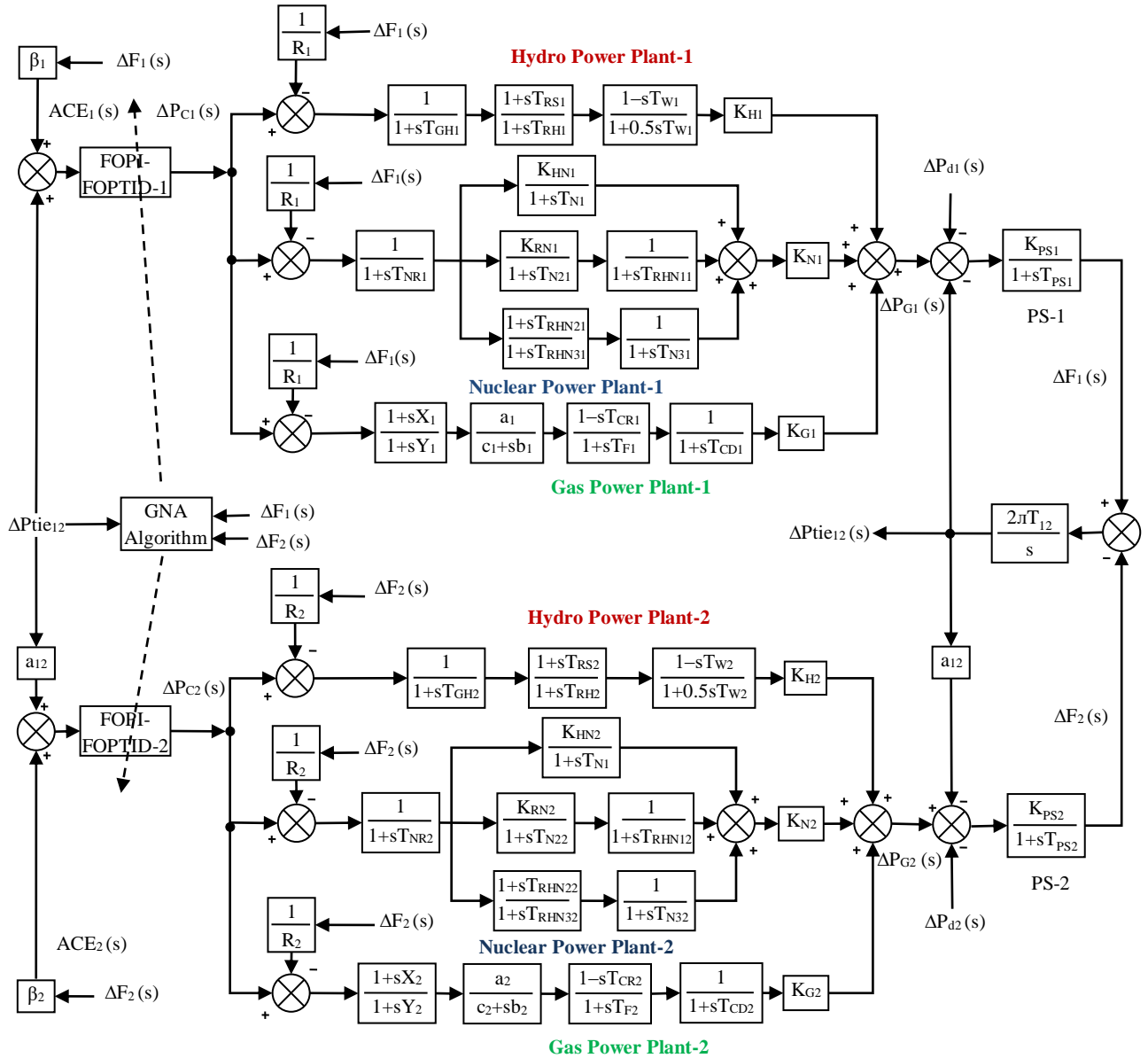


Fig. 7.12 Two-area HNG system.

Table 7.11
Tuned parameters of two-area HNG system with GNA optimized controllers.

Controller used	K_{P1}	K_{I1}	λ_1	K_P	K_I	K_D	λ	μ	K_T	n
GNA:PID	–	–	–	4.0857	5.3365	2.6159	–	–	–	–
GNA:FOPID	–	–	–	4.4657	4.5949	1.8814	0.7178	1.239	–	–
GNA:FOPI-FOPID	3.5831	2.2993	0.2718	2.8765	3.1021	1.0356	0.6473	1.2901	–	–
GNA:FOPI-FOPTID	3.0401	1.1182	0.6569	5.4749	3.3350	1.3849	0.6170	1.3081	2.7166	1.6879

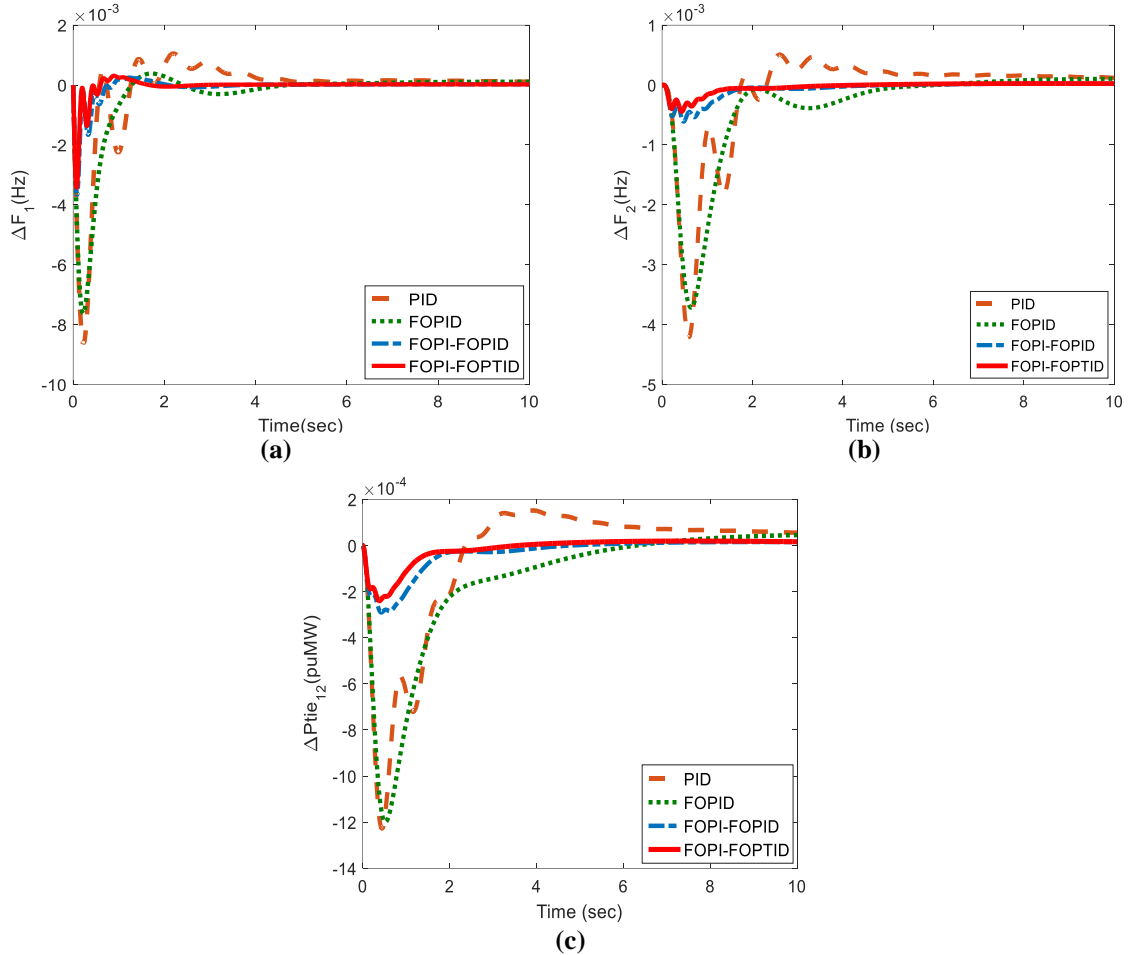


Fig. 7.13 Two-area HNG system response: (a) ΔF_1 , (b) ΔF_2 , and (c) ΔP_{tie12} .

Table 7.12
ST/OS/US/ITAE in two-area HNG system at $\Delta P_{d1} = 0.01$ puMW.

Controller structure	ΔF_1			ΔF_2			ΔP_{tie12}			ITAE
	ST (sec)	OS (Hz)	US (-ve) (Hz)	ST (sec)	OS (Hz)	US (-ve) (Hz)	ST (sec)	OS (Hz)	US (-ve) (Hz)	
GNA:PID	1.212	0.00105	0.00861	1.635	0.000502	0.00421	1.395	0.000149	0.00123	0.0273
GNA:FOPID	1.068	0.00039	0.00760	1.590	0.000103	0.00370	1.338	0.000042	0.00120	0.0172
GNA:FOPI-FOPID	0.623	0.00025	0.00360	0.760	0.000023	0.00061	0.993	0.000021	0.00029	0.0039
GNA:FOPI-FOPTID	0.571	0.00029	0.00342	0.948	0.000021	0.00044	0.656	0.000020	0.00024	0.0035

in terms of STs/USs/OSs and ITAE. Table 7.12 infers that with GNA optimized PID controller the values of ITAE, STs/USs/OSs are ITAE (0.0273), STs ($\Delta F_1 = 1.212$, $\Delta F_2 = 1.635$, $\Delta P_{tie12} = 1.395$), USs ($\Delta F_1 = -0.00861$, $\Delta F_2 = -0.00421$, $\Delta P_{tie12} = -0.00123$) and OSs ($\Delta F_1 = 0.00105$, $\Delta F_2 = 0.000502$, $\Delta P_{tie12} = 0.000149$). For GNA optimized FOPID controller, the values of ITAE, STs/USs/OSs are ITAE (0.0172), STs ($\Delta F_1 = 1.068$, $\Delta F_2 = 1.590$, $\Delta P_{tie12} = 1.338$), USs ($\Delta F_1 = -0.00760$, $\Delta F_2 = -0.00370$, $\Delta P_{tie12} = -0.00120$) and

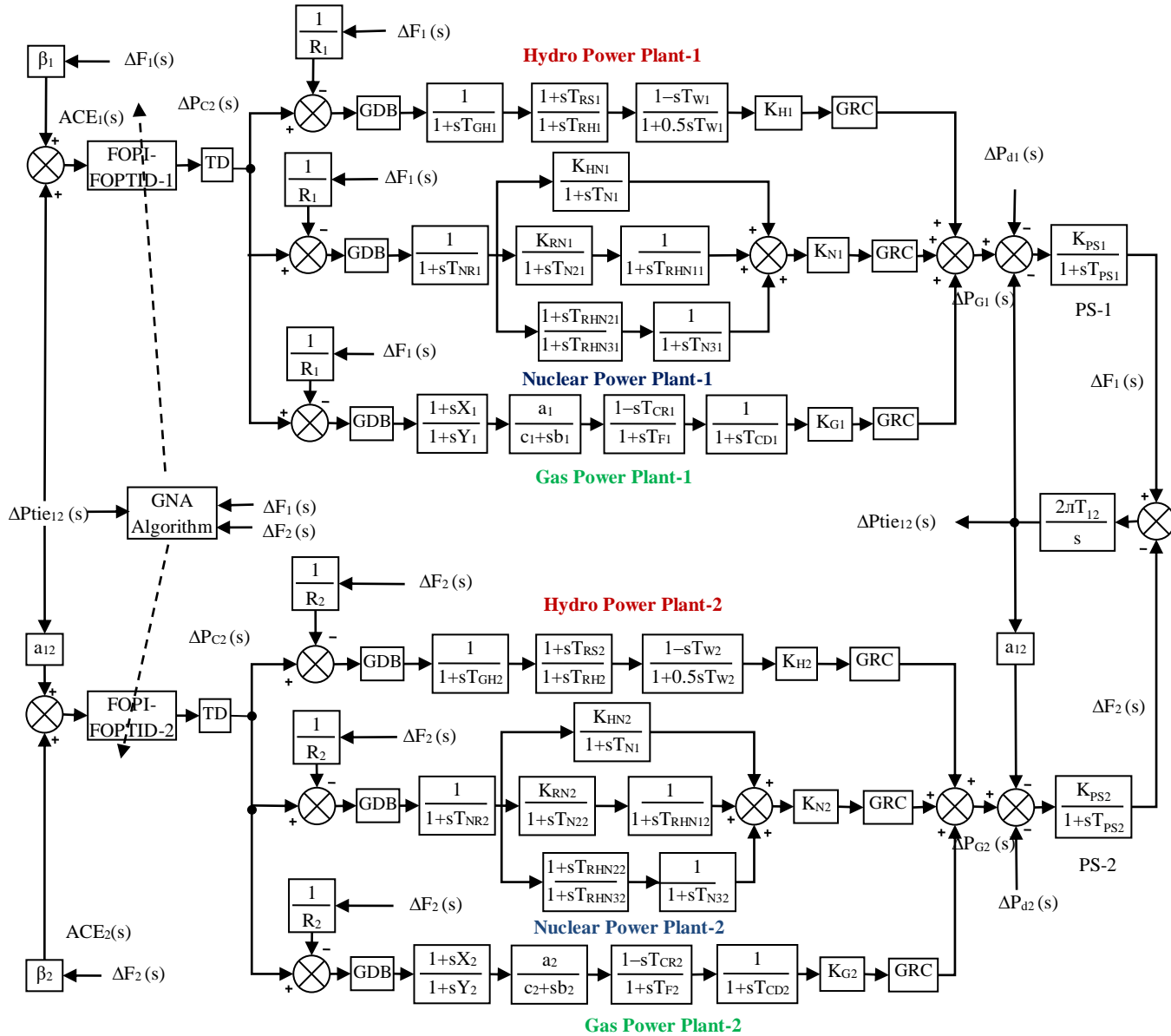
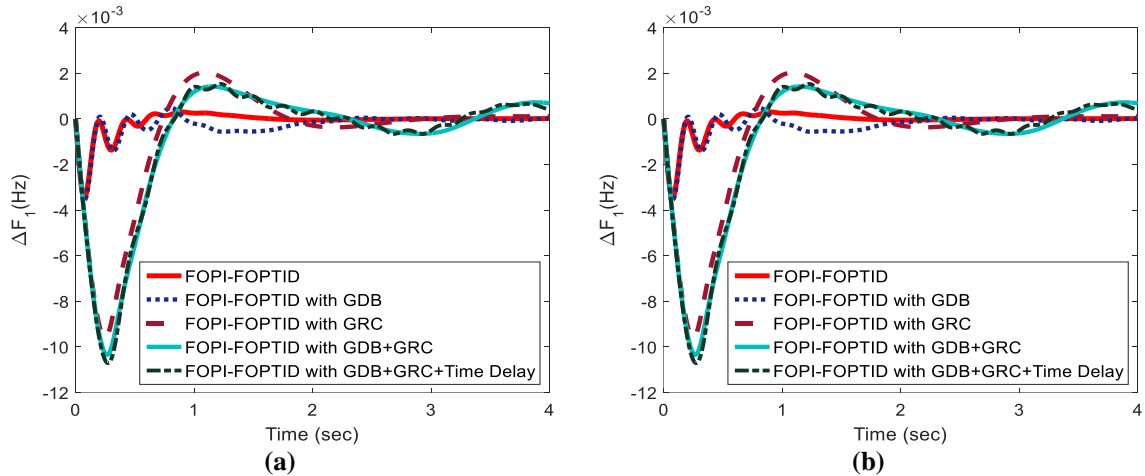


Fig. 7.14 Two-area HNG system with GDB/GRC/Time-delay (TD).

OSs ($\Delta F_1 = 0.00039$, $\Delta F_2 = 0.000103$, $\Delta P_{tie_{12}} = 0.000042$). For GNA optimized FOPI-FOPID controller, the values are ITAE (0.0039), STs ($\Delta F_1 = 0.623$, $\Delta F_2 = 0.760$, $\Delta P_{tie_{12}} = 0.993$), USs ($\Delta F_1 = -0.00360$, $\Delta F_2 = -0.00061$, $\Delta P_{tie_{12}} = -0.00029$) and OSs ($\Delta F_1 = 0.00025$, $\Delta F_2 = 0.000023$, $\Delta P_{tie_{12}} = 0.000021$). For FOPI-FOPTID controller, the values are ITAE (0.0035), STs ($\Delta F_1 = 0.571$, $\Delta F_2 = 0.948$, $\Delta P_{tie_{12}} = 0.656$), USs ($\Delta F_1 = -0.00342$, $\Delta F_2 = -0.00044$, $\Delta P_{tie_{12}} = -0.00024$) and OSs ($\Delta F_1 = 0.00029$, $\Delta F_2 = 0.000021$, $\Delta P_{tie_{12}} = 0.000020$). It is interpreted from Table 7.12 that the best performance is delivered by GNA:FOPI-FOPTID controller as most of the values are least with it and the worst performance is delivered by GNA:PID.

7.5.7. Two-Area Hydro-Nuclear-Gas System with GDB/GRC/TD

Further research is carried out on a two-area multi-source HNG PS including nonlinearities (GDB, GRC, and TD) as shown in Fig. 7.14. Figs. 7.15(a-c) portrays ΔF_1 , ΔF_2 , and $\Delta P_{tie_{12}}$ responses. They reveal that significant enhancement in the system



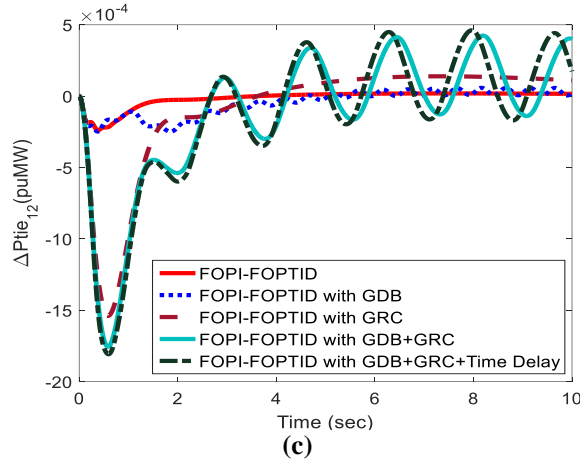


Fig. 7.15 Two-area HNG system response with GDB/GRC/TD: (a) ΔF_1 , (b) ΔF_2 , and (c) $\Delta P_{tie_{12}}$.

performance is detected by the GNA optimized FOPI-FOPTID controller and stabilized results are obtained in the presence of GDB, GRC, and TD.

The FOPI-FOPTID controller's optimized gains match those listed in Table 7.11. For hydro, nuclear, and gas PS, the GDB values are ± 0.002 , ± 0.025 , and ± 0.001 , respectively. The hydro PS has an upper limit of $+0.045$ and a lower limit of -0.06 , whereas the nuclear and gas PS have values of ± 0.2 and ± 0.0033 , respectively. Delay in time (TD) = 0.015 sec.

It is observed that the performance of $\Delta F_1/\Delta F_2/\Delta P_{tie_{12}}$ responses is degraded after adding GRC against the response with/without GDB. The performance of $\Delta F_1/\Delta F_2/\Delta P_{tie_{12}}$ response is deteriorating after adding GDB, GRC and TD when against the response with/without GDB/GRC/TD.

7.6 Conclusion

A GNA optimized cascade FOPI-FOPTID controller is proposed. Initially, the controller is scrutinized on a single-area THG PS. The results attained by the GNA optimized FOPI-FOPTID controller interprets its supremacy against GNA optimized FOPTID+1 controller. Further, the study is extended to single-area nuclear/HN/HNG PSs. Research

is stretched on two-area HN/HNG PS models. It is observed that GNA optimized FOPI-FOPTID ensures enhanced dynamic performance over GNA optimized PID, FOPID, and FOPI-FOPID controllers witnessed least mathematical values of STs/PUs/Pis and ITAE. Finally, the research is stretched on two-area HNG PS with GDB/GRC/TD nonlinearities. It is inferred that PS performance deteriorates in the presence of nonlinearities. However, FOPI-FOPTID controller tuned for linear case by GNA is enough capable to provide a stable performance in the attendance of GDB/GRC/TD nonlinearities.

CHAPTER 8

WHO OPTIMIZED FOID-FOPTID CONTROLLER

8.1 Introduction

In this chapter an effort is carried out for projecting a new cascade fractional order integral derivative-fractional order proportional tilt integral derivative (FOID-FOPTID) controller optimized with a modern wild horse optimization algorithm (WHO) for AGC of THG PSs in single/two-area multi-source.

8.2 Wild Horse Optimization (WHO) Algorithm

Recently several intelligent algorithms are available in literature but the probability of the best solution is more in evolutionary algorithms. The WHO was induced by Naruei and Keynia [215,216]. The WHO is classified into territorial and non-territorial groups. Here, our focus is on non-terrestrial horses. Non-terrestrial horses are herds consisting of stable family groups or harems that include a stallion and one or several mares and offspring. Also, there are single groups, including adult stallions and juvenile horses. Stallions are placed close to mares for communication, and at any instant mating may occur. Foals often begin grazing within their first week of life and, as they age, engage in greater grazing and less rest. The rationale behind the suggested optimization technique is the behavior of non-territorial horses. Here, the utilization of WHO simultaneously optimizes other parameters and controller gains. Five main steps are (1) creating an initial population and forming horse groups and selecting leaders, (2) grazing and mating of horses, (3) leadership and leading the group by the leader (stallion), (4) exchange and selection of leaders, and (5) save the best solution as explained in sections 8.2.1-8.2.7.

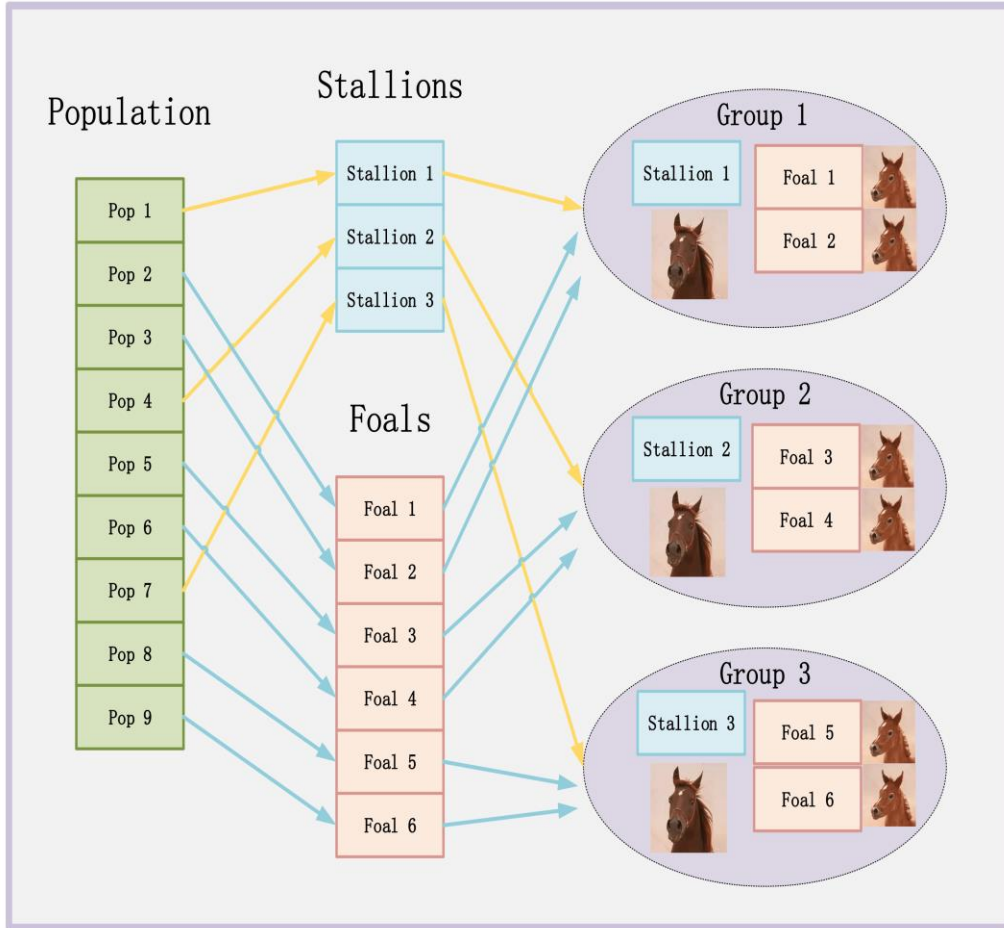


Fig. 8.1 Formation of groups from original population [215].

8.2.1 Generate Initial Population

Define random initial population is specified by Eqn. (8.1):

$$\vec{x} = \{\vec{x}_1, \vec{x}_2, \vec{x}_3, \dots, \vec{x}_n\} \quad (8.1)$$

The target function is used to evaluate this random population. Eqn. (8.2) is used to assess the target function as follows:

$$\vec{O} = \{O_1, O_2, O_3, \dots, O_n\} \quad (8.2)$$

Firstly, to begin with, the population is split up into different categories. The control parameter in this algorithm is the number of groups formulated by $G = [N \times PS]$, where N

denotes total members and PS denotes stallions' percentage. Fig. 8.1 shows this population divide. The stallion is positioned in the middle of the grazing field, while other participants hunt all around it to capture the grazing activity.

8.2.2 Grazing Behavior

The grazing activity is formulated by Eqn. (8.3).

$$\overline{X}_{i,G}^j = 2Z \cos(2\pi RZ) \times (\text{Stallion}^j - X_{i,G}^j) + \text{Stallion}^j \quad (8.3)$$

Here, Stallion^j denotes the group leader position, R denotes uniform distribution in $[-2, 2]$, $\overline{X}_{i,G}^j$ is the new place of group member while grazing, the up-to-date position of foal or mare is $X_{i,G}^j$, The grazing of horses at different angles (360°) of group leader, π is the same as the pi number equal to 3.14, The COS function by combining π and R causes the movement in different radius, Z denotes an adaptive mechanism evaluated by Eqn. (8.4), however P is a vector specified between 0 and 1.

$$P = \overline{R}_1 \leq TDR; \text{IDX} = (P == 0); Z = R_2 \ominus \text{IDX} + \overline{R}_3 \ominus (\square \text{IDX}) \quad (8.4)$$

In the interval $[0,1]$, \overline{R}_1 and \overline{R}_3 are random vectors with uniform distribution, random vector R_2 is in the interval $[0,1]$, IDX is the random vector's index \overline{R}_1 that satisfies $(P == 0)$, and TDR is an adaptive parameter that starts at 1 and drops to 0 as the algorithm begins to execute, as specified by Eqn. (8.5).

$$TDR = 1 - \text{itr} \times \left(\frac{1}{\max \text{iter}} \right) \quad (8.5)$$

Where, the term $\max \text{iter}$ refers to the total number of algorithm iterations and itr denotes the current iteration.

8.2.3 Horse Mating Behavior

It is a unique conduct of horses is that foals separate from the groups and female foals join another family before reaching puberty and select their mate. This behavior prevents father horse to mate with their siblings. This method is implemented as: a male foal leaves group i and female foal leaves group j to join a temporary group. They don't have any common family so their child can join another temporary group k . This behavior of mating is shown in Fig. 8.2 can be simulated using Eqn. (8.6) as:

$$X_{G,K}^P = \text{Crossover}(X_{G,i}^q, X_{G,j}^z) \quad i \neq j \neq k, p = q = \text{end}, \quad \text{Crossover} = \text{Mean} \quad (8.6)$$

$X_{G,K}^P$ is the position of horse p from group k . It will leave the group and a horse will replace it whose parents have left groups i and j . $X_{G,i}^q$ is the position of foal q from group i , who left the group j to mate with the horse z having position $X_{G,j}^z$.

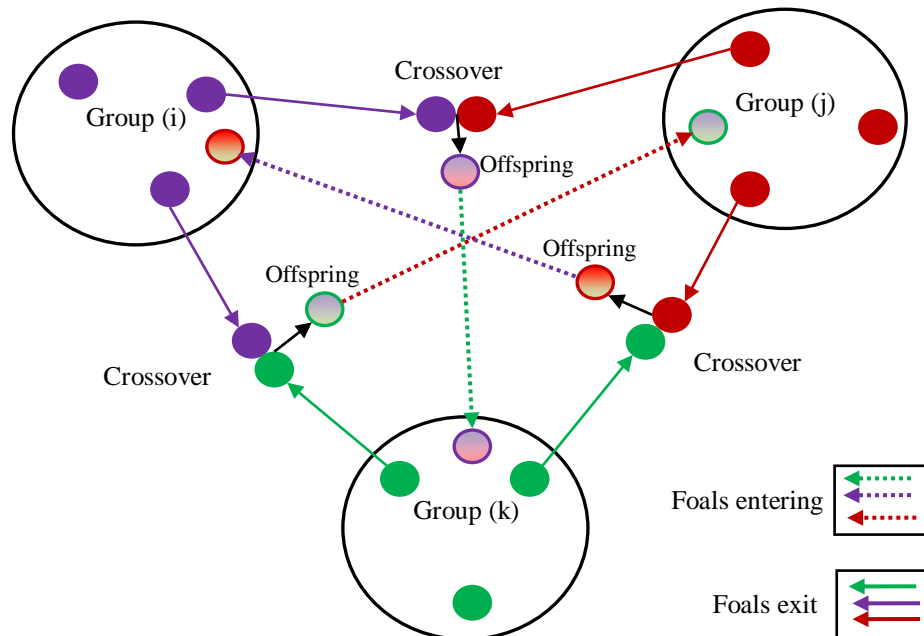


Fig. 8.2 Departure of foals from a group, crossover and reproduction [215].

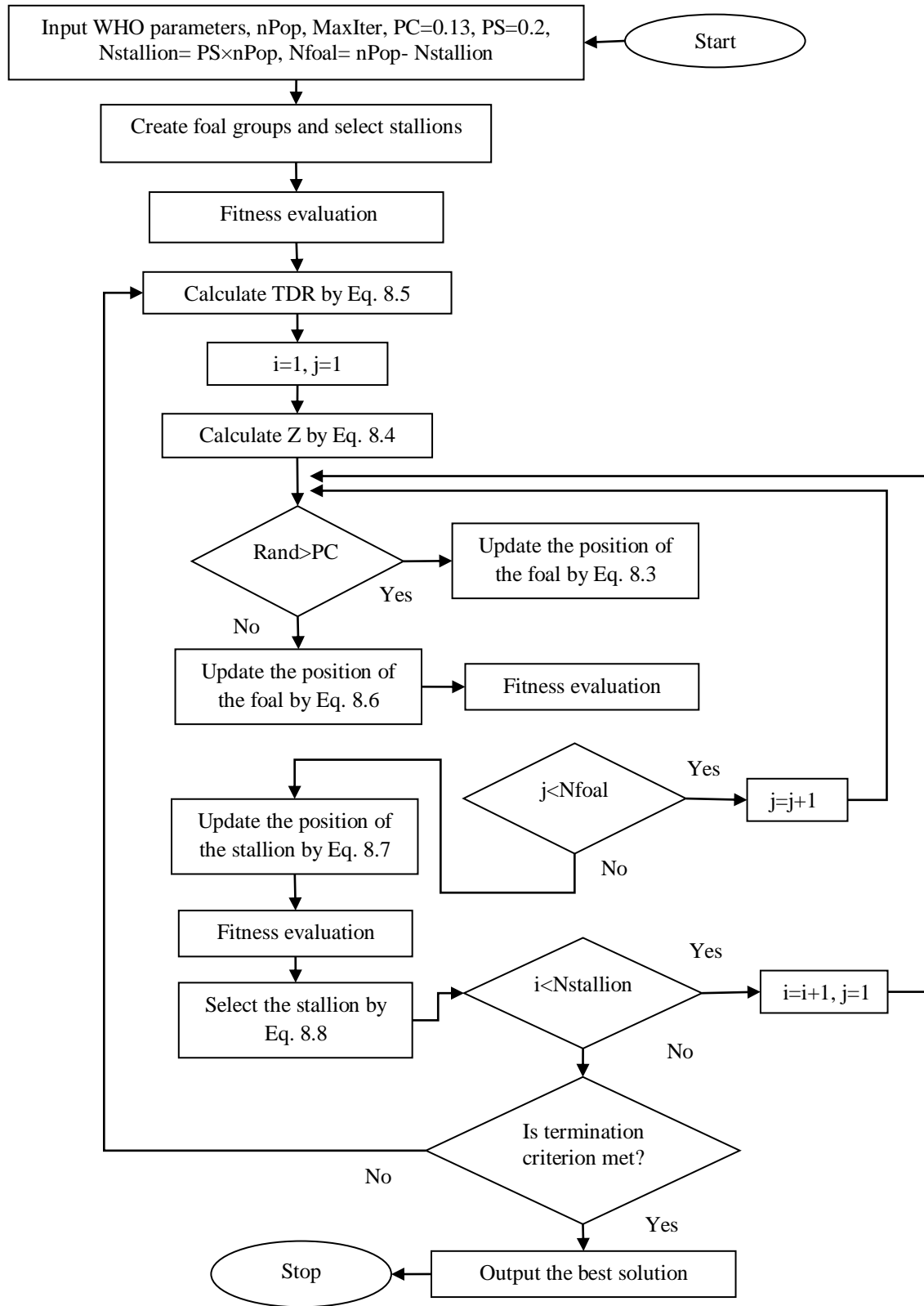


Fig. 8.3 Flowchart of WHO [215].

8.2.4 Group Leadership

The group leader will lead the horses to a suitable area having water. The group which dominates will have the water first and another group moves away. This method will be given by Eqn. (8.7).

$$\overline{Stallion}_{G_i} = \begin{cases} 2Z \cos(2\pi RZ) \times (WH - Stallion_{G_i}) + WH & \text{if } R_3 \geq 0.5 \\ 2Z \cos(2\pi RZ) \times (WH - Stallion_{G_i}) - WH & \text{if } R_3 \leq 0.5 \end{cases} \quad (8.7)$$

Where, $\overline{Stallion}_{G_i}$ and $Stallion_{G_i}$ denotes the next and current positions of the leader of group i, WH is the water hole position, R is a uniform random number exists within range [-2,2], π is the pi number equal to 3.14 and Z is an adaptive mechanism given by Eqn. (8.4).

8.2.5 Selection and Exchange of Leaders

Initially the leaders are selected from the groups randomly and later on selected based on the fitness. The position of the group leader and group members will be interchanged if one of the group members have better fitness than group leader. This method is given by Eqn. (8.8), and the flowchart is shown in Fig. 8.3 for WHO algorithm.

$$Stallion_{G_i} = \begin{cases} X_{G,i} & \text{if } \text{cost}(X_{G,i}) < \text{cost}(Stallion_{G_i}) \\ Stallion_{G_i} & \text{if } \text{cost}(X_{G,i}) > \text{cost}(Stallion_{G_i}) \end{cases} \quad (8.8)$$

8.3 Systems Investigated

Examination of a single-area reheat/non-reheat thermal PS is carried out to compare the WHO and GNA optimization algorithms. Further research is stretched on a single-area multi-source THG PS without GDB/GRC using GNA optimized FOPTID+1 controller, GNA optimized FOPI-FOPTID controller and WHO optimized FOID-FOPTID controllers. Results prove the dominance of WHO optimized controllers over the GNA

tuned controllers. A THG PS components and rated capacity are discussed in chapter 6. Three controllers are connected, one with each plant. Further research is stretched out on a multi-source multi-area THG PS without GDB/GRC. One FOID-FOPTID controller is connected in each area. Both areas are connected with tie-lines. The PS block diagrams investigated are displayed in Fig. 8.5, Fig. 8.7, Fig. 8.9, Fig. 8.11, Fig. 8.13, Fig. 8.15. The PSs nominal parameters are portrayed in Appendix with nomenclature section displays the list of symbols.

8.4 Cascade Fractional Order Integral Derivative-Fractional Order Proportional Tilt Integral Derivative (FOID-FOPTID) Controller

Cascaded FOID-FOPTID controller is used for the AGC of PSs. Literature study reveals the wide employment of FOPID controller in various PSs. The FO controller theory is discussed in Chapter 6. However, the Riemann-Liouville definition used in Chapter 6 is stated in Eqn. (6.1) normally applied in FO calculus. The TF of FOID-FOPTID controller is specified by Eqn. (8.9) and structure displayed in Fig. 8.4.

$$G_{\text{FOID-FOPTID}}(s) = \left[\left\{ \left(\frac{K_{I1}}{s^{\lambda 1}} + K_{D1} s^{\mu 1} \right) - \Delta F(s) \right\} \times \left(K_P + \frac{K_T}{s^{1/n}} + \frac{K_I}{s^{\lambda}} + K_D s^{\mu} \right) \right] \quad (8.9)$$

Where, proportional, integral, derivative and tilt-integral gains of FOPTID controller are K_P , K_I , K_D , K_T while K_{I1} , K_{D1} are integral and derivative gains of FOID controller respectively. $\lambda 1$, $\mu 1$, λ , μ and n are the corresponding orders of integration and differentiation. FOID-FOPTID controller will optimize eleven design parameters against

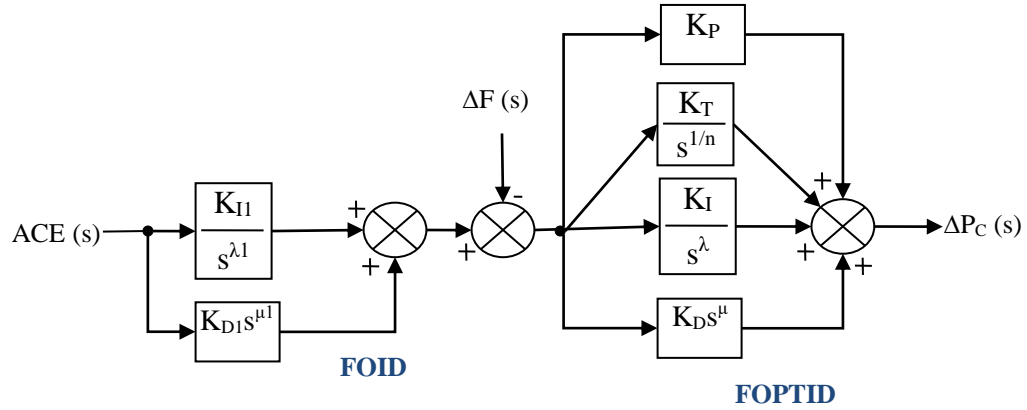


Fig. 8.4 Structure of FOID-FOPTID controller.

the seven parameters required in FOPTID+1 structured controller. The proposed FOID-FOPTID controller involves the suitable design of gains $K_{I1}/K_{D1}/K_P/K_I/K_D/K_T$ and orders $\lambda/\mu/n$ can be any real numbers.

8.5 Optimization Problem

For AGC problem under study, for single/multi-area PS, the objective function (J) employed is ITAE as stated in Eqns. 5.10/(6.11) Chapter 5.

Consequently, a challenge to design the FOID-FOPTID controller gains with optimization for problem solutions with controller parameter restrictions. There are eleven parameters to optimize for the FOID-FOPTID controller in all areas of the multi-area PSs. The lowest and highest values of the parameters given by Eqn. (8.10) are K_{I1} [0 to 5], K_{D1} [0 to 5], λ_1 [0 to 1], μ_1 [0 to 1], K_P [0 to 5], K_I [0 to 5], K_D [0 to 5], λ [0 to 1], μ [0 to 1], K_T [0 to 5], and n [1 to 3]. ACE_1 and ACE_2 are represented by Eqns. (6.13/8.13) and Eqns. (6.14/8.14) [26-27]. The following constraints can be used to define the optimization issue as minimizing J:

$$\begin{aligned}
K_{I1}^{\min} &\leq K_{I1} \leq K_{I1}^{\max} \\
K_{D1}^{\min} &\leq K_{D1} \leq K_{D1}^{\max} \\
\lambda 1^{\min} &\leq \lambda 1 \leq \lambda 1^{\max} \\
\mu 1^{\min} &\leq \mu 1 \leq \mu 1^{\max} \\
K_P^{\min} &\leq K_P \leq K_P^{\max} \\
K_I^{\min} &\leq K_I \leq K_I^{\max} \\
K_D^{\min} &\leq K_D \leq K_D^{\max} \\
\lambda^{\min} &\leq \lambda \leq \lambda^{\max} \\
\mu^{\min} &\leq \mu \leq \mu^{\max} \\
K_T^{\min} &\leq K_T \leq K_T^{\max} \\
n^{\min} &\leq n \leq n^{\max}
\end{aligned} \tag{8.10}$$

8.6 Simulation Results and Discussions

8.6.1 Single-Area Non-Reheat Thermal System

The data provided in the Appendix is used to model a single-area non-reheat thermal PS while taking a 1% SLP at $t = 0$ sec into account. The relationships between the thermal unit and the location of the SLP inputs are clearly illustrated by the system model in Fig. 8.5. The comparison of proposed WHO tuned PID controller and GNA tuned PID controller is shown here. Table 8.1 portrays the tuned gains of the suggested controller and Figs. 8.6(a-b) depicts ΔF responses STs/USs/OSs performance index ITAE. It is inferred that

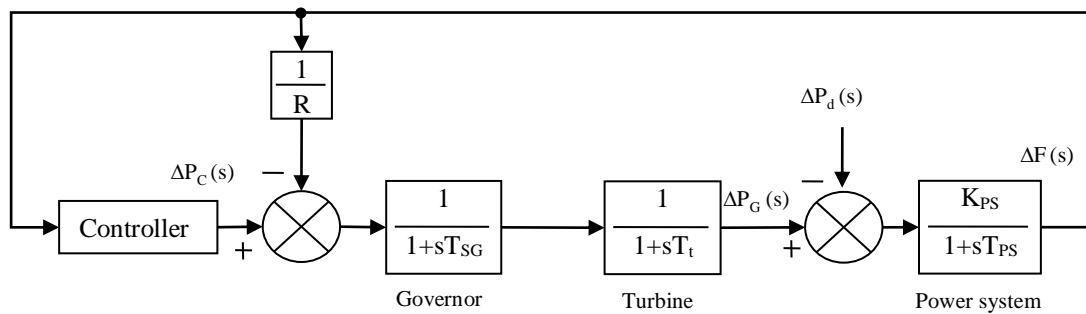


Fig. 8.5 Single-area non-reheat thermal system.

Table 8.1 Tuned parameters of single-area non-reheat thermal system with GNA and WHO optimized PID controller.				
Thermal System Type	Controller Type	K_P	K_I	K_D
Non-Reheat	GNA:PID	2.2814	4.6887	0.4279
	WHO:PID	2.5762	5	0.4716

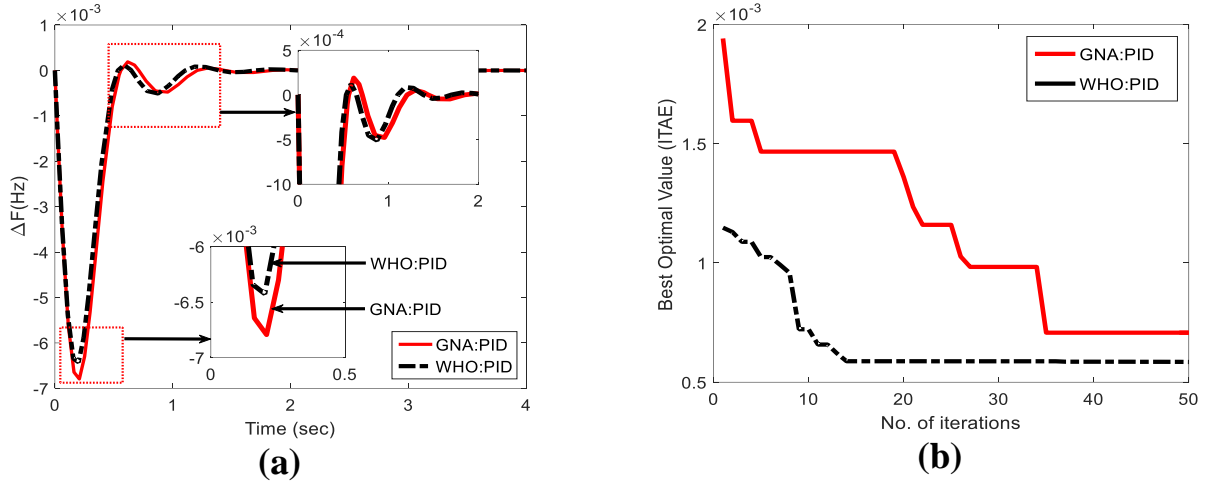


Fig. 8.6 Single-area non-reheat thermal system response: (a) ΔF and (b) Convergence curve.

Table 8.2 ST/OS/US/ITAE in single-area non-reheat thermal system at $\Delta P_d = 0.01$ puMW.				
Controller structure	ST(sec)	OS (Hz)	US (-ve) (Hz)	ITAE
GNA:PID	0.520	0.00682	0.000265	0.000647
WHO:PID	0.506	0.00641	0.000085	0.000586

substantial enhancement is detected with the WHO optimized PID controller against GNA optimized PID controller.

Convergence curve reveals that WHO tuned PID controller shows fast convergence. Table 8.2 portrays the dynamic responses with mathematical values in terms of STs/USs/OSs and ITAE. It is evident from Table 8.2 that ΔF response with WHO optimized PID controller for a tolerance band of ± 0.0005 is better in terms of smaller values of ITAE (0.000586), ST = 0.506 sec, OS = 0.00641, and US = 0.0085. While these values for GNA optimized PID controller are observed ITAE = 0.000647, ST = 0.520 sec, OS = 0.0068, and US = 0.00265. This infers the supremacy of the WHO optimized PID controller.

8.6.2 Single-Area Reheat Thermal System

Further research is stretched to a single-area reheat thermal system. Considering a 1% SLP at $t = 0$ sec, the simulation is carried out on PS displayed in Fig. 8.7. It depicts the connections of thermal unit and location of SLP inputs. The comparison of proposed WHO tuned PID controller efficiency and GNA tuned PID controller is shown here. The tuned controller gains are portrayed in Table 8.3. and Fig. 8.8. depicts the system dynamic results for ΔF responses revealing that significant enhancement is detected with WHO optimized PID controller against GNA optimized PID controller in single-area.

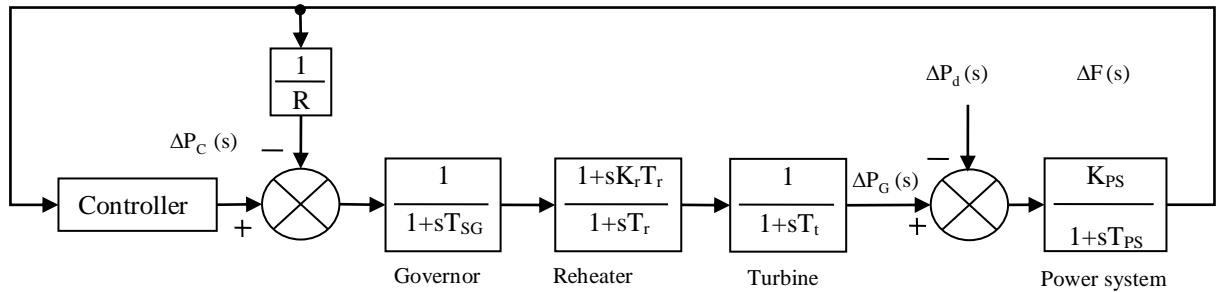


Fig. 8.7 Single-area reheat thermal system.

Table 8.3 Tuned parameters of single-area reheat thermal system without GRC with GNA and WHO optimized PID controller.				
Thermal System Type	Type of Controller used	K_P	K_I	K_D
Reheat	GNA:PID	3.2531	4.5221	0.5535
	WHO:PID	3.6531	4.9989	0.6335

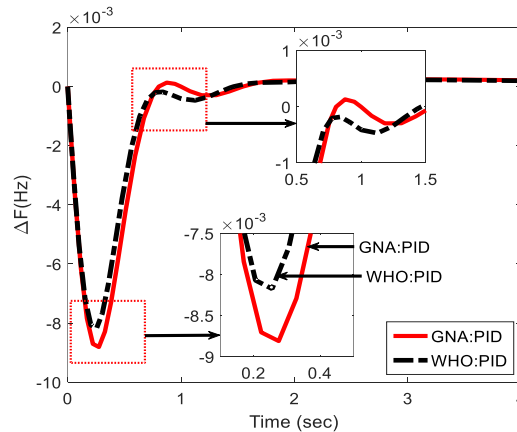


Fig. 8.8 Single-area reheat thermal system response (ΔF).

Table 8.4 ST/OS/US/ITAE in single-area reheat thermal system at $\Delta P_d = 0.01$ puMW.				
Controller structure	ST(sec)	OS (Hz)	US (-ve) (Hz)	ITAE
GNA:PID	0.73	0.000241	0.00877	0.0077
WHO:PID	0.70	0.000203	0.00815	0.0070

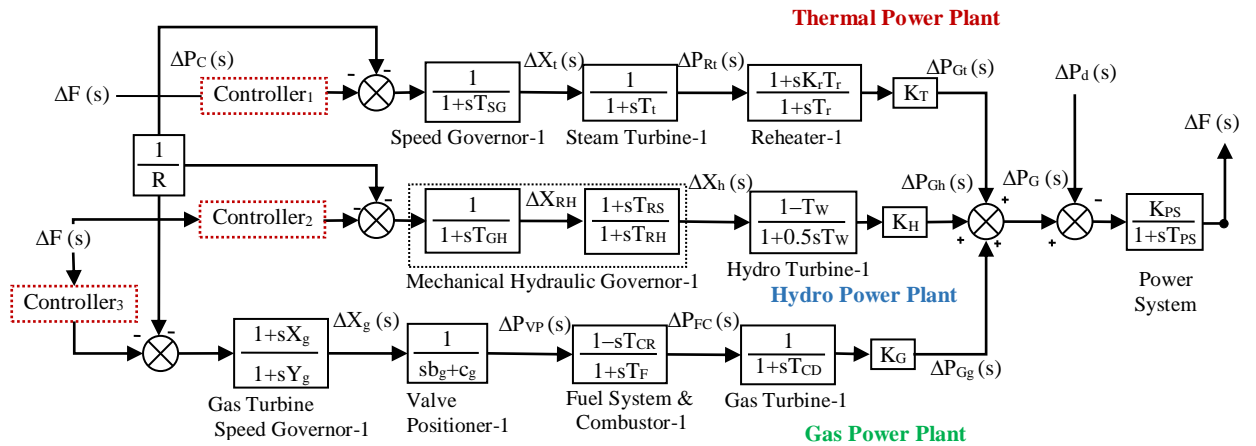


Fig. 8.9 Single-area THG system.

Table 8.4 portrays the mathematical values of STs/USs/OSs and ITAE. In the tolerance band of ± 0.0005 , Table 8.4 infers that ΔF response has lesser ITAE = 0.0070, ST = 0.70 sec, OS = 0.000203, and US = 0.00815 compared to GNA optimized PID controller. This shows the superiority of the WHO optimized PID controller. Further WHO optimization algorithm is suggested for other models.

8.6.3 Single-Area Thermal-Hydro-Gas System

Further research stretched on a single-area THG PS as displayed in Fig. 8.9. Each components of THG PS with rating capacity is discussed in chapter 6. Table 8.5 presents the tuned gains of the controller. For a tolerance band of ± 0.0005 , the system dynamic results are displayed in Fig. 8.10 and Table 8.6. It is inferred from Table 8.6 that, ΔF response for WHO optimized FOID-FOPTID controller has smaller ITAE = 0.0027, ST = 0.82 sec, US = 0.0045, and OS = 0.000021, while these values for GNA optimized FOPI-FOPTID controller are ITAE = 0.0022, ST = 0.67 sec, US = 0.0049, and OS = 0.000207.

Table 8.5

Tuned parameters of single-area THG system with GNA and WHO optimized controllers.

Controller type	K_{P1}	K_{I1}	K_{D1}	λ_1	μ_1	K_{T1}	n_1	K_{P1}	K_{I1}	K_{D1}	λ_1	μ_1
GNA:FOPTID+1	K_{P4}	K_{I4}	K_{D4}	λ_4	μ_4	K_{T1}	n_1	K_{P1}	K_{I1}	K_{D1}	λ_1	μ_1
	-	-	-	-	-	4.3331	1.8018	0.0042	0.4014	4.5687	0.5655	0.8197
	K_{P5}	K_{I5}	K_{D5}	λ_5	μ_5	K_{T2}	n_2	K_{P2}	K_{I2}	K_{D2}	λ_2	μ_2
	-	-	-	-	-	3.9237	1.2135	0.0105	4.8913	3.9787	0.5139	0.1900
	K_{P6}	K_{I6}	K_{D6}	λ_6	μ_6	K_{T3}	n_3	K_{P3}	K_{I3}	K_{D3}	λ_3	μ_3
-	-	-	-	-	1.1250	1.0184	2.3630	4.9787	4.4989	0.8484	0.5190	
GNA:FOPI-FOPTID	K_{P4}	K_{I4}	K_{D4}	λ_4	μ_4	K_{T1}	n_1	K_{P1}	K_{I1}	K_{D1}	λ_1	μ_1
	0.5067	3.2856	-	0.0895	-	3.7045	1.7551	4.3714	2.5027	3.4571	0.8272	0.9999
	K_{P5}	K_{I5}	K_{D5}	λ_5	μ_5	K_{T2}	n_2	K_{P2}	K_{I2}	K_{D2}	λ_2	μ_2
	1.3277	3.9158	-	0.6931	-	0.8016	1.8535	1.5357	2.5558	0.7070	0.5988	0.9674
	K_{P6}	K_{I6}	K_{D6}	λ_6	μ_6	K_{T3}	n_3	K_{P3}	K_{I3}	K_{D3}	λ_3	μ_3
2.6324	3.9439	-	0.2917	-	3.7142	1.9355	1.7651	4.4996	2.9474	0.768	0.5431	
WHO:FOID-FOPTID	K_{P4}	K_{I4}	K_{D4}	λ_4	μ_4	K_{T1}	n_1	K_{P1}	K_{I1}	K_{D1}	λ_1	μ_1
	-	2.2052	2.1573	0.5604	0.0137	0.8972	1.0894	2.7415	3.6027	2.4215	0.2053	0.3305
	K_{P5}	K_{I5}	K_{D5}	λ_5	μ_5	K_{T2}	n_2	K_{P2}	K_{I2}	K_{D2}	λ_2	μ_2
	-	2.5926	0.3364	0.1425	0.1106	0.9519	1.3771	3.6097	0.3087	0.0426	0.6247	0.1922
	K_{P6}	K_{I6}	K_{D6}	λ_6	μ_6	K_{T3}	n_3	K_{P3}	K_{I3}	K_{D3}	λ_3	μ_3
-	3.3369	2.0921	0.5670	0.4114	3.9332	3.0674	3.4631	3.9705	4.9406	0.1220	1.1447	

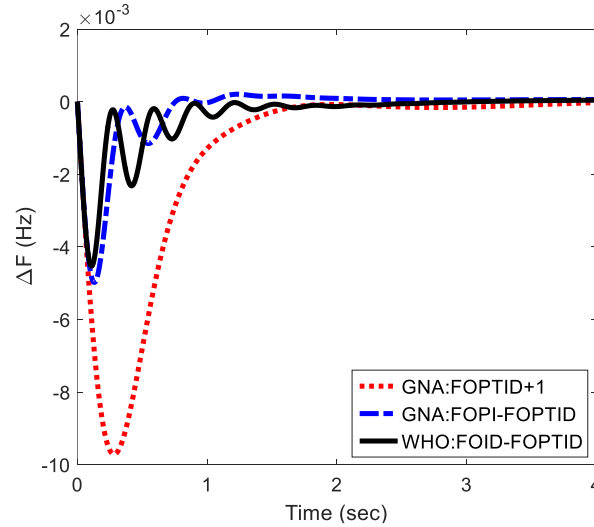
**Fig. 8.10** Single-area THG system response (ΔF).

Table 8.6				
ST/OS/US/ITAE in single-area THG system at $\Delta P_d = 0.01$ puMW.				
Type of controller	ST (sec)	US (Hz) (-ve)	OS (Hz)	ITAE
GNA: FOPTID+1	1.35	0.0096	0.0000386	0.0042
GNA: FOPI-FOPTID	0.67	0.0049	0.000207	0.0022
WHO: FOID-FOPTID	0.82	0.0045	0.000021	0.0027

Table 8.7
Tuned parameters of single-area THG system with WHO optimized controllers.

Controller type	K_{Ii}	K_{Di}	λ_i	μ_i	K_{Ti}	n_i	K_{Pi}	K_{Ii}	K_{Di}	λ_i	μ_i
WHO:PID	K_{I4}	K_{D4}	λ_4	μ_4	K_{T1}	n_1	K_{P1}	K_{I1}	K_{D1}	λ_1	μ_1
	-	-	-	-	-	-	4.0155	1.1685	1.4347	-	-
	K_{I5}	K_{D5}	λ_5	μ_5	K_{T2}	n_2	K_{P2}	K_{I2}	K_{D2}	λ_2	μ_2
	-	-	-	-	-	-	2.9435	2.4371	0.7023	-	-
	K_{I6}	K_{D6}	λ_6	μ_6	K_{T3}	n_3	K_{P3}	K_{I3}	K_{D3}	λ_3	μ_3
-	-	-	-	-	-	3.2554	4.5481	0.4396	-	-	
WHO:TID	K_{I4}	K_{D4}	λ_4	μ_4	K_{T1}	n_1	K_{P1}	K_{I1}	K_{D1}	λ_1	μ_1
	-	-	-	-	4.2293	4.5945	-	0.5695	1.7656	-	-
	K_{I5}	K_{D5}	λ_5	μ_5	K_{T2}	n_2	K_{P2}	K_{I2}	K_{D2}	λ_2	μ_2
	-	-	-	-	3.1007	3.9187	-	0.5307	1.2121	-	-
	K_{I6}	K_{D6}	λ_6	μ_6	K_{T3}	n_3	K_{P3}	K_{I3}	K_{D3}	λ_3	μ_3
-	-	-	-	1.9846	4.7319	-	3.0855	1.2781	-	-	
WHO:FOTID	K_{I4}	K_{D4}	λ_4	μ_4	K_{T1}	n_1	K_{P1}	K_{I1}	K_{D1}	λ_1	μ_1
	-	-	-	-	3.9054	2.6671	-	5.2024	4.6864	0.6474	0.7876
	K_{I5}	K_{D5}	λ_5	μ_5	K_{T2}	n_2	K_{P2}	K_{I2}	K_{D2}	λ_2	μ_2
	-	-	-	-	4.3885	1.1563	-	0.3336	2.8766	0.5677	0.3780
	K_{I6}	K_{D6}	λ_6	μ_6	K_{T3}	n_3	K_{P3}	K_{I3}	K_{D3}	λ_3	μ_3
-	-	-	-	4.7324	2.1505	-	1.8945	1.5149	0.7699	0.9249	
WHO:FOID-FOPTID	K_{I4}	K_{D4}	λ_4	μ_4	K_{T1}	n_1	K_{P1}	K_{I1}	K_{D1}	λ_1	μ_1
	2.2052	2.1573	0.5604	0.0137	0.8972	1.0894	2.7415	3.6027	2.4215	0.2053	0.3305
	K_{I5}	K_{D5}	λ_5	μ_5	K_{T2}	n_2	K_{P2}	K_{I2}	K_{D2}	λ_2	μ_2
	2.5926	0.3364	0.1425	0.1106	0.9519	1.3771	3.6097	0.3087	0.0426	0.6247	0.1922
	K_{I6}	K_{D6}	λ_6	μ_6	K_{T3}	n_3	K_{P3}	K_{I3}	K_{D3}	λ_3	μ_3
3.3369	2.0921	0.5670	0.4114	3.9332	3.0674	3.4631	3.9705	4.9406	0.1220	1.1447	

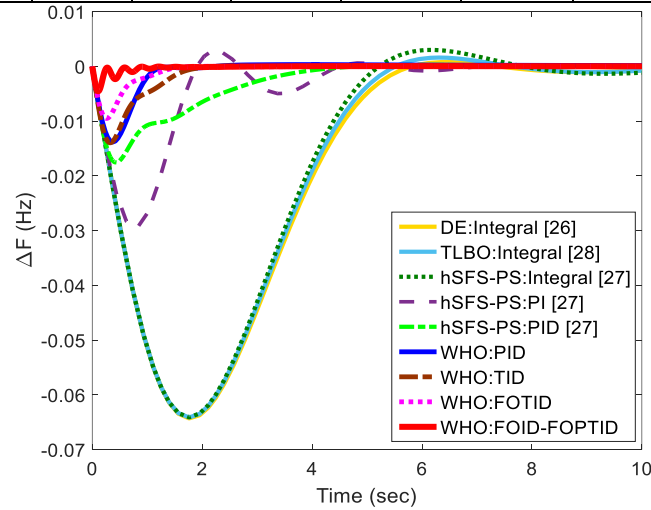


Fig. 8.11 Single-area THG system response (ΔF) with optimized FOID-FOPTID controller.

These values for GNA optimized FOPTID+1 controller are ITAE = 0.0042, ST = 1.35 sec, US = 0.0096, and OS = 0.0000386.

Table 8.8 ST/OS/US/ITAE in single-area THG system at $\Delta P_d = 0.01$ puMW.				
Type of controller	ST (sec)	US (Hz) (-ve)	OS (Hz)	ITAE
DE:Integral [26]	10.35	0.0640	0.00060	0.439
TLBO:Integral [28]	10.48	0.0638	0.00130	0.433
hSFS-PS:Integral [27]	11.15	0.0640	0.00315	0.437
hSFS-PS:PI [27]	6.57	0.0296	0.00280	0.0607
hSFS-PS:PID [27]	4.19	0.0180	0.00027	0.0425
WHO: PID	1.85	0.0140	0.00025	0.0154
WHO: TID	1.81	0.0138	0.000081	0.0075
WHO: FOTID	1.41	0.0095	0.000027	0.0037
WHO: FOID-FOPTID	0.82	0.0045	0.000021	0.0027

It is inferred that WHO:FOID-FOPTID controller considerably offers enhanced performance over FOPI-FOPTID and FOPTID+1 structured controllers. The order of performance is WHO:FOID-FOPTID \rightarrow GNA:FOPI-FOPTID \rightarrow GNA:FOPTID+1.

Next, Table 8.7 shows WHO optimized parameters of PID, TID, and FOTID and suggested FOID-FOPTID controllers. FOID-FOPTID controller parameters are same as given in Table 8.5. System results of ΔF response due to these controllers along with a few existing methodologies are shown in Fig. 8.11 and Table 8.8, reveals that WHO optimized PID controller has supremacy over the published results of hSFS-PS:PID/PI/Integral [27], TLBO:Integral [28], and DE:Integral [26] controllers in terms of lesser ITAE (0.0154), ST (1.85), US (0.0140), and OS (0.00025) values compared to them. It is also evident from Table 8.8, WHO optimized FOID-FOPTID controller has smallest ITAE (0.0027), ST (0.82), US (0.0045), and OS (0.000021), while these values for WHO optimized FOTID controller are ITAE = 0.0037, ST = 1.41 sec, US = 0.0095, and OS = 0.000027. These values for WHO optimized TID controller are ITAE = 0.0075, ST = 1.81 sec, US = 0.0138, and OS = 0.000081. WHO:FOID-FOPTID controller demonstrate considerably better performance than other controllers. Fig. 8.11 and Table

8.8 infers the controller performance decreases in the order WHO:FOID-FOPTID → WHO:FOTID → WHO:TID → WHO:PID → hSFS-PS:PID → hSFS-PS:PI → hSFS-PS:Integral → TLBO:Integral → DE:Integral.

8.6.4 Two-area Thermal-Hydro-Gas System

Further investigation is stretched on a multi-area THG system as displayed in Fig. 8.12. Each components of THG PS with rating capacity is discussed in chapter 6. Table 8.9 depicts the tuned gains of the suggested controller. Figs. 8.13(a-c) portrays results for ΔF_1 , ΔF_2 and ΔP_{tie12} responses at $\Delta P_{d1} = 0.01$ puMW. Fig. 8.14 and Table 8.10 infers that

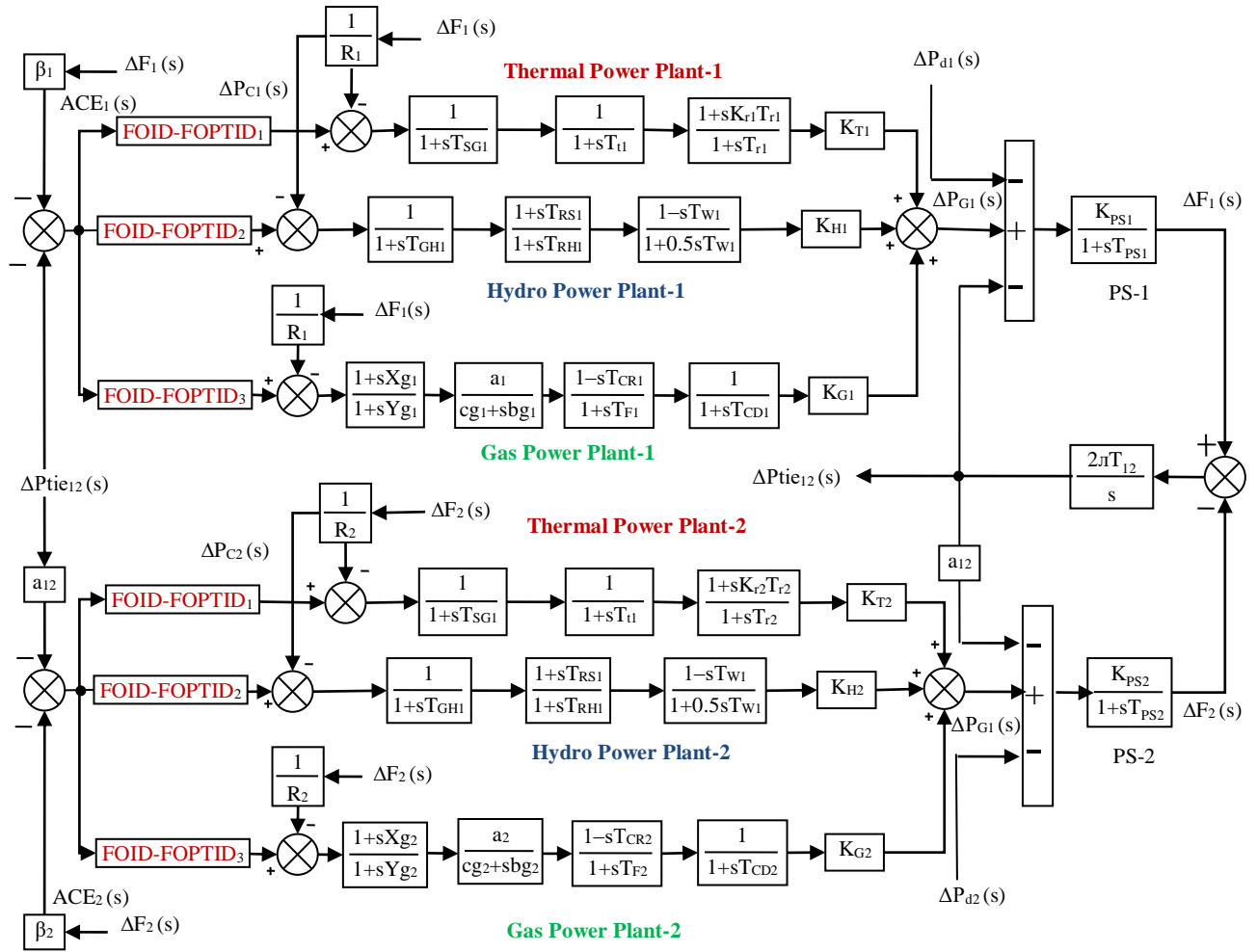


Fig. 8.12 Two-area THG system.

STs/USs/OSs and ITAE. For WHO optimized PID controller the values of ITAE (0.052), the WHO tuned PID controller performance is enhanced over the published results of hSFS-PS:PID [27], TLBO:PID [28], and DE:PID [26] controllers in terms of lesser ($\Delta F_1 = 5.7$, $\Delta F_2 = 3.22$, $\Delta P_{tie_{12}} = 3.36$), USs ($\Delta F_1 = -0.0130$, $\Delta F_2 = -0.0065$, $\Delta P_{tie_{12}} = -0.00179$), and OSs ($\Delta F_1 = 0.000742$, $\Delta F_2 = 0.000140$, $\Delta P_{tie_{12}} = 0.0000678$) are small. However, with WHO:PID, some values like STs ($\Delta P_{tie_{12}} = 3.36$) and USs ($\Delta F_2 = -0.0065$, $\Delta P_{tie_{12}} = -0.00179$) are slightly more than other PID controllers. But, in overall, WHO:PID is better than hSFS-PS:PID [27], TLBO:PID [28], and DE:PID [26] controllers. For WHO optimized FOID-FOPTID controller the values of ITAE (0.0079), STs ($\Delta F_1 = 0.67$, $\Delta F_2 = 0.84$, $\Delta P_{tie_{12}} = 1.75$), USs ($\Delta F_1 = -0.0052$, $\Delta F_2 = -0.000735$, $\Delta P_{tie_{12}} = -0.000326$), and OSs ($\Delta F_1 = 0.000281$, $\Delta F_2 = 0.0000416$, $\Delta P_{tie_{12}} = 0.00000328$)

Table 8.9
Tuned parameters of two-area THG system with WHO optimized controllers.

Controller type	K_{I1}	K_{D1}	λ_1	μ_1	K_{T1}	n_1	K_{P1}	K_{I2}	K_{D2}	λ_2	μ_2
WHO:PID	K_{I4}	K_{D4}	λ_4	μ_4	K_{T1}	n_1	K_{P1}	K_{I1}	K_{D1}	λ_1	μ_1
	-	-	-	-	-	-	4.9111	1.5206	2.1765	-	-
	K_{I5}	K_{D5}	λ_5	μ_5	K_{T2}	n_2	K_{P2}	K_{I2}	K_{D2}	λ_2	μ_2
	-	-	-	-	-	-	2.2865	0.1925	0.3670	-	-
	K_{I6}	K_{D6}	λ_6	μ_6	K_{T3}	n_3	K_{P3}	K_{I3}	K_{D3}	λ_3	μ_3
-	-	-	-	-	-	3.2837	4.8443	2.7460	-	-	
WHO:TID	K_{I4}	K_{D4}	λ_4	μ_4	K_{T1}	n_1	K_{P1}	K_{I1}	K_{D1}	λ_1	μ_1
	-	-	-	-	4.9568	2.6530	-	0.9850	4.1593	-	-
	K_{I5}	K_{D5}	λ_5	μ_5	K_{T2}	n_2	K_{P2}	K_{I2}	K_{D2}	λ_2	μ_2
	-	-	-	-	0.4396	1.5956	-	1.4009	0.7610	-	-
	K_{I6}	K_{D6}	λ_6	μ_6	K_{T3}	n_3	K_{P3}	K_{I3}	K_{D3}	λ_3	μ_3
-	-	-	-	4.9746	2.6676	-	0.7487	0.7239	-	-	
WHO:FOTID	K_{I4}	K_{D4}	λ_4	μ_4	K_{T1}	n_1	K_{P1}	K_{I1}	K_{D1}	λ_1	μ_1
	-	-	-	-	2.5294	1.6115	-	4.2698	4.6210	0.5182	0.9309
	K_{I5}	K_{D5}	λ_5	μ_5	K_{T2}	n_2	K_{P2}	K_{I2}	K_{D2}	λ_2	μ_2
	-	-	-	-	0.3052	1.6281	-	1.4614	4.5922	0.9652	0.2338
	K_{I6}	K_{D6}	λ_6	μ_6	K_{T3}	n_3	K_{P3}	K_{I3}	K_{D3}	λ_3	μ_3
-	-	-	-	1.7188	2.3980	-	3.1729	3.5522	0.4415	1.0731	
WHO: FOID-FOPTID	K_{I4}	K_{D4}	λ_4	μ_4	K_{T1}	n_1	K_{P1}	K_{I1}	K_{D1}	λ_1	μ_1
	4.0345	1.08	0.0059	0.8088	3.7526	1.5016	0.0469	4.6927	3.4767	0.8878	0.7653
	K_{I5}	K_{D5}	λ_5	μ_5	K_{T2}	n_2	K_{P2}	K_{I2}	K_{D2}	λ_2	μ_2
	1.2775	1.1930	0.3374	0.66220	2.8571	1.3715	0.7418	3.1687	4.4135	0.6400	0.4637
	K_{I6}	K_{D6}	λ_6	μ_6	K_{T3}	n_3	K_{P3}	K_{I3}	K_{D3}	λ_3	μ_3
1.5308	0.2153	0.2153	0.6502	0.0922	2.2296	3.6093	1.1669	0.6423	0.5560	0.5580	

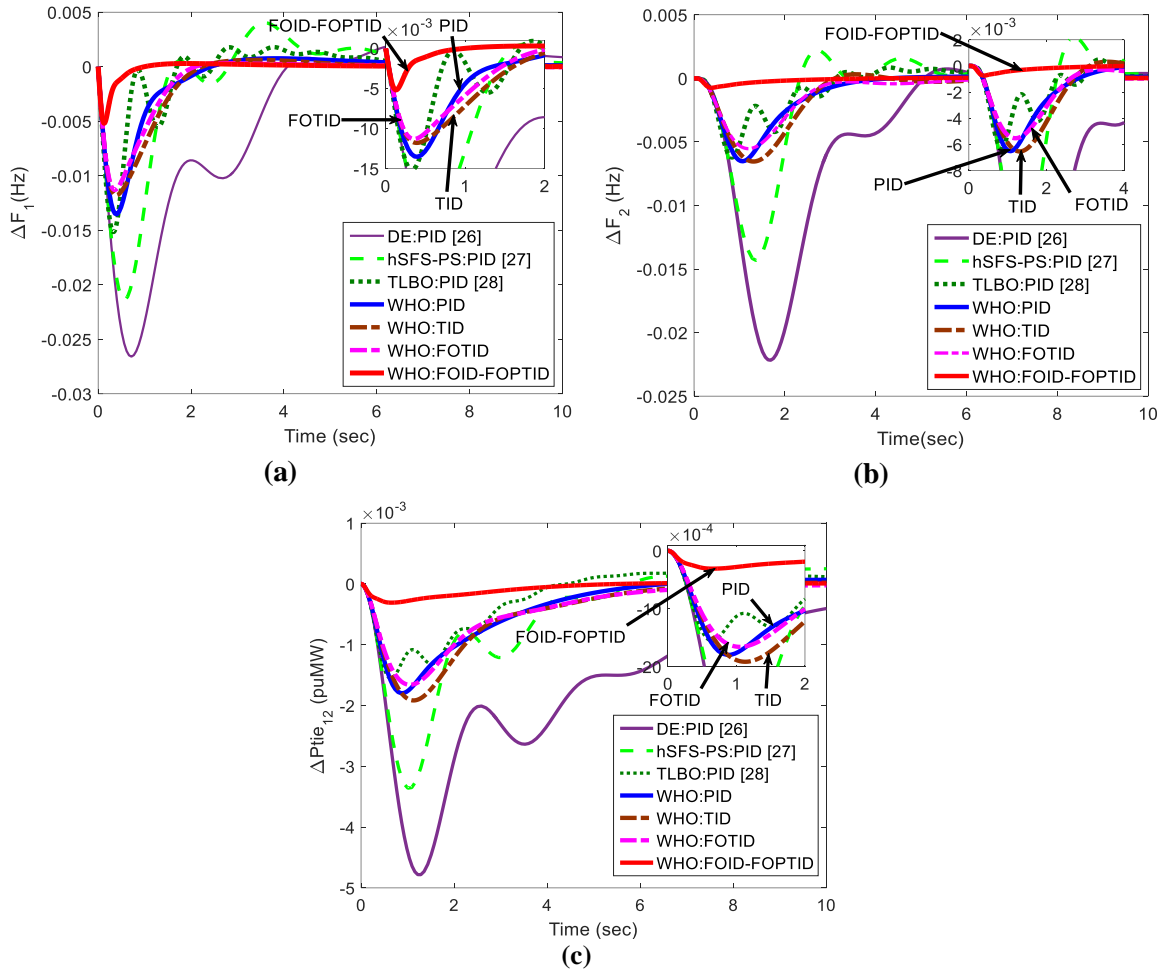


Fig. 8.13 Two-area THG system responses without GDB/GRC: (a) ΔF_1 , (b) ΔF_2 , and (c) $\Delta P_{tie_{12}}$.

Controller structure	ST (sec)			US (-ve) (Hz)		US (-ve) (puMW)	OS (Hz)		OS (puMW)	J
	ΔF_1	ΔF_2	$\Delta P_{tie_{12}}$	ΔF_1	ΔF_2	$\Delta P_{tie_{12}}$	ΔF_1	ΔF_2	$\Delta P_{tie_{12}}$	ITAE
DE: PID	13.097	8.523	9.222	0.0258	0.0215	0.00471	0.00197	0.000764	0.000187	0.290
hSFS-PS: PID [27]	8.58	7.34	3.885	0.0202	0.0134	0.00325	0.00392	0.00218	0.000246	0.129
TLBO: PID [28]	6.27	5.805	2.796	0.0139	0.0055	0.00155	0.00172	0.000825	0.000179	0.067
WHO: PID	5.7	3.22	3.36	0.0130	0.0065	0.00179	0.000742	0.000140	0.0000678	0.052
WHO: TID	4.53	2.86	3.30	0.0118	0.00652	0.00191	0.000853	0.000304	0.0000147	0.050
WHO: FOTID	1.86	2.89	3.25	0.0110	0.0055	0.00160	0.000348	0.000012	0.000011	0.0403
WHO: FOID-FOPTID	0.67	0.84	1.75	0.0052	0.000735	0.000326	0.000281	0.0000416	0.0000328	0.0079

are smallest compared to hSFS-PS:PID [27], TLBO:PID [28], DE:PID [26], and WHO:PID/TID/FOTID controllers. Hence, WHO optimized FOID-FOPTID controller is

enough capable to exhibit better performance than another considered controller. Finally, it is inferred from Table 8.10 and Fig. 8.13 that the performance is decreasing in the order: WHO:FOID-FOPTID \rightarrow WHO:FOTID \rightarrow WHO:TID \rightarrow WHO:PID \rightarrow TLBO:PID \rightarrow hSFS-PS:PID \rightarrow DE:PID.

8.6.5 Two-Area Thermal-Hydro-Gas System with GDB/GRC

Further investigation is stretched to a two-area THG PS including GDB/GRC nonlinearities is displayed by Fig. 8.14. Each components of THG PS with rating capacity is discussed in chapter 6. Three controllers are employed in each area. Both areas are connected with tie-lines. The GRC/GDB limits are discussed in Chapter 6. The

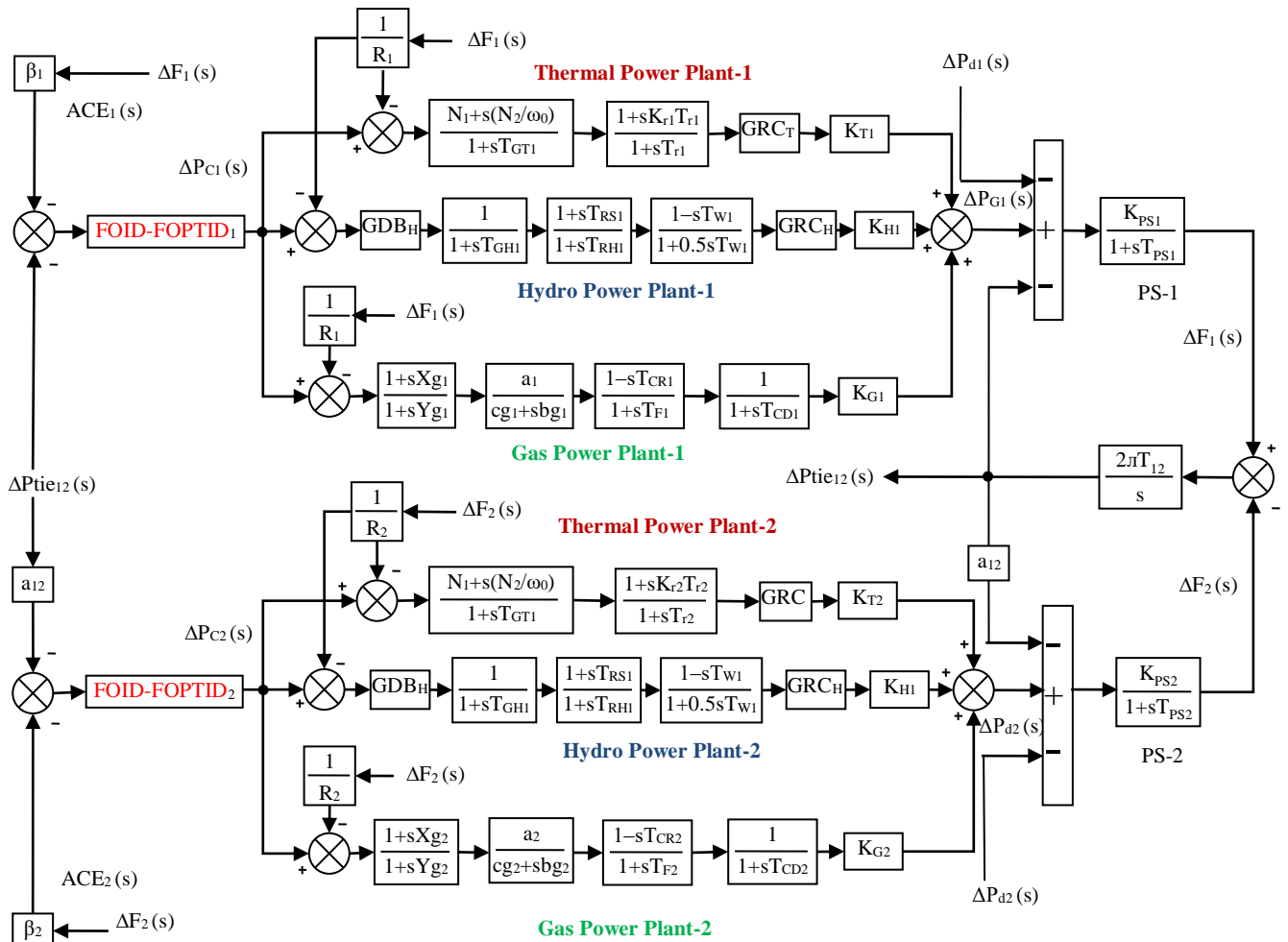


Fig. 8.14 Two-area THG system with GDB/GRC.

significant parameters are presented in Appendix. Table 8.11 depicts the tuned gains of the suggested controller. The results for ΔF_1 , ΔF_2 , and $\Delta P_{tie_{12}}$ responses are shown in Figs. 8.15(a-c) and Table 8.12. Fig. 8.15 and Table 8.12 infers that WHO tuned FOID-FOPTID controller portrays supremacy over the recently published results of Pathfinder algorithm (PFA):PID/TID/FOTID [41] and improved particle swarm optimization (IPSO):PID/TID/FOPID [40] controllers. WHO:FOID-FOPTID tuned controller has minimum ITAE (0.0723), STs ($\Delta F_1 = 8.72$, $\Delta F_2 = 8.21$, $\Delta P_{tie_{12}} = 4.95$), USs ($\Delta F_1 = -0.0047$, $\Delta F_2 = -0.0030$, $\Delta P_{tie_{12}} = -0.00071$), and OSs ($\Delta F_1 = 0.0020$, $\Delta F_2 = 0.00097$,

Controller type	K_{I1}	K_{D1}	λ_1	μ_1	K_{T1}	n_1	K_{P1}	K_{I1}	K_{D1}	λ_1	μ_1
IPSO:PID [40]	K_I	K_D	λ	μ	K_{T1}	n_1	K_{P1}	K_{I1}	K_{D1}	λ_1	μ_1
	-	-	-	-	-	-	0.8576	0.3189	0.6836	-	-
	K_{I3}	K_{D3}	λ_3	μ_3	K_{T2}	n_2	K_{P2}	K_{I2}	K_{D2}	λ_2	μ_2
IPSO:TID [40]	K_I	K_D	λ	μ	K_{T1}	n_1	K_{P1}	K_{I1}	K_{D1}	λ_1	μ_1
	-	-	-	-	0.1884	3.0000	-	0.1238	0.4095	-	-
	K_{I3}	K_{D3}	λ_3	μ_3	K_{T2}	n_2	K_{P2}	K_{I2}	K_{D2}	λ_2	μ_2
IPSO:FOPID [40]	K_I	K_D	λ	μ	K_{T1}	n_1	K_{P1}	K_{I1}	K_{D1}	λ_1	μ_1
	-	-	-	-	-	-	0.8615	1.8463	1.9990	0.6494	0.9990
	K_{I3}	K_{D3}	λ_3	μ_3	K_{T2}	n_2	K_{P2}	K_{I2}	K_{D2}	λ_2	μ_2
PFA:PID [41]	K_I	K_D	λ	μ	K_{T1}	n_1	K_{P1}	K_{I1}	K_{D1}	λ_1	μ_1
	-	-	-	-	-	-	1.6213	2.0000	0.8264	-	-
	K_{I3}	K_{D3}	λ_3	μ_3	K_{T2}	n_2	K_{P2}	K_{I2}	K_{D2}	λ_2	μ_2
PFA:TID [41]	K_I	K_D	λ	μ	K_{T1}	n_1	K_{P1}	K_{I1}	K_{D1}	λ_1	μ_1
	-	-	-	-	2.0000	2.3166	-	2.0000	2.0000	-	-
	K_{I3}	K_{D3}	λ_3	μ_3	K_{T2}	n_2	K_{P2}	K_{I2}	K_{D2}	λ_2	μ_2
PFA:FOTID [41]	K_I	K_D	λ	μ	K_{T1}	n_1	K_{P1}	K_{I1}	K_{D1}	λ_1	μ_1
	-	-	-	-	2.0000	3.0000	-	1.9943	1.3884	1.0001	1.3646
	K_{I3}	K_{D3}	λ_3	μ_3	K_{T2}	n_2	K_{P2}	K_{I2}	K_{D2}	λ_2	μ_2
WHO:FOID-FOPTID	K_I	K_D	λ	μ	K_{T1}	n_1	K_{P1}	K_{I1}	K_{D1}	λ_1	μ_1
	3.2462	1.9149	0.9759	0.9958	3.7816	2.8979	3.7498	4.4252	4.4953	0.7857	0.8252
	K_{I3}	K_{D3}	λ_3	μ_3	K_{T2}	n_2	K_{P2}	K_{I2}	K_{D2}	λ_2	μ_2
	3.3278	2.3191	0.5794	0.8046	3.9934	1.2783	2.3320	0.2134	3.6897	1.5725	1.1493
	4.3355	2.6021	0.7358	0.9995	2.2108	1.4957	1.9712	3.4187	4.5780	0.4446	0.7894
K_{I3}	K_{D3}	λ_3	μ_3	K_{T2}	n_2	K_{P2}	K_{I2}	K_{D2}	λ_2	μ_2	
0.3094	3.8738	0.4267	0.1034	2.6594	1.1761	0.2693	2.0219	0.9446	0.7308	0.9932	

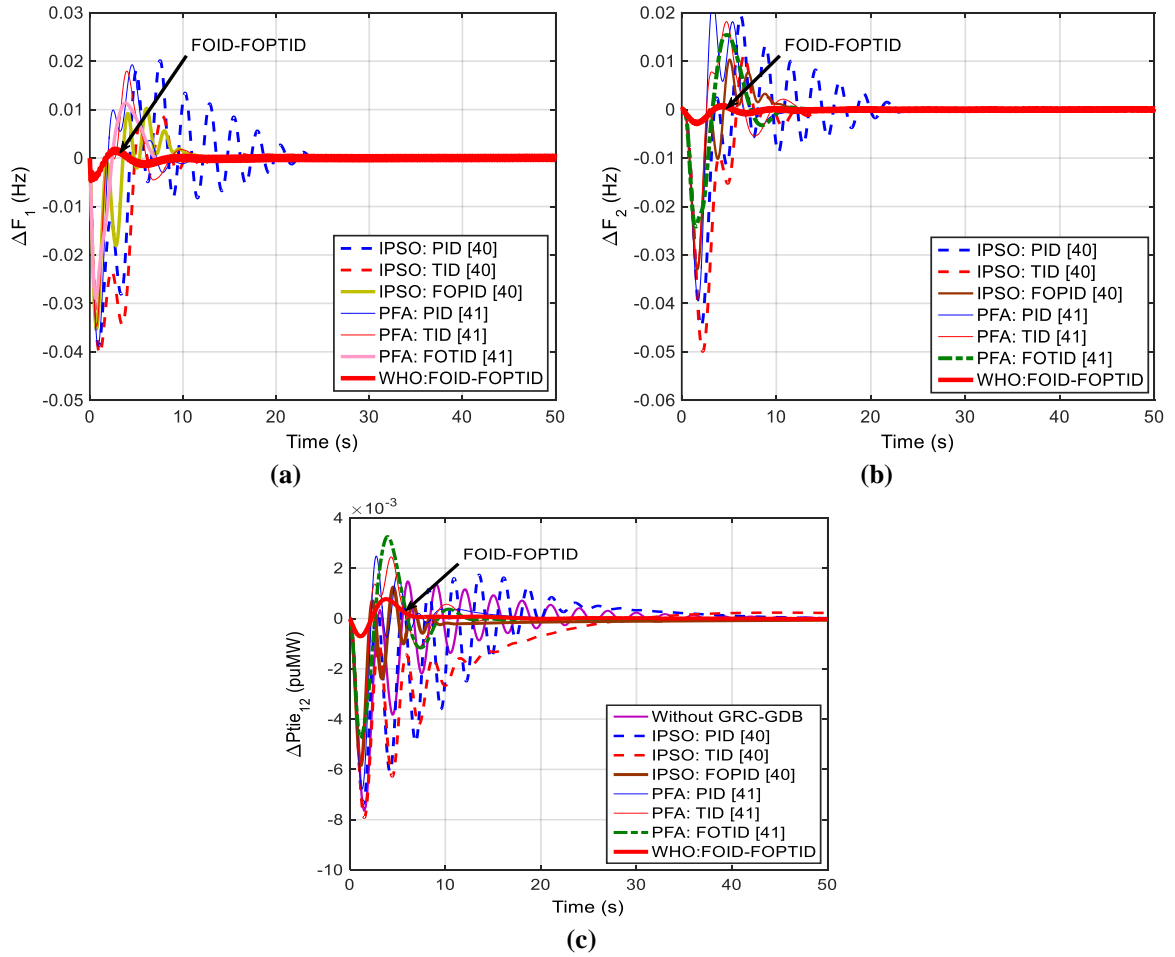


Fig. 8.15 Two-area THG system response with GDB/GRC: (a) ΔF_1 , (b) ΔF_2 , and (c) $\Delta P_{tie_{12}}$.

Controller structure	ST (sec)			US (-ve) (Hz)		US (-ve) (puMW)	OS (Hz)		OS (puMW)	J
	ΔF_1	ΔF_2	$\Delta P_{tie_{12}}$	ΔF_1	ΔF_2	$\Delta P_{tie_{12}}$	ΔF_1	ΔF_2	$\Delta P_{tie_{12}}$	ITAE
IPSO: PID [40]	24.46	24.7	24.2	0.039	0.045	0.0074	0.021	0.020	0.00183	1.176
IPSO: TID [40]	14.28	13.75	21.8	0.040	0.049	0.0089	0.0078	0.0089	0.00017	0.9829
IPSO: FOPID [40]	10.53	10.35	5.38	0.034	0.031	0.0056	0.0076	0.0070	0.00065	0.4677
PFA: PID [41]	10.85	11.1	6.51	0.039	0.040	0.0067	0.019	0.023	0.00248	0.6469
PFA: TID [41]	8.96	10.9	9.01	0.034	0.031	0.00563	0.011	0.012	0.00212	0.4382
PFA: FOTID [41]	11.32	10.8	8.14	0.025	0.022	0.00435	0.011	0.014	0.00323	0.4796
WHO: FOID-FOPTID	8.72	8.21	4.95	0.0047	0.0030	0.00071	0.0020	0.00097	0.00077	0.0723

$\Delta P_{tie_{12}} = 0.00077$) compared to IPSO:PID [40], IPSO:TID [40], IPSO:FOPID [40], PFA:PID [41], PFA:TID [41], and PFA:FOTID [41] controllers.

8.7 Conclusion

For a single-area reheat/non-reheat thermal PS the recommended WHO optimized PID controller has superior performance over the GNA optimized PID controller. Moreover, the dynamic response is enhanced. The research is stretched on a single-area THG PS and the responses of WHO optimized FOID-FOPTID controller are found better than GNA optimized FOPI-FOPTID/FOPTID+1 and WHO optimized PID/TID/FOTID controllers. Finally, then the advantage of WHO optimized FOID-FOPTID is established over WHO optimized PID/TID/FOTID for two-area multi-source THG PS and IPSO:PID/TID/FOPID and PFA:PID/TID/FOTID for two-area multi-source THG PS with nonlinearities.

CHAPTER 9

USE OF ENERGY STORAGE SYSTEMS

9.1 Introduction

Increasing load demand by the consumers has made, the researchers worldwide to recommend various new control strategies, and consider AGC problem actively. For efficient AGC in modern PSs, an extensive number of innovative optimization techniques, controllers, and algorithms have recently been given. But there is always research gap to find new methods for stabilizing power with AGC systems. Hence new ideas like energy storage systems are increasing every day to control the output power.

Energy storage system (ESS) research has recently been introduced to PS in an effort to improve dynamic performance by lessening the impact of disruptions. AGC of various PS [12–16], multi-area multi-source renewable PS [20–30, 32], other systems [34, 36–39], etc. have all seen the expediency of ESS influence. Using the ESS technique to regulate an industrial process has several benefits, including effective output disturbance rejection, robustness to deviations in the plant's gain, steady-state errors, and more.

In light of the above, in this chapter an attempt has been made to investigate the impact of some ESSs and WHO tuned FOID-FOPTID controller employed in single/two-area multi-source THG PS.

9.2 Energy Storage Systems (ESSs)

Recently, several ESSs are available in literature like capacitive ES (CES) [174,205,229–231], superconducting magnetic ES (SMES) [93,112,209,224,225,250, 256], redox flow battery (RFB) [15,16,25,38,48,49,66,94,113,142,228,234], battery ES

(BES) [14,217,254], ultra-capacitor (UC) [12,39,47,125,198], flywheel ES (FES) [220,221,254,255] etc. These ESSs have shown advantage with optimized controllers and intelligent algorithms. The impact of CES, SMES, and RFB are investigated on single-area THG PS and two-area THG PS as explained in sections 9.2.1-9.2.3.

9.2.1 Capacitive Energy Storage (CES)

The CES [229–231] is becoming more and more popular in today's PS because to its high-power density and quick, efficient charging and discharging capabilities. One benefit of CES is its rapid response time and ability to supply power in large quantities as demand rises. It is less priced and simple to use. It is highly efficient and has a long service life. The primary unit of CES system is a super capacitor to store energy [230]. Static charge is stored as energy using capacitor plates. When there is an abrupt demand for power, CES returns stored energy to the grid. The CES model is depicted in Fig. 9.1 [230],

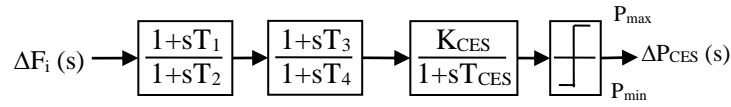


Fig. 9.1 Block CES linearized model [230].

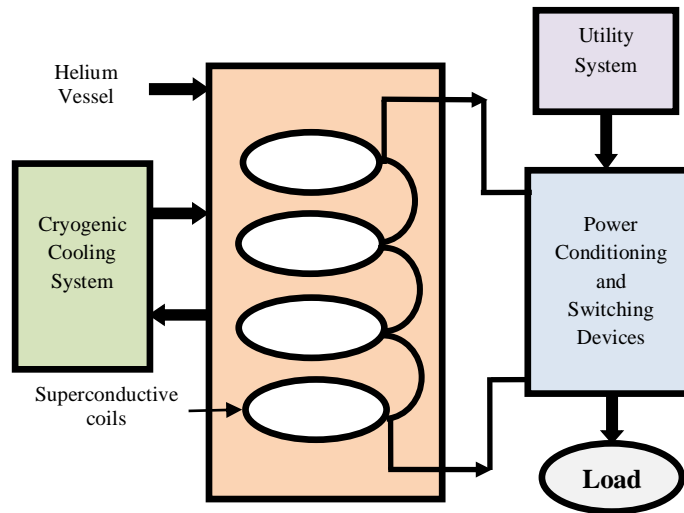


Fig. 9.2 SMES schematic diagram [226].

Where K_{CES}/T_{CES} stand for the CES's gain/time constant, respectively. The formula for the incremental power change of the CES is defined by Eqn. (9.1) [230].

$$\Delta P_{CES} = \left[\frac{K_{CES}}{1+sT_{CES}} \right] \left[\frac{1+sT_1}{1+sT_2} \right] \left[\frac{1+sT_3}{1+sT_4} \right] \Delta F_i \quad (9.1)$$

Where, the phase compensation blocks' time constants with dual-stage are denoted by the variables $i = 1, 2, T_1, T_2, T_3,$ and T_4 . All of the PS's examined regions incorporate CES. Each CES unit receives the frequency deviation (ΔF_i) of area- i as its input control signal. The range $\Delta P_{min} \leq \Delta P_{CES} \leq \Delta P_{max}$ specifies the maximum and minimum power limits. Where, $\Delta P_{max} = 0.01 \text{ puMW}$ and $\Delta P_{min} = -0.01 \text{ puMW}$.

9.2.2 Superconducting Magnetic Energy Storage (SMES)

A coil's magnetic field is used by the SMES device to store electrical power. With very little energy loss, the coil's magnetic field is produced by a superconducting wire. For a

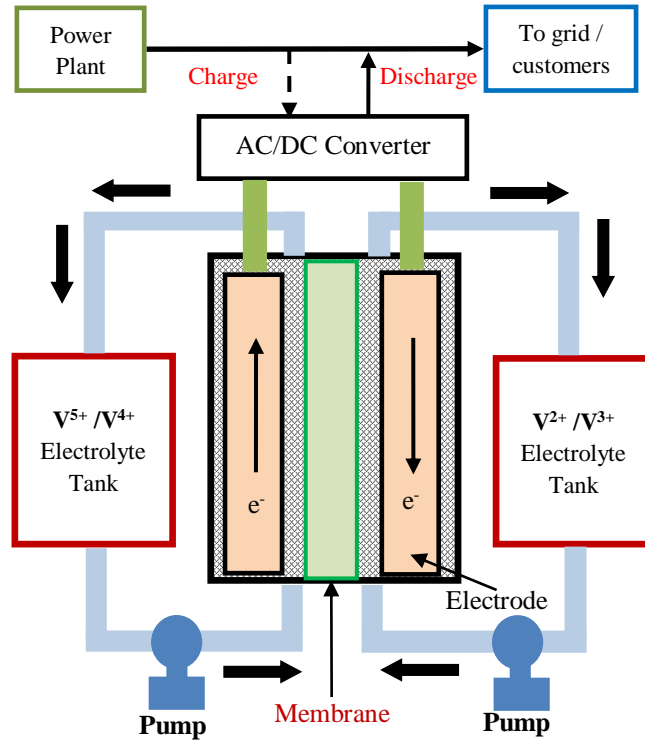


Fig. 9.3 RFB schematic diagram [16].

brief period of time, the SMES [224,225] unit can produce and/or absorb electricity at its rated capacity. The SMES is protected by a cryogenic system and a power conditioning system that keeps its temperature below the superconductor's critical point. To prevent current conduction in the charged superconducting coil, it is submerged in low temperature liquid helium. The utility system supplies power to switching devices and the power conversion/conditioning system. The components of SMES are a step-down transformer, an AC/DC converter, and an inductor-converter unit containing a DC superconducting inductor. When a load demand occurs, the energy that the SMES has stored is released. Fig. 9.2 displays the SMES schematic diagram, and TF is given by the Eqn. (9.2) [225].

$$G_{\text{SMES}}(s) = \frac{K_{\text{SMES}}}{1 + sT_{\text{SMES}}} \quad (9.2)$$

9.2.3 Redox Flow Battery (RFB)

These days, RFB is a quick-rechargeable battery. Electrochemical conversion is a step in the reduction-oxidation (redox) process. A dual converter performs the functions of the rectifier and inverter. When the governor reaction is lagging, rapid storing operation is completed because of the lag time in RFB. This benefit lessens the impact on the environment and gets rid of oscillations. Flow cells, electrolyte tanks, pipes, and pumps make up RFB. The pump moves electrolyte back and forth between the cells and tank. RFB's primary attributes include its adaptability, freed power capacity, abundant efficacy, etc. It has a long performance life, little losses, and ease of operation. When a load need arises, RFB delivers the energy it has stored during charging. Applications in storage durations of two to ten hours are appropriate for RFB [40], with power ratings range in kW to MW. The values of $P_{\text{max}} = 0.01 \text{ puMW}$ and $P_{\text{min}} = -0.01 \text{ puMW}$, is permitted for

the base power of the power system. RFB is a better ESS due to these features. The schematic diagram is displayed in Fig. 9.3 [34,40] and TF is given by the Eqn. (9.3) [16].

$$G_{\text{RFB}}(s) = \frac{K_{\text{RFB}}}{1+sT_{\text{RFB}}} \quad (9.3)$$

9.3 Systems Investigated

A single/two-area multi-source THG PS is examined without/with nonlinearities using WHO optimized FOID-FOPTID controller with energy storage systems (ESS). Components of THG PS is discussed earlier in chapter 6. The transfer function block diagrams of the PSs investigated are portrayed in Fig. 9.4, Fig. 9.6, and Fig. 9.8.

9.4 Simulation Results and Discussions

9.4.1 Single-Area Thermal-Hydro-Gas System with ESS

Considering a 1% SLP at $t = 0$ sec, the data provided in the Appendix is used in modelling a single-area THG PS. The relationships between THG units and the location of SLP inputs are clearly illustrated by the PS model in Fig. 9.4. The ESS block with FOID-FOPTID controller is incorporated in Fig. 9.4. The tuned parameters of the suggested WHO:FOID-FOPTID controller with ESSs like SMES, CES,

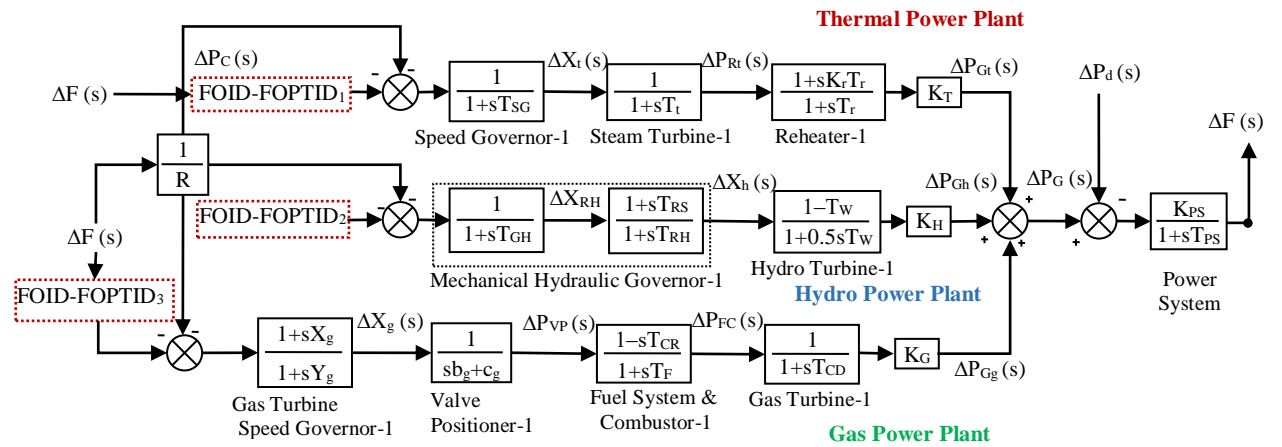


Fig. 9.4 Single-area THG system with ESSs.

Table 9.1
Tuned parameters of single-area THG system with WHO optimized FOID-FOPTID controller and ESSs.

Controller type	K_{Ii}	K_{Di}	λ_i	μ_i	K_{Ti}	n_i	K_{Pi}	K_{Ii}	K_{Di}	λ_i	μ_i
WHO:FOID-FOPTID with SMES	K_{I4}	K_{D4}	λ_4	μ_4	K_{T1}	n_1	K_{P1}	K_{I1}	K_{D1}	λ_1	μ_1
	4.1398	1.7187	0.1744	0.4259	2.8601	3.7555	0.1094	2.6657	2.3192	0.0902	0.9359
	K_{I5}	K_{D5}	λ_5	μ_5	K_{T2}	n_2	K_{P2}	K_{I2}	K_{D2}	λ_2	μ_2
	2.4656	0.9338	0.1487	0.1795	4.9900	2.8480	4.6549	4.9134	2.8006	0.9296	0.8955
WHO:FOID-FOPTID with CES	K_{I4}	K_{D4}	λ_4	μ_4	K_{T1}	n_1	K_{P1}	K_{I1}	K_{D1}	λ_1	μ_1
	4.2210	2.8073	0.3047	0.2896	4.2881	3.9731	2.0502	4.3743	4.2340	0.0885	0.8947
	K_{I5}	K_{D5}	λ_5	μ_5	K_{T2}	n_2	K_{P2}	K_{I2}	K_{D2}	λ_2	μ_2
	3.3297	2.1692	0.6092	0.3707	0.0415	3.4894	2.1272	2.5152	4.9480	0.1234	0.0661
WHO:FOID-FOPTID with RFB	K_{I4}	K_{D4}	λ_4	μ_4	K_{T1}	n_1	K_{P1}	K_{I1}	K_{D1}	λ_1	μ_1
	4.1531	2.2156	0.5008	0.8249	0.8456	3.0075	3.9816	2.6521	2.7456	0.2440	0.0171
	K_{I5}	K_{D5}	λ_5	μ_5	K_{T2}	n_2	K_{P2}	K_{I2}	K_{D2}	λ_2	μ_2
	3.6919	0.3487	0.3177	0.2017	1.9877	2.5174	4.5706	1.3636	1.6296	0.8798	0.3396
WHO:FOID-FOPTID with RFB	K_{I6}	K_{D6}	λ_6	μ_6	K_{T3}	n_3	K_{P3}	K_{I3}	K_{D3}	λ_3	μ_3
	4.9868	0.0617	0.7859	0.8648	3.5392	3.6772	1.3680	0.6879	3.5034	0.6831	0.1747
	K_{I4}	K_{D4}	λ_4	μ_4	K_{T1}	n_1	K_{P1}	K_{I1}	K_{D1}	λ_1	μ_1
	4.1531	2.2156	0.5008	0.8249	0.8456	3.0075	3.9816	2.6521	2.7456	0.2440	0.0171
WHO:FOID-FOPTID with RFB	K_{I5}	K_{D5}	λ_5	μ_5	K_{T2}	n_2	K_{P2}	K_{I2}	K_{D2}	λ_2	μ_2
	3.6919	0.3487	0.3177	0.2017	1.9877	2.5174	4.5706	1.3636	1.6296	0.8798	0.3396
	K_{I6}	K_{D6}	λ_6	μ_6	K_{T3}	n_3	K_{P3}	K_{I3}	K_{D3}	λ_3	μ_3
	4.9990	1.6500	0.4364	0.2921	4.9895	3.6141	4.7684	0.8158	3.2594	0.4674	0.6080

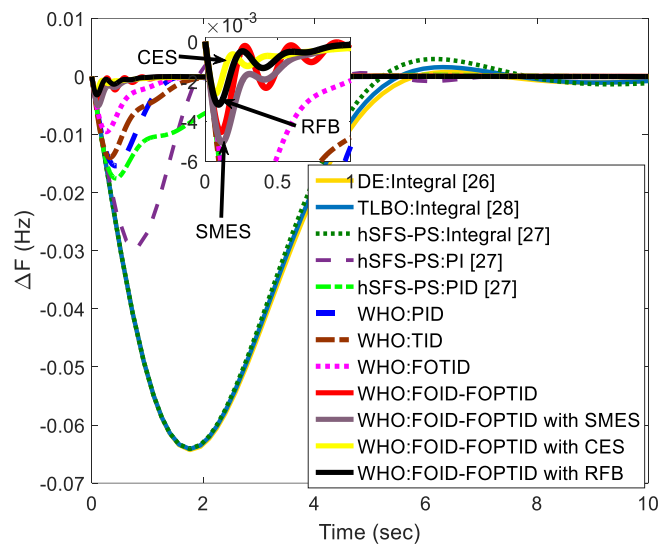


Fig. 9.5 Single-area THG system response (ΔF) with ESS.

and RFB are presented in Table 9.1 and the system dynamic results for ΔF response are shown in Fig. 9.5. Critical examination of responses Fig. 9.5 and Table 9.2 evidently interprets that substantial enhancements are witnessed with new WHO optimized FOID-FOPTID controller against the existing DE:Integral [26], TLBO:Integral [28], hSFS-PS:Integral [27], hSFS-PS:PI [27], hSFS-PS:PID [27], and WHO:PID, WHO:TID,

Type of controller	ST (sec)	US (Hz) (-ve)	OS (Hz)	ITAE
DE:Integral [26]	10.35	0.0640	0.00060	0.439
TLBO:Integral [28]	10.48	0.0638	0.00130	0.433
hSFS-PS:Integral [27]	11.15	0.0640	0.00315	0.437
hSFS-PS:PI [27]	6.57	0.0296	0.00280	0.0607
hSFS-PS:PID [27]	4.19	0.0180	0.00027	0.0425
WHO:PID	1.85	0.0140	0.00025	0.0154
WHO:TID	1.81	0.0138	0.000081	0.0075
WHO:FOTID	1.41	0.0095	0.000027	0.0037
WHO:FOID-FOPTID	0.82	0.0045	0.000021	0.0027
WHO:FOID-FOPTID with SMES	0.78	0.0051	0.000109	0.00110
WHO:FOID-FOPTID with CES	0.73	0.0026	0.0000208	0.00097
WHO:FOID-FOPTID with RFB	0.75	0.00313	0.00000161	0.00086

WHO:FOTID controllers. Next, WHO:FOID-FOPTID with ESSs (SMES/CES/RFB) provides better performance compared to WHO:FOID-FOPTID without ESSs.

It is evident from Table 9.2 that ΔF response observed for WHO:FOID-FOPTID controller with RFB has ITAE = 0.00086, ST = 0.75, US = 0.00313, and OS = 0.00000161, while these values with CES are ITAE = 0.00097, ST = 0.73, US = 0.00260, and OS = 0.0000208. These values for SMES are ITAE = 0.00110, ST = 0.78, US = 0.0051, and OS = 0.000109. This shows the enhanced results are obtained with ESS (SMES, CES, or RFB) compared to WHO:FOID-FOPTID controller without ESS. Without ESS, WHO:FOID-FOPTID controller offers ITAE = 0.0027, ST = 0.82, US = 0.0045, and OS = 0.000021. Here, ITAE/ST values are higher and US/OS are lower than WHO:FOID-FOPTID controller with ESS. In overall, it is observed that the best performance is obtained with ESS specifically with RFB.

9.4.2 Two-Area Thermal-Hydro-Gas System with ESS

Further research is stretched on a two-area THG PS. At $t = 0$ sec, the PS is simulated with a 1% SLP in area-1. The relationships between THG units and the location of SLP inputs

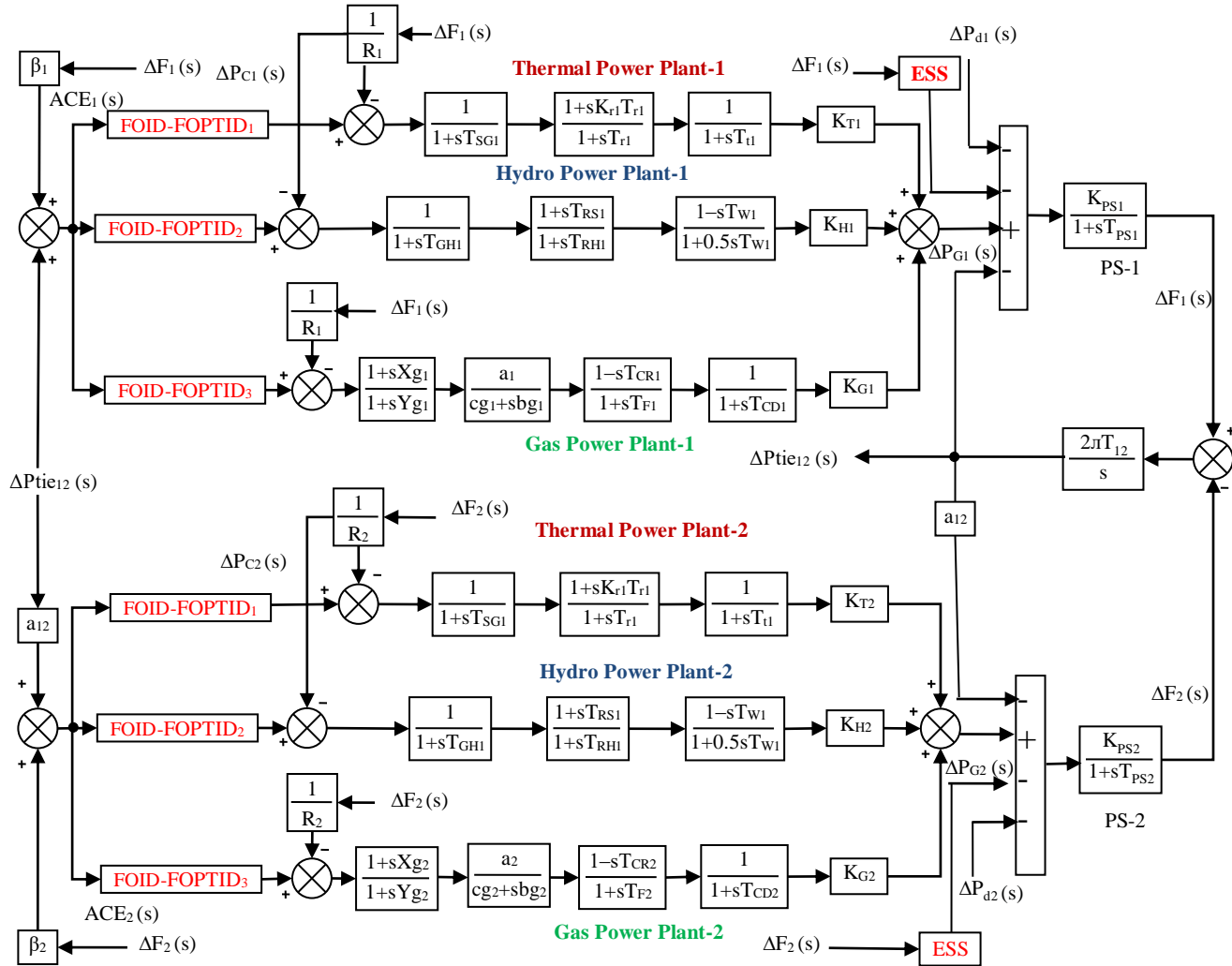


Fig. 9.6 Two-area THG system with ESS.

Table 9.3 Tuned parameters of two-area THG system with ESSs.											
Controller type	K_{Ii}	K_{Di}	λ_i	μ_i	K_{Ti}	n_i	K_{Pi}	K_{Ii}	K_{Di}	λ_i	μ_i
WHO:FOID-FOPTID with CES	K_{I4}	K_{D4}	λ_4	μ_4	K_{T1}	n_1	K_{P1}	K_{I1}	K_{D1}	λ_1	μ_1
	4.6826	2.3770	0.1958	0.6408	4.6651	3.3200	2.3343	3.8221	3.9999	0.6890	0.7566
	K_{I5}	K_{D5}	λ_5	μ_5	K_{T2}	n_2	K_{P2}	K_{I2}	K_{D2}	λ_2	μ_2
	0.7161	2.9353	0.2751	0.2751	3.2480	1.8541	0.6520	0.5703	2.3975	0.3745	0.7698
	K_{I6}	K_{D6}	λ_6	μ_6	K_{T3}	n_3	K_{P3}	K_{I3}	K_{D3}	λ_3	μ_3
	0.4076	1.9402	0.4754	0.3757	2.2426	3.0201	4.6940	4.5684	3.7916	0.8749	0.0187
WHO:FOID-FOPTID with SMES	K_{I4}	K_{D4}	λ_4	μ_4	K_{T1}	n_1	K_{P1}	K_{I1}	K_{D1}	λ_1	μ_1
	2.5700	3.7657	0.4012	0.5060	4.9921	1.3480	3.3912	3.9792	3.6542	0.3572	0.7035
	K_{I5}	K_{D5}	λ_5	μ_5	K_{T2}	n_2	K_{P2}	K_{I2}	K_{D2}	λ_2	μ_2
	3.3984	3.5942	0.4874	0.1900	3.4821	1.5360	0.2277	3.6324	4.4268	0.3466	0.0625
	K_{I6}	K_{D6}	λ_6	μ_6	K_{T3}	n_3	K_{P3}	K_{I3}	K_{D3}	λ_3	μ_3
1.7460	3.8885	0.7735	0.3131	3.4741	2.2026	2.6937	3.9116	1.0773	0.2768	0.5880	
WHO:FOID-FOPTID with RFB	K_{I4}	K_{D4}	λ_4	μ_4	K_{T1}	n_1	K_{P1}	K_{I1}	K_{D1}	λ_1	μ_1
	4.5575	4.8144	0.0315	0.7254	4.3841	1.3868	3.8957	4.3919	0.9390	0.3698	0.8977
	K_{I5}	K_{D5}	λ_5	μ_5	K_{T2}	n_2	K_{P2}	K_{I2}	K_{D2}	λ_2	μ_2
	3.9162	3.03309	0.4247	0.0507	0.4655	2.0857	4.3264	1.6041	3.3263	0.5088	0.4227
	K_{I6}	K_{D6}	λ_6	μ_6	K_{T3}	n_3	K_{P3}	K_{I3}	K_{D3}	λ_3	μ_3
0.6015	0.4253	0.7488	0.9209	4.4202	2.5211	3.3877	2.4279	4.2080	0.8766	0.9082	

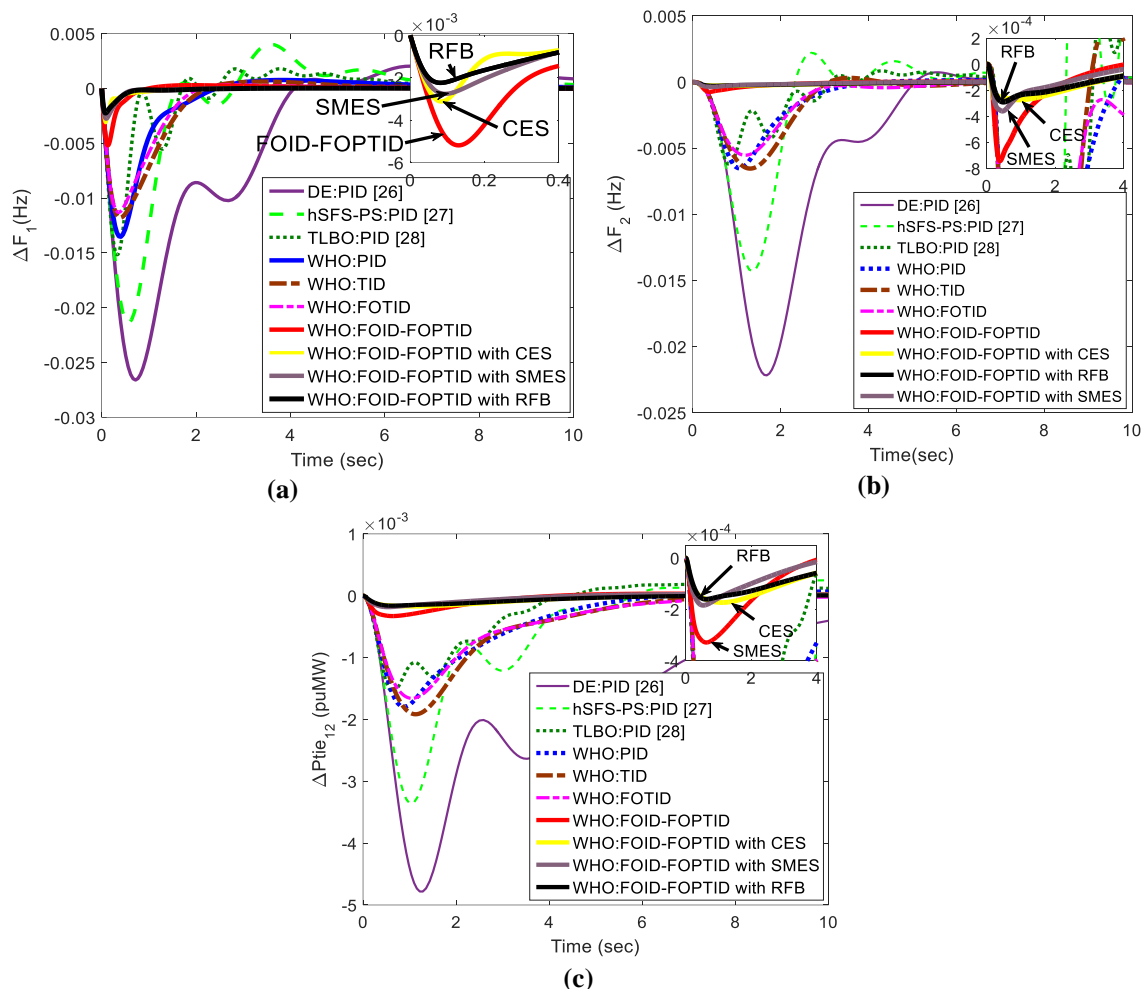


Fig. 9.7 Two-area THG system response with ESS: (a) ΔF_1 , (b) ΔF_2 , and (c) $\Delta P_{tie_{12}}$.

are clearly illustrated by the system model in Fig. 9.6. ESS is incorporated in both areas of the model. The impact of ESS with WHO:FOID-FOPTID controller on the dynamic results is shown here. The tuned parameters of the suggested WHO:FOID-FOPTID controller with ESSs are presented in Table 9.3 and Fig. 9.7(a-c) portrays the PS dynamic results for $\Delta F_1/\Delta F_2/\Delta P_{tie_{12}}$, however the acute scrutiny interprets that significant enhancements are witnessed with new WHO:FOID-FOPTID controller over DE:PID [26], hSFS-PS:PID [27], TLBO:PID [28], WHO:PID, WHO:TID, and WHO:FOTID structured control methods. It is also observed that WHO:FOID-FOPTID controller with ESS offers better results than WHO:FOID-FOPTID controller without ESS as all values

Table 9.4
ST/OS/US/ITAE in two-area THG system with ESS at $\Delta P_{d1} = 0.01$ puMW.

Controller structure	ST (sec)			US (-ve) (Hz)		US (-ve) (puMW)	OS (Hz)		OS (puMW)	J
	ΔF_1	ΔF_2	ΔP_{tie12}	ΔF_1	ΔF_2	ΔP_{tie12}	ΔF_1	ΔF_2	ΔP_{tie12}	ITAE
DE:PID [26]	13.097	8.523	9.222	0.0258	0.0215	0.00471	0.00197	0.000764	0.000187	0.290
hSFS-PS:PID [27]	8.58	7.34	3.885	0.0202	0.0134	0.00325	0.00392	0.00218	0.000246	0.129
TLBO:PID [28]	6.27	5.805	2.796	0.0139	0.0055	0.00155	0.00172	0.000825	0.000179	0.067
WHO: PID	5.7	3.22	3.36	0.0130	0.0065	0.00179	0.000742	0.000140	0.0000678	0.052
WHO: TID	4.53	2.86	3.30	0.0118	0.00652	0.00191	0.000853	0.000304	0.0000147	0.050
WHO:FOTID	1.86	2.89	3.25	0.011	0.0055	0.0016	0.000348	0.000012	0.000011	0.0403
WHO:FOID-FOPTID	0.67	0.84	1.75	0.0052	0.000735	0.000326	0.000281	0.0000416	0.0000328	0.0079
WHO:FOID-FOPTID with CES	0.58	2.26	3.0	0.0032	0.000271	0.000173	0.0000514	0.0000097	0.0000130	0.0052
WHO:FOID-FOPTID with SMES	0.48	1.28	1.98	0.0031	0.000355	0.000184	0.0000748	0.0000307	0.0000266	0.0055
WHO:FOID-FOPTID with RFB	0.50	1.94	2.77	0.0022	0.000290	0.000158	0.0000265	0.00000196	0.0000047	0.0043

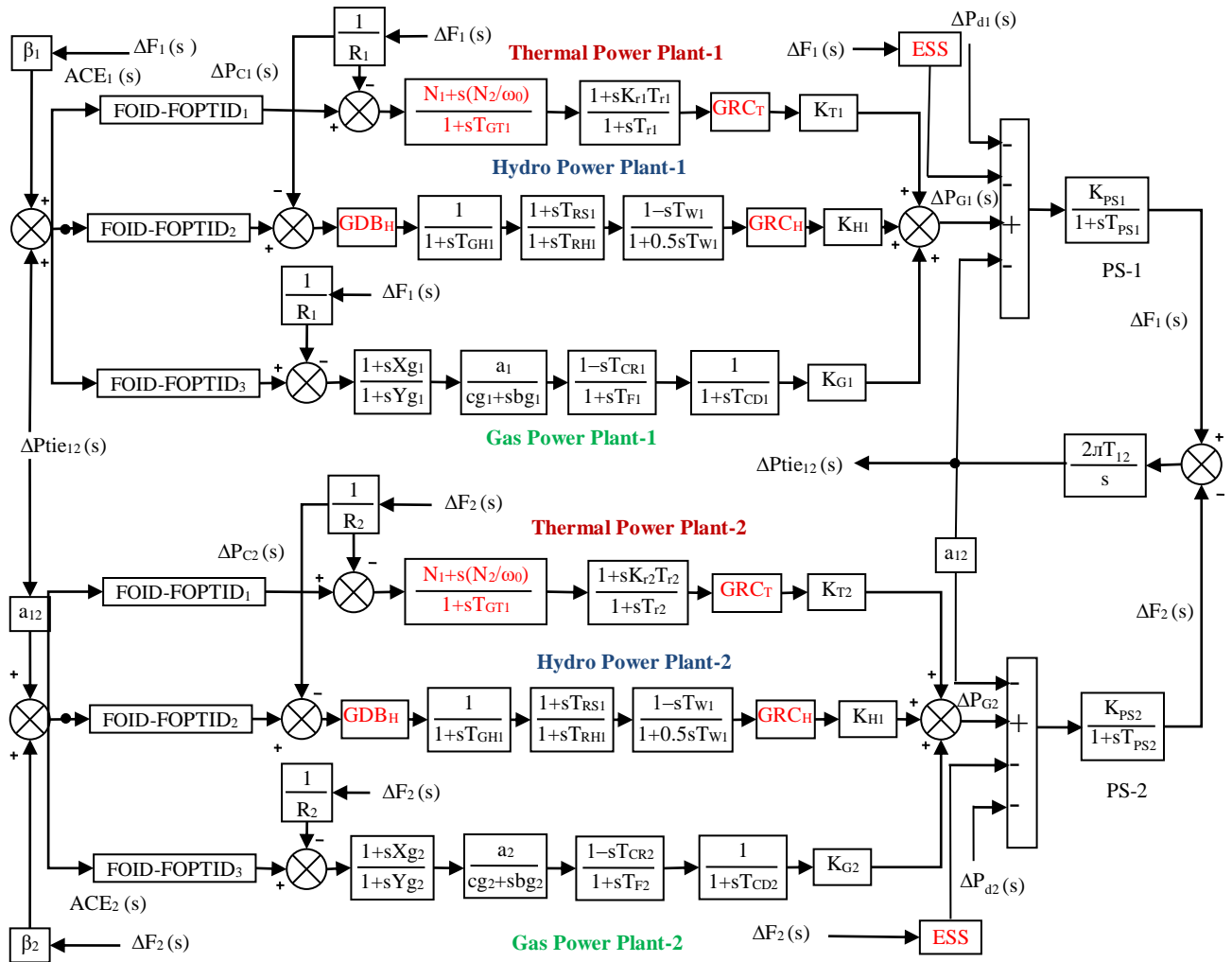


Fig. 9.8 Two-area THG system with GDB/GRC and ESS.

Table 9.5
Optimized parameters of two-area THG system with GRC/GDB and ESS.

Controller Type	K_{I1}	K_{D1}	λ_1	μ_1	K_{T1}	n_1	K_{P1}	K_{I2}	K_{D2}	λ_2	μ_2
WHO:FOID-FOPTID with SMES	K_{I1}	K_{D1}	λ_1	μ_1	K_{T1}	n_1	K_{P1}	K_{I2}	K_{D2}	λ_2	μ_2
	3.3506	0.9764	0.4810	1.2690	3.6155	2.3669	3.9516	1.9264	2.6892	0.7374	0.8144
WHO:FOID-FOPTID with CES	K_{I1}	K_{D1}	λ_1	μ_1	K_{T1}	n_1	K_{P1}	K_{I2}	K_{D2}	λ_2	μ_2
	3.6464	4.8467	0.6053	0.8663	3.2810	2.2551	0.8313	3.1271	1.1910	0.4775	1.0915
WHO:FOID-FOPTID with RFB	K_{I1}	K_{D1}	λ_1	μ_1	K_{T1}	n_1	K_{P1}	K_{I2}	K_{D2}	λ_2	μ_2
	4.3355	2.6021	0.7358	0.9995	2.2108	1.4957	1.9712	3.4187	4.5780	0.4446	0.7894

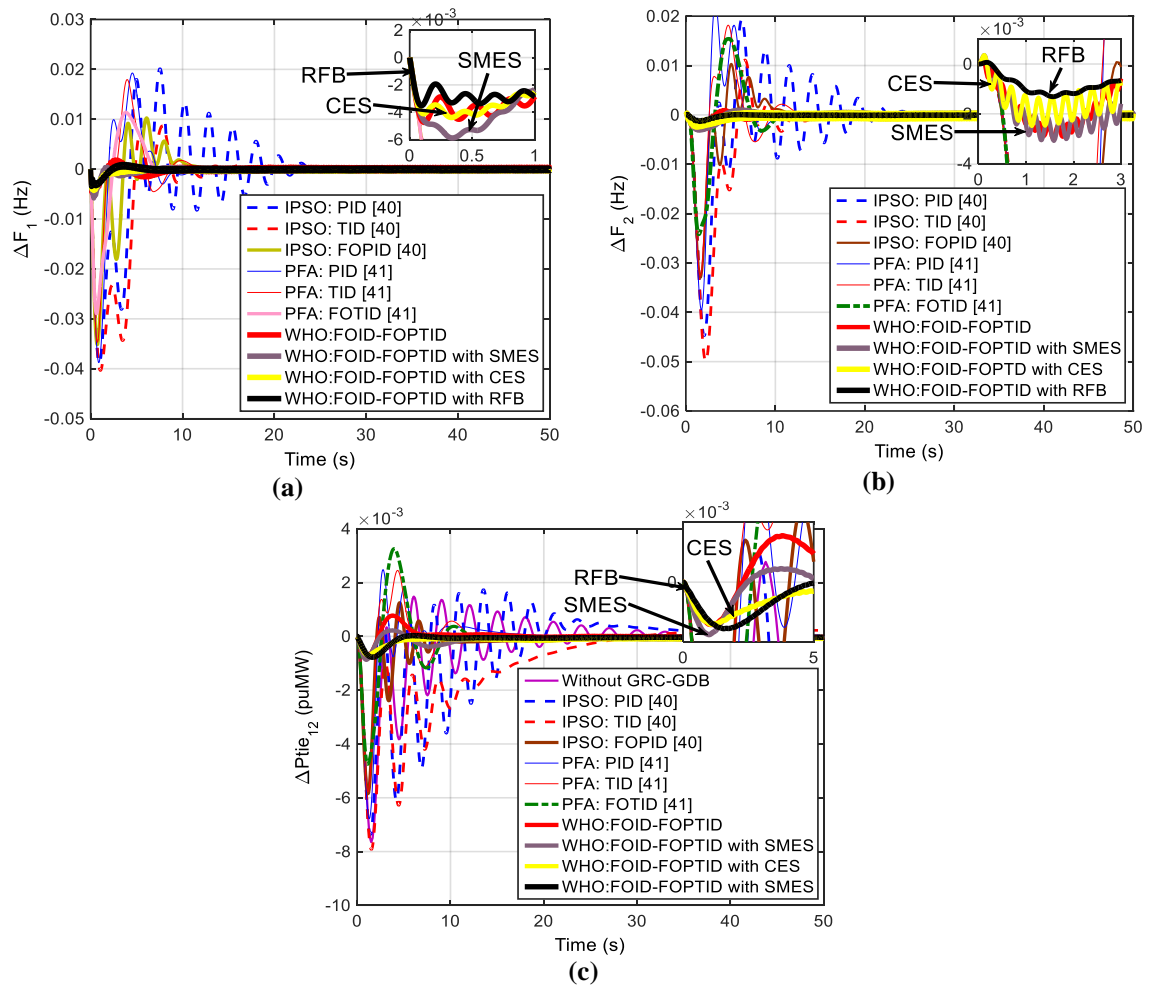


Fig. 9.9 Two-area THG system responses with GDB/GRC and ESS: (a) ΔF_1 , (b) ΔF_2 , and (c) ΔP_{tie12} .

Table 9.6 ST/OS/US/ITAE in multi-area THG system with GDB/GRC and ESS at $\Delta P_{d1} = 0.01$ puMW.										
Controller structure	ST (sec)			US (-ve) (Hz)		US (-ve) (puMW)	OS (Hz)		OS (puMW)	J
	ΔF_1	ΔF_2	$\Delta P_{tie_{12}}$	ΔF_1	ΔF_2	$\Delta P_{tie_{12}}$	ΔF_1	ΔF_2	$\Delta P_{tie_{12}}$	ITAE
IPSO: PID [40]	24.46	24.7	24.2	0.039	0.045	0.0074	0.021	0.020	0.00183	1.176
IPSO: TID [40]	14.28	13.75	21.8	0.040	0.049	0.0089	0.0078	0.0089	0.00017	0.9829
IPSO: FOPIID [40]	10.53	10.35	5.38	0.034	0.031	0.0056	0.0076	0.0070	0.00065	0.4677
PFA: PID [41]	10.85	11.1	6.51	0.039	0.040	0.0067	0.019	0.023	0.00248	0.6469
PFA: TID [41]	8.96	10.9	9.01	0.034	0.031	0.00563	0.011	0.012	0.00212	0.4382
PFA: FOTID [41]	11.32	10.8	8.14	0.025	0.022	0.00435	0.011	0.014	0.00323	0.4796
WHO: FOID-FOPTID	8.72	8.21	4.95	0.0047	0.0030	0.00071	0.0020	0.00097	0.00077	0.0723
WHO: FOID-FOPTID with SMES	5.88	8.35	1.68	0.0058	0.0032	0.00087	0.00046	0.00105	0.000242	0.0638
WHO: FOID-FOPTID with CES	5.51	6.8	2.24	0.0044	0.0025	0.00071	0.00016	0.00047	0.000085	0.0519
WHO: FOID-FOPTID with RFB	5.28	3.22	2.93	0.0035	0.0013	0.00077	0.00096	0.000054	0.0000276	0.0311

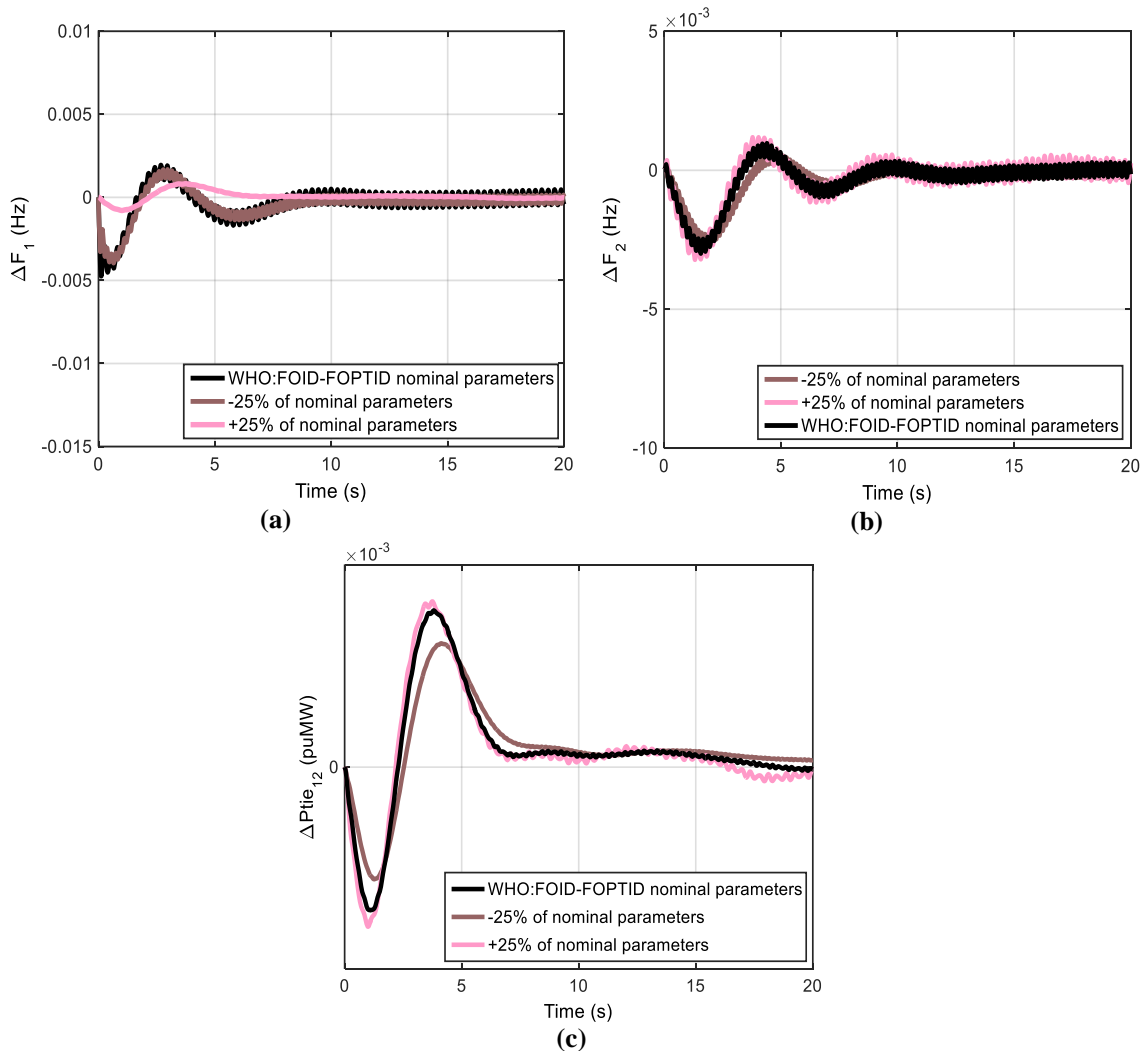


Fig. 9.10 Sensitivity analysis for two-area THG system with GDB/GRC and ESS: (a) ΔF_1 , (b) ΔF_2 , and (c) $\Delta P_{tie_{12}}$.

of ITAE, STs, USs, and OSs are least compared to others except two values of STs of ΔF_2 ($= 0.48$) and $\Delta P_{tie_{12}}$ ($= 1.75$). As most of the values are favorable for WHO:FOID-FOPTID with RFB, so the best performance is obtained with opting RFB as ESS in PS.

9.4.3 Two-Area Thermal-Hydro-Gas System with GDB/GRC and ESS

Further research is stretched on a two-area THG PS with GDB/GRC nonlinearities as shown in Fig. 9.8. Optimized parameters of the suggested WHO:FOID-FOPTID controller with ESSs are given in Table 9.5 while Table 9.6 depicts the mathematical values of STs/USs/OSs and ITAE. Fig. 9.9 and Table 9.4 interprets that WHO:FOID-FOPTID performs greatly compared to the existing IPSO:PID [40], IPSO:TID [40], IPSO:FOPID [40], PFA:PID [41], PFA:TID [41], and PFA:FOTID [41] controllers. Next, performance of WHO:FOID-FOPTID controller is enhanced incorporating ESSs specifically RFB.

9.4.4 Sensitivity Analysis

The study is further extended to investigate the system dynamic performance with WHO:FOID-FOPTID by varying all parameter of two-area THG PS with nonlinearities and ESSs (as shown in Fig. 9.8) by $\pm 25\%$. Figs. 9.10(a-c) portray the response of ΔF_1 , ΔF_2 , and $\Delta P_{tie_{12}}$. The acute analysis of Fig. 9.10(a-c) interprets that the performance of WHO tuned FOID-FOPTID controller is stable under wide variation of PS parameters. It indicates the robust behavior of the proposed controller. Hence, WHO assisted FOID-FOPTID controller may be recommended for realistic two-area multi-source PSs to supply a reliable electric power the consumers.

9.5 Conclusion

For a single/two-area THG PSs with/without nonlinearities, the ESSs have shown enhanced dynamic performance. The proposed WHO optimized FOID-FOPTID controller offers better performance compared to various published and WHO:PID/TID/FOTID controllers. The results with suggested controller interpret that RFB offers better performance compared to other ESSs like CES and SMES. In order to confirm that the recommended controller is robust under significant deviation in the system parameters, a sensitivity study is conducted.

CHAPTER 10

CONCLUSIONS, FUTURE SCOPE, AND SOCIAL IMPACT

10.1 Overview of the Work

A summary of the developments made in the current thesis is given in this chapter. A variety of designs on single-area single-source, single-area multi-source, and multi-area-multi-source PSs' AGC are attempted to be presented in this thesis. This thesis proposes several new control mechanisms to address the AGC problem in PSs. The outcomes acquired are equated with results found in the literature to endorse the performance of the recommended controllers. The following summarizes the primary conclusions of the research included in this thesis:

A. AGC of Single-Area Thermal Power System using ALO and GNA Optimized PID Controller

The optimized PID controllers are planned for single-area non-reheat/reheat thermal PSs with/without GRC. It is inferred that ALO optimized PID controller works satisfactorily with enhanced dynamic response against ALO optimized PI controller. Compared to GNA optimized PI controller, GNA optimized PID controller exhibits a stabilizing influence on PS performance. The dynamic response of reheat thermal PS is slow/poor compared to non-reheat thermal PS. The frequency deviation is found more in the dynamic response of reheat thermal PS with GRC. It is witnessed that the results of thermal PS degrade with nonlinearities. Finally, the results of GNA optimized PID controller is enhanced against ALO optimized PID controller.

B. AGC of Multi-Area Thermal Power System using GNA Optimized 2DOF-PID Controller

GNA optimized PI/PID controllers and 2DOF-PID controller gains are employed in multi-area non-reheat thermal PSs; to get the dynamic response and comparison is made with GNA optimized PI/PID controllers. It is interpreted that GNA optimized 2DOF-PID controller works satisfactorily with enhanced dynamic response in against GNA optimized PI/PID controllers.

C. Multi-Source Multi-Area Power System with Optimized FOPTID+1 Controller

GNA optimized FOPTID+1 controller is projected to resolve AGC problem in multi-area reheat THG PS without GRC and multi-area reheat THG PS with GRC. The dynamic response is evaluated and compared with GNA optimized 2DOF-PID controller. PS system outcomes interpret GNA optimized FOPTID+1 controller outperforms GNA optimized 2DOF-PID controller. It is found that the GNA optimized FOPTID+1 controller outperforms both the traditional and sophisticated control strategies that are often used in the literature. Further research is stretched on multi-area reheat THG PS with GRC with GNA optimized FOPTID+1 controller. Comparison is made with numerous intelligent algorithms optimized PI/PID controller present in the literature published recently. It is inferred that GNA optimized FOPTID+1 controller dominates various intelligent control approaches such as DE/hSFS-PS/TLBO tuned PID controllers in terms of enhanced response holding least mathematical records of STs, OSs, USs and performance index (ITAE).

D. GNA Optimized FOPI-FOPTID Controller

For a multi-source single-area THG PS the research is performed using GNA optimized FOPTID+1 controller and GNA optimized cascaded FOPI-FOPTID controller. It is inferred that GNA optimized FOPI-FOPTID controller dominates the GNA optimized FOPTID+1 control approach. Therefore, GNA optimized FOPI-FOPTID controller is projected for multi-source single-area HN system, single-area HNG, and multi-area HN, multi-area HNG system with/without GDB/GRC PS models. It is inferred that GNA optimized FOPI-FOPTID outperforms GNA optimized FOPID and GNA optimized FOPI-FOPID/ PID controllers in the single-area and multi-area PSs.

E. WHO Optimized FOID-FOPTID Controller

The investigation is performed on a single-area reheat/non-reheat thermal system to compare the WHO and GNA optimization algorithms. The results depict the best performance with WHO optimized FOID-FOPTID controller, compared to GNA optimized FOPI-FOPTID/FOPTID+1 controllers. Then new projected controller is tested for efficacy on a single-area multi-source, two-area multi-source, two-area multi-source THG PS with GRC/GDB. It is inferred that new WHO tuned FOID-FOPTID controller portrays superior performance against the existing DE/TLBO/h-SFS:PS tuned PI/PID controllers. Also, the results with WHO tuned FOID-FOPTID controller are more superior than WHO optimized FOTID/TID/PID controllers.

F. Use of Energy Storage Systems (ESSs)

The study is conducted to check the influence of ESSs on the dynamic response of single-area multi-source THG PS and two-area multi-source THG PS without/with GRC/GDB models with WHO optimized FOID-FOPTID controller. An improved performance is

obtained in the presence of ESS in the single-area and two-area THG PSs. It is inferred that more enhanced results are obtained with ESS such as SMES, CES, and RFB with WHO tuned FOID-FOPTID controller. Further, results with ESS are more superior than WHO tuned FOTID/TID/PID controllers. Given its robustness, the suggested controller could be a good option for handling the AGC issue in a variety of PSs.

10.2 Scope for the Future Research

The current study aims to suggest some effective AGC controller architectures for PSs. The suggested controllers have shown extremely encouraging outcomes. Still, further study is needed to produce improved AGC controller designs for different PS models. The following is a list of these areas:

1. The scope of the current study is restricted to single/multi-area interconnected PSs, but restructured PSs could be the subject of future extension.
2. While GNA is used in this study to create the FOPI-FOPTID controller and WHO is used to design the FOID-FOPTID controllers, other emerging intelligent optimization techniques may yield more successful outcomes.
3. Other types of supplemental controllers include fractional order PIDs with two degrees of freedom (2DOF-FOPID), 2-DOF-FOPTID etc., in addition to certain novel tuning strategies might be used in next research on both standard and restructured PSs.
4. Although AGC controllers are currently designed in continuous mode, discrete mode design may be pursued with additional research.
5. It is considered in this study that the power system's control areas include many power generation sources like thermal-hydro-gas in each area. However, further

studies may be done by considering diverse sources like hydro, thermal, gas, wind, diesel, nuclear, PV etc. in each control area of multi-area traditional/restructured PS.

6. Because of their inertial differences, the current study operates on the assumption that the automated voltage regulator (AVR) loop and the AGC loop do not interact. In future, AGC studies in PSs can be realized in the presence of AVR loop in each area.
7. The AGC problem of multi-area multi-source multi-unit PSs can be solved by researching the effects of different FACTS and additional energy-storing devices.
8. Social impact will be that applications of renewable energy system and ESSs in the AGC of PSs are pollution free.

REFERENCES

- [1] Elgerd, O.I., 1981. Control of electric power systems. *IEEE Cont Sys Magazine*, Vol. 1, Issue. 2, pp. 4–16.
- [2] Kundur, P., 1994. Power system stability and control. *McGraw Hill, New York*.
- [3] Fosha, C.E. and Elgerd, O. I., 1970. The megawatt frequency control problem: A new approach via optimal control theory. *IEEE Tran Pow App Sys*, Vol. PAS-89, Issue. 4, pp. 563–577.
- [4] Cohn, N., 1957. Some aspects of tie-line bias control on interconnected power systems. *Am Inst Elec Eng Tran*, Vol. 75, pp.1415–1436.
- [5] Cohn, N., 1967. Considerations in the regulation of interconnected areas. *IEEE Tran Pow App Sys*, Vol. PAS-86, Issue. 12, pp. 1527–1538.
- [6] Quazza, G. 1966., Noninteracting controls of interconnected electric power systems. *IEEE Tran Pow App Sys*, Vol. 85, Issue. 7, pp. 727–741.
- [7] Elgerd, O.I. and Fosha, C., 1970. Optimum megawatt frequency control of multi-area electric energy systems. *IEEE Tran Pow App Sys*, Vol. 89, Issue. 4, pp. 556–563.
- [8] Das, D., Nanda, J., Kothari, M.L. and Kothari, D.P., 1990. Automatic generation control of hydrothermal system with new area control error considering generation rate constraint. *Elec Mach Pow Sys*, Vol. 18, Issue. 6, pp. 461–471.
- [9] Saikia, L.C., Nanda, J., Mishra, S., 2011. Performance comparison of several classical controllers in AGC for multi-area interconnected thermal system. *Int J Elec Pow Ener Sys*, Vol. 33, Issue. 3, pp. 394–401.
- [10] Sondhi, S. and Hote, Y.V., 2014. Fractional order PID controller for load frequency control. *Ener Conv Man*, Vol. 85, pp. 343–353.
- [11] Sahu, R.K., Panda, S. and Rout, U.K., 2013. DE optimized parallel 2DOF-PID controller for load frequency control of power system with governor dead-band nonlinearity. *Int J Elec Pow Ener Sys*, Vol. 49, pp. 19–33.
- [12] Arya, Y., 2019. Impact of ultra-capacitor on automatic generation control of electric energy systems using an optimal FFOID controller. *Int J Ener Res*, Vol. 43, pp. 8765–8778.
- [13] Bharadwaj, C.K. and Abraham, R.J., 2011. Hydrothermal power system AGC with GA optimized controllers and Capacitive Energy Storage. *IEEE, Int Conf Emer Tre Elec Com Tech*, p. 105–110.

- [14] Aditya, S.K. and Das, D., 2000. Load-frequency control of an interconnected hydro-thermal power system with new area control error considering battery energy storage facility. *Int J Ener Res*, Vol. 24, Issue. 6, pp. 525–538.
- [15] Pilla, R., Gorripotu, T.S. and Azar, A.T., 2021. Design and analysis of search group algorithm-based PD-PID controller plus redox flow battery for automatic generation control problem. *Int J Comp Appl Tech*, Vol. 66, Issue. 1, pp. 19–35.
- [16] Arya, Y., 2017. AGC of restructured multi-area multi-source hydrothermal power systems incorporating energy storage units via optimal fractional-order fuzzy PID controller. *Neu Comp Appl*, Vol. 31, Issue. 3, pp. 851–872.
- [17] Arya, Y., 2019. A new optimized fuzzy FOPI-FOPD controller for automatic generation control of electric power systems. *J Fra Inst*, Vol. 356, Issue. 11, pp. 5611–5629.
- [18] Pathak, N., Verma, A., Bhatti, T.S., et al, 2019. Generation rate constraints physical identification and modeling in AGC of multi-area power systems. *Elec Pow Com Sys*, Vol. 47, pp. 966–984.
- [19] Raju, M., Saikia, L.C. and Sinha, N. 2019. Load frequency control of a multi-area system incorporating distributed generation resources, gate controlled series capacitor along with high-voltage direct current link using hybrid ALO-pattern search optimised fractional order controller. *IET Ren Pow Gen*, Vol. 13, Issue. 2, pp. 330–341.
- [20] Saha, D. and Saikia, L.C., 2017. Performance of FACTS and energy storage devices in a multi area wind-hydro-thermal system employed with SFS optimized I-PDF controller. *J Ren Sust Ener*, Vol. 9, Issue. 2, 024103.
- [21] Hakimuddin, N., Nasiruddin, I., Bhatti, T.S., and Arya, Y., 2020. Optimal automatic generation control with hydro, thermal, gas, and wind power plants in 2-area interconnected power system. *Elec Pow Com Sys*, Vol. 48, Issue. 6-7, pp. 558–571.
- [22] Morsali, J., Zare, K. and Hagh, M.T., 2016. Performance comparison of TCSC with TCPS and SSSC controllers in AGC of realistic interconnected multi-source power system. *Ain Sha Eng J*, Vol. 7, Issue. 1, pp. 143–158.
- [23] Halmous, A, Oubbati Y, Lahdeb M. and Arif, S., 2023. Design a new cascade controller PD-P-PID optimized by marine predators algorithm for load frequency control. *Soft Comp.*, Vol. 27, Issue. 14, pp. 9551–9564.
- [24] Sahu, R.K., Panda, S., Rout, U.K., and Sahoo, D.K., 2016. Teaching learning based optimization algorithm for automatic generation control of power system using 2DOF-PID controller. *Int J Elec Pow Ener Sys*, Vol. 77, pp. 287–301.

- [25] Arya Y., 2017. AGC performance enrichment of multi-source hydrothermal gas power systems using new optimized FOFPID controller and redox flow batteries. *Energy*, Vol. 127, pp. 704–715.
- [26] Mohanty, B. Panda, S. and Hota, P.K., 2014. Controller parameters tuning of differential evolution algorithm and its application to load frequency control of multisource power system, *Int J Elec Pow Ener Sys*, Vol. 54, pp. 77–85.
- [27] Padhy, S. and Panda, S., 2017. A hybrid stochastic fractal search and pattern search technique-based cascade PI-PD controller for automatic generation control of multi-source power systems in presence of plug in electric vehicles, *CAAI Tran Intel Tech*, Vol. 2, pp. 12–25.
- [28] Barisal, A.K., 2015. Comparative performance analysis of teaching learning-based optimization for automatic load frequency control of multi-source power systems, *Int J Elec Pow Ener Sys*, Vol. 66, pp. 67–77.
- [29] Tasnin, W. and Saikia, L.C., 2018. Maiden application of a sine-cosine algorithm optimised FO cascade controller in automatic generation control of multi-area thermal system incorporating dish-stirling solar and geothermal power plants. *IET Ren Pow Gen*, Vol. 12, pp. 585–597.
- [30] Tasnin, W. and Saikia, L.C. 2018. Comparative performance of different energy storage devices in AGC of multi-source system including geothermal power plant. *J Ren Sust Ener*, Vol. 10, 024101.
- [31] Rajbongshi, R. and Saikia, L.C., 2018. Combined voltage and frequency control of a multi-area multisource system incorporating dish-stirling solar thermal and HVDC link. *IET Ren Pow Gen*, Vol. 12, Issue. 3, pp. 323–334.
- [32] Rajbongshi, R. and Saikia, L.C., 2017. Performance of coordinated FACTS and energy storage devices in combined multiarea ALFC and AVR system. *J Ren Sust Ener*, Vol. 9, Issue. 6, 064101.
- [33] Rajbongshi, R. and Saikia, L.C., 2019. Performance of coordinated interline power flow controller and power system stabilizer in combined multi-area restructured ALFC and AVR system. *Int Tran on Elec Ener Sys*, Vol. 29, Issue. 3, pp. e2822.
- [34] Rajbongshi, R. and Saikia, L.C., 2018. Coordinated performance of interline power flow controller and superconducting magnetic energy storage in combined ALFC and AVR system under deregulated environment. *J Ren Sust Ener*, Vol. 10, Issue. 4, 044102.

- [35] Barik, A.K. and Das, D.C., 2018. Expeditious frequency control of solar photovoltaic/biogas/ biodiesel generator based isolated renewable microgrid using grasshopper optimisation algorithm. *IET Ren Pow Gen*, Vol. 12, Issue. 14, pp. 1659–1667.
- [36] Latif, A., Das, D.C., Barik, A.K. et al, 2019. Maiden coordinated load frequency control strategy for ST-AWEC-GEC-BDDG-based independent three-area interconnected microgrid system with the combined effect of diverse energy storage and DC link using BOA-optimised PFOID controller. *IET Ren Pow Gen*, Vol. 13, Issue. 14, pp. 2634–2646.
- [37] Das, C., Sinha, N. and Roy, A.K., 2012. GA based frequency controller for solar thermal-diesel-wind hybrid energy generation/energy storage system. *Int J Electr Pow Ener Syst*, Vol. 43, Issue. 1, pp. 262–279.
- [38] Nosratabadi, S.M., Bornapour, M. and Gharaei, M.A., 2019. Grasshopper optimization algorithm for optimal load frequency control considering predictive functional modified PID controller in restructured multi-resource multi-area power system with redox flow battery units. *Cont Eng Prac*, Vol. 89, pp. 204–227.
- [39] Saha, A. and Saikia, L.C., 2018. Performance analysis of combination of ultra-capacitor and superconducting magnetic energy storage in a thermal-gas AGC system with utilization of whale optimization algorithm optimized cascade controller. *J Ren Sus Ener*, Vol. 10, Issue. 1, 014103.
- [40] Morsali, J., Zare, K. and Hagh, M.T., 2018. Comparative performance evaluation of fractional order controllers in LFC of two-area diverse-unit power system with considering GDB and GRC effects. *J Elec Sys Inf Tech*, Vol. 5, Issue. 3, pp. 708–722.
- [41] Priyadarshani, S., Subhashini, K.R., and Sathapathy, J.K., 2021. Pathfinder algorithm optimized fractional order tilt-integral-derivative (FOTID) controller for automatic generation control of multi-source power system. *Micr Tech*, Vol. 27, pp. 23–35.
- [42] Ullah, K., Basit, A., Ullah, Z., et al, 2022. Automatic generation control in modern power systems with wind power and electric vehicles. *Energies*, Vol. 15, Issue. 5, 1771.
- [43] Sanki, P., Basu, M., Pal, P.S. et al, 2022. Application of a novel PIPDF controller in an improved plug-in electric vehicle integrated power system for AGC operation. *Int J Amb Ener*, Vol. 43, Issue. 1, pp. 4767–4781.
- [44] Padhy, S., Panda, S. and Mahapatra, S., 2017. A modified GWO technique based cascade PI-PD controller for AGC of power systems in presence of plug in electric vehicles. *Eng Sci Tech Int J*, Vol. 20, Issue. 2, pp. 427–442.

- [45] Sonmez, S. and Ayasun, S., 2016. Stability region in the parameter space of PI controller for a single-area load frequency control system with time delay. *IEEE Tran Pow Sys*, Vol. 31, Issue. 1, pp. 829–830.
- [46] Prasad, S., Purwar, S. and Kishor, N., 2019. Load frequency regulation using observer based non-linear sliding mode control. *Int J Elec Pow Ener Sys*, Vol. 104, pp. 178–193.
- [47] Saha, A. and Saikia, L.C., 2017. Utilisation of ultra-capacitor in load frequency control under restructured STPP-thermal power systems using WOA optimised PIDN-FOPD controller. *IET Gen Tran Dist*, Vol. 11, Issue. 13, pp. 3318–3331.
- [48] Saha, A. and Saikia, L.C., 2018. Combined application of redox flow battery and DC link in restructured AGC system in the presence of WTS and DSTS in distributed generation unit. *IET Gen Trans Dist*, Vol. 12, Issue. 9, pp. 2072–2085.
- [49] Arya, Y. and Kumar, N., 2016. Optimal AGC with redox flow batteries in multi-area restructured power systems. *Eng Sci Tech Int J*, Vol. 19, Issue 3, pp. 1145–1159.
- [50] Zare, K., Hagh, M.T. and Morsali, J., 2015. Effective oscillation damping of an interconnected multi-source power system with automatic generation control and TCSC. *Int J Elec Pow Ener Sys*, Vol. 65, pp. 220–230.
- [51] Debbarma, S., Saikia, L.C. and Sinha, N., 2014. Automatic generation control using two degree of freedom fractional order PID controller. *Int J Elec Pow Ener Sys*, Vol. 58, pp. 120–129.
- [52] Rahman, A., Saikia, L.C. and Sinha, N. 2016. Maiden application of hybrid pattern search-biogeography based optimisation technique in automatic generation control of a multi-area system incorporating interline power flow controller. *IET Gen Trans Dist*, Vol. 10, Issue. 7, pp. 1751–8687.
- [53] Dash, P., Saikia, L.C. and Sinha, N., 2015. Comparison of performances of several FACTS devices using cuckoo search algorithm optimized 2DOF controllers in multi-area AGC. *Int J Elec Pow Ener Sys*, Vol. 65, pp. 316–324.
- [54] Debbarma, S., Saikia, L.C. and Sinha, N., 2014. Solution to automatic generation control problem using firefy algorithm optimized $I^{\lambda}D^{\mu}$ controller. *ISA Trans*, Vol. 53, Issue. 2, pp. 358–366.
- [55] Babu, N.R. and Saikia, L.C., 2019. Automatic generation control of a solar thermal and dish-stirling solar thermal system integrated multi-area system incorporating accurate HVDC link model using crow search algorithm optimised FOPI Minus FODF controller. *IET Ren Pow Gen*, Vol. 13, Issue. 12, pp. 2221–2231.

- [56] Babu, N.R. and Saikia, L.C., 2021. Load frequency control of a multi-area system incorporating realistic high-voltage direct current and dish-stirling solar thermal system models under deregulated scenario. *IET Ren Pow Gen*, Vol. 15, Issue. 5, pp. 1116–1132.
- [57] Babu, N.R. and Saikia, L.C., 2019. AGC of a multi-area system incorporating accurate HVDC and precise wind turbine systems. *Int Tran Elec Ener Sys Ren Pow Gen*, Vol. 30, Issue. 4, e12277.
- [58] Tasnin, W. and Saikia, L.C., 2018. Performance comparison of several energy storage devices in deregulated AGC of a multi-area system incorporating geothermal power plant. *IET Ren Pow Gen*, Vol. 12, Issue. 7, pp. 761–772.
- [59] Ayyappan, B.P., Thanigaiselvan, R., Prabakaran, R., and Kanimozhi, R., 2023. Load frequency control of a three-area power system based on the optimal tuning of a fractional-order proportional-integral-derivative controller with multi-objective gray wolf optimization. *J Eng Res*, Vol. 11, Issue. 2B, pp. 127–137.
- [60] Saha, D. and Saikia, L.C., 2018. Automatic generation control of an interconnected CCGT-thermal system using stochastic fractal search optimized classical controllers. *Int Tran Elec Ener Sys*, Vol. 28, Issue. 5, e2533.
- [61] Tasnin, W., Saikia, L.C. and Raju, M., 2018. Deregulated AGC of multi-area system incorporating dish-stirling solar thermal and geothermal power plants using fractional order cascade controller. *Int J Elec Pow Ener Sys*, Vol. 101, pp. 60–74.
- [62] Hussain, I., Das, D.C. and Sinha, N. 2017. Reactive power performance analysis of dish–stirling solar-thermal-diesel hybrid energy system. *IET Ren Pow Gen*, Vol. 11, Issue. 6, pp. 750–762.
- [63] Sharma, M., Saxena, S., Prakash, S., et al, 2022. Frequency stabilization in sustainable energy sources integrated power systems using novel cascade noninteger fuzzy controller. *Ener Sou, Part A: Rec Util Env Eff*, Vol. 44, Issue.3, pp. 6213–6235.
- [64] Kumar, D., Bhushan, R. and Chatterjee, K. 2018. Improving the dynamic response of frequency and power in a wind integrated power system by optimal design of compensated superconducting magnetic energy storage. *Int J Gre Ener*, Vol. 15, Issue. 3, pp. 208–221.
- [65] Rezvani, A., Esmaeily, A., Etaati, H. et al., 2019. Intelligent hybrid power generation system using new hybrid fuzzy-neural for photovoltaic system and RBFNSM for wind turbine in the grid connected mode. *Front Energy*, Vol. 13, Issue. 1, pp. 131–148.

- [66] Dhundhara, S. and Verma, Y.P. 2020. Grid frequency enhancement using coordinated action of wind unit with redox flow battery in a deregulated electricity market. *Int Tran Elect Ener Sys*, Vol. 30, Issue. 3, e12189.
- [67] Zaheeruddin and Singh, K., 2020. Load frequency regulation by de-loaded tidal turbine power plant units using fractional fuzzy based PID droop controller. *Appl Soft Comp*, Vol. 92, 106338.
- [68] Kumar, A. and Shankar, G. 2018. Optimal load frequency control in deloaded tidal power generation plant-based interconnected hybrid power system. *IET Ren Pow Gen*, Vol. 12, Issue. 16, pp. 1864–1875.
- [69] Tasnin, W. and Saikia., L.C. 2019. Impact of renewables and FACT device on deregulated thermal system having sine cosine algorithm optimised fractional order cascade controller. *IET Ren Pow Gen*, Vol. 13, Issue. 9, pp. 1420–1430.
- [70] Ahmed, M., Magdy, G., Khamies, M. et al, 2022. Modified TID controller for load frequency control of a two-area interconnected diverse-unit power system. *Int J Elec Pow Ener Sys*, Vol. 135, 107528.
- [71] Das, D.C., Roy, A.K. and Sinha, N. 2012. GA based frequency controller for solar-thermal-diesel-wind hybrid energy generation/energy storage system. *Int J Elec Pow Ener Sys*, Vol. 43, Issue. 1, pp. 262–279.
- [72] Peddakapu, K., Mohamed, M.R., Srinivasarao, P. et al, 2024. Assessment of energy storage and renewable energy sources-based two-area microgrid system using optimized fractional order controllers. *J Ener Sto*, Vol. 86, 111191.
- [73] Dekaraja, B. and Saikia, L.C., 2022. Impact of electric vehicles and realistic dish-Stirling solar thermal system on combined voltage and frequency regulation of multi-area hydrothermal system. *Energy Storage*, Vol. 4, Issue. 6, e370.
- [74] Revathi, D. and Mohan Kumar, G., 2020. Analysis of LFC in PV thermal-thermal interconnected power system using fuzzy gain scheduling. *Int Tran Elec Ener Sys*, Vol. 30, Issue. 5, e1236.
- [75] Hasanien, H.M. and El-Fergany, A.A., 2019. Salp swarm algorithm-based optimal load frequency control of hybrid renewable power systems with communication delay and excitation cross-coupling effect. *Elec Pow Sys Res*, Vol. 176, 105938.
- [76] Rahman, A., Saikia, L.C. and Sinha, N. 2017. Automatic generation control of an interconnected two-area hybrid thermal system considering dish-stirling solar thermal and wind turbine system. *Ren Ener*, Vol. 105, pp. 41–54.

- [77] Das, D.C., Sinha, N. and Roy, A.K., 2014. Small signal stability analysis of dish-stirling solar thermal based autonomous hybrid energy system. *Int J Elec Pow Ener Sys*, Vol. 63, pp. 485–498.
- [78] Saha, A. and Saikia, L.C., 2019. Renewable energy source-based multi-area AGC system with integration of EV utilizing cascade controller considering time delay. *Int Tran Elec Ene Sys*, Vol. 29, Issue.1, e2646.
- [79] Bhagat, S.K., Babu, N.R., Sakia, L.C., et al, 2020. Maiden application of meta-heuristic techniques with optimized integral minus tilt-derivative controller for AGC of multi-area multi-source system. *EAI End Tran Sca Inf*, Vol. 7, Issue. 8, e5.
- [80] Wang. L., Huang, C-C., 2010. Dynamic stability analysis of a grid connected solar concentrated ocean thermal energy conversion system. *IEEE Tran Sust Ener*, Vol. 1, Issue. 1, pp. 10–18.
- [81] Bevrani, H., Ghosh, A. and Ledwich, G., 2010. Renewable energy sources and frequency regulation: survey and new perspectives. *IET Ren Pow Gen*, Vol. 4, Issue. 5, pp. 438–457.
- [82] Sharma, Y. and Saikia, L.C., 2015. Automatic generation control of a multi-area ST-thermal power system using Grey Wolf Optimizer algorithm based classical controllers. *Elect Pow Ener Sys*, Vol. 73, pp. 853–862.
- [83] Rahman, A., Saikia, L.C. and Sinha, N., 2016. AGC of dish-stirling solar thermal integrated thermal system with biogeography based optimised three degree of freedom PID controller. *IET Ren Pow Gen*, Vol. 10, Issue. 8, pp. 1161–1170.
- [84] Pradhan, C. and Bhende, C.N., 2019. Online load frequency control in power systems using modified Jaya optimization algorithm. *Eng Appl Arti Intel*, Vol. 77, pp. 212–228.
- [85] Li, Y., Choi, S.S. and Vilathgamuwa, D.M., 2018. Primary frequency control scheme for a fixed-speed dish-stirling solar–thermal power plant. *IEEE Tran Pow Sys*, Vol. 33, Issue. 2, pp. 2184–2194.
- [86] Li, Y., Choi, S.S. and Wei, F., 2015. Design of variable-speed dish stirling solar-thermal power plant for maximum energy harness. *IEEE Tran Ener Conv*, Vol. 30, Issue. 1, pp. 394–403.
- [87] Li, Y., Choi, S.S. and Yang, C., 2014. Dish-Stirling solar power plants: modeling, analysis, and control of receiver temperature. *IEEE Trans Sust Ener*, Vol. 5, Issue. 2, pp. 398–407.

- [88] Farooq, Z., Rahman, A., Hussain, S.S. et al, 2022. Power generation control of renewable energy based hybrid deregulated power system. *Energies*, Vol. 15, Issue. 2, 517.
- [89] Ghasemi-Marzbali, A., 2020. Multi-area multi-source automatic generation control in deregulated power system. *Energy*, Vol. 201, 117667.
- [90] Sharma, M., Dhundhara, S. and Sran, R.S., 2023. Impact of hybrid electrical energy storage system on realistic deregulated power system having large-scale renewable generation. *Sust Ener Tech Ass*, Vol. 56, 103025.
- [91] Kumar, R. and Sharma, V.K., 2024. Interconnected power control on unequal, deregulated multi-area power system using three-degree-of-freedom-based FOPID-PR controller. *Elec Eng*, Vol. 106, Issue. 2, pp. 2107–2129.
- [92] Kumar, R. and Sharma, V.K., 2020. Whale optimization controller for load frequency control of a two-area multi-source deregulated power system. *Int J of Fuz Sys*, Vol. 22, Issue. 1, pp. 122–137.
- [93] Kumar, N., Alotaibi, M.A., Singh, A., et al, 2022. Application of fractional order-PID control scheme in automatic generation control of a deregulated power system in the presence of SMES unit. *Mathematics*, Vol. 10, Issue. 3, 521.
- [94] Khamari, D., Sahu, R.K., Gorripotu, T.S. et al, 2020. Automatic generation control of power system in deregulated environment using hybrid TLBO and pattern search technique. *Ain Shams Eng J*, Vol. 11, Issue. 3, pp. 553–573.
- [95] Dutta, A. and Prakash, S., 2022. Utilizing electric vehicles and renewable energy sources for load frequency control in deregulated power system using emotional controller. *IETE J Res*, Vol. 68, Issue. 2, pp. 1500–1511.
- [96] Farooq, Z., Rahman, A. and Lone, S.A., 2021. System dynamics and control of EV incorporated deregulated power system using MBO-optimized cascaded ID-PD controller. *Int. Tran on Elec Ener Sys*, Vol. 31, Issue. 11, e13100.
- [97] Akshay, R.S.R. and Abraham, R.J., 2024. Load following performance in a deregulated power system with static synchronous compensator and super magnetic energy storage. *Ener Sys*, Vol. 15, Issue. 2, pp. 615–634.
- [98] Jain, D., Bhaskar, M.K. and Parihar, M., 2023. Optimization of controller parameters for load frequency control problem of two-area deregulated power system using soft computing techniques. Springer, *In Conf Sma Inn, Sys Tech*, Vol. 364, pp. 385–401.
- [99] Dekaraja, B. and Saikia, L.C., 2023, AGC of two-area deregulated power systems using PSO optimized MFOPIDD controller. *IEEE Sil Sub Conf (SILCON)*, p. 1–6.

- [100] Jain, D., Bhaskar, M.K. and Parihar, M., 2023. PSO-based controller for LFC of deregulated power system. In *Int Conf Par Comm, Comp Data Anal*, Singapore: Springer Nature, p. 607-624.
- [101] Jain, D., Bhaskar, M.K. and Parihar, M., 2022. Comparative analysis of load frequency control problem of multi area deregulated power system using soft computing techniques. *Math Stat Eng Appl*, Vol. 71, Issue. 4, pp. 10713–10729.
- [102] Chandrashekar, M.J. and Jayapal, R., 2019. AGC and AVR implementation in a deregulated power system using optimized controller with renewable integrated DC link. *Int Conf Adv Tech in Intell Cont, Env, Comp Comm Eng (ICATIECE)*, IEEE, p. 355–364.
- [103] Kumar, N., Kumar, J., Chaurasia, R. et al, 2021. Comparison of various load frequency control schemes in restructured power system environment. *J Physics: Conf Ser*, Vol. 2007, Issue 1, pp. 012028.
- [104] Sina, A. and Kaur, D., 2019. An optimal controller for load frequency control in multi-area deregulated power system. *J Elect Sys*, Vol. 15, Issue 1, pp. 142–158.
- [105] Lekshmi, R.R., Swathy, S., Lakshmi, B., et al, 2018. Market clearing mechanism considering congestion under deregulated power system. *Proc Comp Sci*, Vol. 143, pp. 686–693.
- [106] Hota, P.K. and Mohanty, B., 2016. Automatic generation control of multi source power generation under deregulated environment. *Int J Elec Pow Ener Sys*, Vol. 75, pp. 205–214.
- [107] Madrewar, K.T., Gavhane, W.A., Kardile, A.H., et al, 2015. Adaptive approach in deregulation of Indian power system. IEEE, *Int Conf on Ener Sys Appl*, p. 167–172.
- [108] Kumar, N., Tyagi, B. and Kumar, V., 2017. Multiarea deregulated automatic generation control scheme of power system using imperialist competitive algorithm based robust controller. *IETE J. Res.*, Vol. 64, Issue. 4, pp. 528–537.
- [109] Kumar, N., Tyagi, B. and Kumar, V., 2016. Multi-area AGC scheme using imperialist competition algorithm in restructured power system. *Appl. Soft Comp*. Vol. 48, pp.160–168.
- [110] Arya, Y., Kumar, N. and Gupta, S.K., 2017. Optimal automatic generation control of two-area power systems with energy storage units under deregulated environment. *J Ren Sust Ener*, Vol. 9, Issue. 6, 064105.

- [111] Kumar, N., Tyagi, B. and Kumar, V., 2017. Deregulated multi-area AGC scheme using BBBC-FOPID controller. *Arab. J. Sci. Eng.*, Vol. 42, Issue. 7, pp. 2641–2649.
- [112] Mishra, D.K., Złotecka, D. and Li, L., 2022. Significance of SMES devices for power system frequency regulation scheme considering distributed energy resources in a deregulated environment. *Energies*, Vol. 15, Issue. 5, 1766.
- [113] Rangi, S., Jain, S. and Arya, Y., 2023. SSA-optimized cascade optimal-PIDN controller for multi-area power system with RFB under deregulated environment. *Opt Cont Appl Meth*, Vol. 44, Issue. 4, pp. 1972–1994.
- [114] Pathak, N., Bhatti, T.S., Verma, A. et al, 2018. AGC of two area power system based on different power output control strategies of thermal power generation. *IEEE Tran Pow Sys*, Vol. 33, Issue. 2, pp. 2040–2052.
- [115] Shankar, G. and Mukherjee, V., 2016. Quasi oppositional harmony search algorithm based controller tuning for load frequency control of multi-source multi-area power system. *Int J Elec Pow Ener Sys*, Vol. 75, pp.289-302.
- [116] Mohanty, B. and Hota, P.K., 2015. Comparative performance analysis of fruit fly optimisation algorithm for multi-area multi-source automatic generation control under deregulated environment. *IET Gen Tran Dist*, Vol. 9, Issue. 14, pp. 1845–1855.
- [117] Jena, N.K., Patel, N.C., Sahoo, S., et al., 2019. Novel application of selfish herd optimisation based two degrees of freedom cascaded controller for AGC Study. *Int Conf Ren Ener Res Appl*, IEEE, p. 851–856.
- [118] Babu, N.R., Bhagat, S.K., Chiranjeevi, T., et al., 2023. Frequency control of a realistic dish stirling solar thermal system and accurate HVDC models using a cascaded FOPI-IDDN-based crow search algorithm. *Int J Ener Res*, Vol. 2023, Issue.1, 9976375.
- [119] Debbarma, S., Saikia, L.C. and Sinha, N., 2013. AGC of a multi-area thermal system under deregulated environment using a noninteger controller. *Elec Pow Sys Res*, Vol. 95, pp. 175–183.
- [120] Sibtain, D., Rafiq, T., Bhatti, M.H., etal, 2023. Frequency stabilization for interconnected renewable based power system using cascaded model predictive controller with fractional order PID controller. *IET Ren Pow Gen*, Vol. 17, Issue. 16, pp. 3836–3855.
- [121] Ranjan, A. and Mehta, U., 2023. Fractional-order tilt integral derivative controller design using IMC scheme for unstable time-delay processes. *J of Cont Aut Elec Sys*, Vol. 34, Issue. 5, pp. 907–925.

- [122] Naik, A.K., Jena, N.K., Sahoo, S. et al, 2024. Optimal design of fractional order tilt-integral derivative controller for automatic generation of power system integrated with photovoltaic system. *Electrica*, Vol. 24, Issue. 1, pp. 140–153.
- [123] Patel, N.C., Sahu, B.K., Bagarty, D.P., et al., 2021. A novel application of ALO-based fractional order fuzzy PID controller for AGC of power system with diverse sources of generation. *The Int J Elec Eng Edu*, Vol. 58, Issue. 2, pp. 465–487.
- [124] Bhateshvar, Y.K., Mathur, H.D. and Siguerdidjane, H. 2015. Impact of wind power generating system integration on frequency stabilization in multi-area power system with fuzzy logic controller in deregulated environment. *Front Energy*, Vol. 9, Issue. 1, pp. 7–21.
- [125] Bhosale, R. and Agarwal, V., 2018. Fuzzy logic control of the ultra-capacitor interface for enhanced transient response and voltage stability of a DC microgrid. *IEEE Tran Ind Appl*, Vol. 55, Issue. 1, pp. 712–720.
- [126] Peng, B., Zhang, F., Liang, J., et al, 2019. Coordinated control strategy for the short-term frequency response of a DFIG-ES system based on wind speed zone classification and fuzzy logic control. *Int J Elec Pow Ener Sys*, Vol. 107, pp. 363–378.
- [127] Khezri, R., Golshannavaz, S., Shokoohi, S., et al., 2016. Fuzzy logic based fine-tuning approach for robust load frequency control in a multi-area power system. *Elec Pow Comp Sys*, Vol. 44, Issue. 18, pp. 2073–2083.
- [128] Ameli, H., Abbasi, E., Ameli, M.T., et al, 2017. A fuzzy-logic based control methodology for secure operation of a microgrid in interconnected and isolated modes. *Int Tran Elec Ener Sys*, Vol. 27, Issue. 11, e2389.
- [129] Mishra, D., Sahu, P.C., Prusty, R.C. et al, 2022. Power generation monitoring of a hybrid power system with I-GWO designed trapezoidal type-II fuzzy controller. *Int J Mod Sim*, Vol. 42, Issue. 5, pp. 797–813.
- [130] Sabahi, K., Ghaemi, S. and Pezeshki, S., 2014. Application of type-2 fuzzy logic system for load frequency control using feedback error learning approaches. *Appl Soft Comp*, Vol. 21, pp. 1–11.
- [131] Kumar, N.J.V. and Thameem Ansari, M.M., 2015. A new design of dual-mode type-II fuzzy logic load frequency controller for interconnected power systems with parallel AC/DC tie-lines and superconducting magnetic energy storage unit. *Energy*, Vol. 89, pp. 118–137.

- [132] Hooshmand, R. and Moazzami, M., 2012. Optimal design of adaptive under frequency load shedding using artificial neural networks in isolated power system. *Int J Elec Pow Ener Sys*, Vol. 42, Issue. 1, pp. 220–228.
- [133] Al-Majidi, S.D., Kh. AL-Nussairi, M., Mohammed, A.J., 2022. Design of a load frequency controller based on an optimal neural network. *Energies*, Vol. 15, Issue. 17, 6223.
- [134] Nasiruddin, I., Sharma, G., Niazi, K.R., et al., 2017. Non-linear recurrent ANN-based LFC design considering the new structures of Q matrix. *IET Gen Tran Dist*, Vol. 11, Issue. 11, pp. 2862–2870.
- [135] Wang, X., Yan, X., Li, D. et al, 2018. An approach for setting parameters for two-degree-of-freedom PID controllers. *Algorithms*, Vol. 11, Issue. 4, 48.
- [136] Kannan, G., Saravanakumar, G. and Saraswathi, M., 2018. Two-degree of freedom PID controller in time delay system using hybrid controller model. *Int J Auto Cont*, Vol. 12, Issue. 3, pp. 399–426.
- [137] Hussain, I., Das, D.C., Latif, A., et al, 2022. Active power control of autonomous hybrid power system using two degree of freedom PID controller. *Ener Rep*, Vol. 8, pp. 973–981.
- [138] Abdel-hamed, A.M., Abdelaziz, A.Y. and El-Shahat, A., 2023. Design of a 2DOF-PID control scheme for frequency/power regulation in a two-area power system using dragonfly algorithm with integral-based weighted goal objective. *Energies*, Vol. 16, Issue. 1, 486.
- [139] Sahu, R.K., Panda, S., Rout, U.K. et al, 2016. Teaching learning based optimization algorithm for automatic generation control of power system using 2DOF-PID controller. *Int J Elec Pow Ener Sys*, Vol. 77, pp. 287–301.
- [140] Ramoji, S.K. and Saikia, L.C., 2023. Maiden application of fuzzy-2DOF-TID controller in unified voltage-frequency control of power system. *IETE J Res*, Vol. 69, Issue. 7, pp. 4738–4759.
- [141] Debnath, M.K., Satapathy, P., Mallick, R., 2017. 3DOF-PID controller based automatic generation control using TLBO algorithm. *Int J Pure Appl Math*, Vol. 114, Issue. 9, pp. 39–49.
- [142] Tarafdar, SAR., Mishra, D. and Bagarty, D.P. 2020. Crow search algorithm optimized 3DOF-PID controller for AGC of multi-area power system using RFB. Springer: *Adv Elec Cont Sig Sys*, Vol. 2019, pp. 183–197.

- [143] Babu, N.R., Chiranjeevi, T., Saha, A. et al, 2023. Comparative analysis of various energy storage systems in a conventional LFC system considering RDSTS, PWTS and AHVDC models. *J Eng Res*, Vol. 11, Issue. 4, pp. 425–436.
- [144] Hassan, A., Aly, M., Elmelegi, A., et al., 2022. Optimal frequency control of multi-area hybrid power system using new cascaded TID-PI^λD^μN controller incorporating electric vehicles. *Fractal Fract*, Vol. 6, Issue. 10, 548.
- [145] Saha, A. and Saikia, L.C. 2019. Load frequency control of a wind-thermal-split shaft gas turbine-based restructured power system integrating FACTS and energy storage devices. *Int Tran Elec. Ener Sys*, Vol. 29, Issue 3, e2756.
- [146] Sariki, M. and Shankar, R., 2022. Optimal CC-2DOF (PI)-PDF controller for LFC of restructured multi-area power system with IES-based modified HVDC tie-line and electric vehicles. *Eng Sc Tech an Int J*, Vol. 32, 101058.
- [147] Noman, A.M., Aly, M., Alqahtani, M.H. et al, 2024. Optimum fractional tilt based cascaded frequency stabilization with MLC algorithm for multi-microgrid assimilating electric vehicles. *Fractal Fract.*, Vol. 8, Issue. 3, pp.132.
- [148] Jiang, H., Lin, J., Song, Y., et al, 2016. Explicit model predictive control applications in power systems: an AGC study for an isolated industrial system. *IET Gen Tran Dist*, Vol. 10, Issue. 4, pp. 964–971.
- [149] Zheng, Y., Zhou, J., Xu, Y., et al, 2017. A distributed model predictive control based load frequency control scheme for multi-area interconnected power system using discrete-time Laguerre functions. *ISA Tran*, Vol. 68, pp. 127–140.
- [150] Ma, M., Liu, X., Zhang, C. 2017. LFC for multi-area interconnected power system concerning wind turbines based on DMPC. *IET Gen Tran Dist*, Vol. 11, Issue. 10, pp. 2689–2696.
- [151] Sessa, V.P.S.R.V.R.S. and Kesanakurthy, S.S., 2018. Model predictive control approach for frequency and voltage control of standalone micro-grid. *IET Gen Tran Dist*, Vol. 12, Issue. 14, pp. 3405–3413.
- [152] Gulzar, M.M., 2023. Designing of robust frequency stabilization using optimized MPC-(1+PIDN) controller for high order interconnected renewable energy based power systems. *Prot Cont Mod Pow Sys*, Vol. 8, Issue.1, pp. 1–14.
- [153] Elsis, M., Soliman, M., Aboeela, MAS. et al, 2016. Bat inspired algorithm based optimal design of model predictive load frequency control. *Int J Elec Pow Ener Sys*, Vol. 83, pp. 426–433.

- [154] Elsis, M., Aboelela, M., Soliman, M. et al, 2018. Design of optimal model predictive controller for LFC of nonlinear multi-area power system with energy storage devices. *Elec Pow Comp Sys*, Vol. 46, Issue. 11-12, pp. 1300–1311.
- [155] Guo, J., 2019. Application of full order sliding mode control based on different areas power system with load frequency control. *ISA Tran*, Vol. 92, pp. 23–34.
- [156] Wang, C., Mi, Y., Fu, Y. et al, 2018. Frequency control of an isolated micro-grid using double sliding mode controllers and disturbance observer. *IEEE Tran Smart Grid*, Vol. 9, Issue. 2, pp. 923–930.
- [157] Prasad, S., Purwar, S., Kishor, N., 2016. H-infinity based non-linear sliding mode controller for frequency regulation in interconnected power systems with constant and time-varying delays. *IET Gen Tran Dist*, Vol. 10, Issue. 11, pp. 2771–2784.
- [158] Alshabi, M. and Elnady, A., 2019. Recursive smooth variable structure filter for estimation processes in direct power control scheme under balanced and unbalanced power grid. *IEEE Sys J*, Vol. 14, Issue. 1, pp. 971–982.
- [159] Kazemi, M.V., Gholamian, S.A. and Sadati, J., 2019. Adaptive frequency control with variable speed wind turbines using data driven method. *J Ren Sust Ener*, Vol. 11, Issue. 4, 043305.
- [160] Cai, J., Chen C., Liu, P. et al, 2015. Centralized control of parallel connected power conditioning system in electric vehicle charge-discharge and storage integration station. *J Mod Pow Sys Cl Ener*, Vol. 3, Issue. 2, pp. 269–276.
- [161] Pathak, N., Nasiruddin, I. and Bhatti, T.S., 2015. A more realistic model of centralized automatic generation control in real-time environment. *Elec Pow Comp Sys*, Vol. 43, pp. 2205–2213.
- [162] Guha, D., Roy, P.K. and Banerjee, S., 2020. Disturbance observer aided optimised fractional-order three-degree-of-freedom tilt-integral-derivative controller for load frequency control of power systems. *IET Gener Transm Distrib*, Vol. 15, Issue. 4, pp. 716–736.
- [163] Guha, D., Roy, P.K. and Banerjee, S., 2019. Maiden application of SSA optimised CC-TID controller for load frequency control of power systems. *IET Gen Tran Dist*, Vol. 13, Issue. 7, pp. 1110–1120.
- [164] Guha, D., Roy, P.K. and Banerjee, S., 2020. Equilibrium optimizer-tuned cascade fractional-order 3DOF–PID controller in load frequency control of power system having renewable energy resource integrated. *Int Tran Elec Ener Sys*, Vol. 39, Issue 1, e12702.

- [165] Guha, D., Roy, P.K., Banerjee, S., et al, 2020. Small-signal stability analysis of hybrid power system with quasi-oppositional sine cosine algorithm optimized fractional order PID controller. *IEEE Access*, Vol. 8, pp. 155971–155986.
- [166] Dhanasekaran, B., Siddhan, S. and Kaliannan, J., 2020. Ant colony optimization technique tuned controller for frequency regulation of single area nuclear power generating system. *Mic Microsystems*, Vol. 73, 102953.
- [167] Rakhshani, E., Remon, D., Cantarellas, A.M., et al, 2016. Virtual synchronous power strategy for multiple HVDC interconnections of multi-area AGC power systems. *IEEE Tran Pow Sys*, Vol. 32, Issue. 3, pp. 1665–1677.
- [168] Pathak, N., Verma, A., Bhatti, T.S. et al. 2018. Modeling of HVDC tie-links and their utilization in AGC/LFC operations of multi-area power systems. *IEEE Tran Ind Electron*, Vol. 66, Issue. 3, pp. 2185–2197.
- [169] Khanjanzadeh, A., Soleymani, S., Mozafari, B. et al, 2020. Integrated multi-area power system with HVDC tie-line to enhance load frequency control and automatic generation control. *Elec Eng*, Vol. 102, Issue. 3, pp.1223–1239.
- [170] Zhu, J., Booth, C.D., Adam, G.P., et al 2012. Inertia emulation control strategy for VSC–HVDC transmission systems. *IEEE Tran Pow Sys*, Vol. 28, Issue. 2, pp. 1277–1287.
- [171] Rakhshani, E., Rouzbehi, K., Elsharty, M.A. et al, 2017. Heuristic optimization of supplementary controller for VSC-HVDC/AC interconnected grids considering PLL. *Elec Pow Com Sys*, Vol. 45, Issue. 3, pp. 288–301.
- [172] McGill, R., Torres-Olguin, R., Anaya-Lara, O. et al, 2017. Generator response following as a primary frequency response control strategy for VSC-HVDC connected offshore wind farms. *Ener Pro*, Vol. 137, pp.108–118.
- [173] Prakash, A., Murali, S., Shankar, R. et al, 2019. HVDC tie-link modeling for restructured AGC using a novel fractional order cascade controller. *Elec Pow Sys Res*, Vol. 170, pp. 244–258.
- [174] Khadanga, R.K. and Kumar, A., 2019. Analysis of PID controller for the load frequency control of static synchronous series compensator and capacitive energy storage source-based multi-area multi-source interconnected power system with HVDC link. *Int J Bio-Ins Comp*, Vol. 13, Issue. 2, pp.131–139.
- [175] Tavakoli, M., Pouresmaeil, E., Adabi, J., et al, 2018. Load-frequency control in a multi-source power system connected to wind farms through multi terminal HVDC systems. *Comp oper Res*, Vol. 96, pp. 305–315.

- [176] Rakhshani, E., Remon, D., Rodriguez, P. 2016. Effects of PLL and frequency measurements on LFC problem in multi-area HVDC interconnected systems. *Int J Elec Pow Ener Sys*, Vol. 81, pp. 140–152.
- [177] Li, C., Xiao, L., Cao, Y., et al, 2014. Optimal allocation of multi-type FACTS devices in power systems based on power flow entropy. *J Mod Pow Syst Clean Energy*, Vol. 2, Issue. 2, pp. 173–180.
- [178] Ghahremani, E. and Kamwa, I. 2012. Optimal placement of multiple-type FACTS devices to maximize power system loadability using a generic graphical user interface. *IEEE Trans Pow Syst*, Vol. 28, Issue. 2, pp. 764–778.
- [179] Kumar, A. and Shankar, R., 2022. A cascade fractional and fuzzy controller for hybrid power system with FACTS device. *IEEE, Int Conf Eme Fron Elec Ele Tech*, pp. 1-5.
- [180] Sahu, R.K., Panda, S., Biswal, A., et al 2016. Design and analysis of tilt integral derivative controller with filter for load frequency control of multi-area interconnected power systems. *ISA Trans*, Vol. 61, pp. 251–264.
- [181] Marouani, I., Guesmi, T., Alshammari, B.M., et al, 2023. Optimized FACTS devices for power system enhancement: applications and solving methods. *Sustainability*, Vol. 15, Issue. 12, 9348.
- [182] Morsali, J., Zare, K. and Hagh, M.T. 2018. A novel dynamic model and control approach for SSSC to contribute effectively in AGC of a deregulated power system. *Int J Elec Pow Ener Sys*, Vol. 95, pp. 239–253.
- [183] Raj, S. and Bhattacharyya, B., 2018. Optimal placement of TCSC and SVC for reactive power planning using whale optimization algorithm. *Swa Evo Comp*, Vol. 40, pp.131–143.
- [184] Biswas, S., Roy, P.K. and Chatterjee, K. 2023. FACTS-based 3DOF-PID controller for LFC of renewable power system under deregulation using GOA. *IETE J Res*, Vol. 69, Issue 3. pp. 1486–1499.
- [185] Kasireddy, I. and Singh, A.K., 2019. Fractional IMC-based AGC for interconnected power system via its reduced model using genetic algorithm. Springer, *Soft Comp Data Anal Proc Int Conf*, Vol. 2018, pp. 225–235.
- [186] Abdelkader, A., Rabeh, A., Ali, D.M. and Mohamed, J., 2018. Multi-objective genetic algorithm based sizing optimization of a stand-alone wind/PV power supply system with enhanced battery/supercapacitor hybrid energy storage. *Energy*, Vol. 163, pp. 351–363.

- [187] Mohanty, B., Panda, S. and Hota, P.K., 2014. Differential evolution algorithm based automatic generation control for interconnected power systems with non-linearity. *Alex Eng J*, Vol. 53, Issue. 3, pp. 537–552.
- [188] Guha, D., Roy, P.K., Banerjee, S., 2017. Study of differential search algorithm based automatic generation control of an interconnected thermal–thermal system with governor dead-band. *Appl Soft Comp*, Vol. 52, pp. 160–175.
- [189] Panwar, A., Sharma, G., Nasiruddin, I., et al. 2018. Frequency stabilization of hydro-hydro power system using hybrid bacteria foraging PSO with UPFC and HAE. *Elec Pow Sys Res*, Vol. 161, pp. 74–85.
- [190] Guha, D., Roy, P.K. and Banerjee, S., 2016. Load frequency control of interconnected power system using grey wolf optimization. *Swa Evol Comp*, Vol. 27, pp. 97–115.
- [191] Zamani, A., Barakati, S.M. and Yousof-Darmian, S., 2016. Design of a fractional order PID controller using GBMO algorithm for load-frequency control with governor saturation consideration. *ISA Tran*, Vol. 64, pp. 56–66.
- [192] Shankar, R., Chatterjee, K. and Bhushan, R., 2016. Impact of energy storage system on load frequency control for diverse sources of interconnected power system in deregulated power environment. *Int J Elec Pow Ener Sys*, Vol. 79, pp. 11–26.
- [193] Guha, D., Roy, P.K. and Banerjee, S., 2017. Multi-verse optimisation: a novel method for solution of load frequency control problem in power system. *IET Gen Trans Dist*, Vol. 11, Issue. 14, pp. 3601–3611.
- [194] Chidambaram, A., and Paramasivam, B. 2013. Optimized load-frequency simulation in restructured power system with redox flow batteries and interline power flow controller. *Int J Elec Pow Ener Sys*, Vol. 50, Issue. 1, pp. 9–24.
- [195] Arya, Y. and N Kumar., 2017. Design and analysis of BFOA-optimized fuzzy PI/PID controller for AGC of multi-area traditional/ restructured electrical power systems. *Soft Comp*, Vol. 21, Issue. 21, pp. 6435–6452.
- [196] Nayak, P.C., Prusty, R.C. and Panda, S., 2022. Grasshopper optimisation algorithm of multistage $PD_{F+}(1+PI)$ controller for AGC with GDB and GRC nonlinearity of dispersed type power system. *Int J Amb Ener*, Vol. 43, Issue. 1, pp. 1469–1481.
- [197] Khezri, R., Oshnoei, A., Oshnoei, S., et al, 2019. An intelligent coordinator design for GCSC and AGC in a two area hybrid power system. *Appl Soft Comp*, Vol. 76, pp. 491–504.

- [198] Saha, A. and Saikia, L.C., 2017. Utilisation of ultra-capacitor in load frequency control under restructured STPP-thermal power systems using WOA optimised PIDN-FOPD controller. *IET Gen Tran Dist*, Vol. 11, Issue. 13, pp. 3195–3437.
- [199] Bhatshvar, Y.K., Mathur, H.D., Siguerdidjane, H. et al, 2017. Ant colony optimized fuzzy control solution for frequency oscillation suppression. *Elec Pow Comp Sys*, Vol. 45, Issue. 14, pp. 1573–1584.
- [200] Mohammadikia, R. and Aliasghary, M., 2018. A fractional order fuzzy PID for load frequency control of four-area interconnected power system using biogeography-based optimization. *Int Tran Elec Ener Sys*, Vol. 29, Issue. 2, e2735.
- [201] Sathya, M.R., Mohamed, Thameem, Ansari, M., 2016. Design of biogeography optimization based dual mode gain scheduling of fractional order PI load frequency controllers for multi- source interconnected power systems. *Int J Elec Pow Ener Sys*, Vol. 83, pp. 364–381.
- [202] Abdelaziz, A.Y. and Ali, E.S., 2015. Cuckoo Search algorithm based load frequency controller design for nonlinear interconnected power system. *Int J Elec Pow Ener Sys*, Vol. 73, pp. 632–643.
- [203] Arya, Y., 2020. A novel CFFOPI-FOPID controller for AGC performance enhancement of single and multi-area electric power systems. *ISA Trans*, Vol. 100, pp. 126–135.
- [204] Arya, Y., 2018. AGC of two-area electric power systems using optimized fuzzy PID with filter plus double integral controller. *J Fra Inst*, Vol. 355, Issue. 11, pp. 4583–4617.
- [205] Saha, A., Dash, P., Babu, N.R., et al, 2022. Impact of spotted hyena optimized cascade controller in load frequency control of wave-solar-double compensated capacitive energy storage based interconnected power system. *Energies*, Vol. 15, Issue. 19, 6959.
- [206] Sahu, B.K., Pati, T.K., Nayak, J.R., et al, 2016. A novel hybrid LUS-TLBO optimized fuzzy-PID controller for load frequency control of multi-source power system. *Int J Elec Pow Ener Sys*, Vol. 74, pp. 58–69.
- [207] Abd-Elazim, S.M., Ali, E.S., 2016. Load frequency controller design via BAT algorithm for nonlinear interconnected power system. *Int J Elec Pow Ener Sys*, Vol. 77, pp. 166–177.
- [208] Guha, D., Roy, P.K. and Banerjee, S. 2018. Optimal tuning of 3-degree of freedom proportional–integral-derivative controller for hybrid distributed power system using dragonfly algorithm. *Comp Elec Eng*, Vol. 72, pp. 137–153.

- [209] Magdy, G., Mohamed, E.A., Shabib, G., et al, 2018. SMES based a new PID controller for frequency stability of a real hybrid power system considering high wind power penetration. *IET Ren Pow Gen*, Vol. 12, Issue. 11, pp. 1304–1313.
- [210] Abazari, A., Monsef, H., Wu, B. 2019. Load frequency control by de-loaded wind farm using the optimal fuzzy-based PID droop controller. *IET Ren Pow Gen*, Vol. 13, Issue. 1, pp. 180–190.
- [211] Abazari, A., Monsef, H., Wu, B. 2019. Coordination strategies of distributed energy resources including FESS, DEG, FC and WTG in load frequency control (LFC) scheme of hybrid isolated micro-grid. *Int J Elec Pow Ener Sys*, Vol. 109, pp. 535–547.
- [212] Sahu, B.K., Pati, S. and Panda, S., 2014. Hybrid differential evolution particle swarm optimisation optimised fuzzy proportional-integral derivative controller for automatic generation control of interconnected power system. *IET Gen Tran Dist*, Vol. 8, 11, pp. 1789–1800.
- [213] Khadanga, R.K. and Kumar, A., 2017. Hybrid adaptive ‘gbest’-guided gravitational search and pattern search algorithm for automatic generation control of multi-area power system. *IET Gen Tran Dist*, Vol. 11, Issue. 13, pp. 3257–3267.
- [214] Soni, V., Parmar, G. and Kumar, M. 2021. A hybrid grey wolf optimisation and pattern search algorithm for automatic generation control of multi-area interconnected power systems. *Int J Adv Intel Para*. Vol. 18, Issue. 3, 265.
- [215] Naruei, I., Keynia, F. 2021. Wild horse optimizer: a new meta-heuristic algorithm for solving engineering optimization problems. *Eng Comp*, Vol. 38, (Suppl 4), pp. 3025–3056.
- [216] Pathak, P.K. and Yadav, A.K., 2023. Design of optimal cascade control approach for LFM of interconnected power system. *ISA Tran*, Vol. 137, pp. 506–518.
- [217] Liu, P., Zhao, W., Shair, J., et al. 2024. Modeling of battery energy storage systems for AGC performance analysis in wind power systems, *Int J Elec Pow Ener Sys*, Vol. 155, Part A, 109478.
- [218] Cuiping Li, Changsheng Feng, Junhui Li, et al, 2023. Comprehensive frequency regulation control strategy of thermal power generating unit and ESS considering flexible load simultaneously participating in AGC. *J Ener Stor*, Vol. 58, 106394.
- [219] Mohan, N.B., Rajagopal, B. and Krishna, D.H., 2023. Power quality enhancement of hybrid renewable energy source-based distribution system using optimised uPQC, *J Cont Dec*, pp. 1–22. Doi: <https://doi.org/10.1080/23307706.2023.2270481>

- [220] Shen García-Pereira, H., Blanco, M., Martínez-Lucas, et al., 2022. Comparison and influence of flywheels energy storage system control schemes in the frequency regulation of isolated power systems. *IEEE Access*, Vol. 10, pp. 37892–37911.
- [221] Yang, T., Liu, Z., Zeng, D. and Zhu, Y., 2023. Simulation and evaluation of flexible enhancement of thermal power unit coupled with flywheel energy storage array. *Energy*, Vol. 281, 128239.
- [222] Saha, A., Dash, P., Chiranjeevi, T. and Babu, N.R., 2024. Implementation of combined hydrogen aqua electrolyser-fuel cell and redox-flow-battery under restructured situation of AGC employing TSA optimized PDN (FOPI) controller. *J Tai Univ Sci*, Vol. 18, Issue. 1. 2334004.
- [223] Arya, Y., 2019. Impact of hydrogen aqua electrolyzer-fuel cell units on automatic generation control of power systems with a new optimal fuzzy TIDF-II controller. *Ren Energy*, Vol. 139, pp. 468–482.
- [224] Lal, D.K. and Barisal, A.K., 2017. Comparative performances evaluation of FACTS devices on AGC with diverse sources of energy generation and SMES. *Cogent Eng*, Vol. 4, Issue. 1, 1318466.
- [225] Mishra, D.K., Złotecka, D. and Li, L., 2022. Significance of SMES devices for power system frequency regulation scheme considering distributed energy resources in a deregulated environment. *Energies*, Vol. 15, Issue. 5, 1766.
- [226] Sheik Morsali, J., 2022. Fractional order control strategy for superconducting magnetic energy storage to take part effectually in automatic generation control issue of a realistic restructured power system. *J Ener Sto*, Vol. 55, 105764.
- [227] Bhagat, S.K., Saikia, L.C. and Babu, N.R., 2023. Mitigation of AGC problem of the RES integrated hydro-thermal system using FACTS and INEC based AHVDC with ESS considering the 3DOF-TIDN controller. *IETE J Res*, pp. 1–21. doi: <https://doi.org/10.1080/03772063.2023.2210539>
- [228] Sharma, G., Krishnan, N., Arya, Y. et al., 2021. Impact of ultracapacitor and redox flow battery with JAYA optimization for frequency stabilization in linked photovoltaic-thermal system. *Int Tran Elec Ener Sys*, Vol. 31, Issue. 5, e12883.
- [229] Ponnusamy, M., Banakara, B., Das, S.S., et al. 2015. Design of integral controller for load frequency control of static synchronous series compensator and capacitive energy source based multi area system consisting of diverse sources of generation employing imperialistic competition algorithm. *Int J Elect Pow Ener Sys*, Vol. 73, pp. 863–871.

- [230] Dhundhara, S. and Verma, Y.P., 2018. Capacitive energy storage with optimized controller for frequency regulation in realistic multisource deregulated power system. *Energy*, Vol. 147, pp. 1108–1128.
- [231] Arya, Y., Ahmad, R., Nasiruddin, I. et al, 2024. LFC performance advancement of two-area RES penetrated multi-source power system utilizing CES and a new CFOTID controller. *J Ener Sto*, Vol. 87, 111366.
- [232] Çelik, E., Öztürk, N. and Houssein, E.H., 2022. Influence of energy storage device on load frequency control of an interconnected dual-area thermal and solar photovoltaic power system. *Neur Comp Appl*, Vol.34, Issue. 22, pp. 20083–20099.
- [233] Murali, S., Shankar, R., Sharma, P. et al., 2024. Assessment of power system resiliency with new intelligent controller and energy storage systems. *Elec Pow Comp Sys*, Vol. 52, Issue. 8, pp. 1414–1436.
- [234] Jena, N.K., Sahoo, S., Sahu, B.K., et al. 2023. Impact of a redox flow battery on the frequency stability of a five-area system integrated with renewable sources. *Energies*, Vol. 16, Issue. 14, 5540.
- [235] Baral, K.K., Sahu, P.C., Barisal, A.K. et al. 2023. Combined analysis on AGC and ELD of a hybrid power system with D-WCA designed Gaussian type-2 fuzzy controller. *Evol Sys*, Vol. 14, Issue. 2, pp. 263–280.
- [236] Phung, B.N., Wu, Y.-K., Pham, M.-H., 2024. Coordinated frequency regulation between DFIG-VSWTs and BESS hybrid systems. *Energies*, Vol. 17, Issue. 13, 3099.
- [237] Saha, A., Babu, N.R., Dash, P. and Acharya, B., et al. 2023. Dynamic stability assessment of interconnected thermal-SsGT-solar photovoltaic-EV power system with ARO optimized IDN-FOID amalgamated controller. *IET Ren Pow Gen*, Vol. 17, Issue. 10, pp. 2592–2612.
- [238] Mohammed, O.A.A., Peng, L., Amran, G.A., Alsalman, H., Abdalla, M.A.A., Alkawmani, O., Mursil, M., Saleh, B., 2024. Optimal α -variable model-free adaptive barrier function fractional order nonlinear sliding mode control for four area interconnected hybrid power system with nonlinearities. *IEEE Access*, Vol. 12, pp. 61586–61609.
- [239] Jameel, A. and Gulzar, M.M., 2023. Load frequency regulation of interconnected multi-source multi-area power system with penetration of electric vehicles aggregator model. *Elec Eng*, Vol. 105, Issue. 6, pp. 3951–3968.

- [240] Abou, El-Ela, Adel A., et al. 2022. Design of cascaded controller based on coyote optimizer for load frequency control in multi-area power systems with renewable sources. *Cont Eng Prac*, Vol. 121, 105058.
- [241] Khadanga, R.K, Kumar, A. and Panda. S., 2022. A modified grey wolf optimization with Cuckoo Search Algorithm for load frequency controller design of hybrid power system. *Appl Soft Comp*, Vol. 124, 109011.
- [242] Singh, K., Amir, M. and Arya, Y., 2022. Optimal dynamic frequency regulation of renewable energy based hybrid power system utilizing a novel TDF-TIDF controller. *Ener Sou, Part A: Rec, Util Envir Eff*, Vol. 44, Issue. 4, pp. 10733–10754.
- [243] Sobhy, Mohamed A., et al. 2023. Manta ray foraging optimization algorithm-based load frequency control for hybrid modern power systems. *IET Ren Pow Gen*, Vol. 17, Issue. 6, pp. 1466–1487.
- [244] Elsaied, M.M., Abdel Hameed, W.H., Hasanien, etal, 2023. Optimal sliding mode control for frequency stabilization of hybrid renewable energy systems. *IET Ren Pow Gen*, Vol. 17, Issue. 11, pp. 2815–2834.
- [245] Ahmed, M., Khamies, M.and Kamel, S., 2023. A robust control approach integrating with optimal fuel cells to strengthen the frequency stability of a diverse-sources power system including renewable. *ISA Trans*, Vol. 143. pp. 420–439.
- [246] Raj U., Shankar R., 2023. Optimally enhanced fractional-order cascaded integral derivative tilt controller for improved load frequency control incorporating renewable energy sources and electric vehicle. *Soft Comp*, Vol. 27, Issue. 20, pp. 15247–15267.
- [247] Vidyarthi, P.K., Kumar, A., 2024. A cascaded tilt MPC controller for AGC in multi-area interconnected HPS with penetration of RESs and virtual inertia. *Elec Eng*, pp. 1–17. doi: <https://doi.org/10.1007/s00202-024-02398-5>
- [248] Guha, D., Roy, P.K., Banerjee, S., 2021. Observer-aided resilient hybrid fractional-order controller for frequency regulation of hybrid power system. *Int Tran Elec Ener Sys*, Vol. 31, Issue. 9, e13014.
- [249] Kumari, S. and Shankar, G., 2019. Maiden application of cascade tilt-integral-tilt-derivative controller for performance analysis of load frequency control of interconnected multi-source power system. *IET Gen Tran Dist*, Vol.13, Issue. 23, pp. 5326–5338.
- [250] Gouda, E.A., Abd-Alaziz, A. and El-Saadawi, M., 2020. Design modeling, and control of multi-stage SMES integrated with PV system. *J Ener Stor*, Vol. 29, 101399.

- [251] Amiri, F. and Hatami, A., 2023. Load frequency control for two-area hybrid microgrids using model predictive control optimized by grey wolf-pattern search algorithm. *Soft Comp*, Vol. 27, Issue. 23, pp. 18227–18243.
- [252] Babu, N.R., et al., 2022. A comprehensive review of recent strategies on automatic generation control/load frequency control in power systems. *Arch Comp Meth Eng*, Vol. 30, Issue 1, pp. 543–572.
- [253] Mohapatra, A.K., Mohapatra, S., Pattnaik, A. et al, 2024. Design and modeling of an AI governed type-2 Fuzzy tilt control strategy for AGC of a multi-source power grid in constraint to optimal dispatch, *e-Prime - Adv Elec Eng, Elec Ener*, Vol. 7, 100487.
- [254] Shen, L., Cheng, Q., Cheng, Y., et al, 2020. Hierarchical control of DC micro-grid for photovoltaic EV charging station based on flywheel and battery energy storage system. *Elec Pow Sys Res*, Vol. 179, 106079.
- [255] Barelli, L., Bidini, G., Bonucci, F., et al., 2019. Flywheel hybridization to improve battery life in energy storage systems coupled to RES plants. *Energy*, Vol. 173, pp. 937–950.
- [256] Noori, A., Shahbazadeh, M.J. and Eslami, M., 2020. Designing of wide-area damping controller for stability improvement in a large-scale power system in presence of wind farms and SMES compensator. *Int J Elect Pow Ener Sys*, Vol. 119, 105936.
- [257] Nayak, J.R., Shaw, B., Sahu, B.K., et al, 2022. Application of optimized adaptive crow search algorithm based two degree of freedom optimal fuzzy PID controller for AGC system. *Eng Sci Tech an Int J*, Vol. 32, 101061.
- [258] Huang, Chongxin, et al. 2024. DMPC-based load frequency control of multi-area power systems with heterogeneous energy storage system considering SOC consensus. *Elec Pow Sys Res*, Vol. 228, 110064.
- [259] Mirjalili. S., 2015. The antlion optimizer. *Adv in Engg Soft*. Vol. 83, pp. 80–98.
- [260] Alazzam, A and Lewis H.W. 2013. A new optimization algorithm for combinatorial problems. *Int J Adv Res Art Int*, Vol. 2, Issue.5, pp. 63–68.
- [261] Igor Podlubny, 1996. Fractional-order systems and $PI^\lambda D^\mu$ -controller, *IEEE Tran Aut Cont*, Vol. 44, Issue 1, pp. 208–214.
- [262] A. Oustaloup, B. Mathieu, P. Lanusse, 1995. The CRONE control of resonant plants: application to a flexible transmission, *Euro J Cont*, Vol. 1, Issue. 2, pp. 113–121.

Appendix - System Data:

Chapter 4/Chapter 7

Single-Area Non-Reheat Thermal System with/without GRC [1]:

$P_r = 2000$ MW, $\Delta P_d^0 = 1000$ MW, Base power = 2000 MVA, $F^0 = 60$ Hz, $K_{PS} = 120$, $T_{PS} = 20$ sec, $T_{SG} = 0.08$ sec, $T_t = 0.3$ sec, $R = 2.4$ Hz/puMW, $\Delta P_d = 0.01$ puMW, GRC = 0.1 puMW/min

Single-Area Reheat Thermal System with/without GRC [1,203]:

$P_r = 2000$ MW, $\Delta P_d^0 = 1000$ MW, Base power = 2000 MVA, $F^0 = 60$ Hz, $K_{PS} = 120$, $T_{PS} = 20$ sec, $T_{SG} = 0.08$ sec, $T_t = 0.3$ sec, $R = 2.4$ Hz/puMW, $\Delta P_d = 0.01$ puMW, $K_r = 0.5$, $T_r = 10$ sec, GRC = 0.1 puMW/min.

Chapter 5

Two-Area Non-Reheat Thermal System [188]

$P_{r1} = P_{r2} = 2000$ MW, $\Delta P_{d1}^0 = \Delta P_{d2}^0 = 1000$ MW, Base power = 2000 MVA, $F^0 = 60$ Hz, $K_{PS1} = K_{PS2} = 120$, $T_{PS1} = T_{PS2} = 20$ sec, $T_{SG1} = T_{SG2} = 0.08$ sec, $T_{t1} = T_{t2} = 0.3$ sec, $R_1 = R_2 = 2.4$ Hz/puMW, $\Delta P_{d1} = \Delta P_{d2} = 0.01$ puMW, $\beta_1 = \beta_2 = 0.425$ puMW/Hz, $a_{12} = -1$.

Chapter 6/ Chapter 8/Chapter 9

Two-Area Thermal-Hydro-Gas System with/without GDB/GRC [40,41]:

$P_{r1} = P_{r2} = 2000$ MW, $\Delta P_{d1}^0 = \Delta P_{d2}^0 = 1000$ MW, Base power = 2000 MVA, $a_{12} = -1$, $F^0 = 60$ Hz, $P_{tie_max} = 200$ MW, $K_{PS1} = K_{PS2} = 68.9566$ Hz, $R_1 = R_2 = 2.4$ Hz/puMW, $\beta_1 = \beta_2 = 0.4312$ puMW/Hz, $T_{PS1} = T_{PS2} = 11.49$ sec, $a_1 = a_2 = 1$, $c_{g1} = c_{g2} = 1$, $b_{g1} = b_{g2} = 0.05$ sec,

$X_{g1} = X_{g2} = 0.6 \text{ sec}$, $Y_{g1} = Y_{g2} = 1 \text{ sec}$, $T_{F1} = T_{F2} = 0.23 \text{ sec}$, $T_{CR1} = T_{CR2} = 0.01 \text{ sec}$, $T_{CD1} =$
 $T_{CD2} = 0.2 \text{ sec}$, $K_{r1} = K_{r2} = 0.3$, $T_{r1} = T_{r2} = 10 \text{ sec}$, $T_{t1} = T_{t2} = 0.3 \text{ sec}$, $T_{12} = 0.0433$, T_{RS1}
 $= T_{RS2} = 5 \text{ sec}$, $T_{RH1} = T_{RH2} = 28.75 \text{ sec}$, $T_{W1} = T_{W2} = 1 \text{ sec}$, $T_{GH1} = T_{GH2} = 0.2 \text{ sec}$, $K_{T1} =$
 $K_{T2} = 0.543478$, $K_{H1} = K_{H2} = 0.326084$, $K_{G1} = K_{G2} = 0.130438$, $\Delta P_{d1} = \Delta P_{d2} = 0.01 \text{ puMW}$.

Chapter 7/ Chapter 8

Single-Area Thermal-Hydro-Gas System without GDB/GRC [26,27,28]:

$P_r = 2000 \text{ MW}$, Base power = 2000 MVA, $\Delta P_d^0 = 1000 \text{ MW}$, $F^0 = 60 \text{ Hz}$, $T_{PS} = 11.49$
 sec , $K_{PS} = 68.9566 \text{ Hz/puMW}$, $T_{SG} = 0.08 \text{ sec}$, $R = 2.4 \text{ Hz/puMW}$, $a = 1$, $c_g = 1$, $b_g = 0.05$
 sec , $X_g = 0.6 \text{ sec}$, $Y_g = 1 \text{ sec}$, $T_F = 0.23 \text{ sec}$, $T_{CR} = 0.01 \text{ sec}$, $T_{CD} = 0.2 \text{ sec}$, $K_r = 0.3$, $T_r =$
 $= 10 \text{ sec}$, $T_t = 0.3 \text{ sec}$, $T_{RS} = 5 \text{ sec}$, $T_{RH} = 28.75 \text{ sec}$, $T_W = 1 \text{ sec}$, $T_{GH} = 0.2 \text{ sec}$, $K_T =$
 0.543478 , $K_H = 0.326084$, $K_G = 0.130438$, $\Delta P_d = 0.01 \text{ puMW}$.

Single-Area Nuclear System [166]:

$P_r = 2000 \text{ MW}$, Base power = 2000 MVA, $\Delta P_d^0 = 1000 \text{ MW}$, $F^0 = 60 \text{ Hz}$, $R = 2.4$
 Hz/puMW , $K_{PS} = 120 \text{ Hz/puMW}$, $T_{PS} = 20 \text{ sec}$, $K_{HN} = 2$, $T_{N1} = 0.5 \text{ sec}$, $T_{NR} = 0.08 \text{ sec}$,
 $K_{RN} = 0.3$, $T_{N2} = 0.5 \text{ sec}$, $T_{RHN1} = 7 \text{ sec}$, $T_{RHN2} = 6 \text{ sec}$, $T_{RHN3} = 10 \text{ sec}$, $T_{N3} = 9 \text{ sec}$, $\Delta P_d =$
 0.01 puMW .

Single-Area Hydro-Nuclear System [166]:

$P_r = 2000 \text{ MW}$, Base power = 2000 MVA, $\Delta P_d^0 = 1000 \text{ MW}$, $F^0 = 60 \text{ Hz}$, $R = 2.4$
 Hz/puMW , $K_{PS} = 120 \text{ Hz/puMW}$, $T_{PS} = 20 \text{ sec}$, $K_{HN} = 2$, $T_{N1} = 0.5 \text{ sec}$, $T_{NR} = 0.08 \text{ sec}$,

$K_{RN} = 0.3$, $T_{N2} = 0.5$ sec, $T_{RHN1} = 7$ sec, $T_{RHN2} = 6$ sec, $T_{RHN3} = 10$ sec, $T_{N3} = 9$ sec, $K_N = 0.5$, $\Delta P_d = 0.01$ puMW, $T_{GH} = 48.7$ sec, $T_{RS} = 5$ sec, $T_W = 1$, $T_{RH} = 0.513$ sec, $K_H = 0.5$.

Single-Area Hydro-Nuclear-Gas System [166]:

$P_r = 2000$ MW, Base power = 2000 MVA, $\Delta P_d^0 = 1000$ MW, $F^0 = 60$ Hz, $R = 2.4$ Hz/puMW, $K_{PS} = 120$ Hz/puMW, $T_{PS} = 20$ sec, $K_{HN} = 2$, $T_{N1} = 0.5$ sec, $T_{NR} = 0.08$ sec, $K_{RN} = 0.3$, $T_{N2} = 0.5$ sec, $T_{RHN1} = 7$ sec, $T_{RHN2} = 6$ sec, $T_{RHN3} = 10$ sec, $T_{N3} = 9$ sec, $K_N = 0.50$, $\Delta P_d = 0.01$ puMW, $T_{GH} = 48.7$ sec, $T_{RS} = 5$ sec, $T_W = 1$, $T_{RH} = 0.513$ sec, $K_H = 0.25$, $a = 1$, $c = 1$, $b = 0.05$ sec, $a = 1$, $X = 0.6$ sec, $Y = 1.1$ sec, $T_F = 0.239$ sec, $T_{CR} = 0.01$ sec, $T_{CD} = 0.2$ sec, $K_G = 0.25$.

Two-Area Hydro-Nuclear System [166]:

$P_{r1} = P_{r2} = 2000$ MW, $P_{tie_{max}} = 200$ MW, Base power = 2000 MVA, $\Delta P_{di}^0 = 1000$ MW, $F^0 = 60$ Hz, $R_1 = R_2 = 2.4$ Hz/puMW, $a_{12} = -1$, $K_{PS1} = K_{PS2} = 120$ Hz/puMW, $T_{PS1} = T_{PS2} = 20$ sec, $K_{HN1} = 2$, $K_{HN2} = 2$, $T_{N1} = 0.5$ sec, $T_{NR1} = T_{NR2} = 0.08$ sec, $K_{RN1} = K_{RN2} = 0.3$, $T_{N2} = T_{N2} = 0.5$ sec, $T_{RHN1} = T_{RHN2} = 10$ sec, $T_{RHN2} = 6$ sec, $T_{RHN3} = 10$ sec, $T_{N3} = 9$ sec, $K_{N1} = K_{N1} = 0.50$, $\Delta P_{d1} = 0.01$ puMW, $K_{N1} = K_{N2} = 0.25$, $T_{GH1} = T_{GH2} = 48.7$ sec, $T_{RS1} = T_{RS2} = 0.513$ sec, $T_{W1} = T_{W2} = 1$ sec, $T_{RH1} = T_{RH2} = 0.513$ sec, $K_{H1} = K_{H2} = 0.5$.

Two-Area Hydro-Nuclear-Gas System with GDB/GRC [166]:

$P_{r1} = P_{r2} = 2000$ MW, $P_{tie_{max}} = 200$ MW, Base power = 2000 MVA, $\Delta P_{di}^0 = 1000$ MW, $F^0 = 60$ Hz, $R_1 = R_2 = 2.4$ Hz/puMW, $a_{12} = -1$, $K_{PS1} = K_{PS2} = 120$ Hz/puMW, $T_{PS1} = T_{PS2} = 20$ sec, $K_{HN1} = 2$, $K_{HN2} = 2$, $T_{N1} = 0.5$ sec, $T_{NR1} = T_{NR2} = 0.08$ sec, $K_{RN1} = K_{RN2} = 0.3$,

$T_{N2} = T_{N2} = 0.5 \text{ sec}$, $T_{RHN1} = T_{RHN2} = 10 \text{ sec}$, $T_{RHN2} = 6 \text{ sec}$, $T_{RHN3} = 10 \text{ sec}$, $T_{N3} = 9 \text{ sec}$,
 $K_{N1} = K_{N2} = 0.50$, $\Delta P_{d1} = 0.01 \text{ puMW}$, $K_{H1} = K_{H2} = 0.25$, $T_{GH1} = T_{GH2} = 48.7 \text{ sec}$, $T_{RS1} =$
 $T_{RS2} = 0.513 \text{ sec}$, $T_{W1} = T_{W2} = 1 \text{ sec}$, $T_{RH1} = T_{RH2} = 0.513 \text{ sec}$, $K_{H1} = K_{H2} = 0.5$, $a_1 = a_2 = 1$,
 $c_1 = c_2 = 1$, $b_1 = b_2 = 0.05 \text{ sec}$, $a_1 = a_2 = 1$, $X_1 = X_2 = 0.6 \text{ sec}$, $Y_1 = Y_2 = 1.1 \text{ sec}$, $T_{F1} = T_{F2} =$
 0.23 sec , $T_{CR1} = T_{CR2} = 0.01 \text{ sec}$, $T_{CD1} = T_{CD1} = 0.2 \text{ sec}$, $K_{G1} = K_{G1} = 0.25$. **GDB** – Hydro:
 ± 0.002 , Nuclear: ± 0.025 , Gas: ± 0.001 . **GRC** – Hydro: $+0.045$ upper limit and -0.06
lower limit. Nuclear and Gas: ± 0.2 and ± 0.0033 , respectively. **Time delay**: 0.015 sec .

Chapter 9

ESS [16,225,230]

$K_{SMES} = 0.12$, $T_{SMES} = 0.03 \text{ sec}$, $K_{RFB} = 0.67$, $T_{RFB} = 0 \text{ sec}$, $K_{CES} = 0.3$, $T_{CES} = 0.046$, $T_1 =$
 0.280 sec , $T_2 = 0.025 \text{ sec}$, $T_3 = 0.0411 \text{ sec}$, $T_4 = 0.39 \text{ sec}$.

BIO-DATA



Name : Ravi Choudhary
Fathers Name : Sh. Harendra Pal Singh
Mothers Name : Mrs. Sureshna Singh
Date of Birth : 10/10/1981
Email IDs : ravi1nsit@gmail.com, ravichoudhary@msit.in

Academics Qualifications

Qualification	Academic Year	Board/University	Subjects	Division
X	1997	CBSE	H,E,M,S,Sst	Ist
XII	1999	CBSE	P,C,M,H,E	Ist
B.Tech.	2005	UPTU, Lucknow	ECE	Ist
M.Tech.	2015	NSUT, Delhi	Process Control	Ist

Experience (16 Years)

Working as an Assistant Professor with Maharaja Surajmal Institute of Technology, Janakpuri, New Delhi-110058, India.

Subjects Taught: Control System, Circuit System, Digital Electronics

Area of Research interest: Electric Power Systems, advance controller, intelligent techniques, algorithms.

PUBLICATIONS

SCIE Journals

1. Choudhary, R., Rai, J.N. and Arya, Y., 2023. FOPTID+1 controller with capacitive energy storage for AGC performance enrichment of multi-source electric power systems. *Electric Power Systems Research*, Vol. 221,109450. <https://doi.org/10.1016/j.epsr.2023.109450>.
2. Choudhary, R., Rai, J.N. and Arya, Y., 2022. Cascade FOPI-FOPTID controller with energy storage devices for AGC performance advancement of electric power systems. *Sustainable Energy Technologies and Assessment*, Vol. 53(C),102671 <https://doi.org/10.1016/j.seta.2022.102671>.

International Conference

- 1) Choudhary, R., Rai, J.N. and Arya, Y., 2020. Impact of Energy storage device on the performance of AGC using ALO tuned PID controller. *International Conference on Artificial Intelligence and Speech Technology*, pp. 87-95, CRC Press. <https://doi.org/10.1201/9781003150664-10>
- 2) Choudhary, R., Rai, J.N. and Arya, Y., 2019, Automatic generation control for single area power system using GNA tuned PID controller. *Journal of Physics: Conference Series, International Conference on Future of Engineering Systems*, Vol. 1478, Issue. 1, p.012011, IOP Publishing. <https://doi.org/10.1088/1742-6596/1478/1/012011>